White dwarfs, black holes and neutron stars in close binaries

White dwarfs, black holes and neutron stars in close binaries

Witte dwergen, zwarte gaten en neutronensterren in nauwe dubbelsterren

Academisch proefschrift

ter verkrijging van de graad van doctor
aan de Universiteit van Amsterdam,
op gezag van de Rector Magnificus prof. dr. J.J.M. Franse,
ten overstaan van een door het college voor promoties ingestelde commissie,
in het openbaar te verdedigen in de Aula der Universiteit

op

woensdag 28 maart 2001, te 12:00 uur

door
Gijsbert Akijo Nelemans

geboren te Paramaribo, Suriname

PROMOTIECOMMISSIE

PROMOTORES	Ed van den Heuvel	
	Frank Verbunt	(Universiteit Utrecht)
OVERIGE LEDEN	Michiel van der Klis	
	Norbert Langer	(Universiteit Utrecht)
	GertJan Savonije	
	Rens Waters	
	Lev Yungelson	(INASAN, Moskou)

Sterrenkundig Instituut "Anton Pannekoek"
Faculteit der Natuurwetenschappen
Universiteit van Amsterdam

ISBN 90-9014636-9

Cover/Omslag: Image of the dust tail of the binary WR 104 (top left, taken by the Keck Telescope, courtesy Peter Tuthill), doppler tomogram of AM CVn (top right, Chapter 6) and image of the planetary nebula PKS285-02 (bottom, taken witht the Hubble Spce Telescope, courtesy Raghvendra Sahai and the Astrophysical Journal).

VOOR MIJN TWEE OMA'S
voor wie ik veel bewondering heb

Contents

CHAPTER 1

Introduction

1.1 White dwarfs, black holes and neutron stars...

White dwarfs, neutron stars and black holes are remnants of stars that have ended their 'active' life. A star is born when an interstellar gas cloud contracts and forms a sphere which in its centre has a temperature and pressure high enough to start hydrogen fusion. The star remains in this phase for most of its active life and only in the last ten percent of its active life its conditions change dramatically. Then the hydrogen fuel in its centre is exhausted, the energy production by the hydrogen fusion terminates, causing the star's thermal equilibrium to be disturbed, and the core of the star (now consisting mainly of helium) to contract. This causes the temperature and the pressure in the core to rise, until they become high enough for helium fusion to start and the star reaches a new thermal equilibrium. In the meantime a hydrogen-burning shell has formed around the core, and the outer envelope of the star has expanded to giant dimensions. After the helium fuel in the core is exhausted in its turn, the process repeats and during subsequent stages, heavier and heavier elements fuse until an iron core is formed which is no longer able to produce energy by fusion.

The precise temperature and pressure that the core of a star reaches depends also on the mass of the (core of the) star. In some cases the conditions in the core are such that the matter becomes 'degenerate', which has as a most important consequence that a further increase of the temperature does not result in expansion and a decrease of the density. For low-mass stars ($M < 2.3\,\mathrm{M}_\odot$) this happens in the first core-contraction phase and a degenerate helium core is formed. Only when this core has grown to $\sim$0.46 $\mathrm{M}_\odot$ (SWEIGART ET AL. 1990) the pressure becomes high enough for helium fusion to ignite. Because the core now is degenerate the sharp temperature rise produced by the fusion is not accompanied by expansion and cooling. This causes the helium burning to be explosive: the helium flash (HÄRM AND SCHWARZSCHILD 1961). Later in the evolution, for stars less massive than $\sim$8 $\mathrm{M}_\odot$, the core consisting mainly of carbon and oxygen is degenerate. However, during thermally unstable burning of helium in a shell around this core, the envelope of (most of) these stars is expelled before the mass of the core reaches the value for which a carbon-oxygen (CO) flash would happen.

The loss of the hydrogen-rich envelope generally terminates the star's evolution: no fresh helium is added to the core by the hydrogen-burning shell and the naked core of the star remains. In the case of stars less massive than $\sim$8 $\mathrm{M}_\odot$, described above,

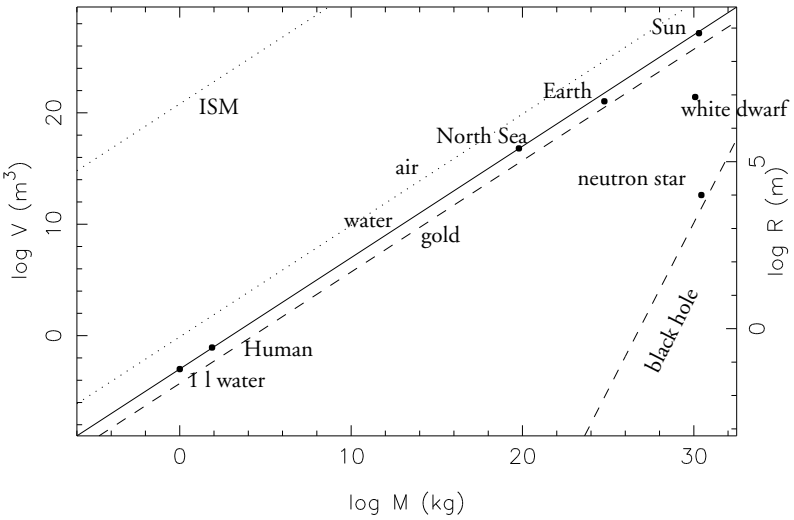

Figure 1.1: Masses and volumes of compact objects, the Earth, the Sun, the North Sea, a Human and 1 litre water. Lines of constant density are plotted for water (solid), gold (dashed) and air (dotted). The top dotted line gives the density of the ISM and the bottom dashed line the Schwarzschild radius for black holes.

the naked degenerate CO core simply cools and it remains observable as an ever fading object, called a white dwarf (e.g. SALPETER 1971). It has a very high density: it has a size comparable to the size of the Earth but a mass similar to that of the Sun (see Fig. 1.1). For a short while the expelled hydrogen envelope is ionised by the intense radiation of the hot core, and can be observed as a so called a planetary nebula, often showing a beautiful shape.

In stars more massive than $\sim$8 $M_\odot$ carbon burning takes place in a non-degenerate CO core. These stars subsequently go through the next burning stages, until an iron core is formed. At that moment the energy production stops and the core can no-longer withstand the gravitational force and collapses. The released energy is partly used to eject the outer envelope in a violent event which is observable as a so-called supernova. Depending on the mass of the (iron) core and possibly other conditions such as rotation and magnetic fields, either a neutron star is formed (an object consisting mainly of neutrons, in which the gravitational force is balanced by the Fermi pressure and nuclear forces between the nuclei) or the star collapses to a black hole (an object which is so compact that no light, and thus information, can escape), when no forces are strong enough to balance the gravitational force. The density of a neutron star is incredibly large: a neutron star is more massive than the Sun, but has a diameter like the city of Amsterdam! (see Fig. 1.1).

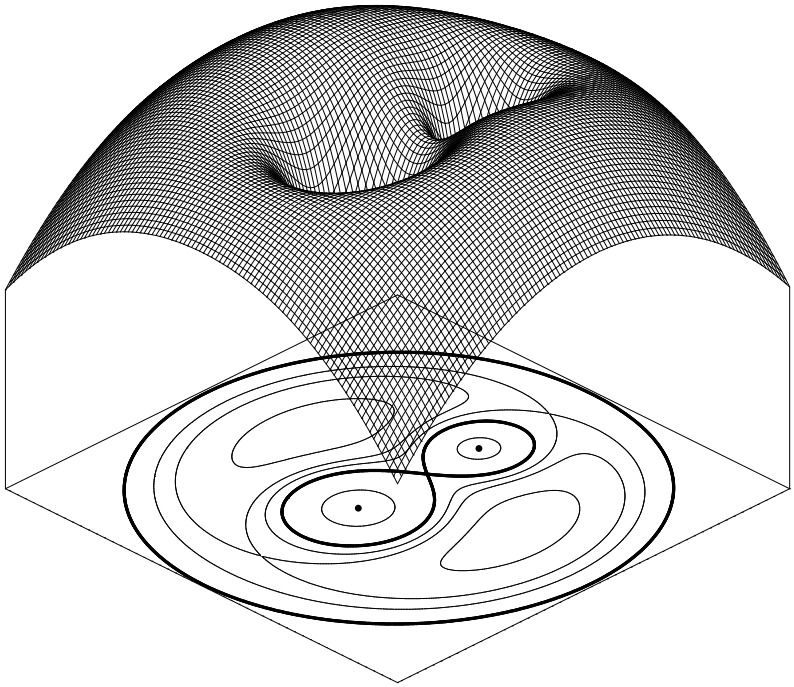

Figure 1.2: Projected equipotential surfaces of a binary system (bottom). The thick solid 8 like shape forms the two Roche lobes. The 3D surface gives the value of the potential. The saddle point in the middle is the first Lagrangian point. If one of the stars becomes big enough matter will flow along this point to the companion. Courtesy Martin Heemskerk.

1.2 ... in close binaries

The above described evolution of stars and the formation of so-called compact objects (white dwarfs, neutron stars and black holes) is complicated if the stars are members of a close pair of stars: a binary system. The importance of considering binary systems follows from the fact that of the known stars in the solar neighbourhood at least some 50% is part of such a pair (DUQUENNOY AND MAYOR 1991).

In a binary system, the effective potential in a co-rotating coordinate system can be approximated by three terms: two for the two (point)masses of the stars and one for the rotation of the coordinate system with the orbital period. The equipotential surfaces have a complex shape. The most important one defines the surface within which the potential of an individual star is the dominant term. This surface is called the Roche equipotential surface, which consists of the two Roche lobes of the two stars (see Fig. 1.2). Outside this surface none of the stellar terms dominates and matter is not bound to one of the two stars but only to the binary system as a whole.

Because their hydrogen-rich envelopes expand drastically during the late stages of the

evolution of stars, sufficiently close binaries will encounter the situation that one of the stars does not fit in its Roche lobe anymore. The first effect of this will be that matter will flow towards the companion star through the 'nozzle' between the two stars of the binary (called the first Lagrangian point, see Fig. 1.2). Since this matter takes along angular momentum and the mass-losing star is fixed in co-rotation with the orbital motion due to tidal coupling, this mass transfer immediately influences the orbital parameters. A second effect is that the mass ratio of the binary changes, causing the orbital parameters to change, even for a constant angular momentum.

The effect of the mass transfer depends totally on the ability of the star to change its radius so that it stays within its Roche lobe. We recognise three types of mass transfer (e.g. POLS AND MARINUS 1994): (i) Stable mass transfer, in which the star can stay inside its Roche lobe and remain in thermal equilibrium (e.g. when the Roche lobe expands because of the changing mass ratio). The mass transfer continues either because of the expansion of the star due its nuclear evolution (the mass transfer then takes place on a nuclear burning time-scale) or because of angular momentum loss from the orbit (e.g. by gravitational wave radiation); in that case the mass transfer proceeds on the typical time-scale of this angular momentum loss. Because the mass-transfer rates are generally low, most transferred matter can probably be accreted by the companion if it is not a neutron star or a black hole. (ii) Thermally unstable mass transfer, in which the star is able to stay inside its Roche lobe, but only because of its adiabatic response to mass loss; the star will try to regain thermal equilibrium but this causes the star to expand and lose mass again. The mass transfer then proceeds on the thermal time-scale, and the amount of transferred matter that is accreted by the companion depends on the nature of the accretor. Compact objects, in particular neutron stars, probably eject most of the transferred mass in some kind of jet. (iii) Dynamically unstable mass transfer (or simply unstable mass transfer), in which the star is not able to keep its radius smaller than its Roche lobe and runaway mass transfer is unavoidable. Hardly any matter is expected to be accreted by the companion.

The first effect of mass transfer on the further evolution of the star is that the hydrogen-rich envelope is removed prematurely. This means that the evolution of the star is halted and the core of the star is exposed. If this core is degenerate a white dwarf is formed directly. In this way two types of white dwarfs can be formed that cannot be formed from single stars: helium white dwarfs, when the envelope of a low-mass star is removed before the helium core has reached the mass for the helium flash, and oxygen-neon-magnesium white dwarfs, which are the cores of stars that would burn all the way to iron if they were left alone, but whose evolution is aborted by the removal of the envelope. Stars up to $\sim$11 $M_\odot$ can produce white dwarfs in this way in binary systems (see BARKAT ET AL. 1974).

If the envelope is removed of a star which has a non-degenerate core, the central burning in the core continues and a star is formed which consists of helium, or even carbon and oxygen, and is supported by nuclear burning. The evolution of this 'naked core' in principle follows the same path as it would have done if it still had its hydrogen-rich envelope. The only difference is that mass loss in a stellar wind, which would normally reduce the mass of the hydrogen-rich envelope and would hardly influence the nuclear

burning evolution of the star, now directly removes mass from the core. For massive helium stars this influences the fate of a star drastically (e.g. WOOSLEY ET AL. 1995). When the core has completed all burning stages it either becomes a CO white dwarf, or the core collapses and a supernova explosion takes place, which, however, looks different from a supernova of a single star because the hydrogen-rich envelope is missing.

A second consequence of the mass transfer in a binary is that the orbital characteristics of the binary change. In particular the effect of runaway mass transfer is believed to be very strong. The runaway mass transfer will produce an envelope surrounding the two stars of the binary system (called a common envelope). If the companion to the mass donor is sufficiently small in mass or radius it may evolve as an object moving through the envelope, slowing down its orbital motion due to frictional forces. As a result the orbital separation is dramatically reduced and the liberated potential energy of the binary may be used to expel the common envelope. This type of evolution is called spiral-in (PACZYŃSKI 1976). It means that after the mass transfer the exposed core of the mass donor resides in a binary which has a much smaller separation than before. In this way close binaries (sometimes with separations smaller than the radius of the Sun) can be formed which contain the remnants of stars that have gone through a phase in which they had radii of hundreds of solar radii. These binaries are the subject of this thesis.

1.3 The study of compact objects in binaries

To study these binaries two approaches can be used. The first one is the study of the physical state of particular (classes of) objects and the second is the study of the formation and evolution of these (classes of) objects. In the first approach observations or physical models are used to determine the physical processes that characterise the observed objects, such as the masses and orbital periods of stars and binaries, the properties of accretion disks, the properties of white dwarfs and pulsars, and properties of stars such as their mass-loss rate and circumstellar environment.

The second approach takes the results of the previous approach as a starting point in order to attempt to understand the further evolution of these stars and binaries and thus to find how different types of objects evolve into others and explain the formation of these types of objects. This approach has be very successful in the explanation of the formation of e.g. X-ray binaries (VAN DEN HEUVEL AND HEISE 1972; VAN DEN HEUVEL 1983), double neutron stars (TUTUKOV AND YUNGELSON 1973; FLANNERY AND VAN DEN HEUVEL 1975), cataclysmic variables (PACZYŃSKI 1976) and double white dwarfs (WEBBINK 1979; TUTUKOV AND YUNGELSON 1981; NATHER ET AL. 1981). In this way a general knowledge of the evolution of binaries was obtained which was used to study whole classes of objects such as double white dwarfs, binary pulsars and X-ray binaries (IBEN AND TUTUKOV 1986b; DEWEY AND CORDES 1987; MEURS AND VAN DEN HEUVEL 1989).

The way such studies are usually performed is by numerical models for the evolution of binary stars. The evolution of a binary is computed using simplified descriptions of stellar and binary evolution. This then is repeated for a large number of binaries,

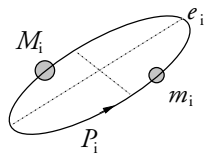

Population Synthesis

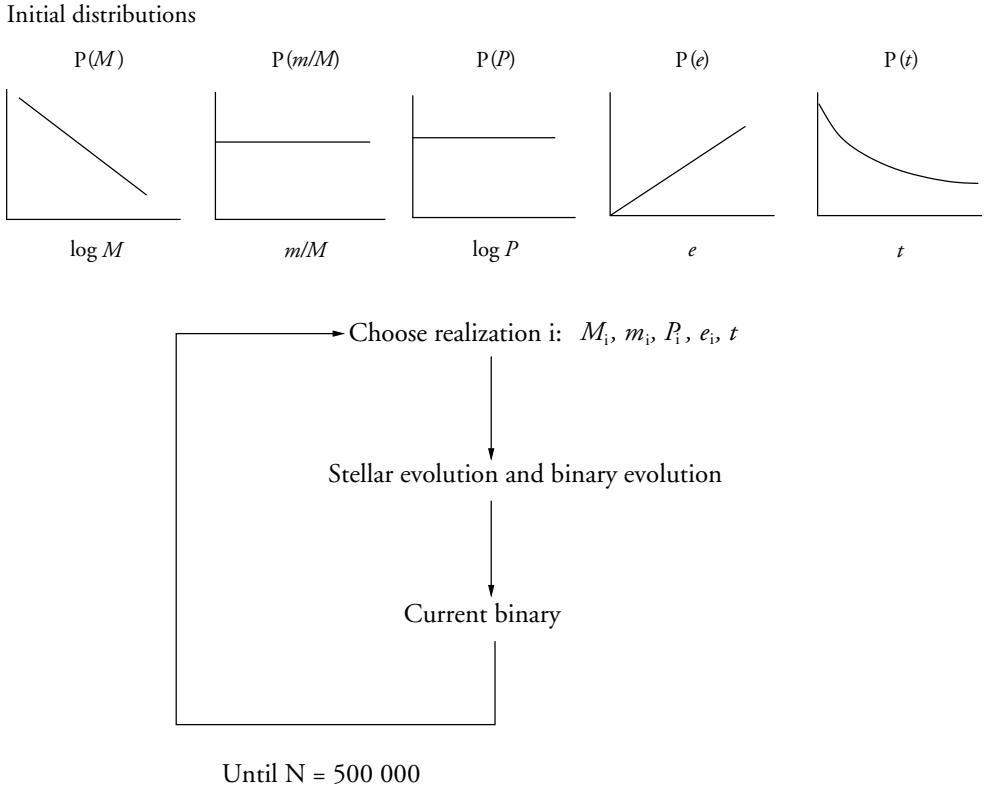

Figure 1.3: The principle of population synthesis. From initial probability distributions of binary parameters (indicated as $P(x)$) the initial mass of the primary M, the mass of the secondary m, the orbital period P, the initial eccentricity e and the age t are randomly chosen. The resulting binary is evolved and the current parameters are determined. Then a new binary is initialised etc. until a sufficiently large number (for example 500,000) is reached.

whose initial parameters are chosen from appropriate distributions derived from the observations. In this way a whole population of binaries is synthesised and this method therefore is called population synthesis (see also Fig. 1.3). The synthesised population can be compared to observed systems after taking selection effects into account. Population synthesis has been applied to the population of cataclysmic variables and related objects (e.g. POLITANO AND WEBBINK 1989; DE KOOL 1992; KOLB 1993), binaries containing neutron stars (e.g. TUTUKOV AND YUNGELSON 1993a), (low-mass) X-ray binaries (e.g. LIPUNOV ET AL. 1995; PORTEGIES ZWART AND VERBUNT 1996; KALOGERA AND WEBBINK 1996, 1998), double neutron stars (e.g. TUTUKOV AND YUNGELSON 1993b; LIPUNOV ET AL. 1997b; PORTEGIES ZWART AND YUNGELSON 1998; BLOOM ET AL. 1999), double white dwarfs (e.g. IBEN AND TUTUKOV 1986b; TUTUKOV AND YUNGELSON 1992; LIPUNOV AND POSTNOV 1988; IBEN ET AL. 1997; HAN 1998), double cores of planetary nebulae (e.g. DE KOOL 1990; YUNGELSON ET AL. 1993; HAN ET AL. 1995) etc.

1.4 This thesis

This thesis consists of three parts. The first and largest part deals with white dwarfs in close binaries, the second with black holes in binaries and the third with all close binaries containing two compact objects – white dwarfs, black holes and neutron stars.

1.4.1 White dwarf binaries

White dwarfs in binaries are the subject of the Chapters 2 to 6. The overall goal is to study the formation and evolution of binaries that consist of two white dwarfs. To achieve this, different research techniques are applied. Chapters 2 and 3 deal with observed characteristics of specific stars and binaries and aim to answer the question of how these objects could be formed and what they teach us about binary evolution.

In Chapters 4 and 5 we use population synthesis to simulate the Galactic population of white dwarf binaries. The resulting simulated populations are compared to the observed populations, after taking into account the selection effects that govern the detection of the observed systems. Finally, in Chapter 6 we study one key object (AM CVn) in detail, using observations obtained with a large telescope.

Chapter 2 deals with the observed phenomenon that not all low-mass white dwarfs, which probably are helium white dwarfs, are found in binaries as is expected from the fact that these objects can only be formed in binaries. We investigate the possibility for planets and brown dwarfs around solar-like stars to fulfil the role of binary companion in the formation of the helium white dwarf. The planet or brown dwarf could be destroyed in the process or be still in orbit around the helium white dwarf but remain undetected because of its low mass.

In Chapter 3 we consider the formation of three well-studied double white dwarf systems. The observed masses of the two stars in these binaries suggest that they are both helium white dwarfs. From these masses we derive the radii of the giants that were the

direct progenitors of the helium white dwarfs, using the core mass – radius relation for giants. This provides constraints on the two phases of mass transfer that must have taken place in these systems and on the properties and applicability of the spiral-in mechanism.

Chapter 4 uses the results of Chapter 3 to simulate the total Galactic population of close double white dwarfs. Using cooling models for helium white dwarfs we are for the first time able to simulate a magnitude-limited sample of close double white dwarfs which we compare to the observed sample. We investigate the period and mass (ratio) distribution of the close double white dwarfs, and also the fraction of observable white dwarfs that is member of a close pair. We compare the current formation rate and number of white dwarfs in our model with the observed formation rate of planetary nebulae and the observed local space density of white dwarfs.

Chapter 5 follows the same method, but now for a different type of binary: binaries in which one white dwarf transfers helium to another white dwarf. These objects are called AM CVn stars. The two possible formation channels for these systems are discussed. One is the further evolution of the double white dwarfs studied in Chapter 4 and the other is the formation of these systems from low-mass helium stars transferring mass to a white dwarf. The Galactic population resulting from the two channels is computed and compared to the six observed systems for which the orbital periods are known.

Chapter 6 deals with high-speed spectroscopic data taken with the 4.2 m William Herschel Telescope of AM CVn, the key object that gave the class of AM CVn stars its name. Even though AM CVn has been known for over 30 years there was still uncertainty about its real orbital period. Up to now periods were only known from photometry. Using the fast spectroscopy we were able to determine which of the two proposed periods is the real orbital period.

1.4.2 Black hole binaries

In the chapters on black hole binaries (Chapters 7 and 8), we study the conditions under which a black hole in a binary system is formed and investigate what we can learn from the observed properties of the black hole binaries about the event in which the black hole is formed and about the preceding evolution of the binary.

In Chapter 7 we use the observed space velocities of the black hole binaries to constrain the amount of mass that is lost in the supernova explosion in which the black hole is formed. Because this mass is lost almost instantaneously it moves away from the binary with the velocity that the exploding star had compared to the centre of mass of the binary. By conservation of momentum, the remaining binary obtains a velocity in the opposite direction.

Chapter 8 deals with the formation of binaries consisting of a black hole and a low-mass star which transfers matter to the black hole. We investigate the possibility that these systems are formed from binaries with such an initial separation that mass transfer takes place only just before the supernova explosion occurs, as has been suggested. We also calculate the effect of reduced mass-loss rates, as have been observed for Wolf-Rayet stars, on the final masses of stars that lose their envelope through mass transfer early in their evolution.

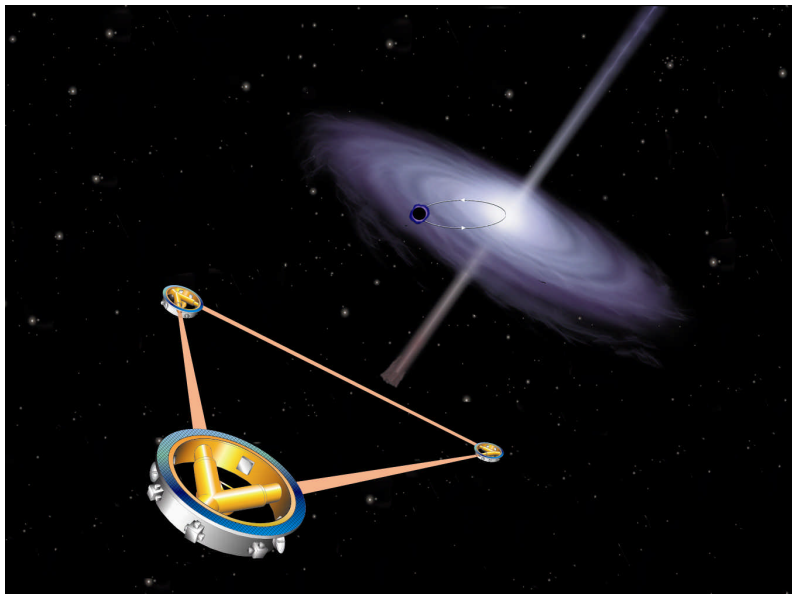

Figure 1.4: Artist impression of the Laser Interferometer Space Antenna (LISA), the joint ESA and NASA gravitational wave detector in space. Courtesy NASA JPL/Caltech.

1.4.3 White dwarf, black hole and neutron star binaries and the Galactic gravitational wave signal

In the last chapter (Chapter 9) we model the Galactic population of binaries containing two compact objects, i.e. white dwarfs, neutron stars or black holes. From these model populations we derive the merger rate for binaries containing neutron stars and/or black holes, which are the prime sources for high frequency gravitational wave detectors like LIGO, VIRGO and GEO600. From the close double white dwarfs (including the AM CVn systems) we calculate the predicted unresolved gravitational wave background at low frequencies for space-borne detectors like LISA (Fig. 1.4). We also predict the population of white dwarf, neutron star and black hole binaries that can be individually resolved by LISA.

CHAPTER 2

Formation of undermassive single white dwarfs and the influence of planets on late stellar evolution

G. Nelemans & T. M. Tauris

Astronomy & Astrophysics, 1998, 335, L85 – L88

ABSTRACT
We propose a scenario to form low-mass, single, slow-rotating white dwarfs from a solar-like star accompanied by a massive planet, or a brown dwarf, in a relatively close orbit (e.g. HD 89707). Such white dwarfs were recently found by MAXTED AND MARSH (1998). When the solar-like star ascends the giant branch it captures the planet and the subsequent spiral-in phase expels the envelope of the giant leaving a low-mass helium white dwarf remnant. In case the planet evaporizes, or fills its own Roche lobe, the outcome is a single undermassive white dwarf. The observed distribution of planetary systems supports the applicability of this scenario.

2.1 Introduction

Recent searches for double degenerates (two white dwarfs in a binary; MARSH 1995; MARSH ET AL. 1995) have resulted in the discovery of two single, low-mass helium white dwarfs – cf. Table 2.1. Similar undermassive white dwarfs ($\lesssim 0.5\,M_\odot$) are usually found in binaries and can not be formed from normal, single-star evolution which leaves a $\gtrsim 0.6\,M_\odot$ carbon-oxygen (CO) white dwarf as a remnant. Any potential single, low-mass progenitor star of these newly discovered undermassive white dwarfs can be excluded, since they would have a main sequence lifetime exceeding the age of our Milky Way. A scenario has been proposed (IBEN ET AL. 1997) in which a double degenerate has merged, due to the emission of gravitational wave radiation. According to MAXTED AND MARSH (1998), this scenario predicts high ($\sim 1000\,\mathrm{km\,s^{-1}}$) rotational

TABLE 2.1: Properties of the two recently discovered undermassive white dwarfs – cf. MARSH ET AL. (1995); MAXTED AND MARSH (1998).

Name	Mass ($M_\odot$)	$v_{\rm rot} \sin i\,(\mathrm{km\,s^{-1}})$	d (pc)
WD 1353+409	0.40	< 50	130
WD 1614+136	0.33	< 50	180

velocities for the remnant of the merged objects in contradiction with their measurements of a maximum projected rotational velocity of only $\sim 50\,\mathrm{km\,s^{-1}}$. Therefore the merger scenario seems questionable – unless there is an extremely efficient removal of angular momentum in the merging process, or the inclination angles for both these systems are extremely small.

In this letter we suggest a different, simple, solution to the formation of these single, low-mass (undermassive) white dwarfs by investigating the influence of massive planets, or brown dwarfs, in relatively close orbits around solar-like stars (Sect. 2.2). A short discussion of the consequences of our planetary scenario is given in Sect. 2.3.

2.2 Planets around solar-like stars

2.2.1 Introduction

We propose a scenario in which a solar-like star is surrounded by a massive planet, or a brown dwarf, in a relatively close orbit. When the star evolves on the giant branch it will become big enough to capture its planet via tidal forces (cf. RASIO ET AL. 1996; SOKER 1996). The planet spirals into the envelope of the giant and a so-called common envelope phase is initiated. The frictional drag on the planet, arising from its motion through the common envelope, will lead to loss of its orbital angular momentum (spiral-in) and deposit of orbital energy in the envelope. The orbital energy is converted into thermal and kinetic energy of the envelope which is therefore being ejected. The result of this common envelope evolution is determined by the energy balance and the fate of the planet. As a result of friction, and the large temperature difference between the envelope of the giant and the equilibrium temperature of the planet, low-mass planets evaporize due to heating. In case the planet evaporizes completely, the outcome will be a single star with a rotating and reduced envelope – otherwise we end up with a planet orbiting the naked core of a giant. The destiny of this white dwarf-planet system is determined by the orbital separation.

In this letter we first present the expected outcome of a common envelope evolution between a giant and a planet; thereafter we look at the important question of the onset of this evolution. We will closely follow the treatment of SOKER (1996, 1998), focusing on the cases where (most of) the envelope is lost in a common envelope, leaving a undermassive white dwarf. Research in this field has been carried out to explain elliptical and

bipolar planetary nebulae (SOKER 1996) and the morphology of the Horizontal Branch in clusters (SOKER 1998).

2.2.2 The outcome of the common envelope phase

Below we outline our scenario in somewhat more detail. By simply equating the difference in orbital energy to the binding energy of the envelope of the giant we can compute the ratio of final to initial separation (WEBBINK 1984). Let α_{ce} describe the efficiency of ejecting the envelope, i.e. of converting orbital energy into the kinetic energy that provides the outward motion of the envelope: $\Delta E_{bind} \equiv \alpha_{ce}\,\Delta E_{orb}$ or (using $m_p \ll M_{env}$):

$$a_f \simeq \frac{\alpha_{ce}\lambda}{2}\,\frac{M_{core}\,m_p}{M\,M_{env}}\,R_g = f\left(\frac{\chi}{1-\chi}\right)\frac{m_p}{M}\,R_g, \tag{2.1}$$

where R_g is the radius of the giant star at the onset of the spiral-in phase, λ is a weighting factor (< 1.0) for the binding energy of the core and envelope of the giant star, $\chi \equiv M_{core}/M$, m_p is the planetary mass and M_{core}, M_{env} and a_f are the mass of the helium core and hydrogen-rich envelope of the evolved star ($M = M_{core} + M_{env}$), and the final separation after all the envelope is expelled, respectively. In our calculations we chose $\lambda = 0.5$ and $\alpha_{ce} = 4$ (cf. TAURIS 1996; PORTEGIES ZWART AND YUNGELSON 1998) and hence $f = 1$.

To model the effect of planetary evaporation we follow SOKER (1998) and equate the local sound speed in the giants envelope to the escape velocity from the (gaseous) planet surface in order to find the approximate location of evaporation:

$$c_s^2 \approx v_{esc}^2 \Longleftrightarrow \gamma\frac{k_B T}{\mu m_u} \approx \frac{2\,G\,m_p}{\eta\,r_p}. \tag{2.2}$$

We use a temperature profile for evolved solar-like stars (cf. Fig. 2.1) of $T \approx 1.78 \times 10^6\,(r/\mathrm{R}_\odot)^{-0.85}\mathrm{K}$, in the entire interval of $R_{core} < r < R_g$, where R_{core} is the radius of the He-core. During the spiral-in the radius of a giant-gas planet, r_p, may expand slightly ($\eta\,r_p$, $\eta > 1$) even though only a small amount of mass ($< 0.1\,m_p$) is believed to be accreted (HJELLMING AND TAAM 1991).

Solving Eq. 2.2, with the temperature dependence given above and assuming $\gamma = 5/3$ and Pop.I chemical abundances (X=0.7; Z=0.02), yields the location of the evaporation:

$$a_{evap} = \left[10\,\eta\left(\frac{M_J}{m_p}\right)\right]^{1.18}\mathrm{R}_\odot, \tag{2.3}$$

where $M_J = 0.001\,\mathrm{M}_\odot$ ($\approx$ a Jupiter mass) and we have assumed $r_p = 0.1\mathrm{R}_\odot$, which is a reasonable assumption for all planets and brown dwarfs in the mass range $0.0001 < m_p/\mathrm{M}_\odot < 0.08$ (HUBBARD 1994).

For a given stellar structure (i.e. core and envelope mass and radius) the final outcome of the common envelope phase is determined only by the mass of the planet. We can

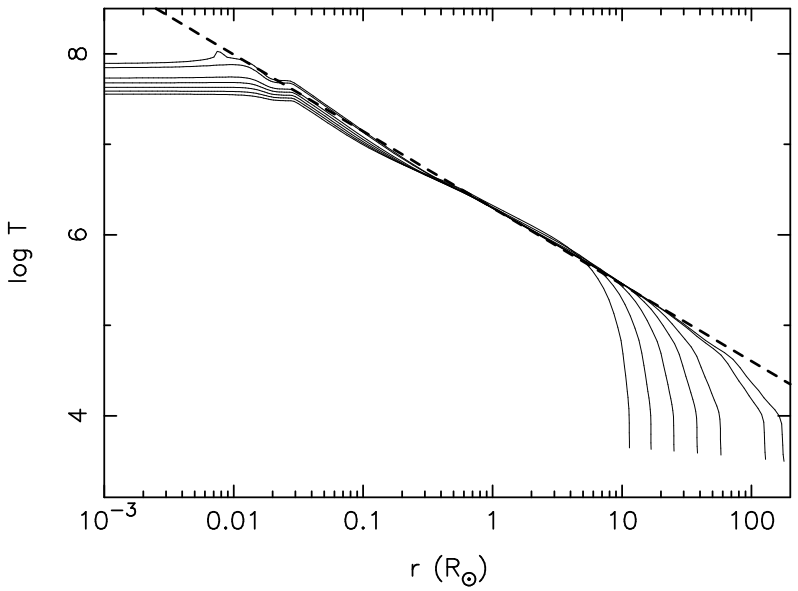

Figure 2.1: The temperature profiles for 1 $M_\odot$ evolved stars on the Red Giant Branch. Notice, that log T is approximately a linear function of log r at all evolutionary stages from the beginning until the tip of the Red Giant Branch (just before the helium flash).

easily compute the critical planetary mass for which the planet evaporizes just at the moment the envelope is completely expelled, i.e. when $a_{\rm evap} = a_{\rm f}$. The mass associated with this critical mass ($m_{\rm crit}$) is found from Eqs. 2.1 and 2.3 ($\eta = 1$):

$$m_{\rm crit} = 10 \left[\left(\frac{1-\chi}{\chi} \right) \left(\frac{M}{\rm M_\odot} \right) \left(\frac{R_{\rm g}}{100\,\rm R_\odot} \right) \right]^{0.46} M_{\rm J}. \tag{2.4}$$

Planets more massive than $m_{\rm crit}$ survive the spiral-in. However, in order to avoid a destructive mass transfer to the white dwarf after the spiral-in, it must have a radius smaller than its Roche lobe given by (PACZYŃSKI 1971):

$$a_{\rm RLO} = \frac{\eta\, r_{\rm p}}{0.462} \left(\frac{M_{\rm WD}}{m_{\rm p}} \right)^{1/3} \rm R_\odot, \tag{2.5}$$

where $M_{\rm WD} = M_{\rm core}$.

If $a_{\rm f} > a_{\rm evap}$ and $a_{\rm f} > a_{\rm RLO}$, the planet will survive and the entire envelope is lost from the giant leaving a low-mass helium white dwarf remnant with a planetary companion. However, if the final separation is small enough, the planetary orbit will decay due to emission of gravitational waves on a time-scale given by:

$$\tau_{\rm gwr} \approx \frac{(a_{\rm f}/60\ R_{\rm WD})^4}{(M_{\rm WD}/\rm M_\odot)^2\ (m_{\rm p}/M_{\rm J})}\ 5.0 \times 10^9\ \ \rm yr. \tag{2.6}$$

Hence, also in this case the final outcome of the evolution might eventually be a single undermassive white dwarf.

Planets less massive than $m_{\rm crit}$ will evaporate (or overflow their Roche lobe if $a_{\rm RLO} > a_{\rm evap}$) before the envelope is expelled completely. However heavy planets deposit significant orbital angular momentum in the envelope of the giant, causing enhanced mass loss due to rotation. This could lead to ejection of the envelope by planets somewhat less massive than $m_{\rm crit}$.

The change in structure of the star may alter the further evolution of the giant considerably. SOKER (1998) suggests that such an evolution could explain the morphology of the Horizontal Branch in clusters.

For the evolution of the giant we used the relations of IBEN AND TUTUKOV (1984a) for the structure of a (Pop.I) giant on the RGB: $R_{\rm g} = 10^{3.5} M_{\rm core}^{4}$, $L = 10^{5.6} M_{\rm core}^{6.5}$, $\dot{M}_{\rm core} = 10^{-5.36} M_{\rm core}^{6.6}$. These equations are valid on the RGB for a low-mass star ($0.8 \leq M/{\rm M}_{\odot} \leq 2.2$).

2.2.3 The onset of the common envelope phase: tidal forces and mass loss on the RGB

The moment the common envelope starts is determined by tidal forces. In the absence of any significant tidal interaction the donor star is only able to capture planets, via Roche-lobe overflow, out to a distance, $a_{\rm i}^{\rm max} \approx 1.6 R_{\rm g}$. Taking tidal effects into account using the equilibrium tide model (ZAHN 1977; VERBUNT AND PHINNEY 1995) we find, following SOKER (1996):

$$a_{\rm i}^{\rm max} \simeq 2.4 R_{\rm g} \left(\frac{1-\chi}{\chi^9}\right)^{1/12} \left(\frac{M}{{\rm M}_{\odot}}\right)^{-11/12} \left(\frac{m_{\rm p}}{10 M_{\rm J}}\right)^{1/8}, \qquad (2.7)$$

where we have used the equations for the structure of the giant as given above. In our calculations (see below) we have also included mass loss, which amounts to as much as $|\Delta M|/M \approx 0.20$ at the tip of the RGB. The mass is lost as a fast isotropic wind with the specific angular momentum of the giant causing the orbital separation of the planet to increase by the same ratio as the total mass of the system decreases. We modelled this effect according to the Reimers formula (KUDRITZKI AND REIMERS 1978) with $\alpha = 0.6$ (cf. RASIO ET AL. 1996).

2.2.4 Results

We will now demonstrate an approximate picture for the fate of stars with planets of different masses and separations to illustrate the applicability of this scenario for producing undermassive single white dwarfs as observed in nature. For the evolution of a solar-like star on the Red Giant Branch we will investigate to which separation (or alternatively which orbital period) a given planet will be captured by the star and compute the outcome of the spiral-in process for different planetary masses.

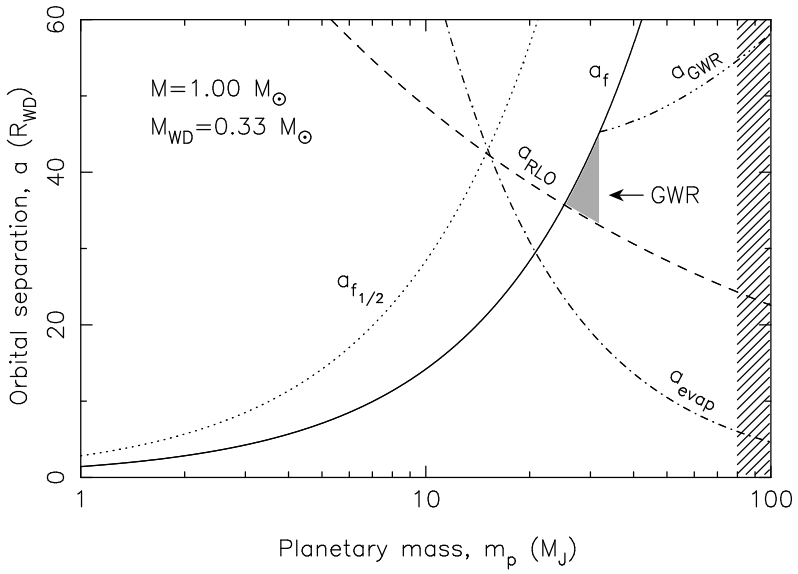

Figure 2.2: Separations of interest (in units of $R_{\rm WD}$ = 10 000 km) after the spiral-in phase for a $1\,{\rm M}_\odot$ star with a core of $0.33\,{\rm M}_\odot$ as a function of planetary mass. The solid line gives the separation for which the liberated orbital energy is equal to the binding energy of the envelope (dotted line for ejecting half of the envelope). The dashed line gives the separation below which the planet fills its Roche lobe. The dash-dotted line gives the separation at which the planet is evaporated. A minimum planetary mass of $\sim 21\,M_{\rm J}$ is needed to expel the entire envelope. planets lighter than this value are seen to be evaporated. However, for $15 < m_{\rm p}/M_{\rm J} < 25$ the planet fills its Roche lobe and is likely to be disrupted as a result. planets more massive than $\sim 25\,M_{\rm J}$ survive the common envelope phase but will later spiral in due to gravitational wave radiation (shaded area indicates a spiral-in time-scale of less than 5 Gyr). Above $0.08\,{\rm M}_\odot$ ($80\,M_{\rm J}$), the companions are heavy enough to ignite hydrogen as stars (hatched region).

In Fig. 2.2 we have plotted the different critical separations discussed above as a function of planetary mass. Our example is based on a $1.0\,{\rm M}_\odot$ star with a core-mass of $0.33\,{\rm M}_\odot$ (cf. WD 1614+136 in Table 2.1). We find $m_{\rm crit} = 21\,M_{\rm J}$. Less massive planets expel only part of the envelope (e.g. a planet with $m_{\rm p} = 15\,M_{\rm J}$ will only expel half of the envelope, neglecting enhanced mass loss of the giant due to the spin-up of the envelope). planets with masses between 15 and $25\,M_{\rm J}$ are presumably disrupted as they fill their Roche lobe during/after the spiral-in[1]. planets more massive than $\sim 25\,M_{\rm J}$ survive the spiral-in and will eject the entire envelope. However if $m_{\rm p} < 32\,M_{\rm J}$, the planet will spiral in, due to emission of gravitational waves, and hence fill its Roche lobe within 5 Gyr.

In Fig. 2.3 (top) we calculated the final outcome of the evolution of a planet orbiting a $1\,{\rm M}_\odot$ star as a function of planetary mass and initial orbital period. We

[1]The final fate of the planet depends on its adiabatic exponent, or actually $(\partial \ln r/\partial \ln m)$ and requires detailed calculations.

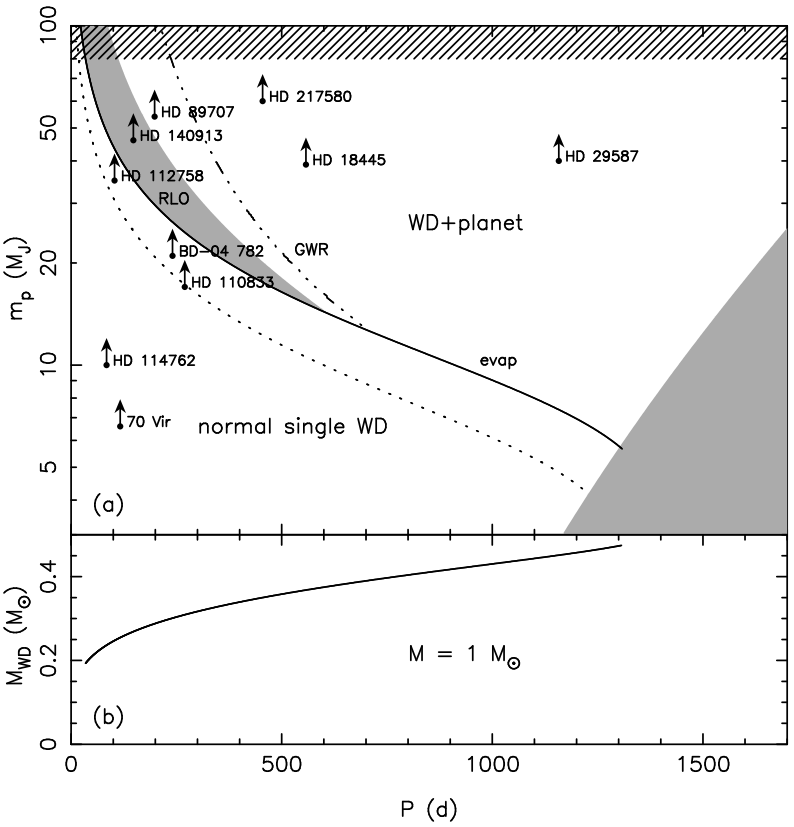

Figure 2.3: **a** Final outcome of the common envelope phase for different planetary masses and initial periods around a 1 $M_\odot$ star. The solid line indicates the critical mass, $m_{\rm crit}$, below which the planet will evaporize during the spiral-in. Above the solid line the planet survives the spiral-in phase and the outcome is an undermassive white dwarf with a planet orbiting it – unless the initial period is sufficiently short leading to a disruption of the planet as it fills its Roche lobe (left shaded area) after the spiral-in. The dash-dotted line indicates the limiting initial periods below which the planet will fill its Roche lobe, after the spiral-in, in less than 5 Gyr due to gravitational wave radiation. The dotted line yields the planetary mass for which half of the envelope is ejected – neglecting rotation (see text). Also indicated in the figure are the observed extrasolar planets and brown dwarfs. In the shaded area to the right, the planet is too far away from the giant to be engulfed in its envelope during evolution on the Red Giant Branch.
b Final mass of the white dwarf in case all of the envelope is expelled (i.e. $m_{\rm p} > m_{\rm crit}$).

also plotted some of the known planetary and brown dwarf systems with solar-like stars (0.70–1.20 $M_\odot$). Data were taken from "The Extrasolar Planets Encyclopaedia" (`http://www.obspm.fr/encycl/encycl.html`). We notice that, of the observed systems HD 89707 and HD 140913 are the best candidates for producing single undermassive white dwarfs. In HD 217580, HD 18445 and HD 29587 the planet is expected to survive the ejection of the envelope. In HD 114762 and 70 Vir they are captured already early on the RGB, where the binding energy of the envelope is too large to be expelled, so these planets will evaporate shortly after contact with the evolved donor star. The solitary white dwarfs resulting from these two systems will therefore be normal CO white dwarfs.

2.3 Discussion

We must bear in mind the uncertainties at work in our scenario, and it is possible that future detailed studies of the interactions between a planet and a common envelope may change the mass limits derived in this letter. Also notice that the two undermassive white dwarfs in Table 2.1 might very well have sub-stellar companions (brown dwarfs or planets) below the observational threshold mass of $\sim 0.1\,M_\odot$.

2.3.1 The final mass of the white dwarf

In the lower panel of Fig. 2.3 we give the final white dwarf mass in case all of the envelope is expelled. We see that white dwarfs with masses between 0.20–0.45 $M_\odot$ can in principle be formed with this scenario. If the common envelope phase initiates while the donor is on the Asymptotic Giant Branch, a CO white dwarf will be formed.

2.3.2 Rotation of the white dwarf

The final rotational period of the white dwarf is essentially determined only by the rotation of the core of the giant: the planet transfers almost all of its angular momentum to the giants envelope which is expelled. The rotation of the core strongly depends on the coupling between the core and the envelope of the giant (SPRUIT 1998), but is in any case in agreement with the the measured upper-limits for the white dwarfs as given in Table 2.1.

2.3.3 A white dwarf ejected from a binary ?

An other possibility for the formation of single undermassive white dwarfs is a binary origin. Consider a compact system with a giant star (the progenitor of the undermassive white dwarf) and a normal white dwarf companion. When the giant fills its Roche lobe it transfers its envelope to the companion leaving a low-mass helium white dwarf as a remnant. The companion may be subsequently lost either because it exploded as a type

Ia SN, or formed a (high velocity) neutron star from an accretion induced collapse – also leading to disruption of the binary.

Acknowledgements. We would like to thank Frank Verbunt for discussions and Bart Bisscheroux for providing Fig. 2.1. This research was supported in part by the NWO Spinoza-grant SPI 78-327. T.M.T. acknowledges the receipt of a Marie Curie Research Grant from the European Commission.

CHAPTER 3

Reconstructing the evolution of double helium white dwarfs: envelope loss without spiral-in

G. Nelemans, F. Verbunt, L. R. Yungelson & S. F. Portegies Zwart

Astronomy & Astrophysics, 2000, 360, 1011 – 1018

ABSTRACT

The unique core-mass – radius relation for giants with degenerate helium cores enables us to reconstruct the evolution of three observed double helium white dwarfs with known masses of both components.

The last mass transfer phase in their evolution must have been a spiral-in. In the formalism proposed by WEBBINK (1984), we can constrain the efficiency of the deposition of orbital energy into the envelope to be $1 \lesssim \alpha \lesssim 6$, for an envelope structure parameter $\lambda = 0.5$. We find that the two standard mass transfer types (stable mass transfer and spiral-in) are both unable to explain the first phase of mass transfer for these three binaries.

We use a parametric approach to describe mass transfer in low-mass binaries, where both stars are of comparable mass and find that the orbital characteristics of the observed double helium white dwarfs can be well reproduced if the envelope of the primary is lost with $\sim$1.5 times the specific angular momentum of the initial binary. In this case no substantial spiral-in occurs.

3.1 Introduction

The long lasting problem that we observe many double stars which are expected to form close pairs of white dwarfs, but yet that of the observed white dwarfs not one seemed to have a close white dwarf companion, was solved by the discovery of such pairs, starting with L870-2 (= WD 0135+052) in 1988 (SAFFER ET AL. 1988). In total 14 close detached binary white dwarfs are known at present, see Table 3.1. The fact

that six of these systems have their orbital period and the masses of both components determined provides an opportunity to test binary evolution theory in detail.

Models for the formation of close double white dwarfs envision two standard scenarios to produce these systems (TUTUKOV AND YUNGELSON 1981; IBEN AND TUTUKOV 1984b; WEBBINK 1984; TUTUKOV AND YUNGELSON 1988; HAN ET AL. 1995; IBEN ET AL. 1997; HAN 1998). In the first scenario, two low-mass ($M \lesssim 2.3\,M_\odot$) stars evolve through two stages of spiral-in. The first spiral-in will shrink the orbit, so the second spiral-in happens in a binary with a much smaller orbital separation. The Roche-lobe filling giant (secondary) now has a small radius and therefore a small core. The white dwarf that is formed last is thus less massive than its companion, with a mass ratio $m_{\rm bright}/m_{\rm dim} \lesssim 0.55$ (e.g. SANDQUIST ET AL. 2000).

In the second scenario, the first phase of mass transfer is stable; the second phase of mass transfer is again a spiral-in. The evolution of the orbit and the growth of the core during the first, slow phase of mass transfer depend on the amount of mass and angular momentum that is lost from the system. If the evolution in this phase is conservative, the expected final mass ratio $m_{\rm bright}/m_{\rm dim} \approx 1.14-1.18$ (TUTUKOV AND YUNGELSON 1988; SANDQUIST ET AL. 2000).

All white dwarfs in close pairs known today have low masses ($M \lesssim 0.5 M_\odot$). Note, however, that the inaccuracy of the mass determinations is as large as $\sim 0.05 M_\odot$ due to uncertainties in model atmospheres and cooling curves for white dwarfs (e.g. NAPIWOTZKI ET AL. 1999). These low masses suggest they are helium white dwarfs, but it cannot be excluded *a priori* that white dwarfs with masses $\gtrsim 0.35\,M_\odot$ are so called hybrid white dwarfs, i.e. having small carbon-oxygen (CO) cores and relatively thick ($\sim 0.1\,M_\odot$) helium envelopes (IBEN AND TUTUKOV 1985). For the most massive ones ($M \gtrsim 0.45\,M_\odot$), this is even the only option, since helium white dwarfs must have a mass below $0.46\,M_\odot$ (SWEIGART ET AL. 1990). For the less massive ones the probability to form hybrid white dwarfs is 4 – 5 times lower than to form helium white dwarfs (Chapter 4).

3.2 Reconstructing the binary evolution

Because of the unique core-mass – radius relation for giants with degenerate helium cores (REFSDAL AND WEIGERT 1970), we can reconstruct the mass transfer phases in which helium white dwarfs are formed. The mass of the brighter star in WD 1101+364 ($0.31\ M_\odot$) indicates that it is a helium white dwarf. In WD 136+768 and WD 0957-666 it cannot be excluded that the brighter stars are hybrid white dwarfs. The low mass of the dimmer companions in these three systems indicates that those are all helium white dwarfs. The white dwarfs in WD 0135-052 and WD 1204+450 are formally inconsistent with being helium white dwarfs, so we will not include them in the discussion anymore. WD 1704+481 probably consists of a helium white dwarf and a dimmer CO white dwarf, but because CO white dwarfs cool faster than helium white dwarfs (DRIEBE ET AL. 1998), it is not clear which of the white dwarfs was formed most recent so we cannot use this system in our present study.

TABLE 3.1: Parameters of known close double white dwarfs with $m_{\rm WD}$ denoting the mass of the brighter white dwarf and $M_{\rm WD}$ denoting its companion. For references see MAXTED AND MARSH (1999)[1] and MAXTED ET AL. (2000).

WD	P(d)	$m_{\rm WD}/{\rm M}_\odot$	$M_{\rm WD}/{\rm M}_\odot$
0135–052	1.556	0.47	0.52
0136+768	1.407	0.44	0.34
0957–666	0.061	0.37	0.32
1101+364	0.145	0.31	0.36
1204+450	1.603	0.51	0.51
1704+481	0.145	0.39	0.56
1022+050	1.157	0.35	
1202+608	1.493	0.40	
1241–010	3.347	0.31	
1317+453	4.872	0.33	
1713+332	1.123	0.38	
1824+040	6.266	0.39	
2032+188	5.084	0.36	
2331+290	0.167	0.39	

[1] For WD 0136+768 we give the masses of components after BERGERON ET AL. (1992), correcting a misprint in MAXTED AND MARSH (1999).

Assuming that the mass of the white dwarf is equal to the mass of the core of the giant at the onset of the mass transfer, the radius of the progenitor of a helium white dwarf can be calculated from the core-mass – radius relation given by IBEN AND TUTUKOV (1984a):

$$R \approx 10^{3.5}\, M_{\rm c}^4 \tag{3.1}$$

(R and $M_{\rm c}$ in solar units). This equation is in good agreement with other equations describing this dependence for giants (e.g. WEBBINK ET AL. 1983). The *mass of the white dwarf progenitor* is however not known, since the above relation is independent of the total mass of the star. However the mass of the giant must be in the range 0.8 – 2.3 $\rm M_\odot$. For less massive stars the main-sequence lifetime is larger than the age of the Galaxy. More massive stars do not form degenerate helium cores.

For the remainder of this article we use the following notation: $M_{\rm i}$ and $M_{\rm WD}$ indicate the initial mass of the original primary and the mass of the white dwarf that it forms, $m_{\rm i}$ and $m_{\rm WD}$ represent the same for the original secondary. If the secondary accretes mass during the first phase of mass transfer, we represent its new mass with $m_{\rm i}'$. For the radii of the stars when they become giants we use $R_{\rm g}$ and $r_{\rm g}$ for the original primary and secondary respectively. With $P_{\rm i}, P_{\rm m}$ and P we indicate the initial period, the period after the first phase of mass transfer, and the current period of the binary.

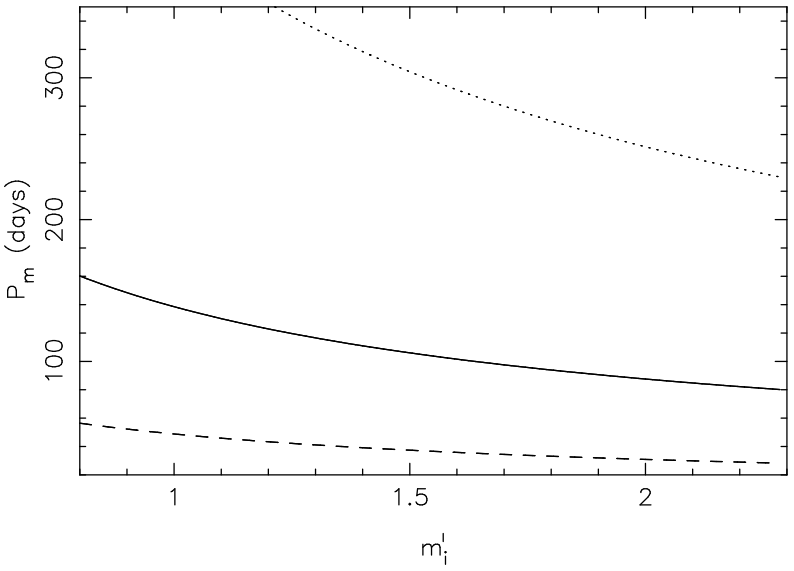

Figure 3.1: Periods before the spiral-in phase in which the younger white dwarf was formed as function of the mass of its giant progenitor. Lines from bottom to top: WD 1101+346, 0957-666 and 0136+768.

3.3 Last mass transfer: spiral-in

Using Eq. (3.1) we calculate the radii of the progenitors of the brighter white dwarfs for the three double helium white dwarfs. Since we know the mass of the white dwarf that orbited this giant and may reasonably assume that it did not accrete anything during the spiral-in phase, we can calculate the orbital separation at the onset of the spiral-in, as function of the mass $m_{\rm i}^{I}$ of the giant,

$$a_{\rm m}(m_{\rm i}^{I}) = \frac{r_{\rm g}(m_{\rm WD})}{r_{\rm L}(M_{\rm WD}/m_{\rm i}^{I})}, \tag{3.2}$$

where $r_{\rm L} \equiv R_{\rm L}/a$ is the dimensionless Roche-lobe radius, given e.g. by EGGLETON (1983) and we assume $r_{\rm g} = R_{\rm L}$. This is shown in Fig. 3.1, where we use Keplers 3$^{\rm rd}$ law to compute the period from the orbital separation. Comparing the periods in Fig. 3.1 with the observed periods in Table 3.1, we see that in the last mass transfer phase the orbital separation must have reduced dramatically. This can only be accomplished if the last mass transfer was a spiral-in.

In a spiral-in, the envelope of the giant is expelled at the expense of the orbital energy of the binary. Balancing the binding energy of the envelope of the giant with the

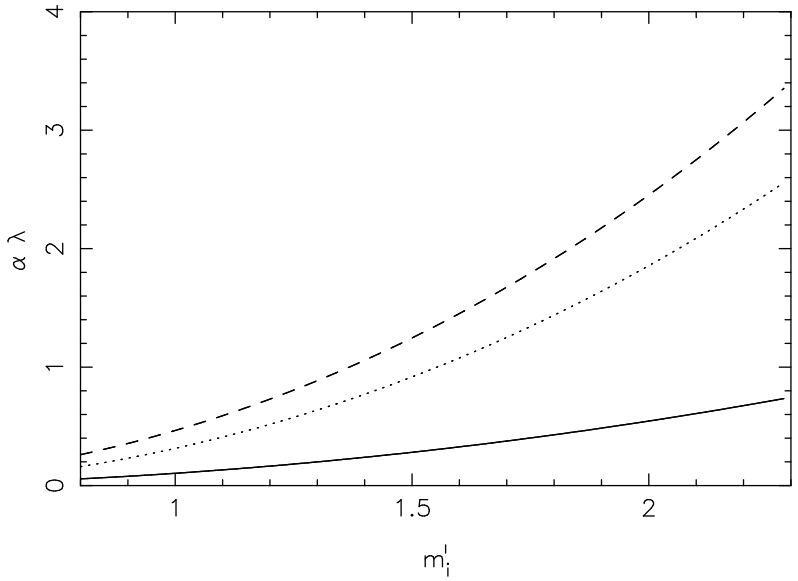

Figure 3.2: The parameter $\alpha\lambda$ for WD 0957-666, 1101+364 and 0136+768 assuming that the brighter component is a helium white dwarf and their orbital periods did not change since the end of the spiral-in stage. Lines from bottom to top are for WD 0957-666, 0136+768 and 1101+364.

difference in orbital energy (WEBBINK 1984) one finds

$$\frac{M_{\rm WD}\,(m_{\rm i}^{\prime}-m_{\rm WD})}{\lambda\,r_{\rm g}} = \alpha\left[\frac{M_{\rm WD}\,m_{\rm WD}}{2\,a_{\rm f}}-\frac{M_{\rm WD}\,m_{\rm i}^{\prime}}{2\,a_{\rm m}}\right]. \tag{3.3}$$

The parameter λ depends on the structure of red giant envelope. The usual assumption is that $\lambda = 0.5$ (DE KOOL ET AL. 1987). The parameter α represents the efficiency of the deposition of orbital energy into the common envelope. To reduce the number of parameters, the product $\alpha\lambda$ is treated as a single parameter in the remainder of this article, but it should be noted that both λ and α will in reality be functions of the evolutionary stage of the stars.

Applying Eq. (3.3) and Eq. (3.2), we find $\alpha\lambda$ as a function of $m_{\rm i}^{\prime}$ for the three systems considered. We plot this in Fig. 3.2, where we assume that the current periods are equal to the post spiral-in periods. This may not be the case in general since close orbits like the those of WD 0957-666 and WD 1101+364 will decay due to the loss of angular momentum by gravitational radiation. However, the estimated ages for these white dwarfs ($\sim 10^7$ yr (MORAN ET AL. 1997) and $\sim 10^9$ yr (using the cooling curves of DRIEBE ET AL. 1998) respectively) are short compared to the orbital decay time-scale.

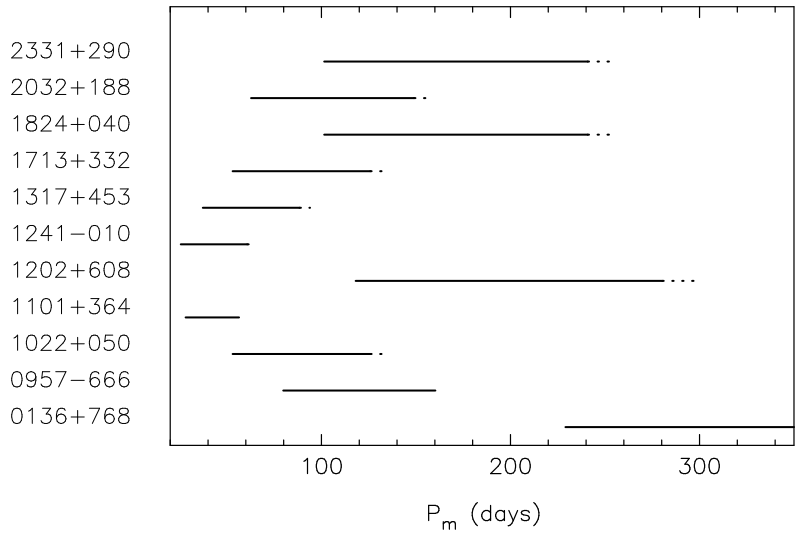

Figure 3.3: Periods before the spiral-in for all double white dwarfs in which the last formed is a helium white dwarf. Limits allow for the (unknown) mass of the progenitor of this white dwarf and the mass of the unseen companion. Solid lines are for a companion mass between 0.2 and 0.65 $M_\odot$. Dotted line gives the limit for a companion mass of 0.65 – 1.4 $M_\odot$.

For the remaining white dwarf pairs listed in Table 3.1 the mass of only one component is known. We assume here that it is the last formed component we observe. Low-mass white dwarfs may have thick hydrogen envelopes which make them cool very slowly (DRIEBE ET AL. 1998) and the situation in which the older white dwarf is really observed cannot be excluded *a priori*. However, as we show in a forthcoming paper (Chapter 4), in the majority of binary white dwarfs we indeed observe the youngest of the two dwarfs.

From Figs. 3.1 and 3.2 we see that we find a range of $P_{\rm m}$'s and $\alpha\lambda$'s for WD 0957-666, 1101+364 and 0136+768 where the mass of the second white dwarf is known. For the remaining systems we can also compute a range of $P_{\rm m}$'s and $\alpha\lambda$'s by determining the ranges for all possible masses of the unseen companion. We do know that the companion almost certainly is another white dwarf, so the mass of this object must be between 0.2 and 1.4 $M_\odot$ and most probably even below 0.65 $M_\odot$ (IBEN ET AL. 1997; HAN 1998, Chapter 4). Having also in mind that the mass of white dwarf progenitor is in the 0.8 – 2.3 $M_\odot$ range we can derive the possible ranges of intermediate periods and $\alpha\lambda$'s for all double white dwarfs, as is shown in Figs. 3.3 and 3.4.

Two conclusions can be drawn from Figs. 3.1 to 3.4:

1. The efficiency of the energy deposition into the common envelopes α must be high.

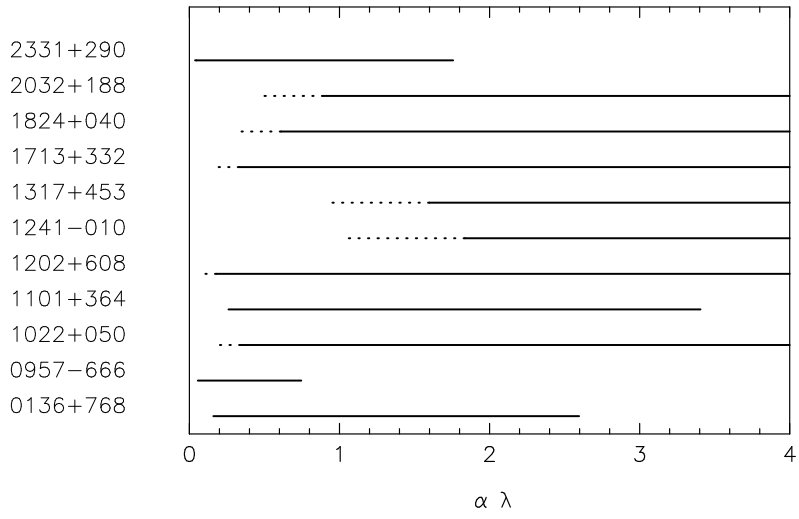

Figure 3.4: The parameter $\alpha\lambda$ for the same cases as in Fig. 3.3.

From model calculations of stellar structure we know that $\lambda \sim 0.5-1.0$. If we assume that α does not depend on the evolutionary state of the giant or the combination of the masses of the giant and the white dwarf, the parameters of all double white dwarfs with two observed helium components can be reproduced with the same $\alpha \sim 4$. The only exception is WD 0957-666 for which the efficiency appears to be much lower (see Sect. 3.6.2 for a different solution). Note that an error in the masses of the white dwarfs of 0.05 $M_\odot$ translates to an error in the value of $\alpha\lambda$ of a factor $\sim$1.5. However even this does not bring the value of α to 4 for WD 0957-666.

Since Eq. (3.3) only considers a rough energy budget, the conclusion $\alpha > 1$ could simply mean that we do not calculate the energy accurately. It does mean that the orbital energy deposition into common envelope has to be highly efficient. It could also mean that sources other than the orbital energy contribute to the process of common envelope expulsion (IBEN AND LIVIO 1993). For example it is possible that the envelope is partially removed before Roche-lobe contact by an enhanced stellar wind due to tidal interaction between the giant and the companion (TOUT AND EGGLETON 1988), yielding a lower value of $\alpha\lambda$.

2. The immediate progenitors of the known close double white dwarfs (i.e. the white dwarf + giant binaries) all had rather wide orbits (25 – >500 days). This has important consequences for the understanding of the first phase of mass transfer.

3.4 The first mass transfer

We compute the evolution of the binary parameters in the first mass transfer, where we start from the initial binary and evolve it forward according to the two standard scenario's. The resulting periods should be equal to the intermediate periods we reconstructed in the previous section.

3.4.1 Spiral-in

In the case when the first mass transfer was also a spiral-in, we can compute the period after the spiral-in by making a (standard) assumption that $\alpha\lambda$ is constant (i.e. here, as derived above $\alpha\lambda = 2$). The initial separation at which the primary fills its Roche lobe is again determined by Eq. (3.1) and a value for $M_{\rm i}$ between 0.8 and 2.3 $M_\odot$. Applying Eq. (3.3), we find $a_{\rm m}$ (and thus $P_{\rm m}$) as a function of $M_{\rm i}$ and $m_{\rm i}$. The maximum period after the spiral-in is given for the case $M_{\rm i} = m_{\rm i}$, which we plot in Fig. 3.5 (bottom three lines). These periods are clearly much smaller than the periods derived in the previous section (see Fig. 3.1). We reproduce the latter on a logarithmic scale as the top three lines in Fig. 3.5. In a recent article SANDQUIST ET AL. (2000) came to the same conclusion, based on the observed mass ratios and also concluded that it is very hard for binaries containing two low-mass stars to survive two spiral-in phases.

It may be argued that $\alpha\lambda$ is different in the first mass transfer phases, because the companion now is a main-sequence star instead of a white dwarf. We can, just as in the case of the second mass transfer determine the value of $\alpha\lambda$ that is required to get the right period after the mass transfer. *If we do this, however, we find* $-15 \lesssim \alpha\lambda \lesssim -5$ *clearly out of the allowed range. This means that a spiral-in phase in the first mass transfer phase for these systems is ruled out.*

3.4.2 Stable mass transfer

For the alternative scenario, to start with a short period zero-age binary and evolve through a phase of stable mass transfer, the zero-age orbital period should be in a narrow interval, such that the primary fills its Roche lobe at the moment it still has a radiative or at least shallow convective envelope. For these stars mass transfer in which the donor stays in thermal equilibrium is possible if the initial mass ratio $q_{\rm i} \equiv m_{\rm i}/M_{\rm i} \gtrsim 0.8$ (TUTUKOV ET AL. 1982). For more extreme mass ratio's; $q_{\rm i} \gtrsim 0.3$, mass transfer can proceed on a time-scale in between the thermal and the dynamical time-scale of the donor (e.g. trial computations for a system with $M_{\rm i} = 2.3 M_\odot$, $m_{\rm i} = 0.8 M_\odot$ and $a_{\rm i} = 12.8 R_\odot$ show that $\log \dot{M}_{\rm i} \lesssim -5.5 M_\odot$ yr^{-1}; A. Fedorova, private communication). However for mass ratio's $q_{\rm i} \lesssim 0.5$, the thermal time-scale of the accretor is much longer than the mass transfer time-scale and the accretor is expected to expand, leading to a contact configuration which is unstable (e.g. KIPPENHAHN AND MEYER-HOFMEISTER 1977), unless the secondary is a convective low-mass main-sequence star (WEBBINK 1977). Since we want to explore the limits of the Algol scenario, we allow all values of $q_{\rm i} > 0.3$ and calculate the possible periods after the Algol phase.

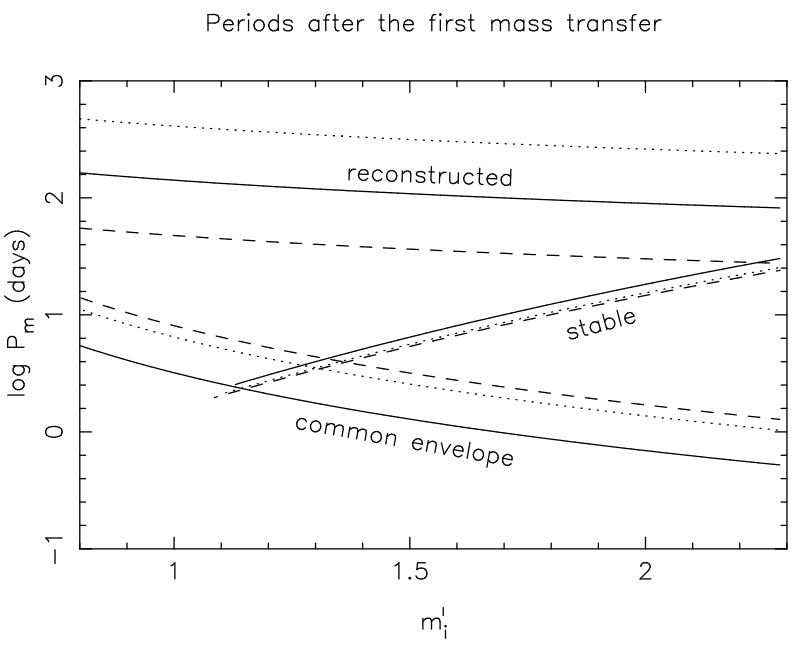

Figure 3.5: Periods after the first phase of mass transfer ($P_{\rm m}$) as function of the mass of secondary at this time ($m_{\rm i}'$). Top three lines are periods needed to explain the mass of the second formed white dwarf (see Fig. 3.1). Middle three lines give the maximum period would the first phase of mass transfer be an Algol phase, lower three ones are for the case the first mass transfer phase was a spiral-in. Solid lines for WD 0957-666, dashed lines for WD 1101+346 and dotted lines for WD 0136+768.

We assume the mass transfer is conservative and for a given total mass of the system $M_{\rm tot} = M_{\rm wd} + m_{\rm i}'$, the initial masses are $M_{\rm i} = M_{\rm tot}/(1+q_{\rm i})$ and $m_{\rm i} = q_{\rm i} M_{\rm i}$. We consider systems in which the primary fills its Roche lobe just before the star develops a relatively deep convective envelope (the outer 50% of the mass is convective). The radii of such stars are obtained by a fit to stellar models by MENGEL ET AL. (1979): $R_{\rm max} \approx 2.4\, M_{\rm i}^{1.56}$ (solar units). Using the approximation to the Roche lobe given by PACZYŃSKI (1967) and the equation for the change in period for conservative mass transfer we find the period after the Algol phase is

$$P_{\rm m} \approx 1.38 \frac{M_{\rm tot}^{7.84}}{(M_{\rm wd}\, m_{\rm i}')^3} \frac{q_{\rm i}^3}{(1+q_{\rm i})^{7.84}} \qquad \text{days.} \tag{3.4}$$

This equation has a maximum for $q_{\rm i} = 0.62$. We compute these maximal periods as function of $m_{\rm i}'$, where of course $M_{\rm i}$ and $m_{\rm i}$ are limited by $M_{\rm i} > 0.8{\rm M}_\odot$, because the primary has to evolve off the main-sequence and $m_{\rm i}' < 2.3{\rm M}_\odot$, because the secondary must still develop a degenerate helium core.

TABLE 3.2: Parameters of wide binaries with giant and white dwarf components. Masses in solar units.

Name	P (d)	M	$m_{\rm WD}$	ref
S1040	42.8	1.5	0.22	LANDSMAN ET AL. (1997)
AY Cet	56.8	2.2	0.25	SIMON ET AL. (1985)

The resulting periods for q = 0.62 are shown as the middle set of lines in Fig. 3.5, where we actually used the equation for the Roche lobe given by EGGLETON (1983), which is better in this mass ratio regime. The obtained periods are clearly not long enough to explain of the origin of WD 0957-666, 1101+364 and 0136+768.

One could argue that the assumption of conservative evolution is not correct. HAN (1998), for example, in his 'best' model assumes 50% of the mass is lost with the specific angular momentum of the donor. This could yield wider orbits than obtained above. Looking at his Fig. 7 one sees that he can indeed explain WD 1101+364, but not WD 0957-666 and especially not WD 0136+768, because for these systems the masses of the last formed white dwarfs (i.e. the periods after the Algol phase) are too large. To get higher masses one needs to lose less angular momentum with the mass, leading to even wider orbits. However, analysis of observed low-mass Algols, which are binaries currently in this stage of stable mass exchange (e.g. REFSDAL ET AL. 1974; MASSEVICH AND YUNGELSON 1975; GIANNUZZI 1981; IBEN AND TUTUKOV 1984b; KRAICHEVA ET AL. 1986; MAXTED AND HILDITCH 1996) shows that their periods are smaller than would be expected with Eq. (3.4). This suggests that descendants of Algol-type systems have orbital separations even smaller than in the case of conservative evolution, which we assumed for Fig. 3.5.

We conclude that with the above assumptions Algol evolution in the first mass transfer stage for WD 0136+768, 0957-66 and 1101+364 is ruled out also.

There are some other observed systems with white dwarfs which probably could not be formed through Algol-type evolution (Table 3.2), since white dwarf + giant binaries with $M_{\rm WD} \lesssim 0.25 {\rm M}_\odot$ end their Algol phase with periods below $\sim$30 d. (KRAICHEVA ET AL. 1986). In another system, HD 185510, with $P_{\rm orb}$=20.7 day, a giant has a hot companion which is classified as a 0.3 $M_\odot$ sdB star from its temperature and gravity (FRASCA ET AL. 1998). However, it also fits the range of temperatures and gravities for $\sim 0.25 {\rm M}_\odot$ helium white dwarfs (DRIEBE ET AL. 1998) and the system may be a viable Algol descendant. If it is an sdB star, which *a priori* is less likely, it actually matches a scenario similar to one for WD 0957-666 rather well (see Sect. 3.6.2).

3.5 Unstable mass transfer revised

Since both standard scenarios for the first phase of mass transfer appear to be ruled out, the situation apparently is more complex. TOUT AND EGGLETON (1988, see also HAN

1998) assume that due to tidal effects of the companion, the star can lose up to 150 times more mass in the stellar wind than without companion. This has of course the desired effect that the orbit widens before the mass transfer starts, and that there is less envelope mass left to be expelled, leading to a less dramatic spiral-in. However, if we recompute the lines for a spiral-in in Fig. 3.5 with reduced envelopes such that they overlap with the reconstructed lines, we find that for WD 1101+364 we need to reduce the envelope by 70% and for the others by even more than 90%.

In searching for a different solution we start by noting that the original spiral-in picture (PACZYŃSKI 1976) considers a companion which orbits inside the envelope of the giant. The companion experiences drag forces while moving in the envelope and frictional effects brake the companion. In this process orbital energy is transformed into heat and motion of the gas and finally into kinetic energy that causes the envelope of the giant to be expelled. This picture is very much based on the situation where there is a tidal instability which causes the decay of the orbit of the companion in systems with a high mass ratios of the components (DARWIN 1908; COUNSELMAN 1973). In the case that the common envelope is caused by a runaway mass transfer, the common envelope will not look much like the equilibrium envelope of the star and worse, the angular momentum of the orbit is so large that the common envelope is in principle easily brought into co-rotation with the orbit. At that moment there are no drag forces anymore.

Since for stars with deep convective envelopes mass loss on a dynamical time-scale seems, in the current state of the art in stellar evolution modelling, inevitable, we have to assume that in the progenitors of the observed double white dwarfs some kind of common envelope engulfing the whole system forms. The parameters of the observed close binary white dwarfs suggest that this envelope is subsequently lost without much spiral-in. The energy to expel the envelope may be supplied by the luminosity of the giant or by tidal heating, or a combination of both. In absence of a detailed physical description we will describe the effects of this mechanism in terms of the angular momentum balance.

We compare the pre- and post-mass transfer binaries, under the assumption that the envelope of the giant is lost completely from the binary (i.e. $m_{\rm i}^{\prime} = m_{\rm i}$), and that this mass loss reduces the angular momentum of the system in a linear way, as first suggested for the general case of non-conservative mass transfer by PACZYŃSKI AND ZIOŁKOWSKI (1967)

$$J_{\rm i} - J_{\rm m} = \gamma J_{\rm i} \frac{\Delta M}{M_{\rm tot}}, \tag{3.5}$$

where $J_{\rm i}$ is the angular momentum of the pre-mass transfer binary and $M_{\rm tot}$ is the total mass of the binary. The change of the orbital period as function of the initial and final masses of the components then becomes

$$\frac{P_{\rm m}}{P_{\rm i}} = \left(\frac{M_{\rm WD} m_{\rm i}^{\prime}}{M_{\rm i} m_{\rm i}} \right)^{-3} \left(\frac{M_{\rm WD} + m_{\rm i}^{\prime}}{M_{\rm i} + m_{\rm i}} \right) \left(1 - \gamma \frac{\Delta M}{M_{\rm i} + m_{\rm i}} \right)^{3}. \tag{3.6}$$

We can estimate γ for the three double helium white dwarf systems, just as for the

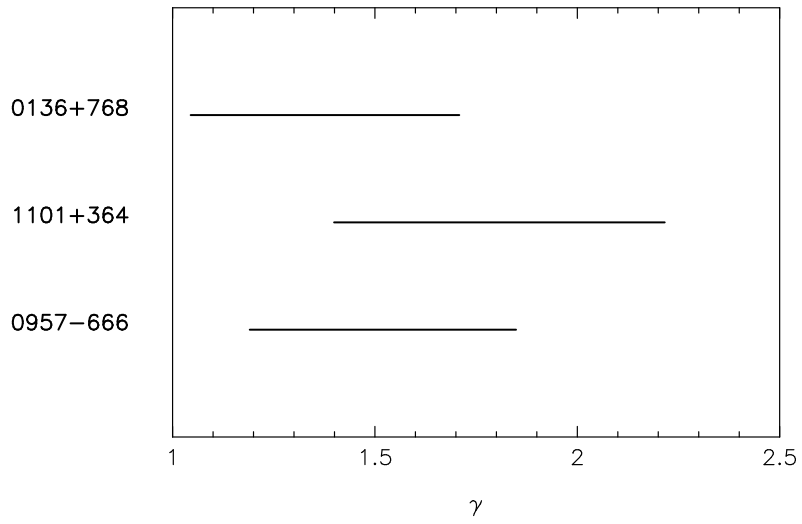

Figure 3.6: Derived range of possible values of γ, for the three double helium white dwarfs.

case of $\alpha\lambda$. It turns out that all three systems are consistent with a value of γ between $\sim$1.4 and $\sim$1.7 (Fig. 3.6).

Thus the mass transfer from a giant to a main-sequence star may in general either be stable (in the case where the giant still has a radiative, or at least not too deep convective envelope), unstable, leading to a spiral-in, or a process in which the envelope is lost without much of a spiral-in. Which systems do and which do not experience a spiral-in is related to the mass ratio of the components. As can be seen from Eq. (3.6) for systems with $\gamma \Delta M \approx M_{\rm i}\,(1+q)$ the periods already become very small and the effect is essentially the same as in the case of a spiral-in.

3.6 Formation of observed systems

From Figs. 3.2 and 3.4 it's clear that WD 0136+768, WD 0957-666 and WD 1101+364 could be formed with $\alpha\lambda$ below 0.8. However from Fig. 3.4 it looks like the extremely short-period system WD 0957-66 falls out of the sample in the sense that the other systems, as well as systems with unobserved companions, are compatible with a value of $\alpha\lambda \sim 2$.

3.6.1 Formation of helium white dwarf pairs

In Fig. 3.7 we show evolutionary scenarios for WD 0136+768 (left) and WD 1101+364 (middle) in which they consist of two helium white dwarfs. We included the effect of stellar winds which was not taken into account in the preceding discussion. Therefore

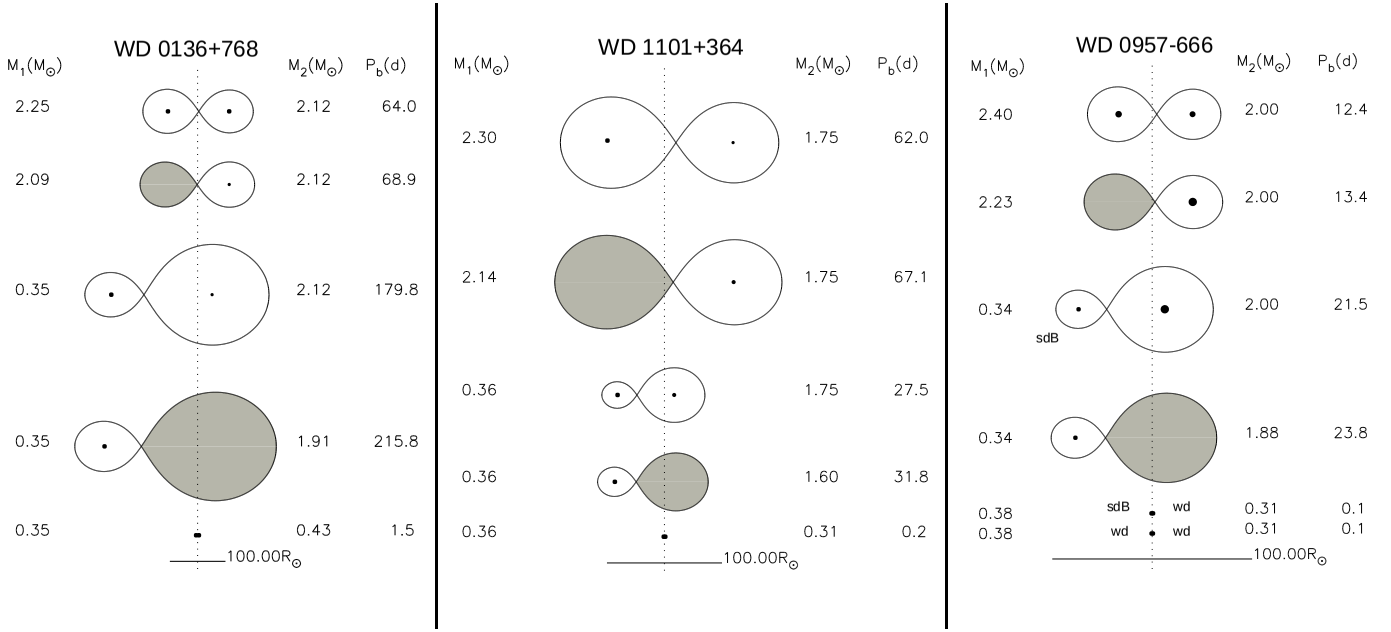

Figure 3.7: Evolutionary scenarios for the formation of WD 0136+768, WD 1101+364 and WD 0957-666 (left to right). In all scenario's the primaries lose their envelope after filling their Roche lobe, causing a change in the orbital period described by Eq. (3.6). Whether the orbit widens (WD 0136+768 and WD 0957-666) or shrinks (WD 1101+364) depends on the mass ratio. The second mass transfer always results in a spiral-in. For WD 0957-666 we present a scenario in which in the first mass transfer a helium star (sdB star) is formed which becomes a hybrid white dwarf only after the companion has become a helium white dwarf in the second phase of mass transfer.

we use slightly different values for γ (1.75 and 1.85 respectively) than the values derived in Fig. 3.6. The difference in the initial mass ratio of the components results in dramatically different orbital periods after the envelope of the primary is lost: almost tripling in the first case and decrease by half in the second. As a result, after the second mass transfer episode the second white dwarf is the more massive member of the pair in WD 0136+768 but the less massive in WD 1101+364. The large difference in periods and especially masses after the first phase of mass transfer, results in rather different final orbital periods.

For WD 0957-666 a scenario in which both components are helium white dwarfs can also be constructed but then one has to assume that $\alpha\lambda$ is atypically small. However we suggest a different scenario.

3.6.2 An alternative scenario for WD 0957-666: carbon-oxygen white dwarf with helium companion

There is another solution which allows us to explain the origin of WD 0957-666 using $\alpha\lambda \approx 2$ and $\gamma \approx 1.75$, like for the other two systems.

The mass of the observable white dwarf in WD 0957-666 system allows it to be a hybrid white dwarf (IBEN AND TUTUKOV 1985). Such white dwarfs descend from stars with initial mass 2.3 $M_\odot$ – 5 $M_\odot$, which fill their Roche lobes in the stage of hydrogen burning in a shell around a non-degenerate helium core, become hot subdwarfs in the core helium-burning stage, but don't experience envelope expansion after the formation of a degenerate carbon-oxygen core. Their masses are between 0.33 and 0.8 $M_\odot$. The formation of hybrid white dwarfs was considered in the study of the population of white dwarfs by TUTUKOV AND YUNGELSON (1992, see their scenario 3) and all their following studies.

In a scenario shown in Fig. 3.7 (right) we start with a system of 2.4 $M_\odot$ and 2.0 $M_\odot$ in a relatively close orbit ($a_0 \approx 37\,R_\odot$). At the instant of Roche-lobe overflow the primary has a deep convective envelope and we apply Eq. (3.6) to compute the change in the orbital period. The primary becomes a compact helium star. A peculiarity of low-mass helium stars is their long lifetime, $\sim 1.1 \times 10^7 M^{-3.75}$ yr for $0.33 \lesssim M/M_\odot \lesssim 0.7$ (POLS ET AL. 1991), comparable to the lifetime of their main-sequence progenitors. As a consequence, the initially slightly less massive secondary fills its Roche lobe and becomes a helium white dwarf while the former primary still burns helium in its core. For some 250 Myr the system could be observed as a hot subdwarf with a companion unseen due to the difference in luminosities. After core helium exhaustion the subdwarf cools and becomes a "hybrid" white dwarf. MORAN ET AL. (1997) estimate from its $T_{\rm eff}$ that the cooling age of this white dwarf is only $\sim 10^7$ yr and that the ratio of the luminosities of components is close to 5. This is compatible with the age of about 250 Myr expected in our scenario for the 0.31 $M_\odot$ companion.

3.7 Conclusion

We followed the binary evolution for three double helium white dwarfs backwards and came to the following conclusions.

1. The last phase of mass transfer (the primary has already become a white dwarf and the secondary fills its Roche lobe) was a spiral-in, for which we can constrain α, which describes the efficiency of orbital energy deposition into the common envelope, to lie between 1 and 6, assuming a structure parameter $\lambda = 0.5$. This efficiency value may be an overestimate since λ may increase towards 1 at the end of the first red giant stage. Our result is in agreement with values of $\alpha \sim 4$ found in population synthesis studies of low-mass X-ray binaries (TAURIS 1996), double neutron stars (PORTEGIES ZWART AND YUNGELSON 1998) and double white dwarfs (Chapter 4).

2. The parameters of all observed double helium white dwarfs may be reproduced with the same $\alpha\lambda \approx 2$.

3. WD 0957-666 is the only system for which $\alpha\lambda$ appears to be lower if both components are helium dwarfs. However, this system might have been formed with $\alpha\lambda \approx 2$ if the immediate precursor of the currently observed white dwarf was a non-degenerate helium star and now it is a hybrid white dwarf.

4. In order to explain the relatively high masses of the observed white dwarfs in close pairs, their direct progenitors (i.e. white dwarf + giant binaries) must have had relatively wide orbits (between 25 and >500 days). The standard cases of mass transfer (Algol evolution and spiral-in) applied to the first phase of mass transfer, can not explain these intermediate wide orbits. Only if the masses of the observed white dwarfs are (much) lower than the current estimates (i.e. below 0.3 $M_\odot$) they could be formed through a phase of stable mass transfer.

5. We suggest that in the first mass transfer phase for low-mass binaries with similar masses of the two stars, most of the mass of the envelope of the evolved star is lost without a significant spiral-in. This suggestion is supported by the fact that the original reasoning for spiral-in (drag forces in the envelope) is not applicable here, because the envelope can easily been spun up to corotate with the binary.

   In the absence of a physical picture for the removal of the envelope, we introduce a simple parameter $\gamma = (\Delta J/\Delta M_{\rm tot})\ (M_{\rm tot}/J)$ to describe the loss of the angular momentum of the system as in the early work of PACZYŃSKI AND ZIOŁKOWSKI (1967). Our analysis of the observed parameters for all observed double helium white dwarfs shows that the material of the envelope of the giant is expelled with 1.4 to 1.7 times the specific angular momentum of the initial binary. The details of this kind of mass transfer should be investigated using 3D gas-dynamical calculations, which are becoming available (e.g. BISIKALO ET AL. 1998), but are not yet accurate enough to make predictions.

6. With some well-constrained assumptions for the masses of the unseen companions in the other eight double white dwarfs, we find similar results as for the double white dwarfs with two helium components.

Acknowledgements. We are indebted to A. Fedorova for making some trial computations of stellar evolution upon our request and to the referee for very useful remarks. LRY acknowledges warm hospitality of the Astronomical Institute "Anton Pannekoek". This work was supported by NWO Spinoza grant 08-0 to E. P. J. van den Heuvel, RFBR grant 99-02-16037, Russian Federal Program 'Astronomy' and by NASA through Hubble Fellowship grant HF-01112.01-98A awarded (to SPZ) by the Space Telescope Science Institute, which is operated by the Association of Universities for Research in Astronomy, Inc., for NASA under contract NAS 5-26555.

CHAPTER 4

Population synthesis for double white dwarfs I. Close detached systems

G. Nelemans, L. R. Yungelson, S. F. Portegies Zwart & F. Verbunt

Astronomy & Astrophysics, 2001, 365, 491 – 507

ABSTRACT

We model the population of double white dwarfs in the Galaxy and find a better agreement with observations compared to earlier studies, due to two modifications. The first is the treatment of the first phase of unstable mass transfer and the second the modelling of the cooling of the white dwarfs. A satisfactory agreement with observations of the local sample of white dwarfs is achieved if we assume that the initial binary fraction is $\sim$50 % and that the lowest mass white dwarfs ($M < 0.3\mathrm{M}_\odot$) cool faster than the most recently published cooling models predict.

With this model we find a Galactic birth rate of close double white dwarfs of 0.05 yr^{-1}, a birth rate of AM CVn systems of 0.005 yr^{-1}, a merger rate of pairs with a combined mass exceeding the Chandrasekhar limit (which may be progenitors of SNe Ia) of 0.003 yr^{-1} and a formation rate of planetary nebulae of 1 yr^{-1}. We estimate the total number of double white dwarfs in the Galaxy as 2.5×10^8. In an observable sample with a limiting magnitude $V_{\mathrm{lim}} = 15$ we predict the presence of $\sim$855 white dwarfs of which $\sim$220 are close pairs. Of these 10 are double CO white dwarfs of which one has a combined mass exceeding the Chandrasekhar limit and will merge within a Hubble time.

4.1 Introduction

Close double white dwarfs form an interesting population for a number of reasons. First they are binaries that have experienced at least two phases of mass transfer and thus provide good tests for theories of binary evolution. Second it has been argued that type Ia

supernovae arise from merging double CO white dwarfs (WEBBINK 1984; IBEN AND TUTUKOV 1984a). Thirdly close double white dwarfs may be the most important contributors to the gravitational wave signal at low frequencies, probably even producing an unresolved noise burying many underlying signals (EVANS ET AL. 1987; HILS ET AL. 1990). A fourth reason to study the population of double white dwarfs is that in combination with binary evolution theories, the recently developed detailed cooling models for (low-mass) white dwarfs can be tested.

The formation of the population of double white dwarfs has been studied analytically by IBEN AND TUTUKOV (1986b, 1987) and numerically by LIPUNOV AND POSTNOV (1988); TUTUKOV AND YUNGELSON (1992, 1994); YUNGELSON ET AL. (1994); HAN ET AL. (1995); IBEN ET AL. (1997, hereafter ITY97), and HAN (1998, hereafter HAN98). Comparison between these sudies gives insight in the differences that exist between the assumptions made in different synthesis calculations.

Following the discovery of the first close double white dwarf (SAFFER ET AL. 1988), the observed sample of such systems in which the mass of at least one component is measured has increased to 14 (MAXTED AND MARSH 1999; MAXTED ET AL. 2000). This makes it possible to compare the models to the observations in more detail.

In this paper we present a new population synthesis for double white dwarfs, which is different from previous studies in three aspects. The first are some differences in the modelling of the binary evolution, in particular the description of a common envelope without spiral-in, in which the change in orbit is governed by conservation of angular momentum, rather than of energy (Sect. 4.2). The second new aspect is the use of detailed models for the cooling of white dwarfs (Sect. 4.4.3), which are important because it is the rate of cooling which to a large extent determines how long a white dwarf remains detectable in a magnitude-limited observed sample. The third new aspect is that we use different models of the star formation history (Sect. 4.5). Results are presented in Sect. 4.7 and discussed in Sect. 4.8. The conclusions are summarised in Sect. 4.9. In the Appendix some details of our population synthesis are described .

4.2 Binary and single-star evolution: the formation of double white dwarfs

The code we use is based on the code described by PORTEGIES ZWART AND VERBUNT (1996) and PORTEGIES ZWART AND YUNGELSON (1998), but has been modified in two respects: the white dwarf masses and the treatment of unstable mass transfer.

4.2.1 White dwarf masses

The masses of white dwarfs in binaries provide important observational constraints on evolution models. Therefore we have improved the treatment of the formation of white dwarfs in our binary evolution models by keeping more accurate track of the growth of the mass of the core. Details are given in Appendix 4.A.1.

4.2.2 Unstable mass transfer

There exist two "standard" scenarios for the formation of close double white dwarfs. In the first, the binary experiences two stages of unstable mass transfer in which a common envelope is formed. The change of the binary orbital separation in a common envelope is treated on the base of a balance between orbital energy and the binding energy of the envelope of the mass-losing star (PACZYŃSKI 1976; TUTUKOV AND YUNGELSON 1979a; WEBBINK 1984; IBEN AND LIVIO 1993). In the second scenario the first-born white dwarf of the pair is formed via stable mass transfer, like in Algol-type binaries (possibly accompanied by some loss of mass and angular momentum from the system) and the second white dwarf is formed via a common envelope.

Reconstruction of the evolution of three double helium white dwarfs with known masses of both components led us to the conclusion that a spiral-in could be avoided in the first phase of unstable mass transfer (Chapter 3). Briefly, when the mass ratio of two stars entering a common envelope is not too far from unity, we assume that the envelope of the evolving giant is ejected without a spiral-in, and that the change in orbital separation is governed by conservation of angular momentum (the equation used is given in Appendix 4.A.2). We parametrise the loss of angular momentum from the binary with a factor γ. If the mass ratio is more extreme, the common envelope leads to a spiral-in, which is governed by the conservation of energy (the equation used is given in Appendix 4.A.2). The efficiency with which the energy of the binary orbit is used to expell the envelope of the giant is parametrised by a factor $\alpha_{ce}\lambda$. We switch between the two descriptions at the mass ratio where both give the same change of the separation (roughly at 0.2). In Chapter 3 we find that values of $\gamma \approx 1.75$ and $\alpha_{ce}\lambda = 2$ give the best agreement of evolution models with the observed parameters of three binaries in which the masses of both white dwarfs are known, and therefore we use these values in our calculations.

Another novelty is what we suggest to call *"double spiral-in"* (see BROWN 1995). It describes the situation when the primary fills its Roche lobe at the time that its companion has also evolved off the main sequence. This kind of evolution can only take place when the initial mass ratio is close to unity. Such a mass transfer phase has hitherto been described with the standard common envelope formalism; in the same way as when the companion is still a main sequence star. However, if the companion is evolved, one might as well argue that the envelope of the smaller star becomes part of the common envelope, and the envelopes of *both* stars will be expelled. We propose to use the energy balance here, since the double core binary will in general not have enough angular momentum to force the envelope into co-rotation. An equation for the change in orbital separation in the case of a "double spiral-in" is derived in Appendix 4.A.2 exactly analogous to the usual common envelope formalism (e.g. WEBBINK 1984).

4.2.3 Examples

Before discussing effects that influence the double white dwarf population as a whole we discuss some typical examples of binary evolution leading to close double white dwarfs, to illustrate some of the assumptions used in our models. For details of the treatment of binary evolution we refer to PORTEGIES ZWART AND VERBUNT (1996) and the Appendix.

Double helium white dwarfs

The most common double white dwarfs consist of two helium white dwarfs (Sect. 4.7.1). These white dwarfs descend from systems in which both stars have $M \lesssim 2.3\,\mathrm{M}_\odot$ and fill their Roche lobes before He ignition in their degenerate cores. In Fig. 4.1 (top, page 42) we show an example of the formation of such a system. We start with a binary with an orbital period of 40 days and components of 1.4 and $1.1\,\mathrm{M}_\odot$. The primary fills its Roche lobe after 3 Gyrs, at which moment it has already evolved up the first giant branch and has lost $\sim 0.13\,\mathrm{M}_\odot$ in a stellar wind. When the star fills its Roche lobe it has a deep convective envelope, so the mass transfer is unstable. We apply the envelope ejection formalism to describe the mass transfer with a γ-value of 1.75 (see Eq. 4.A.20). The core of the donor becomes a $0.31\,\mathrm{M}_\odot$ helium white dwarf. The orbital period of the system hardly changes. After 4 Gyr, when the first formed white dwarf has already cooled to very low luminosity, the secondary fills its Roche lobe and has a deep convective envelope. Mass loss again proceeds on dynamical time-scale, but the mass ratio of the components is rather extreme and a common envelope is formed in which the orbit shrinks dramatically.

Double CO white dwarfs

Most double CO white dwarfs are formed in systems which are initially so wide that both mass transfer phases take place when the star is on the AGB and its core consists already of CO, such that a CO white dwarfs are formed directly. An example is shown in Fig. 4.1 (top, page 43). In the first phase of mass transfer the change of the orbital separation is regulated by the conservation of angular momentum during envelope ejection, according to equation [Eq. (4.A.20)], while in the second phase of mass transfer spiral-in is described by Eq. (4.A.18).

Much less frequently, CO white dwarfs are formed by stars more massive than $2.3\,\mathrm{M}_\odot$ which fill their Roche lobe when they have a nondegenerate core, before helium ignition. Roche-lobe overflow then results in the formation of a low-mass helium star. A brief additional phase of mass transfer may happen, if the helium star expands to giant dimensions during helium shell burning. This is the case for $0.8 \lesssim M_{\mathrm{He}}/\mathrm{M}_\odot \lesssim 3$ (see Appendix 4.A.1). After exhaustion of helium in its core, the helium star becomes a CO white dwarf.

CO white dwarfs with He companions

In Fig. 4.1 (bottom, page 42) we show an example in which the CO white dwarf is formed first. It starts with a more extreme mass ratio and a relatively wide orbit, which shrinks in a phase of envelope ejection. The secondary does not accrete anything and fills its Roche lobe when it ascends the first giant branch, having a degenerate helium core. It then evolves into a helium white dwarf.

In the second example (shown in Fig. 4.1; bottom, page 43), the system evolves through a stable mass exchange phase because the primary has a radiative envelope when it fills its Roche lobe. Part of the transferred mass is lost from the systems (see Appendix 4.A.2). The orbit widens and the primary forms a helium white dwarf when it has transferred all its envelope to its companion. The secondary accretes so much mass that it becomes too massive to form a helium white dwarf. The secondary fills its Roche lobe on the AGB to form a CO white dwarf in a common envelope in which the orbital separation reduces strongly. Because of the differential cooling (Sec. 4.4.3) the CO white dwarf, despite the fact that it is formed last, can become fainter than its helium companion. Since the probability to fill their Roche lobe when the star has a radiative envelope, is low for low-mass stars, the scenario in which the helium white dwarf is formed first is less likely (see Sect. 4.7).

4.3 A model for the current population of white dwarfs in the Galaxy

We model the current population of double and single white dwarfs in the Galaxy using population synthesis and compare our models with the observed populations. We initialise 250,000 "zero-age" binaries and evolve these binaries according to simplified prescriptions for single and binary-star evolution, including stellar wind, mass transfer (which may involve loss of mass and angular momentum from the binary), common envelopes and supernovae.

For each initial binary the mass $M_{\rm i}$ of the more massive component, the mass ratio $q_{\rm i} \equiv m_{\rm i}/M_{\rm i} \leq 1$, where $m_{\rm i}$ is the mass of the less massive component, the orbital separation $a_{\rm i}$ and eccentricity $e_{\rm i}$ are chosen randomly from distributions given by

$$\begin{aligned}
\mathrm{Prob}(M_{\rm i}) &= \mathrm{MS79} \quad \text{for} \quad 0.96\,\mathrm{M}_\odot \leq M_{\rm i} \leq 11\,\mathrm{M}_\odot, \\
\mathrm{Prob}(q_{\rm i}) &\propto \mathrm{const.} \quad \text{for} \quad 0 < q_{\rm i} \leq 1, \\
\mathrm{Prob}(a_{\rm i}) &\propto a_{\rm i}^{-1} \quad \text{for} \quad 0 \leq \log a_{\rm i}/\mathrm{R}_\odot \leq 6, \\
\mathrm{Prob}(e_{\rm i}) &\propto 2e_{\rm i} \quad \text{for} \quad 0 \leq e_{\rm i} \leq 1.
\end{aligned} \tag{4.1}$$

For the primary mass we use the approximation of EGGLETON ET AL. (1989) to the MILLER AND SCALO (1979) IMF indicated as MS79. A primary at the lower mass limit has a main sequence lifetime equal to our choice of the age of the Galactic disk (10 Gyr). The lower mass of less massive component is set to $0.08\,\mathrm{M}_\odot$, the minimum mass for

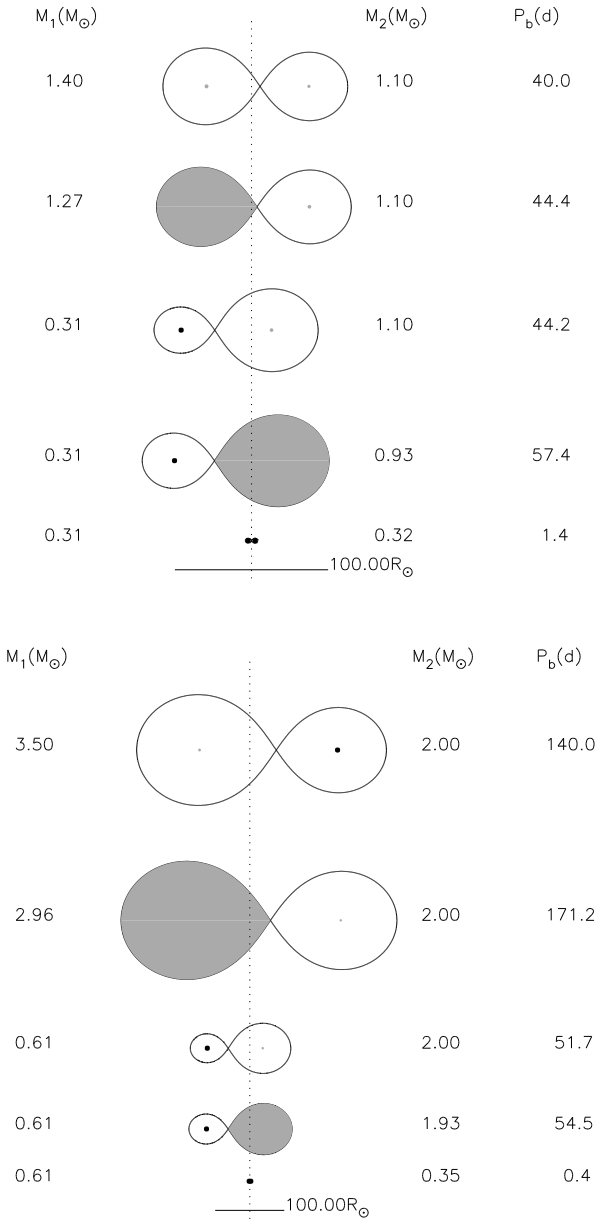

Figure 4.1: Evolutionary scenarios for the formation of a double helium white dwarf (top left), a double CO white dwarf (top right) and the CO+He and He+CO pairs (bottom ones).

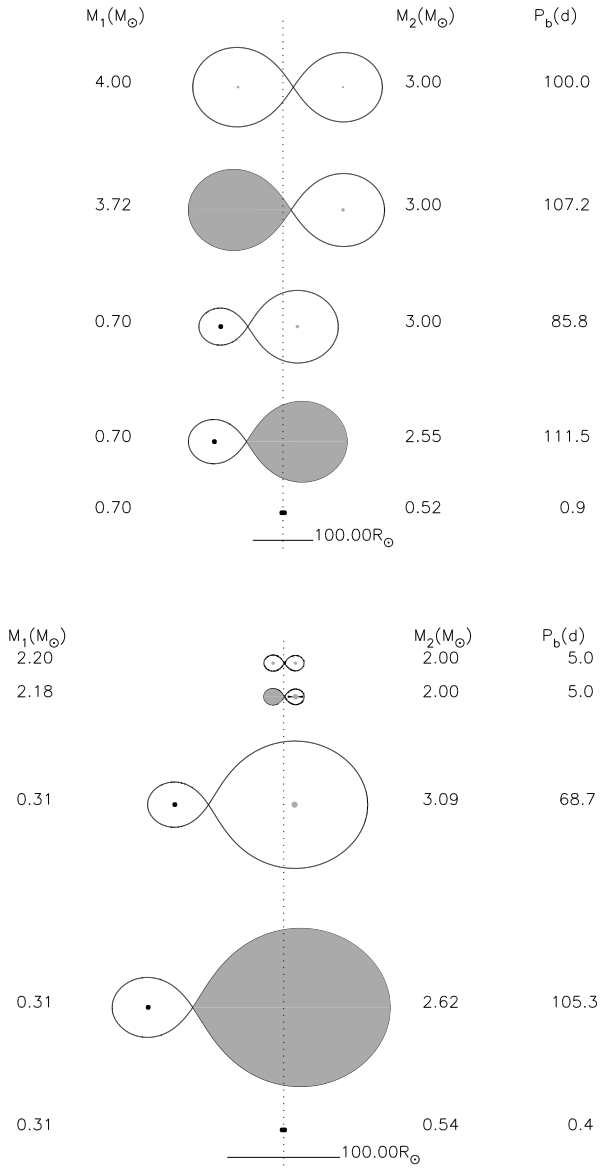

Figure 4.1(continued)
Note that the scales in the panels differ as indicated by the 100 $R_\odot$ rulers at the bottom. For a more detailed discussion see Sect. 4.2.3

TABLE 4.1: Models and their parameters. IMF is always according to MILLER AND SCALO (1979). The SFR is either exponentially decaying [Eq. (4.4)] or constant. The column "% binaries" gives the initial binary fraction in the population, the column "cooling" gives the cooling model (see Sect. 4.4.3).

Model	SFH	% binaries	cooling
A1	Exp	50	DSBH98
A2	Exp	50	Modified DSBH98
A3	Exp	50	100 Myr
B	Exp	100	Modified DSBH98
C	Cnst	50	Modified DSBH98
D	Cnst	100	Modified DSBH98

hydrogen core burning. The distribution over separation is truncated at the lower end by the separation at which the ZAMS binary would be semi-detached.

To investigate the effects of different cooling models (Sect. 4.4.3) and different assumptions about the star formation history (Sect. 4.5) different models have been computed (Table 4.1).

4.4 Modelling the observable population: white dwarf cooling

To model the observable population we have to take orbital evolution and selection effects into account.

4.4.1 Orbital evolution of double white dwarfs

The most important effect of orbital evolution, which is taken into account also in all previous studies of close binary white dwarfs, is the disappearance from the sample of the tightest systems as they merge, due to the loss of angular momentum via gravitational wave radiation. For example an $0.6\,M_\odot + 0.6\,M_\odot$ white dwarf pair with orbital period of 1 hour merges in 3×10^7 yr. If it is located at a distance of 100 pc from the Sun it will disappear abruptly from a magnitude limited sample by merging [1] before the white dwarfs have become undetectable due to cooling.

[1] Note, however, that just before merging white dwarfs may become quite bright due to tidal heating (IBEN ET AL. 1998).

4.4.2 Selection effects

The observed double white dwarfs are a biased sample. First, they were mainly selected for study because of their supposed low mass, since this is a clear indication of binarity (SAFFER ET AL. 1988; MARSH ET AL. 1995). Secondly, for the mass determinations and the measurement of the radial velocities the white dwarfs must be sufficiently bright. A third requirement is that the radial velocities must be large enough that they can be found, but small enough that spectral lines don't get smeared out during the integration. MAXTED AND MARSH (1999) discuss this last requirement in detail. Following them, we include a detection probability in the model assuming that double white dwarfs in the orbital period range between 0.15 hr and 8.5 day will be detected with 100% probability and that above 8.5 day the detection probability decreases linearly from 1 at 8.5 days to 0 at $\sim$35 days (see Fig. 1 in MAXTED AND MARSH 1999).

The second selection effect is related to the brightness of the white dwarfs, which is governed by their cooling curves.

4.4.3 White dwarf cooling

IBEN AND TUTUKOV (1985) noticed that for a $0.6\,M_{\odot}$ white dwarf the maximum probability of discovery corresponds to a cooling age of $\sim 10^8$ yr. In absence of detailed cooling curves for low-mass white dwarfs, it was hitherto assumed in population synthesis studies that white dwarfs remain bright enough to be observed during 10^8 yr, irrespective of their mass. However, recent computations (BLÖCKER 1995; DRIEBE ET AL. 1998, hereafter DSBH98; HANSEN 1999) indicate that helium white dwarfs cool more slowly than CO white dwarfs, for two reasons. First, helium cores contain a higher number of ions than carbon-oxygen cores of the same mass, they store more heat and are brighter at the same age (HANSEN 1999). Second, if the mass of the hydrogen envelope of the white dwarf exceeds a critical value, pp-reactions remain the main source of energy down to effective temperatures well below 10^4 K (WEBBINK 1975; DSBH98; SARNA ET AL. 2000). This residual burning may lead to a significant slow-down of the cooling.

White dwarfs in close binaries form when the evolution of (sub)giants with degenerate cores and hydrogen-rich envelopes is terminated by Roche-lobe overflow. The amount of hydrogen that is left on the white dwarf depends on the details of this process. Fully fledged evolutionary calculations of the formation of helium white dwarfs, (e.g GIANNONE AND GIANNUZZI 1970; SARNA ET AL. 2000), as well as calculations that mimic Roche-lobe overflow by mass loss at fixed constant rate (DRIEBE ET AL. 1998), find that the thickness of the residual envelope around the white dwarf is increasing with decreasing white dwarf mass. As a result the brightness at fixed age decreases monotonically with increasing white dwarf mass (see also Fig. 4.A.2).

However, it is not clear that these calculations are valid for white dwarfs formed in a common envelope. In addition, white dwarfs may lose mass by stellar wind when they still have a high luminosity. Such winds are observed for nuclei of planetary nebulae and post-novae and could also be expected for He white dwarfs. Finally, white dwarfs

with masses between $\sim$0.2 and $\sim$0.3 $M_\odot$ experience thermal flashes (KIPPENHAHN ET AL. 1968; WEBBINK 1975; IBEN AND TUTUKOV 1986a; DRIEBE ET AL. 1999; SARNA ET AL. 2000), in which the envelopes expand. This may lead to additional mass loss in a temporary common envelope, especially in the closest systems with separations $\lesssim 1\,R_\odot$. Mass loss may result in extinguishing of hydrogen burning (IBEN AND TUTUKOV 1986a; SARNA ET AL. 2000).

HANSEN (1999) argues that the details of the loss of the hydrogen envelope are very uncertain and assumes that all white dwarfs have a hydrogen envelope of the same mass. He finds that helium white dwarfs cool slower than the CO white dwarfs, but inside these groups, the more massive white dwarfs cool the slowest. The difference within the groups are small.

We conclude that the cooling models are still quite uncertain, so we will investigate the result of assuming different cooling models in our population synthesis.

The first model we compute (A1; see Table 4.1 for a list of all computed models) uses the cooling curves as given by BLÖCKER (1995) for CO white dwarfs and DSBH98 for He white dwarfs as detailed in Appendix 4.A.1. For the second model (A2) we made a crude estimate of the cooling curves for the case that the thermal flashes or a stellar wind reduce the mass of the hydrogen envelope and terminate the residual burning of hydrogen. We apply this to white dwarfs with masses below 0.3 $M_\odot$, and model all these white dwarfs identically and simply with cooling curves for a more massive (faster cooling) white dwarf of 0.46 $M_\odot$. To compare with the previous investigators, we include one model (A3) in which all white dwarfs can be seen for 100 Myrs. We did not model the cooling curves of HANSEN (1999), because no data for $L > 0.01 L_\odot$ are given.

4.4.4 Magnitude limited samples and local space densities

To convert the total Galactic population to a local population and to compute a magnitude limited sample, we assume a distribution of all single and binary stars in the Galactic disk of the form

$$\rho(R,z) = \rho_0\, e^{-R/H}\, \mathrm{sech}(z/\beta)^2 \quad \mathrm{pc}^{-3}, \tag{4.2}$$

where we use H = 2.5 kpc (SACKETT 1997) and β = 200 pc, neglecting the age and mass dependence of β.

To construct a magnitude limited sample, we compute the magnitude for all model systems from the cooling curves and estimate the contribution of each model system from Eq. (4.2). The absolute visual magnitudes along the cooling curves are derived using bolometric corrections after EGGLETON ET AL. (1989).

From Eq. (4.2) the local (R = 8.5 kpc, z = 30 pc) space density ($\rho_{i,\odot}$) of any type of system is related to the total number in the Galaxy (N_i) by:

$$\rho_{i,\odot} = N_i/4.8 \times 10^{11} \quad \mathrm{pc}^{-3}. \tag{4.3}$$

4.5 Star formation history

Some progenitors of white dwarfs are formed long ago. Therefore the history of star formation in the Galaxy affects the contribution of old stars to the population of local white dwarfs. To study this we compute different models.

For models A and B (see Table 4.1), we model the star formation history of the Galactic disk as

$$\mathrm{SFR}(t) = 15\ \exp(-t/\tau) \quad \mathrm{M}_\odot\ \mathrm{yr}^{-1}, \tag{4.4}$$

where $\tau = 7$ Gyr. It gives a current rate of $3.6\,\mathrm{M}_\odot\ \mathrm{yr}^{-1}$ which is compatible with observational estimates (RANA 1991; VAN DEN HOEK AND DE JONG 1997). The integrated SFR, i.e. the amount of matter that has been turned into stars over the whole history of the Galactic disk (10 Gyr) with this equation is $\sim 8 \times 10^{10}\ \mathrm{M}_\odot$ which is higher than the current mass of the disk, since part of the gas that is turned into stars is given back to the ISM by supernovae and stellar winds.

For models C and D we use a constant SFR of $4\,\mathrm{M}_\odot\ \mathrm{yr}^{-1}$ (as TUTUKOV AND YUNGELSON 1992). We use an age of the disk of 10 Gyr, while TUTUKOV AND YUNGELSON (1992) use 15 Gyr. Model D also allows us to compare our results with previous studies (ITY97 and HAN98; see Sect. 4.8).

Most binary population synthesis calculations take a binary fraction of 100%. Since we want to compare our models with the observed fraction of close double white dwarfs among all white dwarfs, we present models with 100% binaries (models B and D); and with 50% binaries and 50% single stars, i.e. with 2/3 of all stars in binaries (models A and C).

4.6 Observed sample of double white dwarfs

The properties of the observed double white dwarfs with which we will compare our models are summarised in Table 4.2. Only WD 1204+450 and WD 1704+481 are likely to contain CO white dwarfs, having components with masses higher than $0.46\,\mathrm{M}_\odot$, the limiting mass to form a helium white dwarf (SWEIGART ET AL. 1990). The remaining systems are probably helium white dwarfs. In principle in the mass range $M \simeq 0.35 - 0.45\,\mathrm{M}_\odot$ white dwarfs could also be hybrid. However in this range the probability for a white dwarf to be hybrid is 4 – 5 times lower than to be a helium white dwarf, because hybrid white dwarfs originate from more massive stars which fill their Roche lobe in a narrow period range (see, however, an example of such a scenario for WD 0957-666 in Chapter 3). We assume $0.05\,\mathrm{M}_\odot$ for the uncertainty in the estimates of the masses of white dwarfs, which may be somewhat optimistic.

Table 4.2 also includes data on subdwarf B stars with suspected white dwarf companions. Subdwarf B (sdB) stars are hot, helium rich objects which are thought to be helium burning remnants of stars which lost their hydrogen envelope. When their helium burning has stopped they will become white dwarfs. Of special interest are KPD 0422+5421 (KOEN ET AL. 1998; OROSZ AND WADE 1999) and KPD1930+2752

TABLE 4.2: Parameters of known close double white dwarfs (first 14 entries) and subdwarfs with white dwarf companions. *m* denotes the mass of the visible white dwarf or subdwarf. The mass ratio *q* is defined as the mass of the brighter star of the pair over the mass of the companion. For references see MAXTED AND MARSH (1999); MORAN ET AL. (1999); MARSH (2000); and MAXTED ET AL. (2000). The mass of 0136+768 is corrected for a misprint in MAXTED AND MARSH (1999), for 0135+052 the new mass given in BERGERON ET AL. (1997) is taken. Data for the sdB star KPD 0422+5421 are from OROSZ AND WADE (1999) and for KPD 1930+2752 from MAXTED ET AL. (2000). The remaining sdB stars do not have reliable mass estimates.

WD	*P*(d)	q	m	sdB	*P*(d)	q	m
0135–052	1.556	0.90	0.25	KPD 0422+5421	0.090	0.96	0.51
0136+768	1.407	1.31	0.44	KPD 1930+2752	0.095	0.52	0.5
0957–666	0.061	1.14	0.37	0101+039	0.570		
1022+050	1.157		0.35	0940+068	8.33		
1101+364	0.145	0.87	0.31	1101+249	0.354		
1202+608	1.493		0.40	1432+159	0.225		
1204+450	1.603	1.00	0.51	1538+269	2.50		
1241–010	3.347		0.31	2345+318	0.241		
1317+453	4.872		0.33				
1704+481A	0.145	0.7	0.39				
1713+332	1.123		0.38				
1824+040	6.266		0.39				
2032+188	5.084		0.36				
2331+290	0.167		0.39				

(MAXTED ET AL. 2000). With orbital periods as short as 0.09 and 0.095 days, respectively, their components will inevitably merge. In both systems the sdB components will become white dwarfs before the stars merge. In KPD1930+2752 the total mass of the components is close to the Chandrasekhar mass or even exceeds it. That makes this system the only currently known candidate progenitor for a SN Ia.

TABLE 4.3: Birth and event rates and numbers for the different models. All birth and event rates (ν) are in units of yr^{-1} in the Galaxy. All numbers (#) are total numbers in the Galaxy. Close double white dwarfs are represented with (wd, wd). See Sect. 4.7.1 for a discussion of these rates. For comparison (in Sect. 4.8.1) we also include numbers computed by the code from ITY97 but using an age of the Galactic disk of 10 Gyr instead of the 15 Gyr used by ITY97; and numbers of model 1 of HAN98.

Model	SFH	% bin	$\nu_{(wd,wd)}$ (10^{-2})	ν_{merge} (10^{-2})	SN Ia (10^{-3})	ν_{AMCVn} (10^{-3})	#(wd, wd) (10^{8})
A	Exp	50	4.8	2.2	3.2	4.6	2.5
B	Exp	100	8.1	3.6	5.4	7.8	4.1
C	Cnst	50	3.2	1.6	3.4	3.1	1.2
D	Cnst	100	5.3	2.8	5.8	5.2	1.9
ITY97[1]	Cnst	100	8.7	2.4	2.7	12.0	3.5
HAN98[1]	Cnst	100	3.2	3.1	2.9	26	1.0

[1] Note that ITY97 and HAN98 used a normalisation that is higher than we use for model D by factors $\sim$1.4 and $\sim$1.1 respectively (see Sect. 4.8.1).

4.7 Results

Our results are presented in the next subsections. In Sect. 4.7.1 we give the birth rates and total number of double white dwarfs in the Galaxy. These numbers allow a detailed comparison with results of earlier studies, which we defer to Sect. 4.8. They cannot be compared with observations directly, with the exception of the type Ia supernova (SN Ia) rate. For comparison with the observed sample, described in Sect. 4.6, we compute magnitude limited samples in the remaining sections. In Sect. 4.7.2 the distribution over periods and masses is compared with the observations, which constrains the cooling models. Comparison of the mass ratio distribution with the observations gives further support for our new description of a common envelope without spiral-in (Sect. 4.7.3). In Sect. 4.7.4 we compare our model with the total population of single and binary white dwarfs and in Sect. 4.7.5 we compare models that differ in the assumed star formation history with the observed rate of planetary nebula (PN) formation and the local space density of white dwarfs.

4.7.1 Birth rates and numbers

In Table 4.3 the birth rates for all models are given. According to Eq. (4.1) the mass of a binary is on average 1.5 times the mass of a single star. For each binary in models A and C we also form a single star, i.e. per binary a total of 2.5 times the mass of a single star is formed (1.5 for the binary, 1 for the single star). For models B and D only 1.5 times the mass of a single star is formed per binary. Thus for the same SFR in $M_{\odot}yr^{-1}$ the

frequency of each process involving a binary of the models A and C is 0.6 times that in models B and D.

For model A the current birth rate for close double white dwarfs is 4.8×10^{-2} yr^{-1} in the Galaxy. The expected total population of close binary white dwarfs in the Galactic disk is $\sim 2.5 \times 10^{8}$ (see Table 4.3).

The double white dwarfs are of the following types: 53% contains two helium white dwarfs; 25% two CO white dwarfs; in 14% a CO white dwarf is formed first and a helium white dwarf later and in 6% a helium white dwarf is formed followed by the formation of a CO white dwarf. The remaining 1% of the double white dwarfs contains an ONeMg white dwarf. The CO white dwarfs can be so called hybrid white dwarfs; having CO cores and thick helium envelopes (IBEN AND TUTUKOV 1985, 1987). Of the double CO white dwarfs, 6% contains one and 5% two hybrid white dwarfs. In the mixed pairs the CO white dwarf is a hybrid in 20% of the cases.

Forty eight percent of all systems are close enough to be brought into contact within a Hubble time. Most are expected to merge. The estimated current merger rate of white dwarfs is 2.2×10^{-2} yr^{-1}. The current merger rate of pairs that have a total mass larger than the Chandrasekhar limit ($M_{\rm Ch} = 1.44\,{\rm M}_{\odot}$) is 3.2×10^{-3} yr^{-1}. Since the merging of binary CO white dwarfs with a combined mass in excess of $M_{\rm Ch}$ is a viable model for type Ia SNe (see LIVIO 1999, for the most recent review), our model rate can be compared with the SN Ia rate of $\sim (4 \pm 1) \times 10^{-3}$ yr^{-1} for Sbc type galaxies like our own (CAPPELLARO ET AL. 1999). In 19% of the systems that come into contact the ensuing mass transfer is stable and an interacting double white dwarf (identified with AM CVn stars) is formed. The model birth rate of AM CVn systems is 4.9×10^{-3} yr^{-1} (see Table 4.3).

4.7.2 Period – mass distribution: constraints on cooling models

The observed quantities that are determined for all double white dwarfs are the orbital period and the mass of the brighter white dwarf. Following SAFFER ET AL. (1998), we plot in Fig. 4.2 (pages 52 and 53) the $P_{\rm orb} - m$ distributions of the frequency of occurrence for the white dwarfs which are born at this moment and for the simulated magnitude limited sample for the models with different cooling prescriptions, (models A1, A2 and A3; see Table 4.1), where we assume $V_{\rm lim} = 15$ as the limiting magnitude of the sample[2]. For m we always use the mass of the brighter white dwarf. In general the brighter white dwarf is the one that was formed last, but occasionally, it is the one that was formed first as explained in Sect. 4.2.3. For comparison, we also plot the observed binary white dwarfs in Fig. 4.2.

There is a clear correlation between the mass of new-born low-mass (He) white dwarf and the orbital period of the pair. This can be understood as a consequence of the existence of a steep core mass – radius relation for giants with degenerate helium cores (REFSDAL AND WEIGERT 1970). Giants with more massive cores (forming more

[2]The $P-m$ distribution does not qualitatively change if we increase $V_{\rm lim}$ by one or two magnitudes, since we still deal with very nearby objects.

TABLE 4.4: Number of observable white dwarfs, close double white dwarfs and SN Ia progenitors as function of the limiting magnitude of the sample for model A2.

$V_{\rm lim}$	#wd	#wdwd	#SN Ia prog
15.0	855	220	0.9
15.5	1789	421	1.7
16.0	3661	789	3.2
17.0	12155	2551	11.2

massive white dwarfs) have much larger radii and thus smaller binding energies. To expel the envelope in the common envelope, less orbital energy has to be used, leading to a larger orbital period. The spread in the distribution is caused by the difference in the masses of the progenitors and different companion masses.

In the simulated population of binary white dwarfs there are three distinct groups of stars: He dwarfs with masses below $0.45\,M_\odot$, hybrid white dwarfs with masses in majority between 0.4 and 0.5 $M_\odot$ and periods around a few hours, and CO ones with masses above $0.5\,M_\odot$. The last groups are clearly dominated by the lowest mass objects. The lowest mass CO white dwarfs are descendants of most numerous initial binaries with masses of components $1 - 2\,M_\odot$.

The different cooling models result in very different predicted observable distributions. Model A1 where the cooling curves of DSBH98 are applied favours low-mass white dwarfs to such an extent that almost all observed white dwarfs are expected to have masses below $0.3\,M_\odot$. This is in clear contrast with the observations, in which all but one white dwarf have a mass above $0.3\,M_\odot$. Reduced cooling times for white dwarfs with masses below $0.3\,M_\odot$ (model A2) improves this situation. Model A3, with a constant cooling time (so essentially only affected by merging due to GWR), seems to fit all observed systems also nicely. However, a complementary comparison with the observations as given by cumulative distributions of the periods (Fig. 4.3, page 54), shows that model A2 fits the data best, and that model A3 predicts too many short period systems.

The observed period distribution for double white dwarfs shows a gap between 0.5 and 1 day, which is not present in our models. If we include also sdB binaries, the gap is partially filled in. More systems must be found to determine whether the gap is real.

The comparison of our models with observations suggests that white dwarfs with masses below $0.3\,M_\odot$ cool faster than predicted by DSBH98. Mass loss in thermal flashes and a stellar wind may be the cause of this.

The model sample of detectable systems is totally dominated by He white dwarfs with long cooling times. Given our model birth rates and the cooling curves we apply, we estimate the number of double white dwarfs to be detected in a sample limited by $V_{\rm lim} = 15$ as 220 of which only 10 are CO white dwarfs for model A2. Roughly one of these is expected to merge within a Hubble time having a total mass above $M_{\rm Ch}$. For future observations we give in Table 4.4 a list of expected number of systems for different limiting magnitudes.

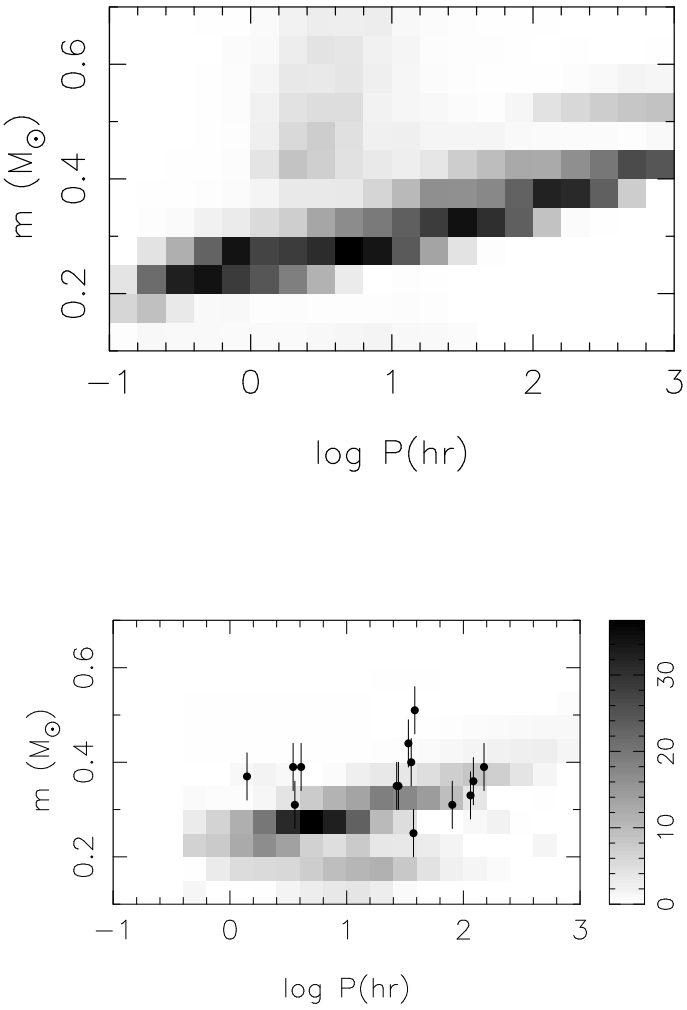

Figure 4.2: Model population of double white dwarfs as function of orbital period and mass of the brighter white dwarf of the pair. Top: distribution of the double white dwarfs that are currently born for models A. This is independent of cooling. In the remaining three plots we show the currently visible population of double white dwarfs for different cooling models: (bottom) cooling according to DSBH98 and BLÖCKER (1995, model A1);

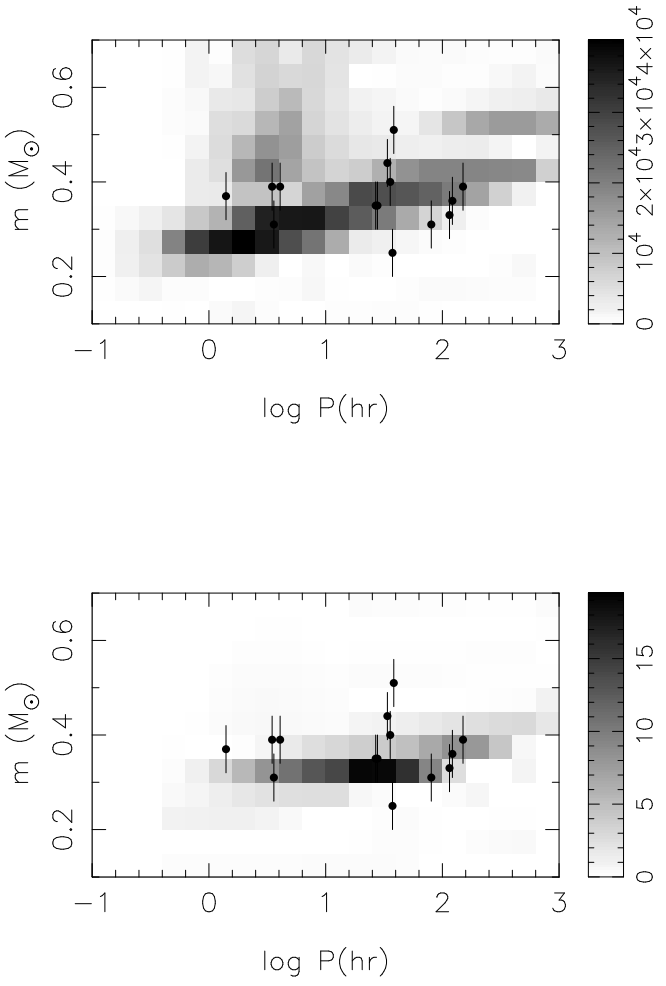

Figure 4.2 (continued)
(bottom) cooling according to DSBH98, but with faster cooling for WD with masses below $0.3\,M_{\odot}$ (model A2). Both plots are for a limiting magnitude $V_{\rm lim}$ = 15; (top) with constant cooling time of 100 Myr (model A3, note that in this case we only obtain the *total number of potentially visible double white dwarfs in the Galaxy* and we can not construct a magnitude limited sample). For comparison, we also plot the observed binary white dwarfs.

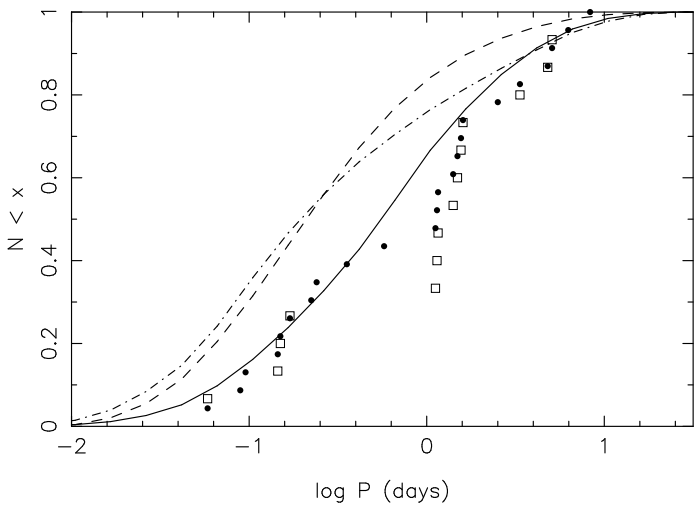

Figure 4.3: Cumulative distribution of periods. Solid line for our best model (A2); DSBH98 cooling, but with lower luminosity due to thermal flashes for white dwarfs with masses below $0.3\,M_{\odot}$. Dashed line for DSBH98 without modifications (model A1) and dash dotted line for constant cooling time of 100 Myr (model A3). Open squares for the observed double white dwarfs, filled circles give the observed systems including the sdB binaries (Table 4.2).

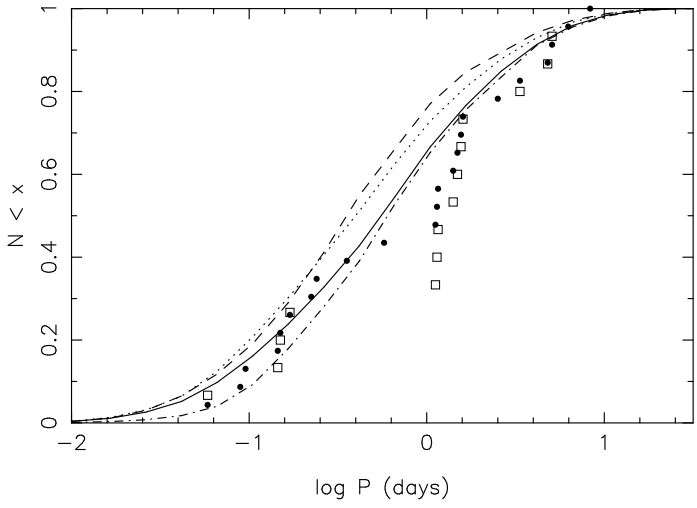

Figure 4.4: Cumulative distribution of periods. Solid line for model A2 as in Fig. 4.3, dashed line for the same model but with $\alpha_{ce}\lambda = 1$, dash-dotted line for a model with $\gamma = 1.5$ and finally the dotted line for model C (constant SFR).

It should be noted that these numbers are uncertain. This is illustrated by the range in birth rates for the different models (Table 4.3) and by the differences with previous studies (see Sect. 4.8.1). Additional uncertainties are introduced by our limited knowledge of the initial distributions [Eq. (4.1)] and the uncertainties in the cooling and the Galactic model [Eq. (4.2)]. For example YUNGELSON ET AL. (1994) compare models with two different q_i distributions (one peaked towards $q_i \sim 1$) and show that the birth rates differ by a factor ~ 1.7. In general the relative statistics of the model are more reliable than the absolute statistics.

Before turning to the mass ratio distribution, we illustrate the influence of the model parameters we choose. We do this by showing cumulative period distributions for some models with different parameters in Fig. 4.4; $\alpha_{ce}\lambda = 1$ (dashed line) and $\gamma = 1.5$ (dash-dotted line). It shows that the change in parameters influences the distributions less than the different cooling models discussed above, although the observations favour a higher $\alpha_{ce}\lambda$. We also included the cumulative distribution for model C (with a constant SFR; dotted line) which differs from that for model A2 in that it has fewer long period systems. This is a consequence of the larger relative importance of old, low-mass progenitor binaries in model A2, which lose less mass and thus shrink less in the first phase of mass transfer (see Eq. 4.A.20).

4.7.3 Period – mass ratio distribution

Our assumption that a common envelope can be avoided in the first phase of mass transfer between a giant and a main-sequence star, is reflected in the mass ratios of the model systems. A clear prediction of the model is that close binary white dwarfs must concentrate to $q = m/M \sim 1$. For the observed systems, the mass ratio can only be determined if both components can be seen which in practice requires that the luminosity of the fainter component is more than 20% of that of the brighter component (MORAN ET AL. 2000). Applying this selection criterium to the theoretical model, we obtain the distribution shown in Fig. 4.5 for the magnitude limited sample. Note that since lower mass white dwarfs cool slower this selection criterium favours systems with mass ratios above unity. In the same figure we also show the observed systems.

For comparison we also computed a run (A′) in which we used the standard common envelope treatment for the first phase of mass transfer, which is done by ITY97 and HAN98. The fraction of double white dwarfs for which the mass ratio can be determined according to the selection criterium of a luminosity ratio greater than 0.2, is 27% for model A2 and 24% for model A′. In a total of 14 systems one thus expects 4 ± 2 and 3 ± 2 systems of which the mass ratio can be determined. Model A2 fits this number better, but the numbers are too small to draw conclusions. The distribution of mass ratios in model A′ (Fig. 4.5, bottom) however clearly does not describe the observations as well as our model A2, as illustrated in more detail in a plot where the cumulative mass ratio distributions of the two models and the observations are shown (Fig. 4.6).

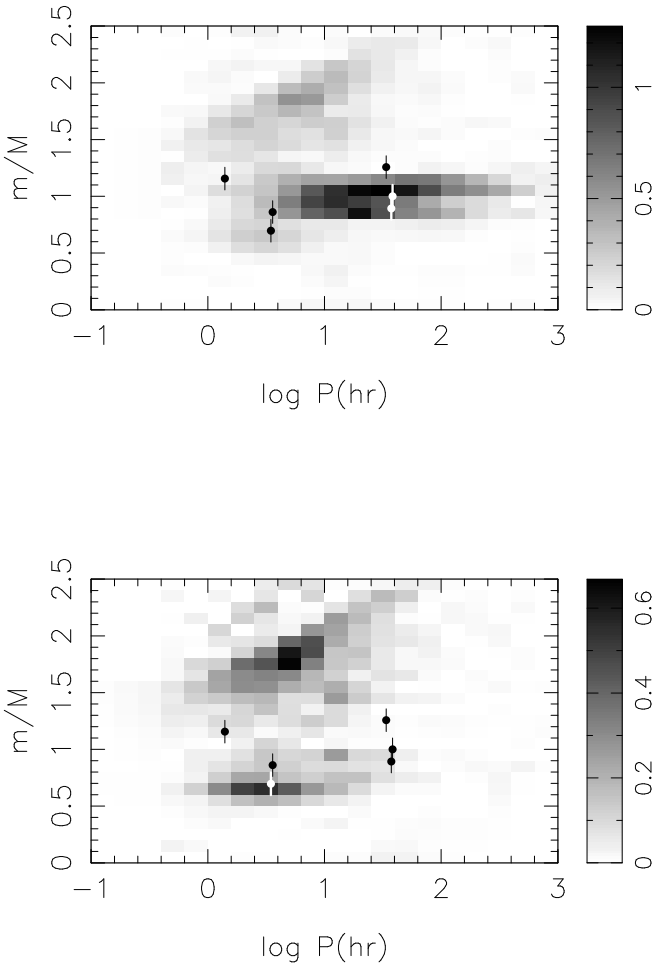

Figure 4.5: **Top:** current population of double white dwarfs as function of orbital period and mass ratio, for model A2, a limiting magnitude of 15 and a maximal ratio of luminosities of 5. **Bottom:** the same for a run in which the first phase of mass transfer is treated as a standard common envelope, as is done by ITY97 and HAN98. For comparison, we also plot the observed binary white dwarfs.

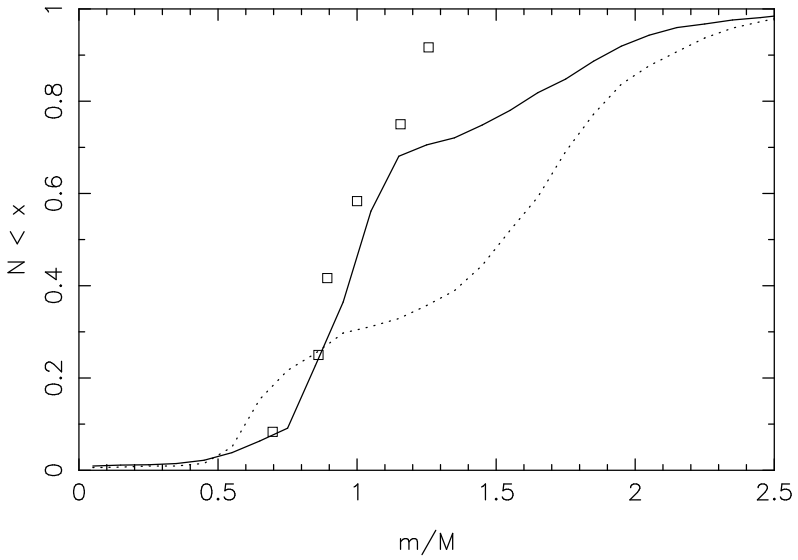

Figure 4.6: Cumulative mass ratio distributions for the models A2 (solid line) and A′ (dotted line) as explained in Sect. 4.7.3. The observed mass ratio's are plotted as the open squares.

4.7.4 Mass spectrum of the white dwarf population: constraints on the binary fraction

Figs. 4.7 and 4.8 show the model spectrum of white dwarf masses for models B and A2, including both single and double white dwarfs for a limiting magnitude $V_{\rm lim}$ = 15. For this plot we consider as "single" white dwarfs all objects that were born in initially wide pairs, single merger products, white dwarfs that became single as a result of binary disruption by SN explosions, white dwarfs in close pairs which are brighter than their main-sequence companions and genuine single white dwarfs for the models with an initial binary fraction smaller than 100%.

These model spectra can be compared to the observed mass spectrum of DA white dwarfs studied by BERGERON ET AL. (1992) and BRAGAGLIA ET AL. (1995), shown in Fig. 4.9. The latter distribution may have to be shifted to higher masses by about 0.05 $M_{\odot}$, if one uses models of white dwarfs with thick hydrogen envelopes for mass estimates (NAPIWOTZKI ET AL. 1999). Clearly, a binary fraction of 50% fits the observed sample better, if indeed helium white dwarfs cool much slower than CO white dwarfs. We can also compare the absolute numbers. MAXTED AND MARSH (1999) conclude that the fraction of close double white dwarfs among DA white dwarfs is between 1.7 and 19 % with 95% confidence. For model B the fraction of close white dwarfs is ∼43% (853 white dwarfs of which 368 are close pairs), for model A2 is is ∼26% (855 white dwarfs and 220 close pairs). Note that this fraction slightly decreases for higher limiting magnitudes because the single white dwarfs are more massive and thus generally dimmer,

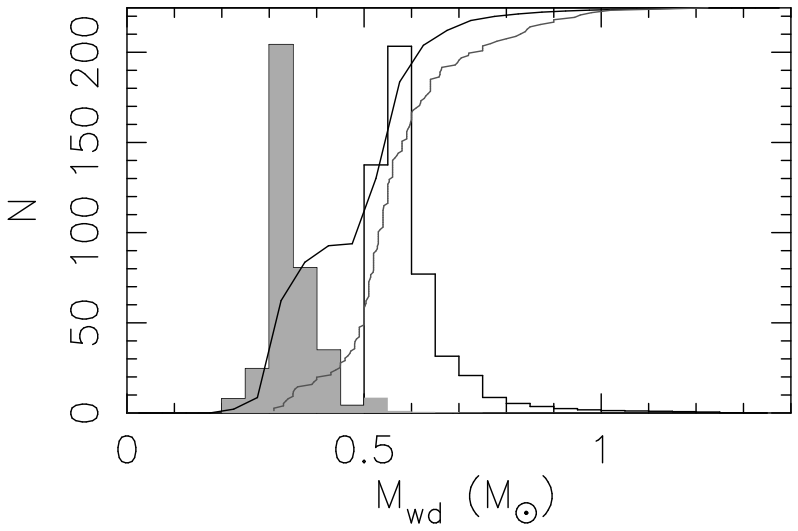

Figure 4.7: Mass spectrum of all white dwarfs for model B (100% binaries). Members of close double white dwarfs are in grey. The cumulative distribution is shown as the solid black line. The grey line shows the cumulative distribution of the observed systems (Fig. 4.9).

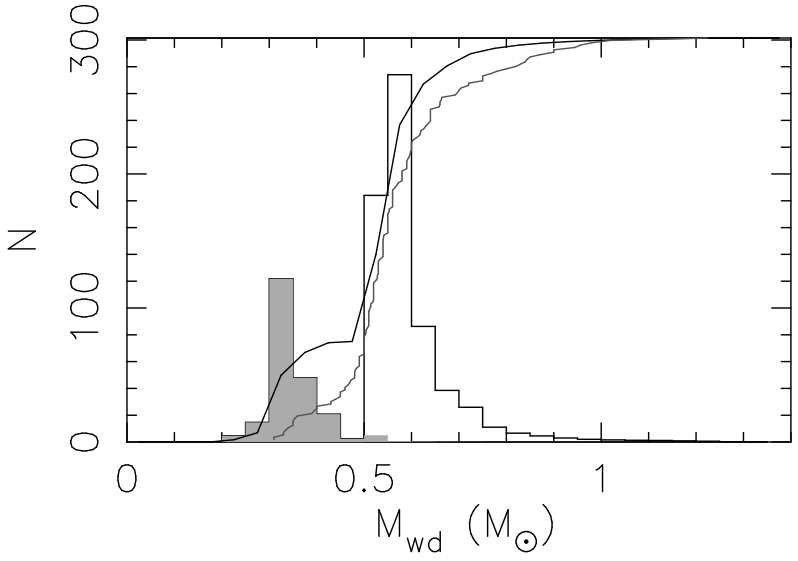

Figure 4.8: Mass spectrum of all white dwarfs for model A2 (initial binary fraction of 50%) Double white dwarfs are in grey. The cumulative distribution is shown as solid black line and cumulative distribution of observed systems as the grey line.

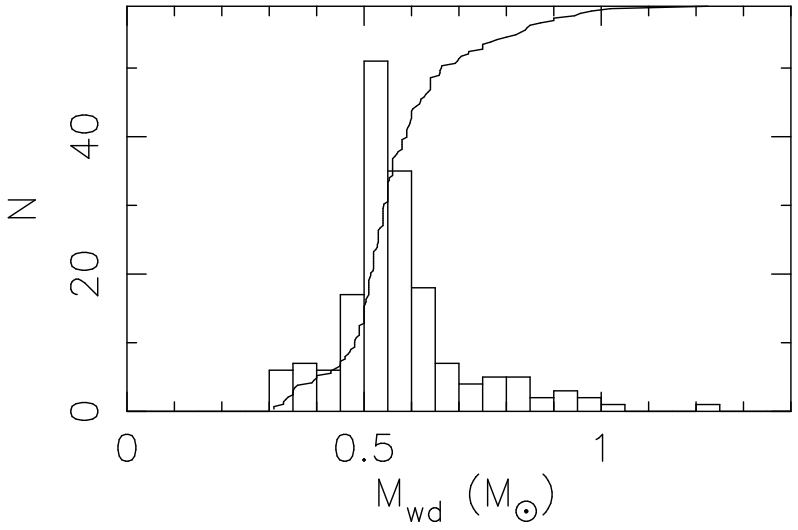

Figure 4.9: Mass spectrum of observed white dwarfs. Data are taken from BERGERON ET AL. (1992) and BRAGAGLIA ET AL. (1995). The solid line is the cumulative distribution.

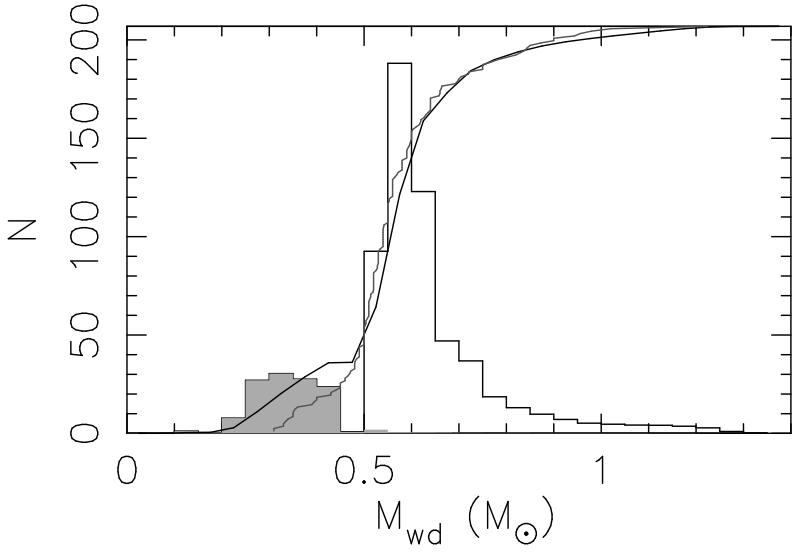

Figure 4.10: Mass spectrum of all white dwarfs as in Fig. 4.8 in a model in which all helium white dwarfs cool like a $0.4\,M_\odot$ dwarf and all CO white dwarfs cool like a $0.6\,M_\odot$ white dwarf. Lines are cumulative distributions for the model (black) and the observations (grey).

TABLE 4.5: Galactic number and local space density of white dwarfs, and Galactic and local PN formation rate for the models A and C. The unit of the PN formation rates is yr^{-1}, the unit for $\rho_{wd,\odot}$ is pc^{-3}. The ranges of observed values are given for comparison. For references and discussion see Sect. 4.7.5.

Model	SFH	% bin	#wd 10^9	ν_{PN}	$\rho_{wd,\odot}$ (10^{-3})	$\nu_{PN,\odot}$ (10^{-12})
A	Exp	50	9.2	1.1	19	2.3
C	Const	50	4.1	0.8	8.5	1.7
Obs					4 – 20	3

sampling a different fraction of Galaxy. An even lower binary fraction apparently would fit the data better, but is in conflict with the estimated fraction of binaries among normal main sequence binaries (ABT 1983; DUQUENNOY AND MAYOR 1991). However this number highly depends on uncertain selection effects.

There are some features in the model mass spectrum in model A2 that appear to be in conflict with observations. The first is the clear trend that with the cooling models of DSBH98, even with our modifications, there should be an increasing number of helium white dwarfs towards lower masses. The observed distribution is flat. A very simple numerical experiment in which we assign a cooling curve to all helium white dwarfs as the one for a $0.414\,M_\odot$ white dwarf according to DSBH98 and a cooling curve as for a $0.605\,M_\odot$ white dwarf according to BLÖCKER (1995) for all CO white dwarfs (Fig. 4.10), shows that an equal cooling time for all helium white dwarfs seems to be in better agreement with the observations. It has a fraction of double white dwarfs of 18%.

Another feature is the absence of stars with $0.45 \lesssim M/M_\odot \lesssim 0.5$ in the model distributions. This is a consequence of the fact that in this interval in our models only hybrid white dwarfs can be present, which have a low formation probability (see Sect. 4.6).

We conclude that an initial binary fraction of 50% can explain the observed close binary fraction in the white dwarf population. The shape of the mass spectrum, especially for the helium white dwarfs is a challenge for detailed mass determinations and cooling models.

4.7.5 Birth rate of PN and local WD space density: constraints on the star formation history

Finally, we compare models A and C (see Table 4.1), which differ only by the assumed star formation history. The star formation rate was probably higher in the past than at present and some (double) white dwarfs descend from stars that are formed just after the Galactic disk was formed. Table 4.5 gives the formation rates of PN and the total number of white dwarfs in the Galaxy for models A and C. The total number of white dwarfs is computed by excluding all white dwarfs in binaries where the companion is

brighter. The local density of white dwarfs and PN rate are computed with Eq. (4.3) as described in Sect. 4.4.4.

We can compare these numbers with the observational estimates for the local PN formation rate of 3×10^{-12} pc^{-3} yr^{-1} (POTTASCH 1996) and the local space density of white dwarfs, which range from e.g. 4.2×10^{-3} pc^{-3} (KNOX ET AL. 1999) through $7.6^{+3.7}_{-0.7} \times 10^{-3}$ pc^{-3} (OSWALT ET AL. 1995) and 10×10^{-3} pc^{-3} (RUIZ AND TAKAMIYA 1995) to $20 \pm 7 \times 10^{-3}$ pc^{-3} (FESTIN 1998).

This list shows the large uncertainty in the observed local space density of white dwarfs. It appears that the lower values are somewhat favoured in the literature. Both models A and C appear for the moment to be consistent with the observed local white dwarf space density and with the PN formation rate. However, we prefer model A2 since it fits the period distribution better (see Fig. 4.4).

The ratio of the local space density of white dwarfs to the current local PN formation rate could in principle serve as a diagnostic for the star formation history of the Galaxy, given better knowledge of $\rho_{\mathrm{wd},\odot}$, which critically depends on the estimates of the incompleteness of the observed white dwarf samples and the applied cooling curves.

4.8 Discussion: comparison with previous studies

We now compare our work with the results of previous studies, in particular the most recent studies of IBEN ET AL. (1997, ITY97) and HAN (1998, HAN98).

4.8.1 Birth rates

In Table 4.3 we show the birth rates of close double white dwarfs for the different models. We also include numbers from HAN98 (model 1) and a set of numbers computed with the same code as used in ITY97, but for an age of the Galactic disk of 10 Gyr, as our models. The numbers of HAN98 are for an age of the disk of 15 Gyr. Our model D is the closest to the models of ITY97 and HAN98, assuming a constant SFR and 100% binaries. To estimate the influence of the binary evolution models only in comparing the different models we correct for their different normalisations.

In the recomputed ITY97 model the formation rate of interacting binaries in which the primary evolves within the age of the Galaxy is 0.35 yr^{-1}. In our model D this number is 0.25 yr^{-1}. In the following we therefore multiply the formation rates of ITY97 as given in Table 4.3 with 0.71.

In the model of HAN98 one binary with a primary mass above 0.8 $M_\odot$ is formed in the Galaxy annually with $\log a_{\mathrm{i}} < 6.76$, i.e. 0.9 binary with $\log a_{\mathrm{i}} < 6$, which is our limit to a_{i}. Correcting for the different assumed age of the Galaxy we estimate this number to be 0.81; in our model this number is 0.73. We thus multiply the the formation rates of HAN98 as given in Table 4.3 with 0.9.

Applying these corrections to the normalisation, we find that some interesting differences remain. The birth rate of double white dwarfs is 0.029, 0.053 and 0.062 per year for HAN98, model D and ITY98 respectively. At the same time the ratio of the

merger rate to the birth rate decreases: 0.97, 0.53 and 0.28 for these models. This can probably be attributed to the different treatment of the common envelope. HAN98 uses a common envelope spiral-in efficiency of 1 in Webbinks (1984) formalism, while we use 4 (for $\lambda = 0.5$, see DE KOOL ET AL. 1987). ITY97 use the formalism proposed by TUTUKOV AND YUNGELSON (1979a) with an efficiency of 1. This is comparable to an efficiency of 4 – 8 in the Webbink formalism. This means that in the model of HAN98, more systems merge in a common envelope, which yields a low formation rate of double white dwarfs. The ones that form (in general) have short periods for the same reason, so the ratio of merger to birth rate is high. In the ITY model the efficiency is higher, so more systems will survive both common envelopes and have generally wider orbits, leading to a much lower ratio of merger to birth rate. Our model D is somewhat in between, but also has the different treatment of the first mass transfer phase (Sect 4.2), in which a strong spiral-in is avoided.

The difference between the models in the SN Ia rate ($\nu_{\rm SN\ Ia}$) is related both to the total merger rate and to the *masses* of the white dwarfs. The former varies within a factor ~ 1.5: 0.017, 0.028, and 0.028 $\rm yr^{-1}$ for ITY97, model D, and HAN98, while $\nu_{\rm SN\ Ia}$ is higher by a factor 2 – 3 in model D compared to the other models. This is caused by the initial - final mass relation in our models, which is derived from stellar models with core overshooting, producing higher final masses.

The difference in the birth rate of interacting white dwarfs ($\nu_{\rm AMCVn}$) is mainly a consequence of our treatment of the first mass transfer, which gives for model D a mass ratio distribution which is peaked to 1 (Sect. 4.7.3), while in ITY97 and HAN98 the mass ratio is in general different from 1 (Sect. 4.8.2), favouring stable mass transfer and the formation of AM CVn systems. An additional factor, which reduces the number of AM CVn systems is the assumption in model D and ITY97 that the mass transfer rate is limited by the Eddington rate. The formation and evolution of AM CVn stars is discussed in more detail in TUTUKOV AND YUNGELSON (1996) and Chapter 5.

4.8.2 Periods, masses and mass ratios

Comparing our Fig. 4.2 with the corresponding Figure in SAFFER ET AL. (1998), we find the same trend of higher white dwarf masses at longer periods. However, in our model the masses are higher than in the model of SAFFER ET AL. (1998) at the same period. This is a consequence of the absence of a strong spiral-in in the first mass transfer phase in our model, contrary to the conventional common envelope model, as discussed in 4.2.2.

In our model the mass ratio distribution is peaked at $q \approx 1$. This is different from the models of ITY97 and SAFFER ET AL. (1998) which predict a strong concentration to $q \sim 0.5 - 0.7$ and from HAN98 who finds typical values of $q \sim 0.5$, with a tail to $q \sim 2$. The difference between these two latter groups of models may be understood as a consequence of enhanced wind in Han's model (see also TOUT AND EGGLETON 1988), which allows wider separations before the second common envelope. The mass ratio distribution of our model, peaked at $q \simeq 1$, appears to be more consistent with the observed mass ratio distribution.

4.8.3 Cooling

To explain the lack of observed white dwarfs with masses below 0.3 $M_\odot$ we had to assume that these white dwarfs cool faster than predicted by the models of DSBH98.

The same assumption was required by VAN KERKWIJK ET AL. (2000), to bring the cooling age of the white dwarf that accompanies PSR B1855+09 into agreement with the pulsar spin-down age, and to obtain cooling ages shorter than the age of the Galaxy for the white dwarfs accompanying PSR J0034–0534 and PSR J1713+0747 .

The absence of the lowest mass white dwarfs may also be explained by the fact that a common envelope involving a giant with a low-mass helium core ($M_c < 0.2-0.25 M_\odot$) always leads to a complete merger, according to SANDQUIST ET AL. (2000). However it can not explain the absence of the systems with $0.25 < M < 0.3 M_\odot$, which would form the majority of the observed systems using the full DSBH98 cooling (model A1; see Fig. 4.2).

4.9 Conclusions

We computed a model of the population of close binary white dwarfs and found good agreement between our model and the observed double white dwarf sample. A better agreement with observations compared to earlier studies is found due to two modifications.

The first is a different treatment of unstable mass transfer from a giant to a main sequence star of comparable mass. The second is a more detailed modelling of the cooling of low-mass white dwarfs which became possible because detailed evolutionary models for such white dwarfs became available. Our main conclusions can be summarised as follows.

1. Comparing the mass distribution of the white dwarfs in close pairs with the observations, we find a lack of observed white dwarfs with masses below 0.3 $M_\odot$. This discrepancy can be removed with the assumption that low-mass white dwarfs cool faster than computed by DRIEBE ET AL. (1998). The same assumption removes discrepancies between observed and derived ages of low-mass white dwarfs that accompany recycled pulsars, as shown by VAN KERKWIJK ET AL. (2000). Faster cooling is expected if the hydrogen envelopes around low-mass white dwarfs are partially expelled by thermal flashes or a stellar wind.

2. Our models predict that the distribution of mass ratios of double white dwarfs, when corrected for observational selection effects as described by MORAN ET AL. (2000), peaks at a mass ratio of unity, consistent with observations. The distributions predicted in the models by IBEN ET AL. (1997) and HAN (1998) peak at mass ratios of about 0.7 and above 1.5 and agree worse with the observations even after applying selection effects.

3. Our models predict a distribution of orbital periods and masses of close double white dwarfs in satisfactory agreement with the observed distribution.

4. Amongst the observed white dwarfs only a small fraction are members of a close pair. To bring our models into agreement with this, we have to assume an initial binary fraction of 50% (i.e. as many single stars as binaries).

5. In our models the ratio of the local number density of white dwarfs and the planetary nebula formation rate is a sensitive function of the star formation history of the Galaxy. Our predicted numbers are consistent with the observations.

6. Using detailed cooling models we pridict that an observed sample of white dwarfs near the Sun, limited at the magnitude V = 15, contains 855 white dwarfs of which 220 are close pairs. Of these pairs only 10 are double CO white dwarfs and only one is expected to merge having a combined mass above the Chandrasekhar mass. The predicted merger rate in the Galaxy of double white dwarfs with a mass that exceeds the Chandrasekhar mass is consistent with the inferred SN Ia rate.

   ITY97 estimated, depending on α_{ce}, to find one such pair in a sample of $\sim$200 to $\sim$600 white dwarfs. Reversing this argument, when the statistics become more reliable, the observed number of systems with different types of white dwarfs could provide constraints on the cooling models for these white dwarfs.

Acknowledgements. We thank the referee A. Gould for valuable comments. LRY and SPZ acknowledge the warm hospitality of the Astronomical Institute "Anton Pannekoek". This work was supported by NWO Spinoza grant 08-0 to E. P. J. van den Heuvel, the Russian Federal Program "Astronomy" and RFBR grant 99-02-16037 and by NASA through Hubble Fellowship grant HF-01112.01-98A awarded (to SPZ) by the Space Telescope Science Institute, which is operated by the Association of Universities for Research in Astronomy, Inc., for NASA under contract NAS 5-26555.

Appendix 4.A Population synthesis code SeBa

We present some changes we made to the population synthesis code SeBa (see PORTEGIES ZWART AND VERBUNT 1996; PORTEGIES ZWART AND YUNGELSON 1998).

4.A.1 Stellar evolution

As before, the treatment of stellar evolution in our code is based on the fits to detailed stellar evolutionary models (EGGLETON ET AL. 1989; TOUT ET AL. 1997), which give the luminosity and the radius of the stars as a function of time and mass. In addition to this we need the mass of the core and the mass loss due to stellar wind. These we obtain as follows.

Core mases and white dwarf masses

For the mass of the helium core m_c at the end of the main sequence we use (EGGLETON, private communication, 1998)

$$m_c = \frac{0.11\, M^{1.2} + 7 \times 10^{-5}\, M^4}{1 + 2 \times 10^{-4} M^3}. \tag{4.A.5}$$

The mass of the core during the further evolution of the star is computed by integrating the growth of the core resulting from hydrogen shell burning:

$$\dot{m}_c = \eta_H \frac{L}{X} \tag{4.A.6}$$

where

$$\eta_H = 9.6 \times 10^{-12} \mathrm{M}_\odot\ \mathrm{yr}^{-1}\ \mathrm{L}_\odot^{-1} \tag{4.A.7}$$

and X is the mass fraction of hydrogen in the envelope. During core helium burning we assume that half of the luminosity of the star is produced by hydrogen shell burning, while in the double shell burning phase we assume that all of the luminosity is produced by the hydrogen shell burning.

When giants have degenerate cores, application of a core mass - luminosity relation gives more accurate results than direct integration of the growth of the core.

For degenerate helium cores of stars with $M \lesssim 2.3\mathrm{M}_\odot$ we use (BOOTHROYD AND SACKMANN 1988)

$$M_c = 0.146\, L^{0.143} \tag{4.A.8}$$

(all quantities in solar units). For degenerate CO cores of stars with $M \lesssim 8\mathrm{M}_\odot$ on the AGB we use (GROENEWEGEN AND DE JONG 1993)

$$\begin{aligned} M_c &= 0.015 + \sqrt{\frac{L}{47488} + 0.1804} && L < 15725 \\ M_c &= 0.46 + \frac{L}{46818}\, M^{-0.25} && L > 15725 \end{aligned} \tag{4.A.9}$$

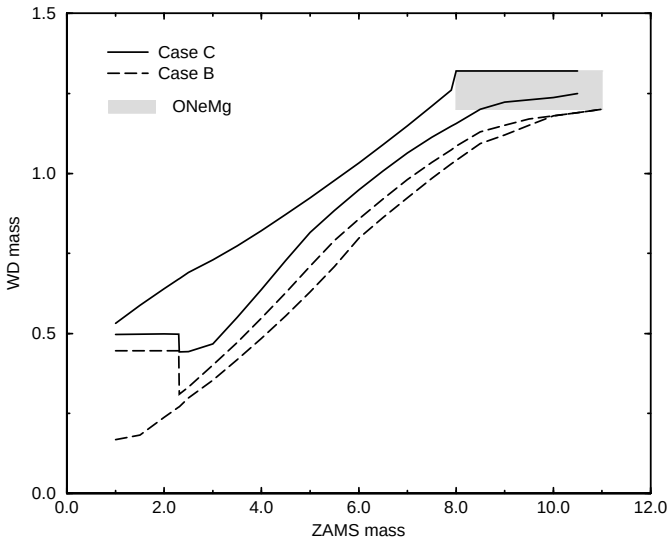

Figure 4.A.1: White dwarf masses as function of the ZAMS mass. Dashed lines are for case B mass transfer. The white dwarfs that descend from stars with ZAMS masses below 2.3 $M_\odot$ in case B mass transfer are helium white dwarfs. The two dashed lines give the minimum and maximum mass of the white dwarf, which depends on the orbital separation at the onset of the mass transfer. Solid lines are for case C mass transfer, which results in the formation of a CO white dwarf. When the ZAMS mass is above 8 $M_\odot$ the stripping of the envelope in case C mass transfer may prevent the formation of a neutron star, leading to the formation of a white dwarfs with a core consisting of O, Ne and Mg (shaded region).

where the transition between the two fits occurs at $M_c \approx 0.73 M_\odot$ in stars $\sim 3.5 M_\odot$ where the two relations fit together reasonably. We changed the power of the dependence on M from –0.19 in the original paper to –0.25 because the maximum luminosities given by our fits otherwise lead to white dwarf masses too high compared to initial - final mass relations as found from observations (see GROENEWEGEN AND DE JONG 1993).

The masses of CO cores formed by central He burning inside the helium core are defined in the same way as we define the relation between the mass of helium stars and their CO cores (see Sect. 4.A.1).

A white dwarf forms if a component of a binary with $M < 10 M_\odot$ loses its hydrogen envelope through RLOF either before core helium burning (case B mass transfer) or after helium exhaustion (case C). The masses of white dwarfs formed in cases B and C as function of initial mass are shown in Fig. 4.A.1.

Helium stars

A helium star is formed when a star more massive than 2.3 $M_\odot$ loses its hydrogen envelope in case B mass transfer. The helium star starts core helium burning and forms a CO core. In our code, this core grows linearly at a rate given by the ratio of 65% of the initial mass of the helium star and the total lifetime of the helium star. This is suggested by computations of HABETS (1986) and gives a CO core of the Chandrasekhar mass for a 2.2 $M_\odot$ helium star: the minimum mass to form a neutron star in our code.

Helium stars with $0.8 \lesssim M \lesssim 3 M_\odot$ expand again after core helium exhaustion and can lose their remaining helium envelope in so called case BB mass transfer. The amount of mass that can be lost is defined as increasing linearly from 0 to 45% for stars between 0.8 and 2.2 $M_\odot$ and stays constant above 2.2 $M_\odot$. The maximum mass of the CO white dwarf thus formed is 1.21 $M_\odot$. helium stars of lower mass ($M < 0.8 M_\odot$) do not expand and retain their thick helium envelopes, forming hybrid white dwarfs (IBEN AND TUTUKOV 1985).

Stellar wind

We describe mass loss in a stellar wind in a very general way in which the amount of wind loss increases in time according to

$$\Delta M_{\rm w} = M_{\rm lost} \left[\left(\frac{t + \Delta t}{t_{\rm f}} \right)^{\eta} - \left(\frac{t}{t_{\rm f}} \right)^{\eta} \right]. \qquad (4.A.10)$$

The exponent $\eta = 6.8$ is derived from fitting stellar wind mass loss on the main sequence of massive stars ($M \gtrsim 15 M_\odot$ MEYNET ET AL. 1994), but we apply it also for low and intermediate mass stars. For these stars $t_{\rm f}$ is the duration of the evolutionary phase that the star is in (as given by EGGLETON ET AL. 1989). For the different evolutionary phases, the parameters $M_{\rm lost}$ is defined as follows.

- In the Hertzsprung gap $M_{\rm lost}$ is 1% of the total mass of the star.
- For the first giant branch (hydrogen shell burning), we use a fit to models of SWEIGART ET AL. (1990) for stars with degenerate helium cores

  $$M_{\rm lost} = (2.5 - M)/7.5 \quad M_\odot \qquad (4.A.11)$$

  which we extend to all low and intermediate mass stars by setting $M_{\rm lost} = 0$ above $M = 2.5 M_\odot$.
- On the horizontal branch $M_{\rm lost}$ is 5% of the envelope mass.
- For the AGB phase we take $M_{\rm lost}$ equal to 80% of the mass of the envelope of the star when it enters the early AGB phase.

Radii of gyration

In the previous version of the SeBa code all gyration radii were set to 0.4. The gyration radius plays a role in the determination of the stability of the mass transfer (PORTEGIES ZWART AND VERBUNT 1996, Appendix C.1). We now use the following values.

For main-sequence stars we use a fit to the results by CLARET AND GIMÉNEZ (1990). Further we classify stars either as radiative (stars in Hertzsprung gap and helium stars) or as convective (red giants, AGB stars). A summary of radii of gyration are given in Table 4.A.1.

TABLE 4.A.1: Gyration radii for various types of stars.

Type	k^2
Radiative stars	0.03
Convective stars	0.2
White dwarfs	0.4
Neutron stars	0.25[a]
Black holes	$1/(c\,R^2)$

(a) GUNN AND OSTRIKER (1969)

White dwarf evolution: luminosity and radius

We model the cooling of white dwarfs according to the results of BLÖCKER (1995) and DRIEBE ET AL. (1998).

Luminosity
The luminosity of white dwarfs as function of time t can be reasonably well modelled by

$$\log L = L_{\rm max} - 1.4 \log(t/10^6 {\rm yr}) \qquad (4.A.12)$$

where $L_{\rm max}$ is a linear fit given by

$$L_{\rm max} = 3.83 - 4.77\, M_{\rm WD} \quad \text{for } 0.18 < M_{\rm WD} < 0.6 \qquad (4.A.13)$$

(mass and luminosity in solar units). Outside these limits $L_{\rm max}$ stays constant (i.e. $L_{\rm max} = 3$ below $M_{\rm WD} = 0.18$ and $L_{\rm max} = 1$ above $M_{\rm WD} = 0.6$). For white dwarf masses below $0.6 {\rm M}_\odot$ the luminosity is constrained to be below $\log L/{\rm L}_\odot = -0.5$, for more massive white dwarfs below $\log L/{\rm L}_\odot = 2$. In Fig. 4.A.2 we show the fits and the results of BLÖCKER (1995) and DRIEBE ET AL. (1998).

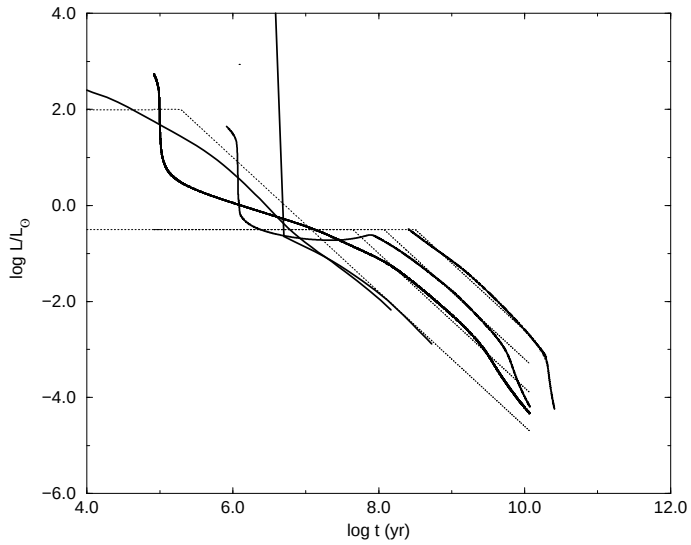

Figure 4.A.2: White dwarf cooling tracks from DRIEBE ET AL. (1998) and BLÖCKER (1995). Straight lines are the fits to these curves. The curves are for masses of 0.179, 0.300, 0.414, 0.6 and 0.8 from top right to bottom left.

Radius
We fitted the models of DRIEBE ET AL. (1998) and BLÖCKER (1995), and interpolated between the fits. The fits are given by

$$\frac{R}{R_\odot} = a - b\log(t/10^6\mathrm{yr}) \quad \text{for } M_{\mathrm{WD}} < 0.6\,\mathrm{M}_\odot. \tag{4.A.14}$$

The coefficients a and b are given in Table 4.A.2. Fig. 4.A.3 shows the fits and the corresponding detailed calculations.

For more massive white dwarfs we use the mass-radius relation for zero-temperature spheres (NAUENBERG 1972)

$$\frac{R}{R_\odot} = 0.01125\sqrt{\left(\frac{M_{\mathrm{WD}}}{M_{\mathrm{Ch}}}\right)^{-2/3} - \left(\frac{M_{\mathrm{WD}}}{M_{\mathrm{Ch}}}\right)^{2/3}} \tag{4.A.15}$$

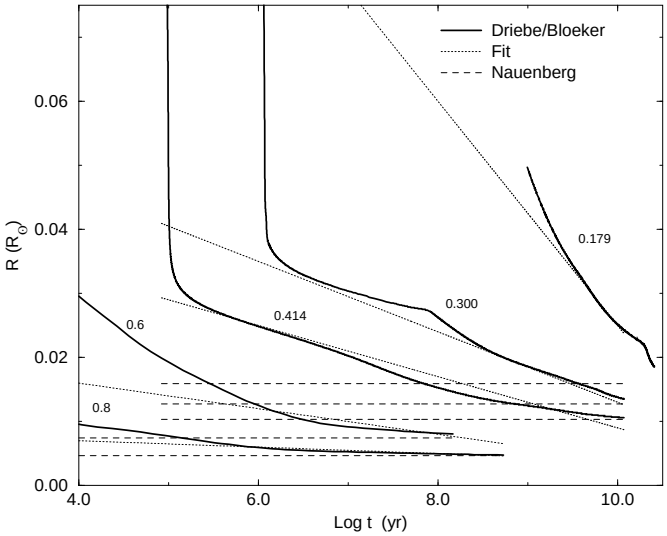

Figure 4.A.3: White dwarf radii from DRIEBE ET AL. (1998) and BLÖCKER (1995). Straight lines are the fits to these curves. The curves are for masses of 0.179, 0.300, 0.414, 0.6 and 0.8 from top right to bottom left.

Modified DSBH98 cooling

Our modification to the cooling described above reduces the cooling time-scale for white dwarfs with masses below $0.3 M_{\odot}$. For these white dwarfs we use the cooling curve and the radius of a more massive, thus faster cooling white dwarf of $0.46\ M_{\odot}$ (see Sect. 4.4.3).

TABLE 4.A.2: Coefficients for the fits to the white dwarf radii.

$M_{\rm WD}$	a	b
0.2	0.1	0.0175
0.4	0.03	0.0044
0.6	0.017	0.001
0.8	0.011	0.0005

4.A.2 Mass transfer in binary stars

As suggested in Chapter 3, we distinguish four types of mass transfer with different outcomes: stable mass transfer, common envelope evolution, envelope ejection and a double spiral-in.

Stable mass transfer

The amount of mass that can be accreted by a star is limited by its thermal time-scale

$$\dot{M}_{\rm max} \approx \frac{M}{\tau_{\rm th}} \approx \frac{R\,L}{G\,M}. \tag{4.A.16}$$

If not all mass can be accreted, we assume that the excess of mass leaves the system taking with it $n_{\rm J}$ times the specific angular momentum of the binary.

This assumption gives for the variation of orbital separation

$$\frac{a_{\rm f}}{a_{\rm i}} = \left(\frac{M_{\rm f}\,m_{\rm f}}{M_{\rm i}\,m_{\rm i}}\right)^{-2} \left(\frac{M_{\rm f}+m_{\rm f}}{M_{\rm i}+m_{\rm i}}\right)^{2n_{\rm J}+1} \tag{4.A.17}$$

We use $n_{\rm J} = 2.5$, which gives good agreement for the periods of low-mass Algols and Be X-ray binaries (PORTEGIES ZWART 1996)

Standard common envelope

When the mass transfer is unstable due to a tidal instability, the accretor is a compact object, or the envelope ejection equation gives a smaller orbital separation, we apply the standard common envelope equation $E_{\rm bind} = \alpha_{\rm ce}\,\Delta E_{\rm orb}$ (WEBBINK 1984):

$$\frac{M_{\rm i}\,(M_{\rm i}-M_{\rm f})}{\lambda\,R} = \alpha_{\rm ce}\,\left[\frac{M_{\rm f}\,m}{2\,a_{\rm f}} - \frac{M_{\rm i}\,m}{2\,a_{\rm i}}\right] \tag{4.A.18}$$

where $\alpha_{\rm ce}$ is an efficiency parameter and λ a parameter describing the structure of the envelope of the giant. Both are uncertain so we use them combined: $\alpha_{\rm ce}\,\lambda = 2$.

Envelope ejection

In the case of envelope ejection (Chapter 3), we assume that the complete envelope is lost and that this mass loss reduces the angular momentum of the system linearly proportional to the mass loss, as first suggested for the general case of non-conservative mass transfer by PACZYŃSKI AND ZIOŁKOWSKI (1967)

$$J_{\rm i} - J_{\rm m} = \gamma J_{\rm i} \frac{\Delta M}{M_{\rm tot}}, \tag{4.A.19}$$

where J_i is the angular momentum of the pre-mass transfer binary and M_tot is the total mass of the binary. The companion does not accrete al all (see discussion in Sect. 4.2.2 and Chapter 3). The change in orbital separation is given by

$$\frac{a_\mathrm{f}}{a_\mathrm{i}} = \left(\frac{M_\mathrm{f}\, m_\mathrm{f}}{M_\mathrm{i}\, m_\mathrm{i}}\right)^{-2} \left(\frac{M_\mathrm{f}+m_\mathrm{f}}{M_\mathrm{i}+m_\mathrm{i}}\right) \left(1-\gamma\frac{M_\mathrm{i}-M_\mathrm{f}}{M_\mathrm{i}+m_\mathrm{i}}\right)^2 . \tag{4.A.20}$$

In this work we use $\gamma = 1.75$.

Double spiral-in

If mass transfer is unstable when both stars are evolved (which can only happen if the mass ratio is close to unity), we model the evolution as a common envelope in which the two cores spiral-in. The energy needed to expel the complete envelope is computed analogously to the case of a standard common envelope (WEBBINK 1984, see also Sect. 4.A.2):

$$\frac{M_\mathrm{i}\,(M_i-M_\mathrm{f})}{\lambda\, R} + \frac{m_\mathrm{i}\,(m_\mathrm{i}-m_\mathrm{f})}{\lambda r} = \alpha_\mathrm{ce} \left[\frac{M_\mathrm{f}\, m_\mathrm{f}}{2\, a_\mathrm{f}} - \frac{M_\mathrm{i}\, m_\mathrm{i}}{2\, a_\mathrm{i}}\right]$$

If the final separation is too small for the two cores to form a detached binary, the cores merge and we compute the fraction of the envelopes that is lost with the (practical) assumption that both stars lose the same fraction of mass, retaining fM, i.e

$$\frac{M_\mathrm{i}(1-f)M_\mathrm{i}}{\lambda\, R} + \frac{m_\mathrm{i}(1-f)m_\mathrm{i}}{\lambda r} = \alpha_\mathrm{ce} \left[\frac{fM_\mathrm{i}\, fm_\mathrm{i}}{2\, a_\mathrm{RLOF}} - \frac{M_\mathrm{i}\, m_\mathrm{i}}{2\, a_\mathrm{i}}\right]$$

where a_RLOF is the separation at which one of the cores fills its Roche lobe. This is solved for f.

CHAPTER 5

Population synthesis for double white dwarfs II. Semi-detached systems: AM CVn stars

G. Nelemans, S. F. Portegies Zwart, F. Verbunt & L. R. Yungelson

Astronomy & Astrophysics, in press

ABSTRACT

We study two models for AM CVn stars: white dwarfs accreting (i) from a helium white dwarf companion and (ii) from a helium-star donor. We show that in the first model possibly no accretion disk forms at the onset of mass transfer. The stability and the rate of mass transfer then depend on the tidal coupling between the accretor and the orbital motion. In the second model the formation of AM CVn stars may be prevented by detonation of the CO white dwarf accretor and the disruption of the system. With the most favourable conditions for the formation of AM CVn stars we find a current Galactic birth rate of $6.8 \times 10^{-3}\,\mathrm{yr}^{-1}$. Unfavourable conditions give $1.1 \times 10^{-3}\,\mathrm{yr}^{-1}$. The expected total number of the systems in the Galaxy is 9.4×10^{7} and 1.6×10^{7}, respectively. We model very simple selection effects to get some idea about the currently expected observable population and discuss the (quite good) agreement with the observed systems.

5.1 Introduction

AM CVn stars are helium-rich faint blue objects that exhibit variability on time-scales of ∼1000 seconds. SMAK (1967) discovered that the prototype of the class, AM CVn (=HZ 29), shows photometric variability with a period ∼ 18 min and suggested that it is a binary. PACZYŃSKI (1967) realised that it could be a semi-detached pair of degenerate dwarfs in which mass transfer is driven by loss of angular momentum due to gravitational wave radiation. After flickering, typical for cataclysmic binary systems, was found in AM

CVn by WARNER AND ROBINSON (1972), this model was used to explain AM CVn by FAULKNER ET AL. (1972). There are currently 8 AM CVn candidates (Table 5.2) which have been studied photometrically in detail (for reviews see ULLA 1994; WARNER 1995; SOLHEIM 1995). AM CVn stars also attracted attention as possible sources of gravitational waves (HILS AND BENDER 2000, and references therein).

After the introduction of the concept of common envelope evolution for the formation of cataclysmic variables and X-ray binaries (PACZYŃSKI 1976), the formation of close double white dwarfs through two of such phases was anticipated by TUTUKOV AND YUNGELSON (1979b, 1981). The emission of gravitational waves would subsequently bring the two white dwarfs into a semi-detached phase. NATHER ET AL. (1981) independently suggested this scenario for the formation of AM CVn itself. In an alternative scenario the white dwarf donor is replaced by a helium star that becomes semi-degenerate during the mass transfer (IBEN AND TUTUKOV 1991).

Throughout this paper we use the term AM CVn for binaries in which a white dwarf accretes from another white dwarf or from a semi-degenerate helium star, irrespective how they would be classified observationally.

This paper continues our study on the formation and evolution of the Galactic population of close double white dwarfs (Chapter 3; Chapter 4). Here we study the population that becomes semi-detached and transfers mass in a stable way. In addition we examine the alternative case where the donor is a semi-degenerate helium star.

In Sect. 5.2 we outline the evolution of binaries driven by gravitational wave radiation. We review the models for the formation of AM CVn stars and discuss the stability of the mass transfer in Sect.5.3. The results of our population synthesis and a comparison with observations are presented in Sect. 5.4. The differences with previous studies are discussed in Sect. 5.5 after which the conclusions follow.

5.2 Mass transfer in close binaries driven by gravitational wave radiation

The rate of angular momentum loss ($\dot{J}$) of a binary system with a circular orbit due to gravitational wave radiation (GWR) is (LANDAU AND LIFSHITZ 1971):

$$\left(\frac{\dot{J}}{J}\right)_{\rm GWR} = -\frac{32}{5}\,\frac{G^3}{c^5}\,\frac{M\,m\,(M+m)}{a^4}. \tag{5.1}$$

Here M and m are the masses of the two components and a is their orbital separation.

In a binary with stable mass transfer the change of the radius of the donor exactly matches the change of its Roche lobe. This condition combined with an approximate equation for the size of the Roche lobe (PACZYŃSKI 1967),

$$R_{\rm L} \approx 0.46\,a\left(\frac{m}{M+m}\right)^{1/3} \qquad \text{for } m < 0.8M, \tag{5.2}$$

may be used to derive the rate of mass transfer for a semi-detached binary in which the

mass transfer is driven by GWR (PACZYŃSKI 1967)

$$\frac{\dot{m}}{m} = \left(\frac{\dot{J}}{J}\right)_{\rm GWR} \times \left[\frac{\zeta(m)}{2} + \frac{5}{6} - \frac{m}{M}\right]^{-1}. \tag{5.3}$$

Here $\zeta(m)$ is the logarithmic derivative of the radius of the donor with respect to its mass ($\zeta \equiv \partial \ln r / \partial \ln m$). For the mass transfer to be stable, the term in brackets must be positive, i.e.

$$q \equiv \frac{m}{M} < \frac{5}{6} + \frac{\zeta(m)}{2}. \tag{5.4}$$

The mass transfer becomes dynamically unstable when this criterion is violated, probably causing the binary components to coalesce (PRINGLE AND WEBBINK 1975; TUTUKOV AND YUNGELSON 1979b).

5.3 The nature of the mass donor: two formation scenarios

5.3.1 Close double white dwarfs as AM CVn progenitors

From the spectra of AM CVn stars it is inferred that the transferred material consists mainly of helium. FAULKNER ET AL. (1972) suggested two possibilities for the helium rich donor in AM CVn: (i) a helium star with a mass of $0.4 - 0.5\ M_\odot$ and (ii) a helium white dwarf. The first possibility is excluded because the helium star would dominate the spectrum and cause the accretor to have large radial velocity variations, none of which is observed. Thus they concluded that AM CVn stars are interacting double white dwarfs. Their *direct progenitors* may be detached close double white dwarfs which are brought into contact by loss of angular momentum due to GWR within the lifetime of the Galactic disk (for which we take 10 Gyr). The less massive white dwarf fills its Roche lobe first and an AM CVn star is born, if the stars do not merge (see Sect. 5.3.2). We discussed the formation of such double white dwarfs in Chapter 4.

To calculate the stability of the mass transfer and the evolution of the AM CVn system, one needs to know the mass-radius relation for white dwarfs. This depends on the temperature, chemical composition, thickness of the envelope etc. of the white dwarf. However, PANEI ET AL. (2000) have shown that after cooling for several 100 Myr the mass – radius relation for low-mass helium white dwarfs approaches the relation for zero-temperature spheres. As most white dwarfs that may form AM CVn stars are at least several 100 Myr old at the moment of contact (TUTUKOV AND YUNGELSON 1996), we apply the mass – radius relation for cold spheres derived by ZAPOLSKY AND SALPETER (1969), as corrected by RAPPAPORT AND JOSS (1984). For helium white dwarfs with masses between 0.002 and 0.45 $M_\odot$, it can be approximated to within 3% by (in solar units)

$$R_{\rm ZS} \approx 0.0106 - 0.0064\ \ln M_{\rm WD} + 0.0015 M_{\rm WD}^2. \tag{5.5}$$

We apply the same equation for the radii of CO white dwarfs, since the dependence on chemical composition is negligible in the range of interest.

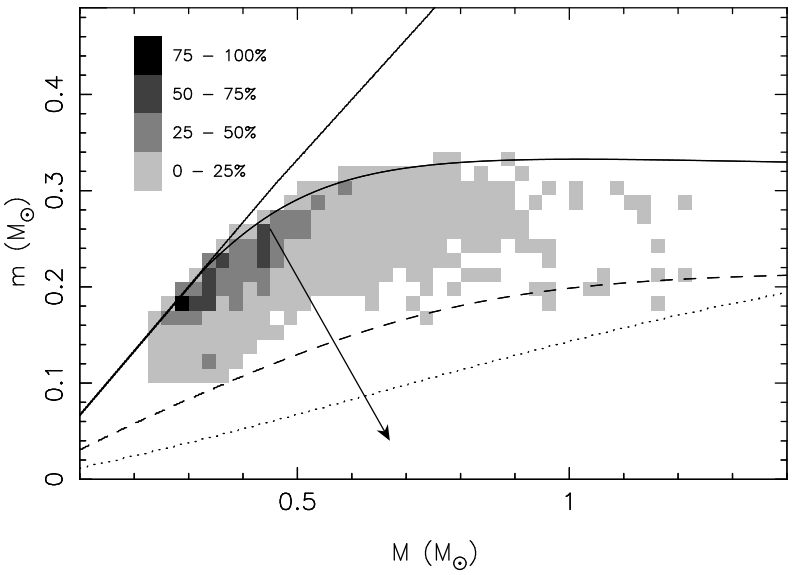

Figure 5.1: Stability limits for mass transfer in close double white dwarfs. Above the upper solid curve the mass transfer is dynamically unstable. Below the lower solid line the systems have mass transfer rates below the Eddington limit in the case of an efficient tidal coupling between the accretor and the orbital motion. If the coupling is inefficient, this limit shifts down to the dashed line. Above the dotted line the stream hits the companion directly at the onset of the mass transfer and no accretion disk forms. As the evolution proceeds (parallel to the arrow) a disk eventually forms. The gray shades give the current model birth rate distribution of AM CVn stars that form from close binary white dwarfs. The shading is scaled as a fraction of the maximum birth rate per bin, which is 1.4×10^{-4} yr^{-1}.

5.3.2 Stability of the mass transfer between white dwarfs

In Fig. 5.1 we show the limiting mass ratio for dynamically stable mass transfer [Eq. (5.4)] as the upper solid line, with $\zeta(m)$ derived from Eq. (5.5). The initial mass-transfer rates, as given by Eq. (5.3), can be higher than the Eddington limit of the accretor (TUTUKOV AND YUNGELSON 1979b). The matter that cannot be accreted is lost from the system, taking along some angular momentum. The binary system may remain stable even though it loses extra angular momentum. However heating of the transferred material, may cause it to expand and form a common envelope in which the two white dwarfs most likely merge (HAN AND WEBBINK 1999). Therefore, we impose the additional restriction to have the initial mass transfer rate lower than the Eddington accretion limit for the companion ($\sim 10^{-5}\,M_\odot$ yr^{-1}). This changes the limiting mass ratio below which AM CVn stars can be formed to the lower solid line in Fig. 5.1. In this Figure we over-plotted our model distribution of the current birth rate of AM CVn stars that form from close binary white dwarfs (see Sect. 5.4).

In the derivation of the Eq. (5.3) it is implicitly assumed that the secondary rotates synchronously with the orbital revolution and that the angular momentum which is drained from the secondary is restored to the orbital motion via tidal interaction between the accretion disk and the donor star (see, e.g. VERBUNT AND RAPPAPORT 1988, and references therein).

However, the orbital separation when Roche-lobe overflow starts is only about 0.1 $R_\odot$ and the formation of the accretion disk is not obvious; the matter that leaves the vicinity of the first Lagrangian point initially follows a ballistic trajectory, passing the accreting star at a minimum distance of $\sim 10\%$ of the binary separation (LUBOW AND SHU 1975), i.e. at a distance comparable to the radius of a white dwarf ($\sim 0.01 R_\odot$). So, the accretion stream may well hit the surface of the accretor directly instead of forming an accretion disk around it (WEBBINK 1984).

The minimum distance at which the accretion stream passes the accretor is computed by LUBOW AND SHU (1975, their $\widetilde{\omega}_{\rm min}$), which we fit with

$$\begin{aligned}\frac{r_{\rm min}}{a} &\approx 0.04948 - 0.03815\ \log(q) \\ &\quad + 0.04752\ \log^2(q) - 0.006973 \log^3(q).\end{aligned} \tag{5.6}$$

The value of q at which the radius of the accretor equals $r_{\rm min}$ is presented as a dotted line in Fig. 5.1; above this line the accretion stream hits the white dwarfs' surface directly and no accretion disk is formed.

In absence of the disk the angular momentum of the stream is converted into spin of the accretor and mechanisms other than disk – orbit interaction are required to transport the angular momentum of the donor back to the orbit. The small separation between the two stars may result in tidal coupling between the accretor and the donor which is in synchronous rotation with the orbital period. The efficiency of this process is uncertain (SMARR AND BLANDFORD 1976; CAMPBELL 1984), but if tidal coupling between accretor and donor is efficient the stability limit for mass transfer is the same as in the presence of the disk [Eq. (5.4)]. In the most extreme case all the angular momentum carried with the accretion stream is lost from the binary system. The lost angular momentum can be approximated by the angular momentum of the ring that would be formed in the case of a point-mass accretor: $\dot{J}_{\dot{m}} = \dot{m}\sqrt{GMar_{\rm h}}$, where $r_{\rm h}$ is the radius of the ring in units of a. This sink of angular momentum leads to an additional term $-\sqrt{(1+q)r_{\rm h}}$ in the brackets in Eq. (5.3). As a result the condition for dynamically stable mass transfer becomes more rigorous:

$$q < \frac{5}{6} + \frac{\zeta(m)}{2} - \sqrt{(1+q)r_{\rm h}}. \tag{5.7}$$

This limit (with $r_{\rm h}$ given by VERBUNT AND RAPPAPORT (1988) and again the additional restriction of a mass transfer rate below the Eddington limit) is shown in Fig. 5.1 as the dashed line.

Figure 5.1 shows that, with our assumptions, none of the AM CVn binaries which descend from double white dwarfs (which we will call the *white dwarf family*) forms a

disk at the onset of mass transfer. After about 10^7 yr, when the donor mass has decreased below 0.05 $M_\odot$ (see Fig. 5.4) and the orbit has become wider a disk will form.

Only one of the currently known 14 close double white dwarfs possibly is an AM CVn progenitor; WD 1704+481A has $P_{\rm orb}$ = 3.48 hr, $m = 0.39 \pm 0.05\,M_\odot$ and $M = 0.56 \pm 0.05\,M_\odot$ (MAXTED ET AL. 2000). It is close to the limit for dynamical stability, but because the initial mass transfer rate is expected to be super-Eddington it may merge.

5.3.3 Binaries with low-mass helium stars as AM CVn progenitors: a semi-degenerate mass donor

Another way to form a helium transferring binary in the right period range was first outlined by SAVONIJE ET AL. (1986). They envisioned a neutron star accretor, but the scenario for an AM CVn star, with a white dwarf accretor, is essentially the same (IBEN AND TUTUKOV 1991). One starts with a low-mass, non-degenerate helium burning star, a remnant of so-called case B mass transfer, with a white dwarf companion. If the components are close enough, loss of angular momentum via GWR may result in Roche-lobe overflow before helium exhaustion in the stellar core. Mass transfer is stable if the ratio of the mass of the helium star (donor) to the white dwarf (accretor) is smaller than ~ 1.2 (TUTUKOV AND FEDOROVA 1989; ERGMA AND FEDOROVA 1990)[1]. When the mass of the helium star decreases below $\sim 0.2\,M_\odot$, core helium burning stops and the star becomes semi-degenerate. This causes the exponent in the mass-radius relation to become negative and, as a consequence, mass transfer causes the orbital period to increase. The minimum period is $\sim$10 min. With strongly decreasing mass transfer rate the donor mass drops below $0.01 M_\odot$ in a few Gyr, while the period of the system increases up to ~ 1 hr; in the right range to explain the AM CVn stars. The luminosity of the donor drops below $10^{-4}\,L_\odot$ and its effective temperature to several thousand K. We will call the AM CVn stars that formed in this way the *helium star family*. Note that in this scenario a disk will always form because the orbit is rather wide at the onset of the mass transfer. The equations for efficient coupling thus hold.

The progenitors of these helium stars have masses in the range 2.3 – 5 $M_\odot$. The importance of this scenario is enhanced by the long lifetimes of the helium stars: $t_{\rm He} \approx 10^{7.15} M_{\rm He}^{-3.7}$ yr (IBEN AND TUTUKOV 1985), comparable to the main-sequence lifetime of their progenitors, so that there is enough time to lose angular momentum by gravitational wave radiation and start mass transfer before the helium burning stops.

Our simulation of the population of helium stars with white dwarf companions, suggests that at the moment they get into contact the majority of the helium stars are at the very beginning of core helium burning. This is illustrated in Fig. 5.2. Having this in mind, we approximate the mass-radius relation for semi-degenerate stars by a power-law fit to the results of computations of TUTUKOV AND FEDOROVA (1989) for a $0.5\,M_\odot$ star, which filled its Roche lobe shortly after the beginning of core helium burning (their

[1] This stability limit is the same as for hydrogen-rich stars with radiative envelopes.

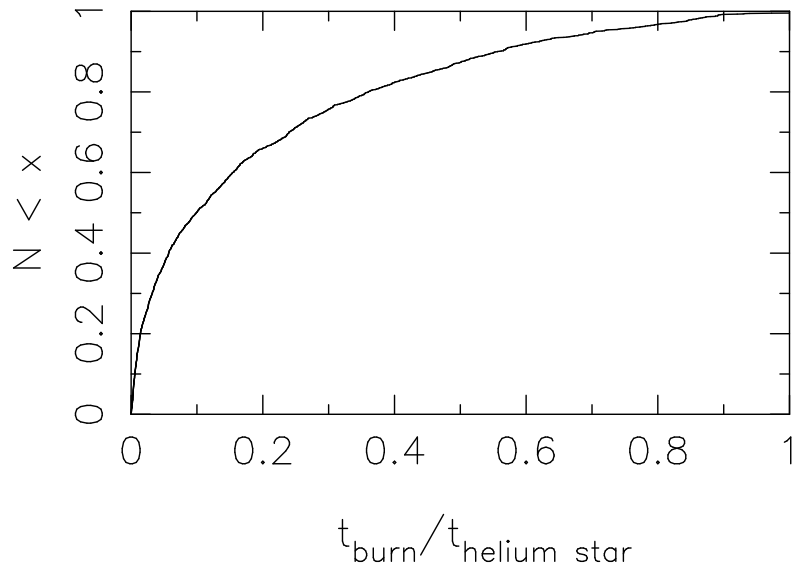

Figure 5.2: Cumulative distribution of the ratios of the helium burning time that occurred *before* the mass transfer started and the total helium burning time for the model systems.

model 1.1). For the semi-degenerate part of the track we obtain (in solar units):

$$R_{\rm TF} \approx 0.043\, m^{-0.062}. \tag{5.8}$$

Trial computations with the relation $R \approx 0.029\, m^{-0.19}$ from the model of SAVONIJE ET AL. (1986) which had $Y_{\rm c} = 0.26$ at the onset of the mass transfer reveals a rather weak dependence of our results on the mass – radius relation.

As noticed by SAVONIJE ET AL. (1986), severe mass loss in the phase before the period minimum, increases the thermal time-scale of the donor beyond the age of the Galactic disk and thus prevents the donor from becoming fully degenerate and keeps it semi-degenerate.

Another effect of the severe mass loss is the quenching of the helium burning in the core. TUTUKOV AND FEDOROVA (1989) show that during the mass transfer the central helium content hardly changes (especially for low-mass helium stars). Therefore, despite the formation of an outer convective zone, which penetrates inward to regions where helium burning took place, one would expect that in the majority of the systems the transferred material is helium-rich down to very low donor masses. However, donors with He-exhausted cores at the onset of mass transfer ($Y_{\rm c} \lesssim 0.1$) may in the course of their evolution start to transfer matter consisting of a carbon-oxygen mixture (see Fig. 3 in ERGMA AND FEDOROVA 1990, who used the same evolutionary code as TUTUKOV AND FEDOROVA).

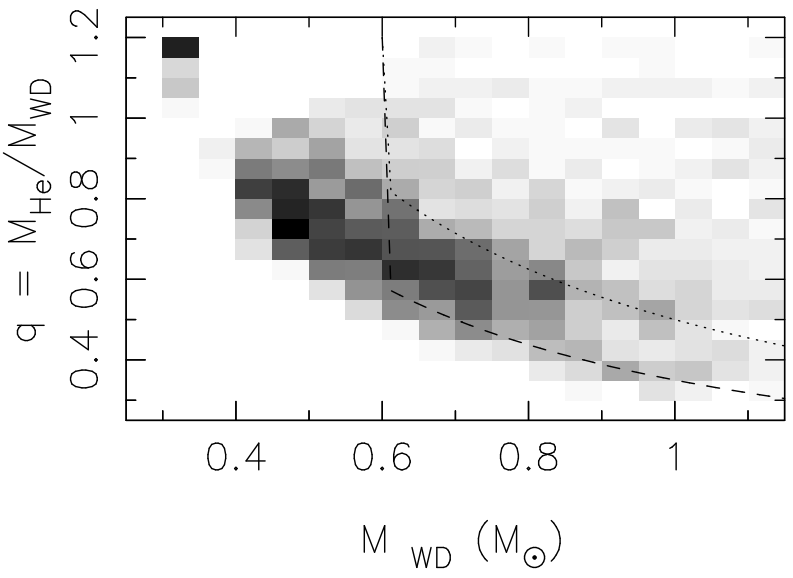

Figure 5.3: Distribution of helium stars with white dwarf companions that currently start stable mass transfer. In the systems to the right of the dotted and dashed lines the white dwarfs accrete at least $0.3\,M_\odot$ and $0.15\,M_\odot$ before ELD, respectively, at high accretion rates. These lines show two choices of mass limits above which, with our assumption, the binaries are disrupted by edge-lit detonation before they become AM CVn systems. The systems in the top left corner are binaries with helium white dwarf accretors.

Figure 5.3 shows the population of low-mass helium stars with white dwarf companions which currently start mass transfer, (i.e. have $q \lesssim 1.2$), derived by means of population synthesis. It is possible that only a fraction of them evolves into AM CVn stars. Upon Roche lobe overflow, before the period minimum, most helium donors lose mass at an almost constant rate close to $3 \times 10^{-8}\,M_\odot\ \mathrm{yr}^{-1}$. Accretion of He at such rates by a carbon-oxygen (CO) white dwarf may trigger a detonation in the layer of the accumulated matter (TAAM 1980). This may further cause the detonation of the underlying CO dwarf, so-called edge-lit detonation, ELD (LIVNE 1990; LIVNE AND GLASNER 1991; WOOSLEY AND WEAVER 1994; LIVNE AND ARNETT 1995). The conditions for ELD to occur: the mass of the white dwarf, the range of accretion rates, the mass of the accumulated layer, etc. are still actively debated.

However, examples computed by LIMONGI AND TORNAMBÈ (1991) and WOOSLEY AND WEAVER (1994) show that if $\dot{M} \gtrsim 10^{-8}\,M_\odot\ \mathrm{yr}^{-1}$ the helium layer inevitably detonates if $\Delta M_{\mathrm{He}} \gtrsim 0.3\,M_\odot$ and $M_{\mathrm{CO}} \gtrsim 0.6\,M_\odot$. Therefore, as one of the extreme cases, we reject all systems which satisfy these limits from the sample of progenitors of AM CVn stars, assuming that they will be disrupted before the helium star enters the semi-degenerate stage. As another extreme, we assume that only $0.15\,M_\odot$ has to

be accreted for ELD (as a compromise between results of LIMONGI AND TORNAMBÈ 1991, and WOOSLEY AND WEAVER 1994). The relevant cut-offs are shown in Fig. 5.3.

For CO white dwarf accretors less massive than $0.6\,M_\odot$ we assume that accretion of helium results in "flashes" in which the He layer is ejected or lost via a common envelope formed due to expansion of the layer. Such events may be repetitive.

LIMONGI AND TORNAMBÈ (1991) show that for accretion rates below $10^{-8}\,M_\odot\ \mathrm{yr}^{-1}$ more than $\sim 0.4\,M_\odot$ helium has to be accreted before detonation. For systems in which the donor becomes semi-degenerate and the mass accretion rates are low we limit the accumulation of He only by adopting the Chandrasekhar mass as a maximum to the total mass of the accreting white dwarf.

5.3.4 Summary: two extreme models for AM CVn progenitors

We recognise two possibilities for each family of potential AM CVn systems, which are: efficient or non-efficient tidal coupling between the accretor and the orbital motion in the white dwarf family, and two limits for the disruption of the accretors by ELD in the helium star family. We compute the populations for every possible solution and combine them into two models: model I, in which there is no tidal coupling and ELD is efficient in the destruction of potential progenitor systems (an "inefficient" scenario for forming AM CVn systems) and an "efficient" model II, in which there is an effective tidal coupling and ELD is efficient only in systems with the most massive donors. However, we give the birth rates and number of the objects for the four different solutions separately in Table 5.1.

Figure 5.4 presents two examples of the evolution of the orbital period and the mass transfer rate for both families of AM CVn systems. Initially the mass transfer rate is very high but within a few million years it drops below $10^{-8}\ M_\odot\ \mathrm{yr}^{-1}$. In the same time interval the orbital period increases from a few minutes, in the case of the white dwarf family, or from a little over 10 minutes, for the helium star family, to a few thousand seconds. The semi-degenerate donor systems have lower mass transfer rates and larger periods for the same donor mass due to their larger radii. The fact that the period is independent of the accretor mass (M) is a consequence of Eq. (5.2) and Keplers 3rd law leading to $P \propto (R^3/m)^{1/2}$.

5.4 The population of AM CVn stars

We used the population synthesis program SeBa, as described in detail in PORTEGIES ZWART AND VERBUNT (1996), PORTEGIES ZWART AND YUNGELSON (1998) and Chapter 4 to model the progenitor populations. We follow model A of Chapter 4, which has an IMF after MILLER AND SCALO (1979) and flat initial distributions over the mass ratio of the components and the logarithm of the orbital separation and a thermal eccentricity distribution. We assume an initial binary fraction of 50% and that the star formation decreases exponentially with time, which is different from other studies of close double white dwarfs that assume a constant star formation rate. The mass transfer

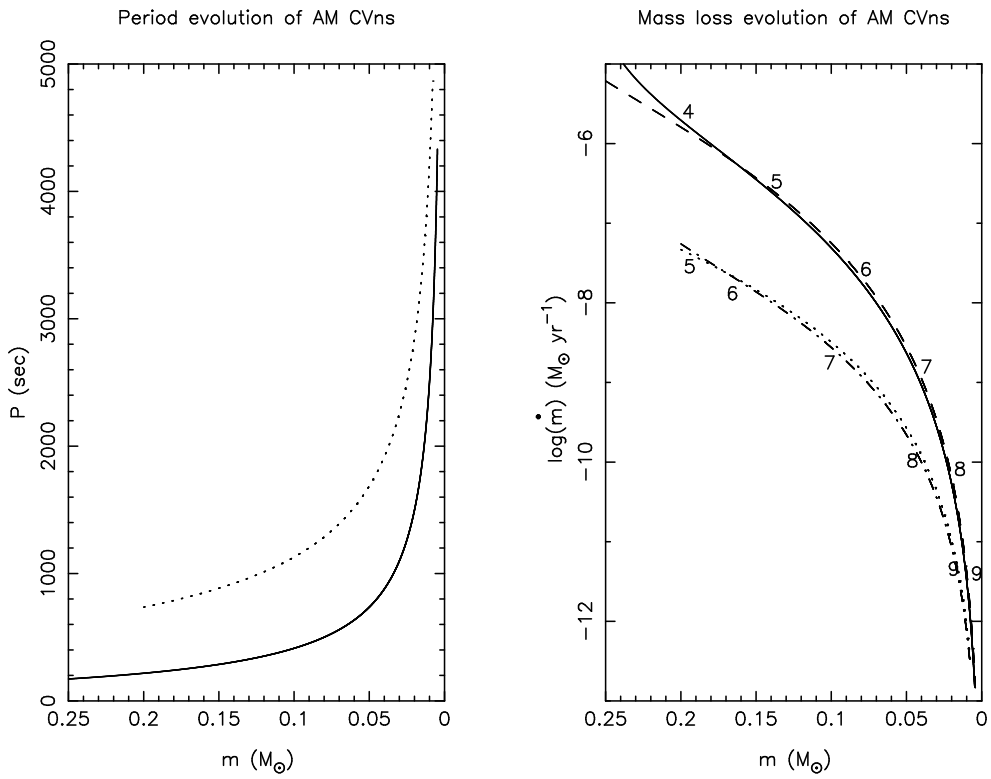

Figure 5.4: Examples of the evolution of AM CVn systems. The left panel shows the evolution of the orbital period as function of the mass of the secondary (donor) star. The right panel shows the change in the mass transfer rate during the evolution. The solid and dashed lines are for white dwarf donor stars of initially $0.25\,M_\odot$ transferring matter to a primary of initial mass of 0.4 and $0.6\,M_\odot$, respectively, assuming efficient coupling between the accretor spin and the orbital motion. The dash-dotted and dotted line are for a helium star donor, starting when the helium star becomes semi-degenerate (with a mass of $0.2\,M_\odot$). Primaries are again 0.4 and $0.6\,M_\odot$. The numbers along the lines indicate the logarithm of the time in years since the beginning of the mass transfer.

between a giant and a main-sequence star of comparable mass is treated with an "angular momentum formalism" which does not result in a strong spiral-in (Chapter 3).

5.4.1 The total population

We generate the population of close double white dwarfs and helium stars with white dwarf companions and select the AM CVn star progenitors according to the criteria for the formation of the AM CVn stars as described above. We calculate the birth rate of AM CVn stars, and evolve every system according to the recipe described in Sect. 5.2, to

TABLE 5.1: Birth rate and number of AM CVn systems in the Galaxy. The first column gives the model name (Sect. 5.3.4) followed by the current Galactic birth rate (ν in yr^{-1}), the total number of systems in the Galaxy (#) and the number of observable systems with $V < 15$ (# obs). The last column (σ in pc^{-3}) gives the local space density of AM CVn stars for each model. Due to selection effects the number of observable systems is quite uncertain (see Sect. 5.4.2).

Mod.	white dwarf family			He-star family			
	ν	#	# obs	ν	#	# obs	σ
	10^{-3}	10^7		10^{-3}	10^7		10^{-4}
I	0.04	0.02	1	0.9	1.8	32	0.4
II	4.7	4.9	54	1.6	3.1	62	1.7

obtain the total number of systems currently present in the Galaxy (Table 5.1) and their distribution over orbital periods and mass-loss rates (Fig. 5.5).

The absence of an effective coupling between the accretor spin and the orbital motion (model I) reduces the current birth rate AM CVn stars from the white dwarf family by two orders of magnitude as compared to the case of effective coupling (model II). The fraction of close double white dwarfs which fill their Roche lobes and continue their evolution as AM CVn stars is 21% in model II but only 0.2% in model I (see also Fig. 5.1, page 76).

In model I the population of AM CVn stars is totally dominated by the helium star family. In model II where tidal coupling is efficient both families have a comparable contribution to the population. Increasing the mass of the critical layer for ELD from $0.15\,M_\odot$ to $0.3\,M_\odot$ almost doubles the current birth rate of the systems which are able to enter the semi-degenerate branch of the evolution. In the latter case almost all helium star binaries that transfer matter to a white dwarf in a stable way eventually become AM CVn systems (see Fig. 5.3).

In Fig. 5.5 we show the total current population of AM CVn systems in the Galaxy in our model. The evolutionary paths of both families are indicated with the curves (see also Fig. 5.4). Table 5.1 gives the total number of systems currently present in the Galaxy. The evolution of the systems decelerates with time and as a result the vast majority of the systems has orbital periods larger than one hour. The evolutionary tracks for the two families do not converge, since the mass-loss of the helium stars prevents their descendants from recovering thermal equilibrium in the lifetime of the Galactic disk (see sect.5.3.3).

The minimum donor mass attainable within the lifetime of the Galactic disk is $\sim 0.005\,M_\odot$ for the descendants of the helium white dwarfs and $\sim 0.007\,M_\odot$ for the descendants of the helium stars. This is still far from the limit of $\sim 0.001\,M_\odot$ where the electrostatic forces in their interiors will start to dominate the gravitational force, the mass-radius relation will become $R \propto M^{1/3}$ (ZAPOLSKY AND SALPETER 1969), and the mass transfer will cease.

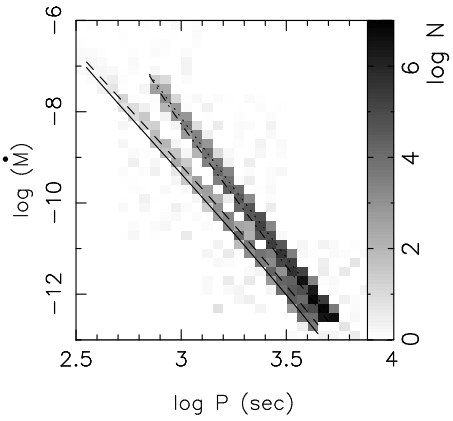

Figure 5.5: The current Galactic population of AM CVn systems of the two families for models I (above) and II (next page). The grey scale indicates the *logarithm* of the number of systems. The upper branch is the helium star family; the lower branch the white dwarf family.

In Table 5.1 we give the local space density of AM CVn systems estimated from their total number and the Galactic distribution of stars, for which we adopt

$$\rho(R,z) = \rho_0 \, e^{-R/H} \, \mathrm{sech}(z/\beta)^2 \quad \mathrm{pc}^{-3} \tag{5.9}$$

as in (Chapter 4). Here H = 2.5 kpc (SACKETT 1997) and β = 200 pc, neglecting the age and mass dependence of β. These estimates can not be compared directly to the space density, estimated from the observations: 3×10^{-6} pc^{-3} (WARNER 1995). In our model the space density is dominated by the long-period, dim systems, while Warner's estimate is based on the observed systems which are relatively bright. For a comparison of the observed and predicted populations we have to consider selection effects.

5.4.2 Observational selection effects: from the total population to the observable population

The known systems are typically discovered as faint blue stars (and identified with DB white dwarfs), as high proper motion stars, or as highly variable stars (see for the history of detection of most of these stars ULLA 1994; WARNER 1995). The observed systems thus do not have the statistical properties of a magnitude limited sample.

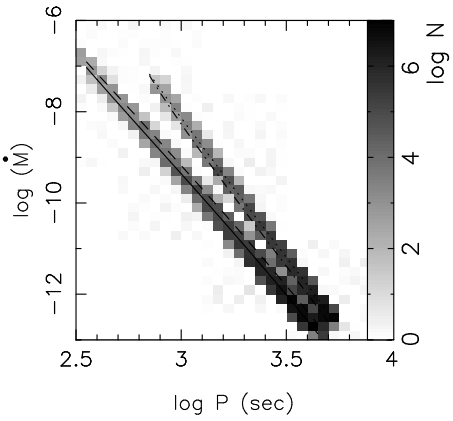

Figure 5.5 (continued)
The lines show the orbital period and mass transfer rate evolution and correspond to the lines in Fig. 5.4.

Moreover, the luminosity of AM CVn stars comes mainly from the disk in most cases. Despite the fact that several helium disk models are available (e.g. SMAK 1983; CANNIZZO 1984; TSUGAWA AND OSAKI 1997; EL-KHOURY AND WICKRAMASINGHE 2000) there is no easy way to estimate magnitude of the disk. Therefore, we compute the visual magnitude of the systems from very simple assumptions, to get a notion of the effect of observational selection upon the sample of interacting white dwarfs.

The luminosity provided by accretion is

$$L_{\rm acc} \approx 0.5\, G\, M \dot{m} \left(\frac{1}{R} - \frac{1}{R_{\rm L1}} \right). \tag{5.10}$$

Here R is the radius of the accretor and $R_{\rm L1}$ is the distance of the first Lagrangian point to the centre of mass of the accretor. We use an "average" temperature of the disk (see WADE 1984), which may be then obtained from $L = S\sigma T^4$, where S is the total surface of the disk:

$$S = 2\pi(R_{\rm out}^2 - R_{\rm WD}^2). \tag{5.11}$$

We use $R_{\rm out} = 0.7 R_{\rm L1}$. The visual magnitude of the binary is then computed from the effective temperature and the bolometric correction (taken from KUIPER 1938), assuming that the disk is a black body . This allows us to construct a magnitude limited sample

by estimating the fraction of the Galactic volume in which any system in our theoretical sample may be observed as it evolves.

We derive $P-\dot{M}$ diagrams for both models, similar to the ones for the total population, but now for the "observable" population, which we limit by V = 15. Changing $V_{\rm lim}$ doesn't change the character of graphs, since only the nearby systems are visible. The expected number of observable systems for the two families of progenitors is given in Tab. 5.1 and shown in Fig. 5.6 (pages 89 and 90). The observable sample comprises only one star for every million AM CVn stars that exists in the Galaxy. A large number of AM CVn stars may be found among very faint white dwarfs which are expected to be of the non-DA variety due to the fact, that the accreted material is helium or a carbon-oxygen mixture.

In the "inefficient" model I about one in 30 observed systems is from the white dwarf family. This is a considerably higher fraction than in the total AM CVn population where it is only one out of 100 systems. In the "efficient" model II, the white dwarf family comprises $\sim$ 60% of the total population and $\sim$ 50% of the "observable" one. The ratio of the total number of systems of the white dwarf family in models I and II is not proportional to the ratio of their current birth rates. This reflects the star formation history and the fact that the progenitors of the donors in model I are low mass stars that live long before they form a white dwarf. In model I the fraction of the observable systems which belong to the white dwarf family is higher than the fraction of the total number of systems that belong to this family. This is caused by the fact that the accretors in these systems are more massive (see Fig. 5.1, page 76), thus smaller, giving rise to higher accretion luminosities.

To compare our model with the observations, we list the orbital periods and the observed magnitude ranges for the known and candidate AM CVn stars in Table 5.2. For AM CVn we give $P_{\rm orb}$ as inferred by PATTERSON ET AL. (1993) and confirmed as a result of a large photometry campaign (SKILLMAN ET AL. 1999) and a spectroscopic study (Chapter 6). For the remaining systems we follow the original determinations or WARNER (1995). Most AM CVn stars show multiple periods, but these are close together and do not influence our qualitative analysis. KL Dra is identified as an AM CVn type star by its spectrum (JHA ET AL. 1998), but still awaits determination of its period. The periods of the observed AM CVn stars are shown in Fig. 5.6 as the vertical dotted lines. The period of RX J1914+24 is not plotted because this system was discovered as an X-ray source and it is optically much fainter than the limit used here.

Figures 5.5 and 5.6 show that the uncertainty in both models and observational selection effects make it hard to argue which systems belong to which family. According to model I the descendants of close double white dwarfs are very rare. However, in that case one might not expect two observed systems at short periods (AM CVn and HP Lib). In both models I and II, systems with long periods (like GP Com) are more likely to descend from the helium star family. In the spectrum of GP Com, however, MARSH ET AL. (1991) found evidence for hydrogen burning ashes in the disk, but no traces of helium burning, viz. very low carbon and oxygen abundances. It is not likely that any progenitor of the helium star family completely skipped helium burning. More probably,

TABLE 5.2: Orbital periods, visual magnitudes and theoretical mass estimates for known and candidate AM CVn stars. Theoretical mass estimates (in $M_{\odot}$) obtained from Eq. (5.5) are labelled by ZS, estimates from Eq. (5.8) by TF.

Name	Period sec	m_v	m (ZS)	m (TF)	Ref.
AM CVn	1028.7	14.1-14.2	0.033	0.114	1
HP Lib	1119	13.6	0.030	0.099	2
CR Boo	1471.3	13.0–18.0	0.021	0.062	3
V803 Cen	1611	13.2–17.4	0.019	0.054	2
CP Eri	1724	16.5–19.7	0.017	0.048	2
GP Com	2970	15.7–16.0	0.008	0.019	2
RX J1914+24	569	> 19.7	0.068	-	4
KL Dra		16.8–20			5

References: (1) PATTERSON ET AL. (1993), (2) WARNER (1995), (3)PROVENCAL ET AL. (1997), (4) CROPPER ET AL. (1998), (5) SCHWARTZ (1998)

this system belongs to the white dwarf family.

Most systems in the "observable" model population have orbital periods similar to the periods of the observed AM CVn stars that show large brightness variations; thus most modelled systems are expected to be variable. These brightness variations have been interpreted as a result of a thermal instability of helium disks (SMAK 1983). In Fig. 5.6 we show the thermal stability limits for helium accretion disks as derived by TSUGAWA AND OSAKI (1997): above the solid line the disks are expected to be hot and stable; below the horizontal dashed lines the disks are cool and stable and in between the disks are unstable. Note that the vast majority of the total Galactic model population (Fig. 5.5) is expected to have cool stable disks according to the thermal instability model, preventing them from being detected by their variability.

The period distributions of the "observable" population in our models agree quite well with the observed population of AM CVn stars. Better modelling of the selection effects is, however, necessary.

5.4.3 Individual systems

Table 5.2 (page 87)gives theoretical estimates of the masses of the donor stars in the observed AM CVn stars, derived from the relation between the orbital period and the mass of the donor (see Sect. 5.3.4 and Fig. 5.6).

AM CVn stars may be subject to tidal instability due to which the disk becomes eccentric and starts precessing. Such instabilities are used to explain the superhump phenomenon in dwarf novae (WHITEHURST 1988).

For AM CVn and CR Boo the observed 1051.2 s (SOLHEIM ET AL. 1998) and 1492.8 s (PROVENCAL ET AL. 1997) periodicities are interpreted as superhump periods. Following WARNER (1995) we compute the mass ratio of the binary system using the orbital period ($P_{\rm orb}$) and the superhump period ($P_{\rm s}$) via:

$$\frac{P_{\rm s}}{P_{\rm s}-P_{\rm orb}} \approx 3.73\,\frac{1+q}{q}. \tag{5.12}$$

This results is q = 0.087 and 0.057 for AM CVn and CR Boo respectively. Assuming that they belong to the white dwarf family their accretor masses are $M = 0.38\,{\rm M}_\odot$ and $M = 0.37\,{\rm M}_\odot$. These values are at the lower end of the predicted distribution. If we apply the semi-degenerate mass – radius relation, the estimated masses of the accretors are high, even close to the Chandrasekhar mass for AM CVn. The formation of systems with high-mass accretors has a low probability (see Fig. 5.3), which suggests that either Eq. (5.12) is not applicable for helium disks or alternatively that these binaries do not belong to the helium star family.

Maybe the most intriguing system is RX J1914.4+245: detected by *ROSAT* (MOTCH ET AL. 1996) and classified as an intermediate polar, because its X-ray flux is modulated with a 569 s period, typical for the spin periods of the white dwarfs in intermediate polars. CROPPER ET AL. (1998) and RAMSAY ET AL. (2000) suggest that it is a double degenerate polar with an orbital period equal to the spin period of the

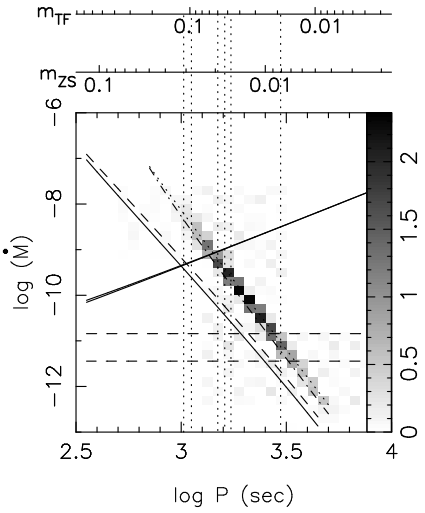

Figure 5.6: Magnitude limited sample ($V_{\rm lim}$ = 15) of the theoretical population of AM CVn stars for model I. The grey scale gives the number of systems, like in Fig. 5.5 but now on a linear scale (upper branch for the helium star family; lower branch for the white dwarf family). The selection criteria are described in Sect. 5.4.2. The periods of the observed systems (Table 5.2) are indicated with the vertical dotted lines.

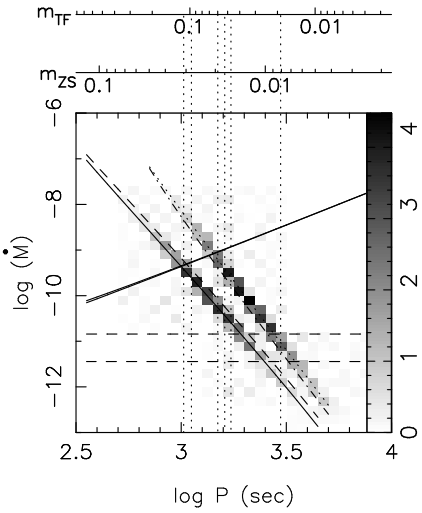

Figure 5.6 (continued)
The same for model II. The stability limits for the helium accretion disk according to TSUGAWA AND OSAKI (1997) are plotted as the slanted solid and dashed horizontal lines. Between these lines the disk is expected to be unstable. The upper dashed line is for an accretor mass of 0.5 $M_{\odot}$, the lower for a 1.0 $M_{\odot}$accretor. The rulers at the top indicate the theoretical relation between the period and the mass for the mass-radius relations of the two AM CVn star families given by Eqs. (5.5) and (5.8).

accreting white dwarf. The mass transfer rate in this system, inferred from its period ($\dot{m} \approx 1.8 \times 10^{-8}\,M_\odot\ yr^{-1}$) is consistent with the value deduced from the *ROSAT* PSPC data (CROPPER ET AL. 1998) if the distance is $\sim$100 pc.

Even though polars have no disk, the coupling between the accretor and donor is efficient due to the strong magnetic field of the accretor. We therefore anticipate that Eq. (5.4) applies without the correction introduced by Eq. (5.7). It may well be that magnetic systems in which the coupling is maintained by a magnetic field form the majority of stable AM CVn systems of the white dwarf family. We do not expect this system to belong to the helium star family, since its period is below the typical period minimum for the majority of the binaries in this family.

RX J0439.8-809 may be a Large Magellanic Cloud relative of the Galactic AM CVn systems. This system was also first detected by *ROSAT* (GREINER ET AL. 1994). Available X-ray, UV- and optical data suggest, that the binary may consist of two degenerate stars and have an orbital period < 35 min (VAN TEESELING ET AL. 1997, 1999).

RX J1914.4+245 and RX J0439.8-809 show that it is possible to detect optically faint AM CVn stars in supersoft X-rays, especially in other galaxies. The possibility of supersoft X-rays emission by AM CVn stars was discussed by TUTUKOV AND YUNGELSON (1996). There are two probable sources for the emission: the accreted helium may burn stationary at the surface of the white dwarf if $\dot{m} \sim 10^{-6}\,M_\odot\ yr^{-1}$ and/or the accretion disk may be sufficiently hot in the same range of accretion rates. However, the required high accretion rate makes such supersoft X-ray sources short-living (see Fig. 5.4) and, therefore, not numerous. Note that AM CVn, CR Boo, V803 Cen, CP Eri and GP Com are also weak X-ray sources (e.g. ULLA 1995).

The most recently found suspected AM CVn star, KL Dra, is also variable. Therefore we expect it to lie in the same period range as CR Boo, V803 Cen and CP Eri. Taking the limits for stability as given by TSUGAWA AND OSAKI (1997) we expect the orbital period to be between 20 and 50 minutes (Fig. 5.6).

5.5 Discussion

A population synthesis study for AM CVn stars (and related systems) was done by TUTUKOV AND YUNGELSON (1996), who considered only an "efficient" model. Their derived birth rate for the white dwarf family is $1.3 \times 10^{-2}\ yr^{-1}$, a factor three higher than the value in our "efficient" model. This difference can in part be explained by the different treatment of the mass transfer from a giant to a main sequence star of comparable mass (see Chapter 3; Chapter 4). Most close double white dwarfs in our model have a mass ratio close to unity for which stable mass transfer is impossible (Sect. 5.2), while in the model of TUTUKOV AND YUNGELSON (1996) they predominantly have $q \sim 0.5 - 0.7$ which is more favourable for stable mass transfer. Our higher integrated star formation rate only partly compensates for the loss of stable systems.

Another difference is that TUTUKOV AND YUNGELSON (1996) conclude that the helium star family (non-degenerate helium stars in their terminology) do not contribute significantly to the AM CVn population. This is a consequence of their assumption that

these systems, after the period minimum, live only for 10^8 yr. In contrast, our calculations show that their evolution is limited only by the lifetime of the Galactic disk. TUTUKOV AND YUNGELSON estimate the total number of AM CVn stars from the helium star family as $(1.9-4.6) \times 10^5$ depending on the assumptions about the consequences of the accretion of helium. We find 2×10^7 even when we let ELD destroy the systems which accrete only 0.15 $M_\odot$.

An additional complication is the possibility of the formation of a common envelope for systems where the accretion rate exceeds the rate of stationary helium burning at the surface of the accreting white dwarf ($\sim 10^{-6}\,M_\odot$ yr^{-1}). If such a common envelope forms the components of system may well merge. If it happens, it will occur directly after the Roche-lobe contact, when the highest accretion rate occurs. We do not consider this possibility in our model, because it involves too many additional (and unknown) parameters. Applying only the requirement that stable systems should accrete below the Eddington rate, we may overestimate the birth rate of AM CVn stars.

We did not discuss the Roche-lobe overflow by low-mass stars with almost exhausted hydrogen cores ($X_c \sim 0.01$) which may also result in the formation of helium transferring systems with orbital periods ~ 10 min (TUTUKOV ET AL. 1987) because of its extremely low probability.

The prescription for ELD is related to the problem of SN Ia progenitors. In model I almost all accretors in the helium star family with initial $M \geq 0.6\,M_\odot$ "explode" and the ELD rate is close to 0.001 yr^{-1}. If ELDs really produce SNe Ia, they may contribute about 25% of their currently inferred Galactic rate. In model II $0.3\,M_\odot$ must be accreted prior to the explosion, and the ELD rate is only about 4×10^{-4} yr^{-1}. Even in model I we find a much lower ELD rate than TUTUKOV AND YUNGELSON (1996, who find 0.005). This is partly due to a lower birth rate, but also to the different treatment of the mass transfer from a giant to a main sequence star of comparable mass (Chapter 3), which causes the accretors in our model mainly to have masses below 0.6 $M_\odot$. Such systems probably never experience ELD.

In model II the accretors in both families may accrete so much matter that they reach the Chandrasekhar mass. The rates for the white dwarf and helium star families for this process are 3×10^{-6} and 5×10^{-5} yr^{-1}.

In both families the accretors can be helium white dwarfs (see Figs. 5.1 and 5.3). It was shown by NOMOTO AND SUGIMOTO (1977) that accretion of helium onto helium white dwarfs with $\dot{m} = (1-4) \times 10^{-8}\,M_\odot$ yr^{-1} results either in a helium shell flash (at the upper limit of the accretion rates) or in central detonation which disrupts the white dwarf (for lower $\dot{m}$). The detonation occurs only when the mass of the accretor grows to $\sim 0.7\,M_\odot$. In our calculations this happens for the helium star family at a rate of $\sim 4 \times 10^{-6}$ yr^{-1}. For the white dwarf family it happens only in model II, at a rate of $\sim 2 \times 10^{-6}$ yr^{-1}.

5.6 Conclusions

We study the formation of AM CVn stars from (i) close detached double white dwarfs which become semi-detached and (ii) helium stars that transfer matter to a white dwarf and stop burning helium due to mass loss and become dim and semi-degenerate.

We find that, with our assumptions, in all cases where a double white dwarf potentially can form an AM CVn star no accretion disk will be formed in the initial phase of mass transfer. Normally the disk provides the feedback of angular momentum to the orbit, stabilising the mass transfer. In absence of a disk, the stability of the mass transfer in the semi-detached white dwarf binary depends critically on the efficiency of the coupling between the accretor and the donor. If this coupling is not efficient most systems merge, and the formation rate of AM CVn stars from double white dwarfs becomes very low. In this case it is possible that magnetically coupled systems are almost the only ones to survive. RX J1914.4+245 may be such a system.

In the second channel the formation of AM CVn stars may be prevented by explosive burning of the accumulated helium layer which may cause detonation of the CO white dwarf accretor and the disruption of the system.

We combine our population synthesis results into two models, an "efficient" model in which the stability of mass transfer is not affected by the absence of an accretion disk and the explosive helium burning disrupting the system happens when 0.3 $M_\odot$ is accumulated and an "inefficient" model in which the absence of an accretion disk is very important and the explosive helium disrupting the system happens already when 0.15 $M_\odot$ is accumulated. Applying very simple selection effects we estimate that in the "inefficient" model only one in 30 potentially observed systems descends from double white dwarfs. In the "efficient" model both families produce comparable numbers of observable systems. The observed systems fall roughly in the expected range of periods for a magnitude limited sample.

We conclude that to learn more about the AM CVn population both theory (stability of the mass transfer and helium accretion disks) and observations (especially the distances and the completeness of the sample) need to be improved.

Acknowledgements. We thank the referee Jan-Erik Solheim for valuable comments. LRY and SPZ acknowledge the warm hospitality of the Astronomical Institute "Anton Pannekoek". This work was supported by NWO Spinoza grant 08-0 to E. P. J. van den Heuvel, RFBR grant 99-02-16037, the "Astronomy and Space Research Program" (project 1.4.4.1) and by NASA through Hubble Fellowship grant HF-01112.01-98A awarded (to SPZ) by the Space Telescope Science Institute, which is operated by the Association of Universities for Research in Astronomy, Inc., for NASA under contract NAS 5-26555.

CHAPTER 6

Spectroscopic evidence for the binary nature of AM CVn

G. Nelemans, D. Steeghs & P. J. Groot

Monthly Notices of the Royal Astronomical Society, submitted

ABSTRACT

We analysed archival spectroscopic data of AM CVn taken with the William Herschel Telescope in 1996. In the literature two orbital periods are proposed. A clear S-wave in the He I 4471, 4387 and 4143 Å lines is revealed when the spectra are folded on the 1029 s period. No signature of this S-wave is seen when folded on 1051 s. Doppler tomography of the line profiles shows a clear signature of the hot spot. Using this we can constrain the value of K_2 to lie between 210 and 280 km s^{-1}. Our work confirms the binary nature of AM CVn beyond any doubt, establishes 1028.73 s as the true orbital period and supports the interpretation of AM CVn as a permanent superhump system.

6.1 Introduction

AM CVn (HZ 29) was found as a faint blue object by HUMASON AND ZWICKY (1947) and shows broad He I absorption lines (GREENSTEIN AND MATTHEWS 1957) and no hydrogen. Periodic brightness variations on a period of ∼18 min. (SMAK 1967) and flickering (WARNER AND ROBINSON 1972) suggested mass transfer in a very compact binary. A model in which a degenerate helium white dwarf transfers helium to another white dwarf, driven by the loss of angular momentum due to gravitational wave radiation was proposed by PACZYŃSKI (1967) and FAULKNER ET AL. (1972). See for details on the models for AM CVn stars and a list of the 8 currently known systems Chapter 5.

Since the discovery of the periodic brightness variations and the flickering, AM CVn has been extensively studied with high speed photometry (e.g SKILLMAN ET AL. 1999; SOLHEIM ET AL. 1998) yielding multiple periodicities on 1051, 1011 and 1029 s (see also SOLHEIM ET AL. 1991; HARVEY ET AL. 1998). Spectroscopic observations

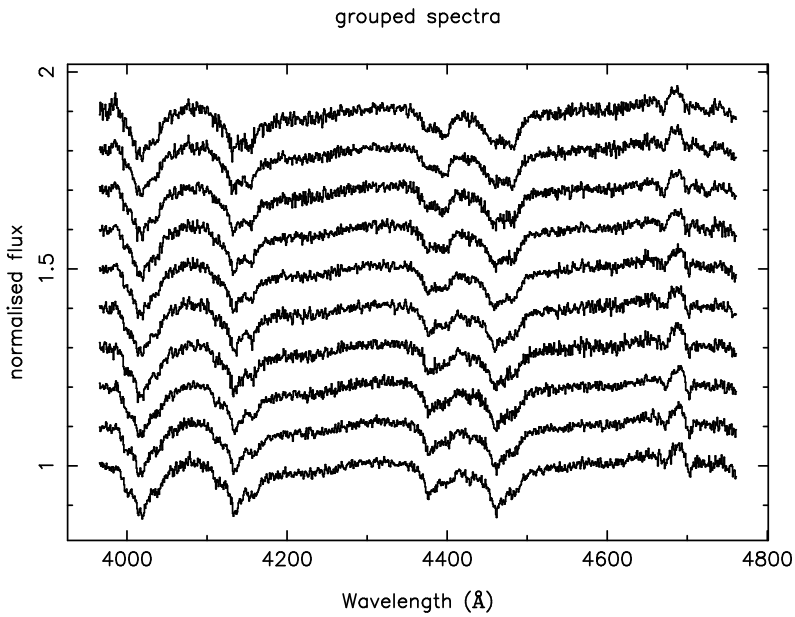

Figure 6.1: Spectra of the second night averaged into 10 groups of 40 consecutive spectra added together after normalising the continuum. The spectra show the change in the shape of the absorption lines over the 5 hours of the observation (see Sect. 6.3.4).

(PATTERSON ET AL. 1993) show a 13.38 hr periodicity in the skewness of the He I absorption lines.

According to SOLHEIM ET AL. (1998) the dominant 1051 s photometric period is the orbital period and the 1029 s a beat between the orbital period and the 13.38 hr precession period of the accretion disk. However, SKILLMAN ET AL. (1999) argue that 1029 s is the orbital period and 1051 s is the beat period. In the latter case, the system would be similar to the permanent superhump systems among the hydrogen rich cataclysmic variables (SKILLMAN ET AL. 1999).

To discern between these two possibilities and to establish beyond doubt the binary nature of AM CVn, a spectroscopic signature at either period is needed. In this article we describe a spectroscopic study of AM CVn in which we found a clear signature on the 1029 s period, proving that this is the orbital period of the system.

6.2 Data reduction

We analysed archival spectroscopic data obtained on the 4.2m William Herschel Telescope on February 26 and 27, 1996, with the ISIS spectrograph. In the first night a dichroic was used with both the ISIS red and blue arm. Because of ripples in the blue part of the spectrum introduced by the dichroic, it was removed on the second night

and only blue spectra were taken. Because of the ripples and the lack of flat-fields of high quality for the first night we mainly discuss the data taken on the second night. In the blue arm the spectra were obtained with the R600B grating covering 3960-4760 Å at a resolution of 2.0 Å.

There are 403 spectra taken on the second night (173 on the first), each with an integration time of 30 s. Wavelength calibration lamp exposures were taken approximately every 50 spectra (about every 40 minutes). The spectra were reduced using the standard data reduction package MIDAS. After bias subtraction and flatfielding the spectra were extracted and wavelength calibrated. The wavelength calibration was very stable (less than half a pixel change between the subsequent arc spectra) and the calibration of each arc spectrum was used for the 25 spectra taken before and the 25 spectra taken after the arc without interpolation. The flat-field for the first night was taken at the beginning of the second night and had to be corrected for a small wavelength shift.

The continuum of the wavelength calibrated spectra was fitted with a cubic spline of order 3 to line free areas and used to normalise all spectra with respect to their continuum level. In Fig. 6.1 we show the resulting spectra of the second night after averaging them into 10 groups over the whole night.

6.3 Data analysis

6.3.1 A period search

In order to search for line profile variations on the uncertain orbital period of the binary, an equivalent width (EW) lightcurve was constructed using the combined EW of the four strongest He I lines. A Lomb-Scargle power spectrum (Fig. 6.2) indeed reveals a clear peak around 3.5 cycles/hour, close to the expected orbital period of 17 minutes.

Because the accuracy of the candidate orbital periods as derived from the photometric studies of AM CVn exceeds the accuracy of our period determination using the EW lightcurve, we folded the data set on the two proposed orbital periods, 1028.73 s (SKILLMAN ET AL. 1999) and 1051.2 s (SOLHEIM ET AL. 1998). Both periods lie very close to the peak in our power spectrum.

An emission component is seen to be moving periodically through the line profiles when the spectra are folded on 1029 s, but not when they are folded on 1051 s (Figure 6.3). This S-wave is a characteristic signature in the line profiles of accreting binaries caused by the impact of the gas stream onto the accretion disk around the primary (e.g. MARSH 1990; SPRUIT AND RUTTEN 1998; MARSH 1999). The phase resolved spectroscopy thus provides a definite spectroscopic signature of the true orbital period of AM CVn, and firmly establishes its binary nature.

The S-wave is most clearly visible in the He I lines at 4387 and 4471 Å, but can also be discerned in the line at 4143 Å. The He II lines at 4686 and 4199 Å, however, do not show any evidence for S-waves on the orbital period. The S-wave is strongest moving from redshift to blueshift, but only barely present when moving from blue to red. This reflects the fact that the hot spot is mainly visible when it is at the front of the system

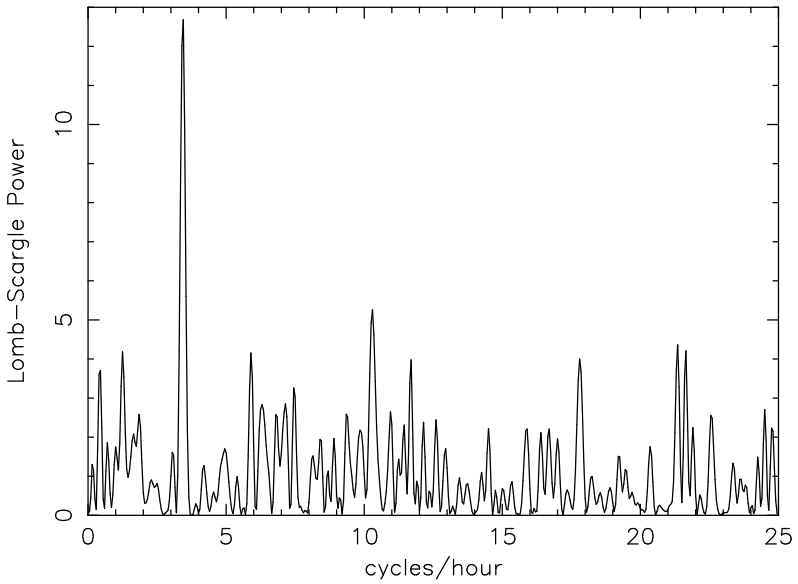

Figure 6.2: Lomb-Scargle power spectrum of the equivalent width lightcurve of the 4 strongest He I lines. The peak at 3.5 cycles/hour points to an orbital period around 1030s.

as observed from Earth. Note that when the spot comes to the front the velocity of the stream and of the disk at the impact point are directed away from the observer and thus redshifted.

6.3.2 Doppler tomography

As a next step we applied Doppler tomography in order to reveal the velocity structure in the lines as well as to establish the exact velocity of the S-wave. Doppler mapping (MARSH AND HORNE 1988) uses the time dependent line profile shapes to reconstruct the distribution of line emission/absorption in the corotating frame of the binary. Each point in the corotating frame contributes to the line profiles with a particular velocity amplitude and phase, so the phase resolved profiles can be converted to two dimensional velocity patterns. Doppler mapping is a widely applied tool in the study of the strong emission lines in CVs. It has revealed a variety of structures associated with the accretion disk around the primary in interacting binaries such as bright spots, spiral arms and magnetic streams (MARSH 2001).

So far we have used an arbitrary zero point for our orbital phases since the absolute phase is not known from the photometry. In order to estimate the absolute orbital phase of the binary, where phase 0.0 is defined as superior conjunction of the primary star, we analysed the line profile behaviour when folded on the 1029 s orbital period. The line profiles are complex with a mix of absorption and emission components present at any

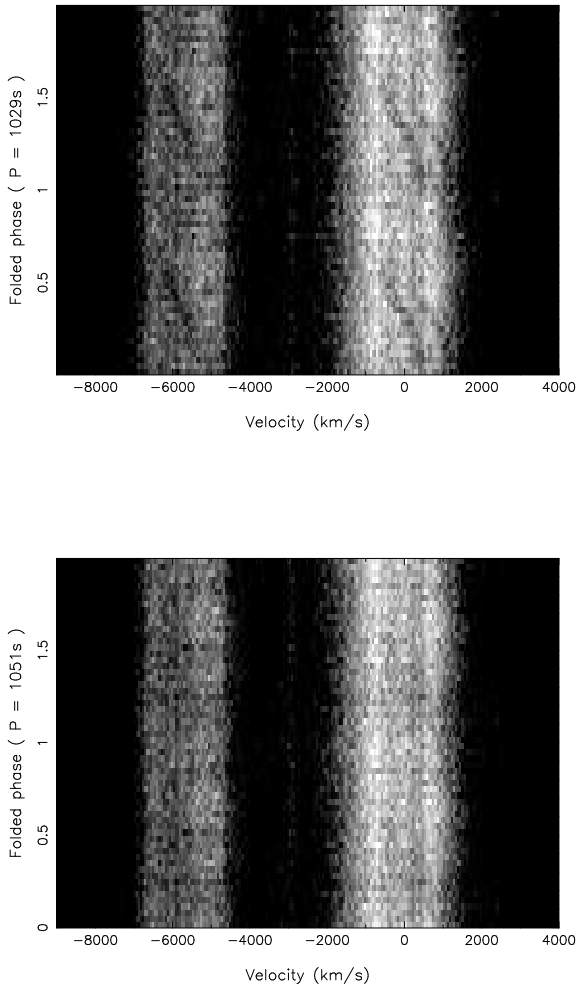

Figure 6.3: Trailed spectrogram of the He I 4387 and 4471 Å line profiles (absorption in white). **Top:** after folding on the candidate orbital period of 1028.73 s. **Bottom:** after folding on 1051.2 s. The gray scale is chosen in order to highlight the weak emission components in the core of the lines. A clear emission component is visible in both lines when the data are folded on 1029 s only, indicating that this is indeed the true orbital period of AM CVn.

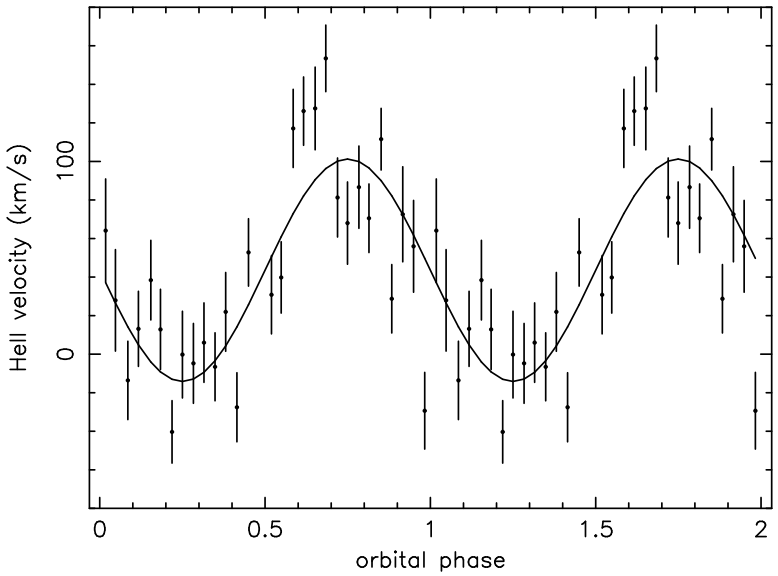

Figure 6.4: The radial velocities of the He II line, derived from a Gaussian fit as a function of orbital phase. A sinusoidal fit is used to establish the absolute orbital phases and derive an upper limit to the radial velocity of the primary.

given time. The He II 4686 Å line is an exception and consist of a single emission component superimposed on an absorption trough, and shows no evidence for an S-wave. We fitted the He II emission component with a simple Gaussian, in order to measure its radial velocity as a function of binary phase. The radial velocity of the He II line shows a systematic variation with an amplitude of 53 ± 6km s^{-1} when fitted with a simple sine-function (Fig. 6.4). If the emission is associated with the accretion flow around the primary, this gives us an indication of the motion of the primary white dwarf. Care must be taken since asymmetries in the distribution of the He II emission around the primary also introduces apparent radial velocity shifts. So rather than assuming that the derived velocity is indeed the projected velocity of the white dwarf (K_1), we merely use the relative phasing in order to construct a more reliable zero point for our phases. The derived velocity amplitude can be taken as an upper limit to the projected velocity of the white dwarf. Using the convention that orbital phase zero corresponds to superior conjunction of the primary, we then derive the following orbital ephemeris for AM CVn:

$$T_0(HJD) = 2450140.6135(2) + 0.011906623(3)E$$

with the formal uncertainty of the zero point indicated between brackets and the period taken from SKILLMAN ET AL. (1999). In all plots, the orbital phases shown are the result of folding using the above ephemeris.

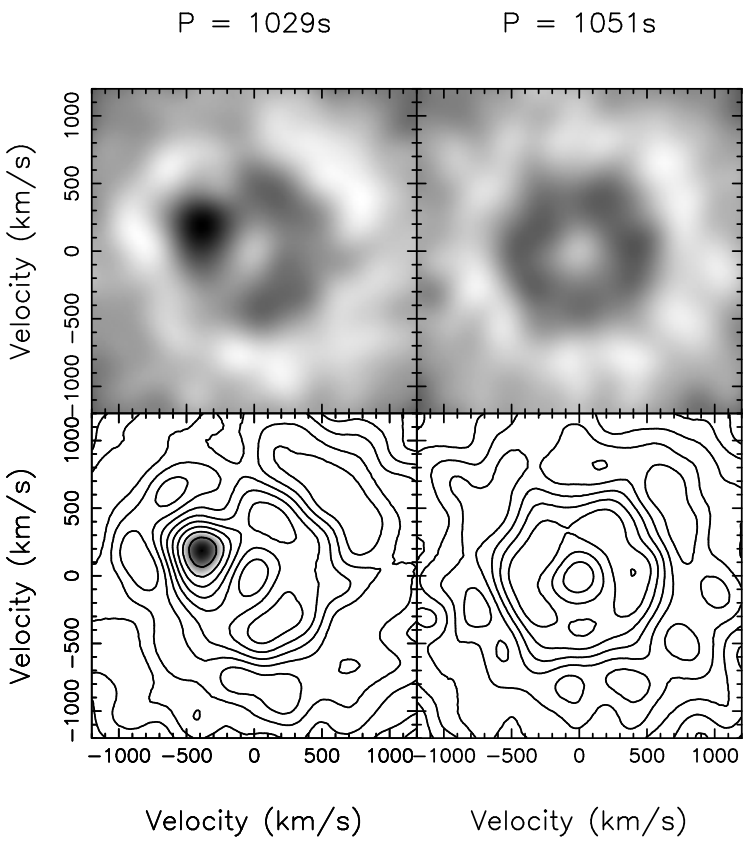

Figure 6.5: Filtered back-projection of the He I 4471 Å line profiles on the orbital period of 1029 s as well as the photometric period of 1051 s. The hot spot produces a prominent spot superposed on weak disk emission if folded on the correct period only. (Darker indicates more emission). The bottom two panels are the same images displayed as a contour plot. Any emission significantly brighter than the emission from the disk ring is overplotted as a gray scale, revealing the strong spot in the left tomogram.

There are two methods of calculating Doppler tomograms from phase resolved spectroscopy. One is a straightforward back projection in conjunction with a Fourier filter (HORNE 1991), the other applies maximum entropy regularisation (MARSH AND HORNE 1988). Our goal is to isolate the weak emission components in the cores of the He I absorption lines. To this end the filtered back projection method is preferred, since a maximum entropy reconstruction requires pure emission line profiles. Although more prone to reconstruction artifacts, the back-projection method can be applied to the complex line profiles of AM CVn without additional data processing. The results of back projecting the line profiles of the He I 4471 Å line are plotted in Fig. 6.5. Again we

compare the back projection of the line profiles folded on the two periods; 1029 s and 1051 s. In the case of 1029 s, the S-wave maps into a prominent spot in the Doppler tomogram that is absent when folded on 1051 s. The location of the emission spot is where hot spot emission is indeed expected, giving us confidence in the orbital ephemeris that is derived and our previous interpretation of the S-wave as due to the hot spot on the outer edge of the accretion disk.

6.3.3 The radial velocity of the mass donor

Apart from the hot spot itself, a weak ring of emission is visible in Fig. 6.5 from the rest of the accretion disk. At higher velocities this weak emission turns into absorption which produces the broad deep absorption wings in the lines. Having established the true orbital period of AM CVn, we can also constrain other system parameters using the position of the bright spot. The hot spot is the result of local heating and dissipation at the outer rim of the disc where the infalling gas stream impacts. In most cases, the emission has the velocity of the free falling stream (e.g. MARSH AND HORNE 1990). However, in other cases the velocity of the hot spot gas appears to be a mix of the fall velocity as well as the local velocity flow in the disk at the impact point (MARSH 1990). This unfortunately means that a straightforward fit to the position of the hot spot using single particle trajectories is unreliable. However, some interesting limits can still be obtained. First of all the velocity amplitude of the spot itself (403 ± 15 km s^{-1}) provides an upper limit to the possible projected velocity of the mass donor star (K_2), since the velocity of its centre of mass cannot be larger than that of the hot spot itself. Very low values of K_2 also lead to gas stream trajectories that are incompatible with the data. For a given choice of K_1, K_2, we can calculate the trajectory of the gas stream as well as the velocity vector of the disk flow in order to isolate those parts in the tomogram where hot spot emission is possible. We shall see later that the mass ratio $q(= M_2/M_1)$ of AM CVn is most likely 0.087, which means that for a given choice of K_2, K_1 is derived from $K_1 = qK_2$.

If we assume that the hot spot velocities in AM CVn reflect the velocity of the ballistic gas stream, we can achieve a good fit to the observed tomogram using $K_2 = 260$ km s^{-1} and $K_1 = 23$ km s^{-1} (Fig. 6.6). If we relax our assumptions and only require that the observed velocities of the hot spot lie anywhere between the trajectory of the gas stream, and that of the disc, we can constrain K_2 to lie between 210 and 265 km s^{-1}. The assumed value of the mass ratio has only a small effect on the derived values for K_2.

The least constrained range for K_2 is obtained if we also consider the zero point of our orbital phases to be a free parameter. Then, in principle, K_2 can lie between 200 and 400 km s^{-1}. Note, however, that in order to fit the data with $K_2 > 280$ km s^{-1}, we need to apply an arbitrary phase shift in order for the stream to cross the hot spot, which also leads to an unrealistic impact radius that is very close to the white dwarf. We can thus firmly constrain the value of K_2 to lie between 210 and 280 km s^{-1}.

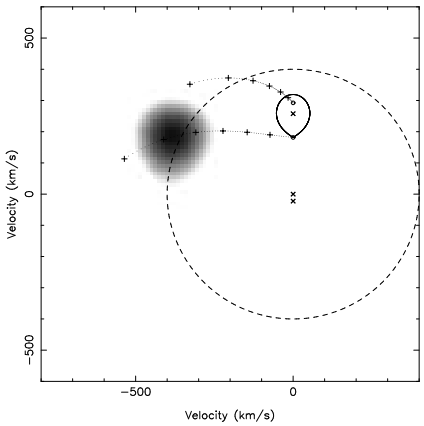

Figure 6.6: Ballistic trajectories that fit to the location of the hot spot. The observed position of the hot spot is plotted as a gray scale. Overplotted is the best fit ballistic stream trajectory, if the hot spot corresponds to pure free fall velocities. The corresponding velocities of the disk are indicated by the second trajectory above the ballistic one. The observed hot spot velocities need to lie in between these two trajectories for a given choice of K_2, leading to possible K_2 values between 210 and 265 km s^{-1}. The Roche lobed shape indicates the location of the mass donor star in the tomogram and the three crosses the centres of mass of the two components and the binary system.

6.3.4 Disk precession and superhumps

PATTERSON ET AL. (1993) have found a 13.38 hr period in the skewness of the He I absorption lines. From Fig. 6.1 (page 96) we see indeed that the shape of the absorption lines changes during the 5 hrs of the total observation. This can be interpreted as the varying double peaked absorption profiles of a precessing accretion disk. We measured the skewness of the line profiles in our data by fitting multiple Gaussians to the absorption lines as follows. Since there is evidence for emission in the line cores, which modulates on the much shorter orbital period compared to the slow changes in the absorption lines on the precessing periods, the central emission was masked. Double Gaussians were fitted to the absorption components in order to measure the relative strength of the blue shifted absorption relative to the redshifted absorption. The spectra of both nights were grouped into bins of 10 consecutive spectra to improve signal to noise and the line asymmetry was measured accordingly. This double Gaussian method was found to be more reliable that calculating the formal skewness of the line as a whole since the emission components can be masked so as not to distort the measurements. Fig. 6.7 plots the derived line asymmetry together with a sinusoidal least squares fit. We do not cover the full precession cycle, so cannot improve on the precession period derived by Patterson

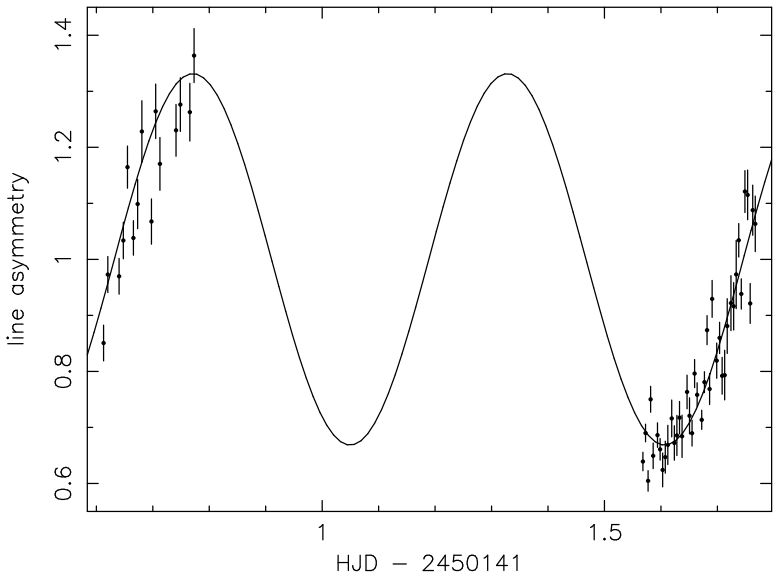

Figure 6.7: The change in relative absorption on the redshifted versus the blueshifted side across the 13.38 hour precession cycle. Plotted is the line asymmetry derived from a double Gaussian fit as a function of HJD. A least squares sinusoidal fit is overplotted.

et al. (13.38 hours) and fixed the period in the fit. The asymmetry is expressed as the ratio between the depths of both Gaussians. The relative contribution of the red versus blue shifted side of the disk thus changes with an amplitude of 33% across the precessing cycle.

TABLE 6.1: System parameters for the two different mass radius relations: deg. for fully degenerate mass – radius relation for white dwarfs and semi for the semi-degenerate mass radius relation for the final products of helium CVs (from TUTUKOV AND FEDOROVA 1989, see Chapter 5). The inclination is determined assuming K_2 = 260 km s^{-1}.

	M_2 ($M_\odot$)	M_1 ($M_\odot$)	K1/sin i (km s^{-1})	K2/sin i (km s^{-1})	i °
deg.	0.033	0.38	55.5	637.4	24.1
semi	0.114	1.31	83.7	961.8	15.7

6.4 Discussion

The fact that AM CVn behaves very similarly to the hydrogen rich superhump systems (PATTERSON ET AL. 1993) suggests that the superhump phenomena has the same origin (WARNER 1995). The precession of the disk in superhump systems is caused by a tidal resonance between the disk and the companion which is expected for mass transferring systems with a mass ratio smaller than 0.22 (e.g. WHITEHURST 1988). The numerical simulations of HIROSE AND OSAKI (1990, 1993) show that there is a relation between the precession period, the orbital period and the mass ratio (WARNER 1995)

$$\frac{P_{\rm prec}}{P_{\rm orb}} = A\frac{1+q}{q} \tag{6.1}$$

where $A \approx 3.73$ for systems with $q < 0.1$. Because of the tidal origin of the phenomenon there is no reason to expect a different relation for helium discs. Using 1028.73 s for the orbital period and 13.38 hr for the precession period, this relation gives a mass ratio for AM CVn of 0.087.

From the well known fact that for a Roche-lobe filling star the period only depends on the mass and radius of the donor we can calculate the mass of the donor in AM CVn from the period and the mass – radius relation. From the two evolutionary scenarios that are proposed to lead to AM CVn stars, two mass – radius relations for the donor stars are found (WARNER 1995, Chapter 5). From the mass ratio the companion mass is found. In Table 6.1 we give the two solutions for AM CVn using the mass – radius relation as given in Chapter 5.

From the system parameters we can calculate the radial velocities of the two components, which we can compare to the values of K_2 as derived from the Doppler tomograms. In Table 6.1 we give the expected values of the radial velocities ($K_{1,2}/\sin i$) and the resulting values for the inclination assuming K_2 = 260 km s^{-1}.

The derived inclinations are low, consistent with the fact that no eclipses are observed (which means $i < 78°$ for q = 0.087). The only clue to discern the two mass – radius relations (and thus the formation scenario) may be the fact that the hot spot is obscured

when moving from blue to red, implying not too low inclination. This would slightly favour the fully degenerate mass radius relation.

The value of K_1 derived from the mass ratio of 0.087 (23 km s^{-1}) seems incompatible with the interpretation of the radial velocity of the He II line as being caused by the motion of the primary. However it could be that the mass ratio determined from the superhump period is incorrect for AM CVn. For example for a mass ratio of 0.2, the value of K_1 would be 52 km s^{-1}. This also would bring the mass of the primary down, which rules out the fully degenerate mass – radius relation, but gives somewhat more realistic value for the primary mass in the case of the semi-degenerate mass – radius relation (see for more details Chapter 5).

Evidence for time variability of the strength of the hot spot was found by folding both nights separately. Using the the first night only, no discernible S-wave could be identified. However, the second night alone, resulted in a clearly visible S-wave in several lines. This offers opportunities to study the strength and position of the hot spot as a function of the precessing cycle, allowing a straightforward determination of the mass ratio provided adequate signal to noise can be obtained.

6.5 Conclusion

We found a clear S-wave in spectra of AM CVn when folded on a period of 1029 s, confirming the binary nature of AM CVn beyond any possible remaining doubt and establishing 1028.73 s as the true orbital period. The dominant photometrical period of 1051.2 s can be interpreted as the beat between the orbital period and the 13.38 hr period that has been found in the skewness of the absorption lines, making the system the helium equivalent of the permanent superhump systems. The 13.38 hr period then is interpreted as the precession period of the accretion disk. The shape of the absorption lines in our data set changes on the same period. By applying Doppler tomography we were able to constrain the value of K_2 between 210 and 265 km s^{-1}, which given the formation channels implies a low inclination (between $\sim 15°$ and $\sim 25°$).

Our results open a new field of studying the details of these intriguing ultra-compact binaries by phase resolved spectroscopy and Doppler tomography.

Acknowledgements. We thank Tom Marsh for motivating discussion and the use of the MOLLY data reduction package. This paper makes us of data obtained from the Isaac Newton Group Archive which is maintained as part of the Astronomical Data Centre at the Institute of Astronomy, Cambridge. The William Herschel Telescope is operated on the island of La Palma by the Isaac Newton Group in the Spanish Observatorio del Roque de los Muchachos of the Instituto de Astrofisica de Canaria. GN is supported by NWO Spinoza grant 08-0 to E. P. J. van den Heuvel, DS is supported by a PPARC fellowship and PJG is supported by a CfA fellowship.

CHAPTER 7

Constraints on mass ejection in black hole formation derived from black hole X-ray binaries

G. Nelemans, T. M. Tauris & E. P. J. van den Heuvel

Astronomy & Astrophysics, 1999, 352, L87 – L90

ABSTRACT

Both the recently observed high runaway velocities of Cyg X-1 ($\sim$ 50 km s^{-1}) and X-ray Nova Sco 1994 ($\geq$ 100 km s^{-1}) and the relatively low radial velocities of the black hole X-ray binaries with low-mass donor stars, can be explained by symmetric mass ejection in the supernovae (SNe) which formed the black holes in these systems.

Assuming symmetric mass ejection in black hole formation, we estimate the amount of mass that must have been ejected in the stellar core collapse in order to explain the velocities of the above X-ray binaries. We find that at least 2.6 $M_\odot$ and 4.1 $M_\odot$ must have been ejected in the formation of Cyg X-1 and Nova Sco, respectively. A similar mass-loss fraction (f = 0.35) for the black hole binaries with low-mass donors, gives low velocities, in agreement with the observations.

We conclude that the black holes in X-ray binaries are all consistent with being formed in a successful SN in which mass is ejected. A possible kick at the formation of the black hole is not needed to explain their space velocities.

7.1 Introduction

The light curve and spectrum of the abnormally luminous type Ic SN 1998bw (GALAMA ET AL. 1998) suggest that in this event a black hole was formed (IWAMOTO ET AL. 1998). The observations imply that a considerable fraction of the mass of the progenitor (a massive C/O core) was ejected in the explosion (IWAMOTO ET AL. 1998). Similarly, the observed overabundance of the elements O, Mg, Si and S in the atmosphere of the

TABLE 7.1: Properties of black hole X-ray binaries. The velocity of Cyg X-1 is its space velocity, all other velocities are radial velocities, so are lower limits.

Source	$M(M_\odot)$	$m(M_\odot)$	P (d)	v (km s^{-1})
Nova Sco 1994	6.29–7.60	1.6–3.1	2.62	106±19
Cyg X-1	3.9–15.2	11.7–19.2	5.6	49±14
V 404 Cyg	6–12.5	0.6	6.5	8.5±2.2
A 0620-00	3.3–4.24	0.15–0.38	0.32	15±5
Nova Muscae	>4.45±0.46	0.7	0.43	26±5
Nova Oph 1977	5–7	0.7	–	38±20
GRO J0422+32	3.25–3.9	0.39	0.21	11±8
GS2000+25	6.04–13.9	0.26–0.59	0.35	18.9±4.2

Masses and periods from ERGMA AND VAN DEN HEUVEL (1998) and references therein, velocities from BRANDT ET AL. (1995) and references therein, except for GRO J0422+32 (HARLAFTIS ET AL. 1999) and GS2000+25 (HARLAFTIS ET AL. 1996) which are heliocentric γ-velocities. For Nova Sco 1994 we changed the velocity according to the new γ-velocity of 142 km s^{-1} (SHAHBAZ ET AL. 1999). Space velocity for Cyg X-1 is from KAPER ET AL. (1999).

companion of Nova Sco 1994, indicates considerable mass ejection in the formation of this black hole (ISRAELIAN ET AL. 1999).

From a study of the z-distribution of the population of black hole X-ray binaries with low-mass donors, WHITE AND VAN PARADIJS (1996) conclude that the velocity dispersion of these X-ray binaries is of the order of 40 km s^{-1}. Since the velocity dispersion of the progenitor systems is expected to be around 17 km s^{-1}, they estimate the extra velocity that is given to the system in the formation of the black hole to be 20 – 40 km s^{-1}. This requires substantial mass ejection in the formation of a black hole if no asymmetric kicks are involved.

Recent determinations of the space velocity of Cyg X-1 (KAPER ET AL. 1999) and the radial velocity of Nova Sco (BAILYN ET AL. 1995) demonstrate that these black hole binaries have significantly higher runaway velocities than the black hole X-ray binaries with low-mass donors.

In Table 7.1 we have listed the relevant properties of the Galactic black hole binaries for which one, or more, of its velocity components have been measured.

7.2 Origin of the black hole binary runaway velocities

There are two effects to accelerate a binary system by a supernova explosion. The first is caused by the ejection of material from the binary (BLAAUW 1961). The centre of mass of the ejected matter will continue to move with the orbital velocity of the black hole

progenitor. To conserve momentum, the binary will move in the opposite direction. The second one is an additional velocity kick, which is produced by asymmetries in the supernova explosion itself and for which there is strong evidence in the case of the formation of a neutron star (e.g. LYNE AND LORIMER 1994; HARTMAN 1997).

The current status quo of supernova simulations is that in order to get a successful supernova, in which the shock is reversed and matter is ejected, one needs to form a neutron star (BETHE AND WILSON 1985). If the supernova is not so energetic, there may be considerable fall back, turning the neutron star into a black hole (e.g COLGATE 1971; WOOSLEY AND WEAVER 1995). Formation of a black hole without an intermediate neutron star would then not result in mass ejection. However, if other mechanisms than neutrino heating will be found to reverse the supernova shock (e.g rotation), this conjecture of both mechanisms may be broken.

BRANDT ET AL. (1995) have listed a number of scenarios for reproducing the high radial velocity measured in Nova Sco. They show that though mass ejection alone can explain the velocity of Nova Sco 1994, the allowed range of initial masses is very small. They therefore conclude that Nova Sco is formed in a delayed black hole formation, in which the kick, which is imparted to the initial neutron star, is responsible for a considerable fraction of the present system velocity. The black holes in the other binaries would then be formed by a direct collapse without mass ejection and kicks. The velocity dispersion found by WHITE AND VAN PARADIJS (1996) can be explained by scattering at molecular clouds and density waves, since these binaries could be an old population (PODSIADLOWSKI, private communication; see also BRANDT ET AL. 1995).

With the new discovery of the relatively high velocity of Cyg X-1, we think the above is unlikely, because now the two systems with highest mass companions must have formed through a delayed black hole formation, while the systems with low-mass companions form in a direct collapse. This would mean that the success of the SN in which the black hole is formed is related to the nature of its binary companion, for which we see no reason

TUTUKOV AND CHEREPASHCHUK (1997) discuss the system velocities of the X-ray binaries containing black holes and conclude that all velocities can be explained with mass ejection alone. However, they only consider the maximum velocity that can be obtained with the observed limits on the masses of both stars, assuming the shortest possible period at the moment of the SN and the maximum amount of mass that can be ejected without disrupting the binary. In that case, the pre-SN mass ratio is not independent of the final (observed) mass ratio and it would be better to use the current (observed) mass ratio, with which their equation (7) would become

$$v_{\rm max} = 192 \left(\frac{q_{\rm obs}}{1 + q_{\rm obs}} \right)^{0.72} \qquad {\rm km\ s^{-1}}. \tag{7.1}$$

See also the discussion in section 7.5.

We now investigate the effect of the mass ejection in more detail, assuming possible kicks are (relatively) unimportant.

7.3 Runaway velocities from symmetric SNe

Consider a circular pre-SN orbit of a binary consisting of a helium star with mass $M_{\rm He}$ (the progenitor of the black hole) and a companion star with mass m. Assume that the helium star explodes in a symmetric SN during which an amount of mass, ΔM is ejected instantaneously and decouples gravitationally from the system. If $\Delta M = M_{\rm He} - M_{\rm BH} < 0.5\,(M_{\rm He} + m)$ the binary will remain bound. The post-SN eccentricity, period and orbital separation are given by BHATTACHARYA AND VAN DEN HEUVEL (1991)

$$e_{\rm postSN} = \frac{\Delta M}{M_{\rm BH} + m} = \frac{1-\mu}{\mu} \tag{7.2}$$

$$P_{\rm postSN} = P_{\rm i}\,\frac{\mu}{(2\mu-1)^{3/2}}, \tag{7.3}$$

where we define

$$\mu = \frac{M_{\rm BH} + m}{M_{\rm He} + m} = \frac{M_{\rm He} + m - \Delta M}{M_{\rm He} + m} \tag{7.4}$$

and subscripts i denote the pre-SN system. Since the observed black hole binaries all have short orbital periods (< 7 days) tidal forces act to re-circularize the post-SN orbit. The parameters of the re-circularized orbit are given by

$$P_{\rm re-circ} = P_{\rm postSN}(1 - e^2_{\rm postSN})^{3/2} = P_{\rm i}/\mu^2. \tag{7.5}$$

And similarly $a_{\rm re-circ} = a_{\rm i}/\mu$. Here we have ignored the effects of the impact of the ejected shell on the companion star and assume there is no mass loss or transfer during the re-circularization phase. From conservation of momentum one finds an expression for the resulting runaway velocity (recoil) of the system

$$v_{\rm sys} = \frac{\Delta M\, v_{\rm He}}{M_{\rm BH} + m}, \tag{7.6}$$

where $v_{\rm He}$ is the pre-SN orbital velocity of the exploding helium star in a centre-of-mass reference frame. Together with Keplers third law we find

$$v_{\rm sys} = (G\,2\pi)^{1/3}\,\Delta M\, m\, P^{-1/3}_{\rm re-circ}\,(M_{\rm BH} + m)^{-5/3}. \tag{7.7}$$

For convenience this equation can be expressed as

$$v_{\rm sys} = 213 \left(\frac{\Delta M}{M_\odot}\right) \left(\frac{m}{M_\odot}\right) \left(\frac{P_{\rm re-circ}}{\rm day}\right)^{-\frac{1}{3}} \left(\frac{M_{\rm BH} + m}{M_\odot}\right)^{-\frac{5}{3}} {\rm km\ s^{-1}}. \tag{7.8}$$

If we know the masses of the stellar components and the orbital period after the re-circularization ($M_{\rm BH}, m, P_{\rm re-circ}$) we can calculate ΔM from the observed runaway velocity, $v_{\rm sys}$. However, we observe mass-transferring binaries which might have evolved

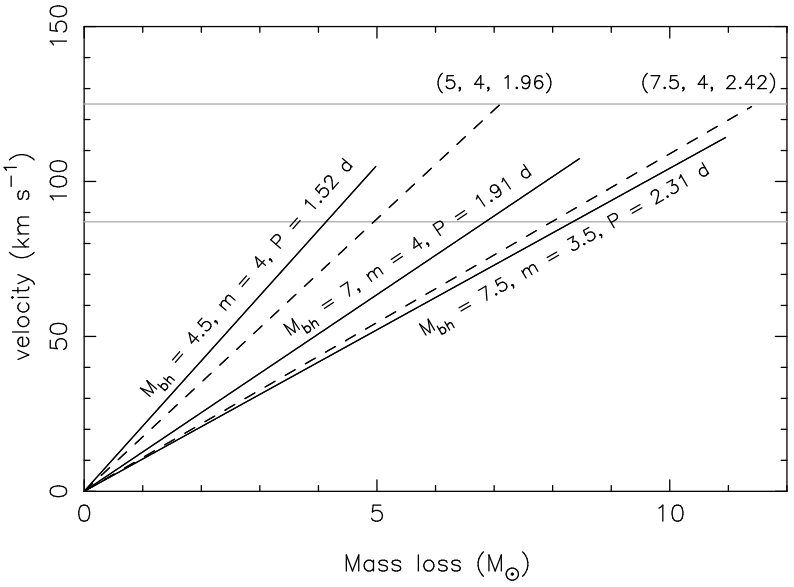

Figure 7.1: Limits on the amount of mass ejected in the SN explosion that is required to explain the measured velocities for Nova Sco 1994 with three possibilities of the binary parameters at the onset of the X-ray phase (solid lines; see text) and the two possibilities in the case 0.5 $M_\odot$ has been lost draining angular momentum (dashed lines).

due to loss of angular momentum by gravitational radiation or magnetic braking before the mass transfer started and/or might have transferred already a significant amount of mass from the donor to the black hole. Before applying equation (7.8) to the observed systems we have to correct for these effects.

Also, one has to check whether the binary before the SN would be detached, i.e. that both stars do not fill their Roche lobes at the moment the SN explodes.

7.4 Results

7.4.1 Nova Sco 1994

SHAHBAZ ET AL. (1999) have recently determined the present stellar masses in Nova Sco 1994 (GRO J1655-40). They find $M_{\rm BH} = 5.5-7.9\,M_\odot$ and $m = 1.7-3.3\,M_\odot$. The mass transfer in Nova Sco 1994 may already have been going on for a long period of time. From the luminosity and effective temperature of the donor star in this system one finds, using stellar evolution tracks, that the donor can not have started out with a mass larger than $4.0\,M_\odot$ at the onset of the X-ray phase (VAN DER HOOFT ET AL. 1998). As an example of combinations of present masses we use $(M_{\rm BH}, m) = (6, 2.5)$ and (7.75, 3.25). Assuming conservative mass transfer ($P_{\rm re-circ}/P_{\rm obs} = [(M_{\rm BH,obs} m_{\rm obs})/$

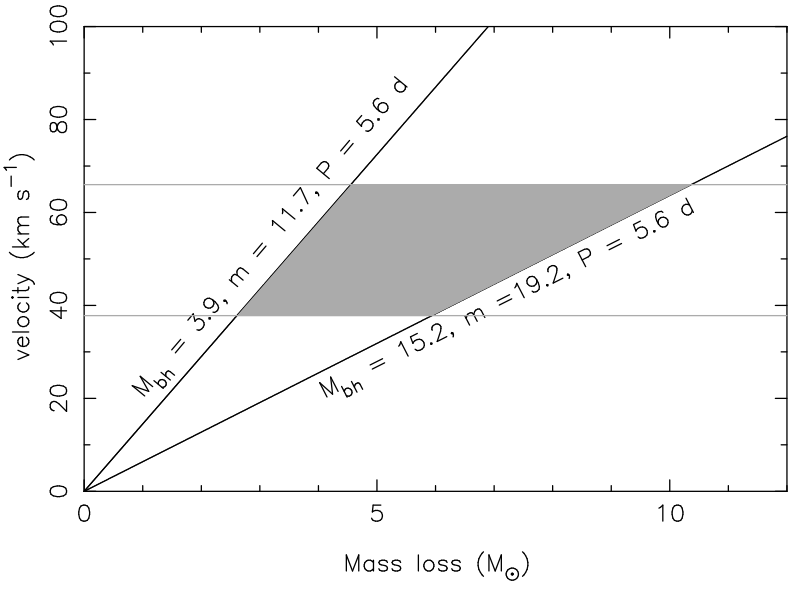

Figure 7.2: The same as Fig. 7.1 but for Cygnus X-1 with two different solutions for the companion mass.

$(M_{\rm BH}m)]^3$) some possibilities for the system configuration at the onset of mass transfer are the following combinations of $(M_{\rm BH}, m, P_{\rm re-circ})$: (4.5, 4.0, 1.52), (7.0, 4.0, 1.91) and (7.5, 3.5, 2.31). With these values and Eq. (7.8) we find that the present runaway velocity of 106 km s^{-1} is obtained for ΔM = 5.0, 8.4 and 10.2 $M_\odot$ respectively. This is shown in Fig. 7.1 (solid lines). Note that all these lines are terminated at the amount of mass ejection that would result in a pre-SN orbit in which the companion would fill its Roche lobe. The minimum amount of mass that must be lost is 4.1 $M_\odot$ in the case of a black hole of 4.5 $M_\odot$, given $v_{\rm sys} > 87$ km s^{-1}.

Relaxing the assumption of conservative mass transfer (as is suggested by the observation of jets from Nova Sco), and assuming the lost material drags along three times the specific angular momentum (POLS AND MARINUS 1994), we calculated the orbits for the first two cases, assuming 0.5 $M_\odot$ was lost from the system. The resulting system parameters at the onset of the mass transfer then become (5, 4, 1.96) and (7.5, 4, 2.42) for the first two examples. These curves are plotted as dashed lines in Fig. 7.1. In this case at least 5 and 8 $M_\odot$ are lost, respectively.

7.4.2 Cygnus X-1

For Cygnus X-1 the presently best estimate of the masses of the stellar components is $M_{\rm BH}$ = 10.1 $M_\odot$ and m = 17.8 $M_\odot$. Extremes of the allowed masses are given by $(M_{\rm BH}, m)$ = (3.9, 11.7) and (15.2, 19.2) respectively (HERRERO ET AL. 1995). We

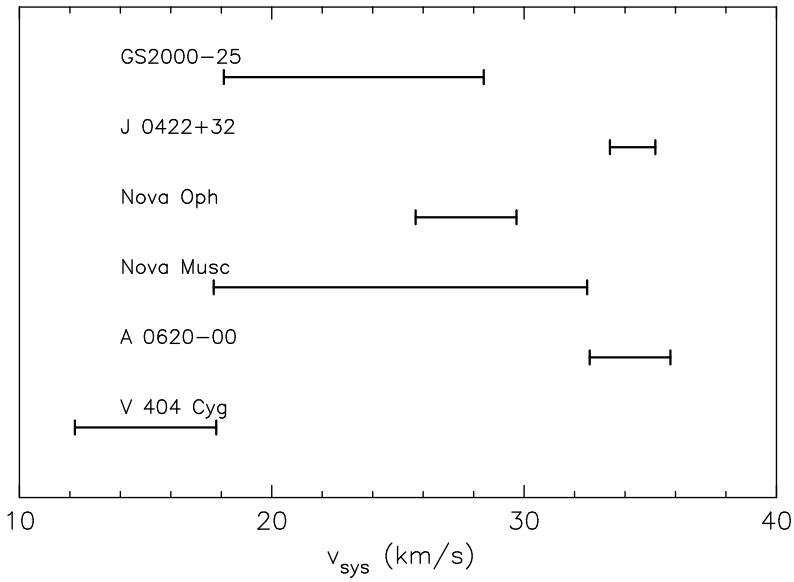

Figure 7.3: Our estimated 3-D recoil velocity for the black hole X-ray binaries with low-mass donors, for a supernova mass-loss fraction $f \equiv \Delta M/M_{\rm He} = 0.35$. The limits represent the uncertainty in the black hole mass as given in Table 7.1.

assume no orbital evolution since the beginning of the mass transfer phase, because Roche-lobe overflow can not have started long ago since the expected mass transfer rates then would be much higher. We use the values of the masses as given above and the present day orbital period of 5.6 days. We also neglect the small eccentricity that the orbit still has. Fig. 7.2 shows the resulting allowed range of mass ejected in the formation of the black hole. For a present black hole mass of 3.9 $M_\odot$ at least 2.6 $M_\odot$ must have been ejected to produce the observed space velocity. For a black hole of 15.2 $M_\odot$ at least 6 $M_\odot$ must have been ejected.

7.4.3 The remaining black hole X-ray transients

Table 7.1 shows that all the black hole X-ray binaries with low-mass donors have low velocities. As derived by WHITE AND VAN PARADIJS (1996), the expected additional velocity component of these X-ray binaries is of the order of 20 – 40 km s^{-1}. In Cyg X-1 and Nova Sco at least 28 and 48% of the mass of the progenitor must have been ejected in the SN. Therefore we computed the velocities for these systems assuming a constant fraction of 35% of the helium star mass to be ejected and show the obtained range in velocities given the range in black hole masses in Fig. 7.3. The last five systems are all expected to have evolved during mass transfer to smaller periods, and all seem to be compatible with an initial systems close to (m, P) = (1 $M_\odot$, 0.74 d), cf. ERGMA AND

FEDOROVA (1998). The systems shrink due to magnetic braking, so we assume $P_{\rm re-circ}$ = 1 d (see e.g. KALOGERA 1999). For V 404 Cyg we assumed a re-circularized period of 4 days and a donor mass of 1 $M_\odot$.

7.5 Discussion and conclusions

In this Letter we show that both the high observed velocities of Cyg X-1 and Nova Sco, and the low velocities of the black hole X-ray binaries with low-mass donors can be explained by ejection of $\gtrsim$30% of the mass of the exploding helium star in the SN that formed the black hole. This removes the need to invoke a large kick for Nova Sco (and Cyg X-1) and at the same time a small or no kick for the remaining systems (BRANDT ET AL. 1995), which seems highly unlikely to us.

The radial velocity of Nova Sco can only be explained by large mass-loss fractions ($\gtrsim$ 50%) and the assumption that the mass transfer has already started some time ago. If this mass transfer was non-conservative (consistent with observed jets), the velocity can be explained more easily. This may also be needed if Nova Sco also has a transverse velocity component.

TUTUKOV AND CHEREPASHCHUK (1997) state that the high velocity of Nova Sco could be obtained by having the pre-SN mass ratio above 0.24, i.e. $M_{\rm He} \leq 9.6$ (they use 2.3 and 4 $M_\odot$ for the current masses). However, this is not in agreement with the assumption in their equation, that the maximal amount of mass is lost. Using our modification [Eq. (7.1)] to their equation, we find indeed that for their masses it is impossible to obtain a velocity higher than 93 km s $^{-1}$, in agreement with our findings that the post-SN orbit must be different from the current orbit.

The fact that black holes in X-ray binaries may have lost several tens of percents of their progenitor mass in the SN, makes it necessary that some of their progenitor (helium) stars must have had masses above 10 $M_\odot$, which is in clear disagreement with the suggestion from some stellar evolution models that all Wolf-Rayet stars have a mass $\lesssim 3.5\,M_\odot$ at the moment they explode in a supernova (WOOSLEY ET AL. 1995).

Finally, it should be noticed that the conclusion that black holes eject a substantial amount of material during their formation has consequences for the orbital period distribution of close black hole pairs, which are expected to be prime sources for ground based gravitational wave detectors. Mass ejection will widen the orbit, which happens twice during the formation of a black hole pair, possibly preventing black holes to form in a close orbit at all. Only kicks from an asymmetry in the SN could then form close pairs. But as shown above, there is not much evidence for kicks and the magnitude of any kicks is severely limited to < 40 km s^{-1} by the black hole X-ray binaries with low-mass donors, unless the black holes in these systems formed in a direct collapse.

Acknowledgements. We thank Philipp Podsiadlowski and the referee for comments that improved this article and Lex Kaper who made us aware of the proper motion of Cyg X-1.

CHAPTER 8

The formation of black hole low-mass X-ray binaries: through case B or case C mass transfer?

G. Nelemans & E. P. J. van den Heuvel

to be submitted

ABSTRACT

The formation of low-mass X-ray binaries containing a rather massive ($M \gtrsim 7\mathrm{M}_\odot$) black hole is problematic because in most recent stellar evolutionary calculations the immediate progenitors of these black holes (Wolf-Rayet stars) lose so much mass via their stellar wind that their final masses are well below the observed black hole masses. We discuss the recently proposed solution that these binaries are formed through case C mass transfer (i.e. mass transfer after core helium burning is completed), avoiding a long Wolf-Rayet phase and thus significant mass loss. We show that only some of the currently available models for the evolution of massive stars allow this formation channel. We also investigate the effect of the downward revised Wolf-Rayet mass-loss rate as is suggested by observations, and conclude that in that case the Wolf-Rayet stars end their lifes with significantly higher masses than previously found and may be able to form a black hole.

8.1 Introduction

In low-mass X-ray binaries a neutron star or a black hole accretes from a low-mass ($M \lesssim 1\mathrm{M}_\odot$) companion. A scenario to form such binaries begins with a relatively wide binary of a massive star and a low-mass companion. When the massive star becomes a giant, mass transfer is unstable and a common-envelope forms in which the companion spirals down towards the core of the giant, leaving a close binary consisting of the helium core of the giant and the low-mass companion (VAN DEN HEUVEL 1983). The helium star explodes in a supernova and depending on the (core) mass of the helium

star, a neutron star or black hole is formed. With the discovery of A0620-00 (EYLES ET AL. 1975; ELVIS ET AL. 1975) and the determination of the mass function of 3.18 (MCCLINTOCK AND REMILLARD 1986), the existence of the class of black hole low-mass X-ray binaries was established. Currently we know 6 to 8 such systems depending on the membership criteria (CHARLES 1998; BAILYN ET AL. 1998). An evolutionary scenario for these objects is given in DE KOOL ET AL. (1987).

To make a black hole, the initial mass of the primary must exceed a critical value, which currently is believed to be around 20 $M_\odot$ (FRYER 1999). However, large mass-loss rates for massive stars and Wolf-Rayet stars have been inferred from observations (DE JAGER ET AL. 1988) and are found from the comparison of Wolf-Rayet models with these observations (LANGER 1989a). Applying these rates to evolutionary calculations resulted in the conclusion that even massive single stars might end their evolution as relatively low-mass objects when they explode (SCHALLER ET AL. 1992; MEYNET ET AL. 1994; WOOSLEY ET AL. 1995) and are thus unable to produce the observed black holes. For massive stars in close binaries, which lose their hydrogen envelopes due to mass transfer early in their evolution the situation is even worse; the most recent calculations predict masses of helium stars as they explode as low as 3 $M_\odot$, almost independent of their initial mass (WELLSTEIN AND LANGER 1999).

In this article we first discuss the formation of black hole low-mass X-ray binaries through case C evolution: mass transfer starting after core-helium burning has been completed (KIPPENHAHN AND WEIGERT 1967). In this case a long-duration Wolf-Rayet phase in which the star loses a lot of mass is avoided (Sect. 8.2). Then we discuss the most recently observed mass-loss rates for Wolf-Rayet stars and the implication of lower mass-loss rates on the final helium-star masses of exploding stars in binaries (Sect. 8.3). At the end we discuss uncertainties and possible alternatives for the formation of black hole low-mass X-ray binaries (Sect. 8.4) and end with our conclusions (Sect. 8.5).

8.2 Case C mass transfer

It has been suggested that case C mass transfer could be invoked to avoid a long-duration Wolf-Rayet phase in the evolution of the massive star, in order that this star does not lose too much mass and still is able to form a massive black hole (BROWN ET AL. 1999; WELLSTEIN AND LANGER 1999).

The occurrence of case C mass transfer depends on the radius evolution of massive stars. For supergiants the radius of the star is not very well defined, since the outer layers of the giant envelope are extremely dilute. However, the best we can do is use the calculated values of the radii of giants. We also neglect the interaction between the wind of the massive star and the companion which may influence the separation of the two stars.

We calculate the initial separation with which a binary should start in order to undergo case C mass transfer as follows (see also PORTEGIES ZWART ET AL. 1997). The

separation at the moment the Roche-lobe overflow (RLOF) starts is given by

$$a_{\rm RLOF} = \frac{R}{r_{\rm L}} \tag{8.1}$$

where R is the radius of the star and $r_{\rm L}$ is the dimensionless Roche-lobe radius (the ratio of the Roche-lobe radius and the binary separation). We use the EGGLETON (1983) equation for $r_{\rm L}$. For mass ratios between 10 and 50, the value of $r_{\rm L}$ is between about 0.6 and 0.7. During the evolution the star loses mass and the separation increases according to

$$a' = a\frac{M}{M'}, \tag{8.2}$$

where M denotes the total mass of the binary. So to start Roche-lobe overflow at time t when the star has a radius $R(t)$, the initial separation is given by

$$\begin{aligned} a_{\rm i} &= a_{\rm RLOF}(t)\,\frac{M(t)}{M_{\rm i}} \\ &= \frac{R(t)}{r_{\rm L}}\,\frac{M(t)}{M_{\rm i}}. \end{aligned} \tag{8.3}$$

We now compute the separations at which massive stars fill their Roche lobes as function of initial mass and initial separation and determine whether the mass transfer is case B or case C. In Fig. 8.1 (top) we show this for the evolutionary calculations of SCHALLER ET AL. (1992, see also Fig. 4 of KALOGERA AND WEBBINK 1998). For a star of initially 15 $M_\odot$ case C mass transfer occurs for initial separation between 1000 and 1320 $R_\odot$. For a 20 $M_\odot$ star, these limits are 1300 and 1550 $R_\odot$. For a 25 $M_\odot$ star case C is not possible anymore. The two other panels in Fig. 8.1 show the same, but for the stellar evolution models of HURLEY ET AL. (2000, middle) and HEGER ET AL. (2000, bottom). For these models case C is not possible for stars more massive than around 19 $M_\odot$. A recent estimate of the number of black hole low-mass X-ray binaries that can form through the narrow case C interval of the SCHALLER models shows that even such a narrow interval might be enough to explain the whole Galactic population (BROWN ET AL. 2001).

We conclude that since case C evolution depends strongly on the radius evolution of massive stars which is very uncertain, it is not clear whether black hole low-mass X-ray binaries can be formed in this way.

8.3 Case B mass transfer

A different way to avoid too much mass loss may be the fact that observed mass loss rates (which are the basis for the mass-loss rates used in the evolutionary calculations) are revised downward (HAMANN AND KOESTERKE 1998; NUGIS AND LAMERS 2000), which may make it possible to prevent helium stars in binaries to lose so much mass that

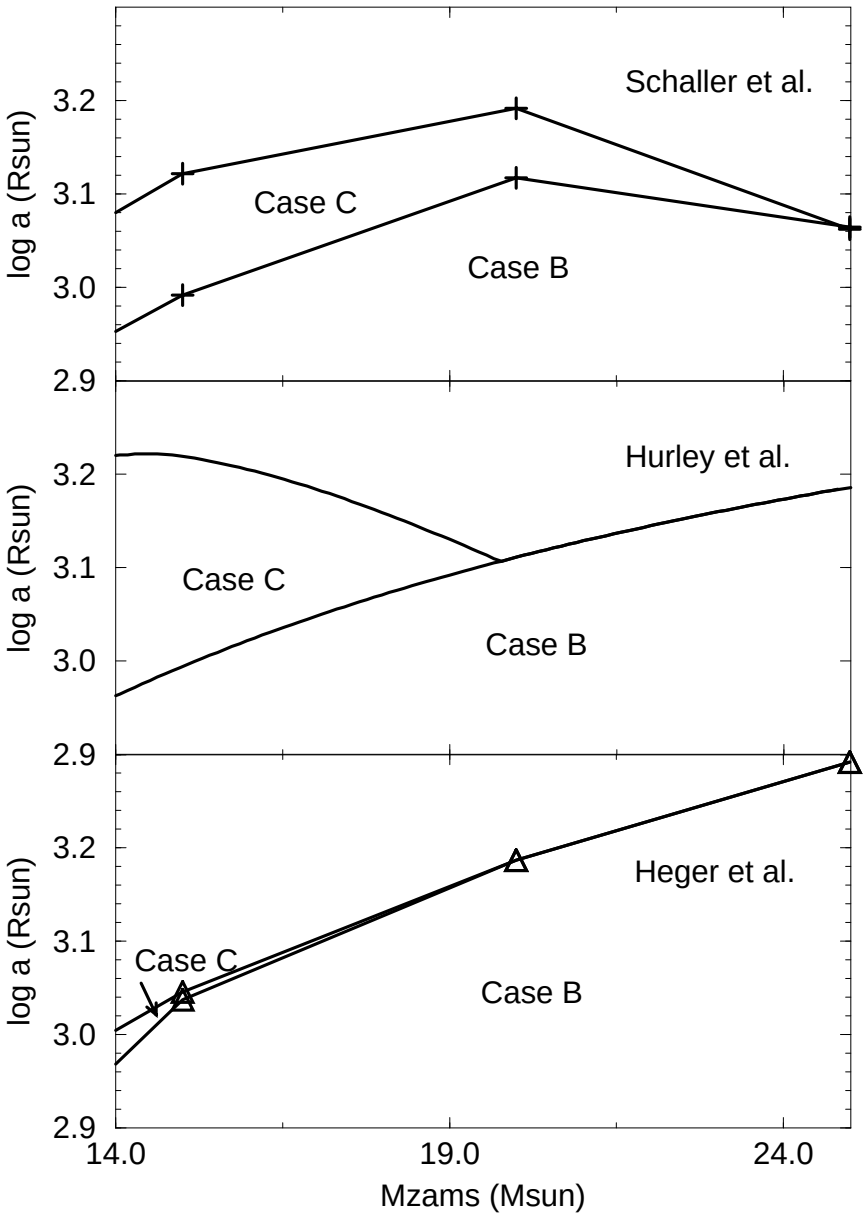

Figure 8.1: Initial separations a_i for which case B and case C mass transfer occurs as function of ZAMS mass, for a 1 $M_\odot$ companion. **Top** for the SCHALLER ET AL. (1992) models, **middle** for the HURLEY ET AL. (2000) models, **bottom** for the HEGER ET AL. (2000) models.

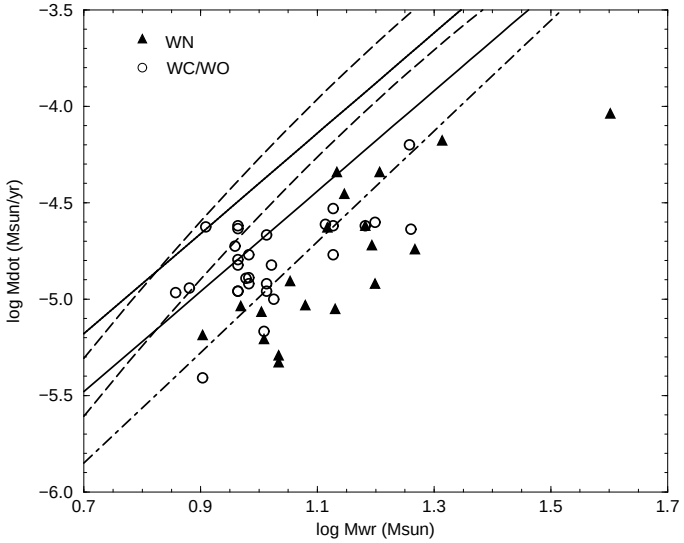

Figure 8.2: Mass-loss rates for Wolf-Rayet stars as observed (triangles and circles, from NUGIS AND LAMERS 2000) and various relations used for evolutionary calculations. The solid lines are the relations assumed by WOOSLEY ET AL. (1995) for WC (upper) and WN (lower) stars. The dashed lines are the ones used by WELLSTEIN AND LANGER (1999), where we converted the mass loss – luminosity relations to mass loss - mass relations using the mass - luminosity relation of LANGER (1989b). The upper dashed line is for their standard case, the lower for their reduced mass loss case. The dash-dotted line is a rectangular least square fit to all points (see also the text and Eq. (8.4)).

they no longer can become black holes. As shown by KALOGERA (1999) the helium stars that were the progenitors of the black holes in binaries cannot have lost more than half of their initial mass. This includes both mass loss in the stellar wind and in the supernova explosion.

A recent compilation of observed mass-loss rates for Wolf-Rayet stars is made by NUGIS AND LAMERS (2000). In Fig. 8.2 we show these inferred mass-loss rates for WN and WC/WO stars (without the hydrogen rich Wolf-Rayet stars). We overplotted mass-loss rates for WN and WC stars as used by WOOSLEY ET AL. (1995) as the solid lines. The mass-loss rates used recently by WELLSTEIN AND LANGER (1999) are shown as the dashed lines, where we used the luminosity – mass relation as given by LANGER (1989b) to convert the mass loss – luminosity relation used by these authors, to a mass loss – mass relation. The top dashed line is their standard case, the bottom the reduced mass-loss rate, which they used to account for the lower observed mass-loss rates.

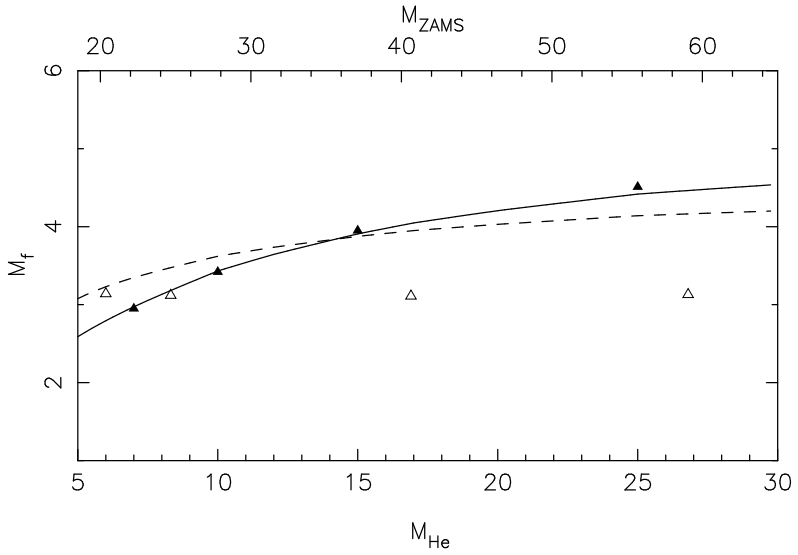

Figure 8.3: Final helium star masses as function of the initial helium star mass with the mass-loss rates according to WOOSLEY ET AL. (1995, solid line, some of their results are potted as solid triangles) and WELLSTEIN AND LANGER (1999, dashed line) assuming a helium star lifetime as given by WOOSLEY ET AL. (1995). A selection of their results is plotted as the open triangles. The numbers at the top give an estimate of the ZAMS mass of the progenitor of the helium star.

The most recently determined mass-loss rates thus suggest that the rates used by WELLSTEIN AND LANGER (1999) are still too high. We will investigate the effect of using a lower mass-loss rate law, which is shown in the figure as the dash-dotted line and is given by

$$\dot{M} = -1.38 \times 10^{-8} M^{2.87} \tag{8.4}$$

and is obtained by a 'rectangular least square fit' (LANGER 1989a) to the data (i.e. minimising the rectangular distances to the line, rather than the vertical distances). The fit is different from the one obtained by NUGIS AND LAMERS (2000) because we excluded the hydrogen rich Wolf-Rayet stars.

For a mass-loss rate of the form

$$\dot{M} = -k M^{\alpha} \tag{8.5}$$

the final helium stars mass $M_{\rm f}$ can be computed from the initial mass $M_{\rm i}$ and the helium star lifetime (τ) from

$$M_{\rm f} = \left[M_{\rm i}^{1-\alpha} + (\alpha - 1)\, k \tau \right]^{1/(1-\alpha)}. \tag{8.6}$$

If the mass-loss rate is given in terms of the luminosity, the final mass is obtained by numerical integration of the mass evolution. In Fig. 8.3 we show the final masses

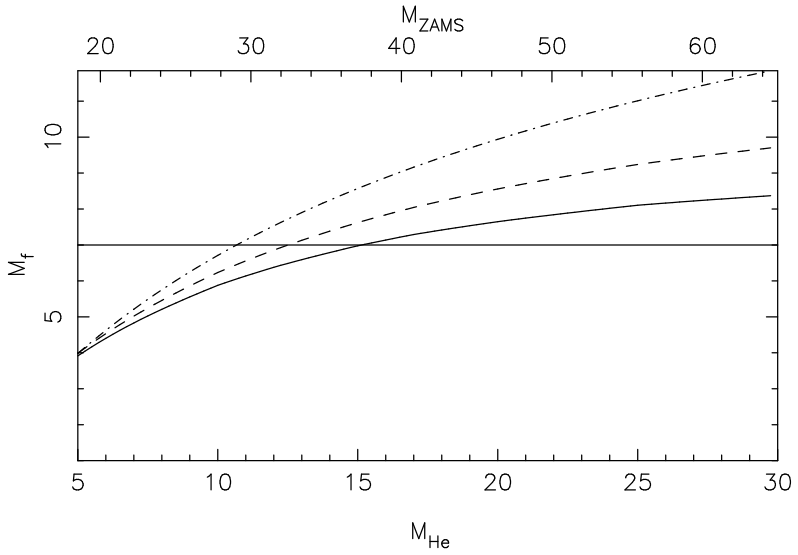

Figure 8.4: Final helium star masses as function of initial helium star mass with the mass-loss rates given by Eq. (8.4) using a helium-star lifetime as given by WOOSLEY ET AL. (1995, solid line) and the given by POLS ET AL. (1991, dash-dotted line) and one with a helium-star lifetime in between these two (dashed line). ZAMS masses for the helium star progenitors are indicated at the top.

that we obtain using the top two lines (dashed and solid) from Fig. 8.2 and the helium star lifetimes as given by WOOSLEY ET AL. (1995) and compare these with the results obtained with the same mass-loss rates by WOOSLEY ET AL. (1995) and WELLSTEIN AND LANGER (1999). For the highest mass-loss rate the final masses do not completely agree with the masses obtained by WELLSTEIN AND LANGER (1999), probably because these high mass-loss rates lead to even longer lifetimes.

We now calculated the final masses for the revised mass-loss rate given by Eq. (8.4), which yields

$$M_{\rm f} = \left[M_{\rm i}^{-1.87} + 2.6 \times 10^{-8}\,\tau \right]^{-1/1.87}. \qquad (8.7)$$

In Fig. 8.4 we show these masses for the helium star lifetimes from WOOSLEY ET AL. (1995, solid line). The lifetime of the helium star depends on the assumed mass-loss rate because mass-losing helium stars become less massive, thus less luminous and can live longer. For example the helium star lifetimes as given by WOOSLEY ET AL. (1995) are substantially longer than the ones collected by POLS ET AL. (1991) for models without mass loss. We thus expect the lifetimes for the helium stars with reduced mass-loss rates to be shorter. In Fig. 8.4 we also plotted the final helium star masses assuming a lifetime which is between the lifetimes given by WOOSLEY ET AL. (1995) and POLS ET AL. (1991, dashed line) and the one given by POLS ET AL. (1991, dash-dotted line).

The horizontal line is at 7 $M_\odot$, the typical observed mass of the black holes in the low-mass X-ray binaries. The limiting ZAMS mass for which the final helium star mass exceeds 7 $M_\odot$with the masses loss rate used here is $\sim 30 - 37 M_\odot$.

We thus conclude that with revised mass-loss rates helium stars end their lives with significantly higher masses than previously found and may be able to form black holes even after case B mass transfer.

8.4 Discussion

The analyses in Sect. 8.2 neglects the influence of the wind of the massive star on the companion star. The companion moves through the wind and already feels friction, which counteracts the widening of the orbit due to the stellar wind. However, even for a wind mass-loss rate of $10^{-3} M_\odot$ yr^{-1}, the density in the wind at the companion is almost four orders of magnitude lower than the density at the edge of the giant for a giant with radius of 1000 $R_\odot$and a binary separation of 1600 $R_\odot$.

The whole argument presented in Sect. 8.3 is based on the observed mass-loss rates. However, it should be noted that *all* mass-loss rates proposed for Wolf-Rayet stars and used in evolutionary calculations are based on the observed rates. The valid question still remains what the uncertainty is in the observed mass-loss rates and in the inferred stellar masses and how this could influence our main conclusion.

The mass-loss rates as determined by NUGIS AND LAMERS (2000) are the most accurate, but still suffer from the general problem that not all quantities (mass, mass-loss rate and luminosity) can be determined independently. They therefore use the mass – luminosity relation of SCHAERER AND MAEDER (1992) to obtain the final mass estimates from the luminosity. Using a different mass – luminosity relation may change the resulting mass/mass-loss rate combinations.

Taking the masses and mass-loss rates as plotted in Fig. 8.2, one would not say that there is a unique mass-loss rate – mass relation, as is expected on theoretical grounds (LANGER 1989b). The scatter is larger than the quoted uncertainty in the observations. This either points to underestimates of the errors in the observations, to variability or to additional physical processes, which were not taken into account in the calculations by LANGER (1989b) and can change the mass-loss rate for a given Wolf-Rayet star mass. One could think of rotation, magnetic fields or maybe the evolutionary history.

In the last respect it might be that stars in binaries that lose their hydrogen envelopes by mass transfer evolve differently from stars that lose their envelopes due to their own stellar winds (which possibly is enhanced by a companion). The question which stars actually form black holes and which neutron stars is considerably more complex than the question of the final mass of helium stars (e.g. FRYER 1999). In particular the evolution of the core is important. As long as the collapse of the core is not understood this question will remain unanswered.

Finally, it should be noted that to form a black hole low-mass X-ray binary the companion must survive the common-envelope phase. The outcome of the common envelope depends on the binding energy and density structure of the giants envelope,

which are quite different for giants that undergo case B and case C mass transfer. It could for instance be that that all binaries that undergo case B mass transfer to a low-mass companion will completely merge. That would mean that we *need* the small allowed initial separation range for case C.

8.5 Conclusion

We calculated the possible initial separations for which case C mass transfer is likely to occur for massive stars, using different stellar evolution models. We find that case C mass transfer becomes impossible for stars more massive than around 19 $M_\odot$ for the models of HEGER ET AL. (2000) and HURLEY ET AL. (2000) and more massive than around 25 $M_\odot$ for the models by SCHALLER ET AL. (1992). Unless the current models for massive stars underestimate the radius expansion after the end of core helium burning the chances for forming black holes in binaries through case C mass transfer are therefore quite limited.

We also investigated the influence of the assumed mass-loss rate on the final mass of helium stars in binaries and conclude that with a downward revised mass-loss rate as suggested by the observations (e.g. NUGIS AND LAMERS 2000) helium stars end their lives with significantly higher masses than previously found and may be able to form black holes even after case B mass transfer for primaries more massive than $\sim 30 - 40 M_\odot$.

Acknowledgements. We thank Jasinta Dewi and Norbert Langer for helpful discussion and trial calculations of helium star evolution and Alexander Heger for providing details of his evolutionary calculations. This work was supported by NWO Spinoza grant 08-0 to E. P. J. van den Heuvel.

CHAPTER 9

The gravitational wave signal from the Galactic disk population of binaries containing two compact objects

G. Nelemans, L. R. Yungelson & S. F. Portegies Zwart

to be submitted

ABSTRACT

We review the properties of binaries containing two compact objects in the Galactic disk, as derived from population synthesis. Using this information we calculate the gravitational wave signal of these binaries. At frequencies below $f \lesssim 2$ mHz the double white dwarf population forms an unresolved background for the low-frequency gravitational wave experiment LISA. Above this limit some few thousand double white dwarfs and a few tens of binaries containing neutron stars will be resolved in frequency. Of the double white dwarfs ~ 500 have a total mass above the Chandrasekhar limit of which ~ 95 have a measurable frequency change allowing a measurement of their chirp mass. We discuss the properties of the resolved binaries.

9.1 Introduction

The interest in gravitational waves, predicted by Einstein's theory of general relativity, was greatly enhanced by the signals supposedly detected by resonant gravitational wave (GW) antennas (WEBER 1969) and the discovery of the pulsar B1916+13 in a relativistic binary (HULSE AND TAYLOR 1975; TAYLOR AND WEISBERG 1982). Currently, about ten projects for ground and space-based gravitational wave detectors are already operating or under development (see, e.g. FLANAGAN 1998). They will open the windows in the frequency bands 10 to 10^4 Hz from the ground and 10^{-4} to 1 Hz from space.

Recently the first upper limits on detections from the Japanese TAMA300 detector were reported (TAGOSHI ET AL. 2001).

At high frequencies the merging events of extra-galactic binaries containing neutron stars and/or black holes are among the most promising sources. The estimates of the merger rates of these systems are highly uncertain (e.g. PHINNEY 1991; PORTEGIES ZWART AND YUNGELSON 1998; KALOGERA AND LORIMER 2000). An upper limit for the rate of neutron star – neutron star mergers in our Galaxy of $10^{-4}\,\mathrm{yr}^{-1}$ is found both from observations (ARZOUMANIAN ET AL. 1999) and theory (TUTUKOV AND YUNGELSON 1993b). However, BAILES (1996) provided a strong observational argument that this upper limit is $\lesssim 10^{-5}\ \mathrm{yr}^{-1}$ in the Galaxy. Extrapolated to cosmic scales, these estimates show that the perspectives for detection of such events by the first generation GW detectors are not very good (see also KALOGERA ET AL. 2000). They could be better for black hole – black hole or for black hole – neutron star mergers (TUTUKOV AND YUNGELSON 1993b; LIPUNOV ET AL. 1997a; PORTEGIES ZWART AND MCMILLAN 2000).

At low frequencies, it was first expected that contact W UMa binaries will dominate the gravitational wave spectrum (MIRONOVSKII 1965). However, it was shown that the gravitational wave background formed by Galactic disk systems is totally dominated by detached double white dwarfs and that their number is so large that they will form a confusion limited background for the currently planned detectors (EVANS ET AL. 1987; LIPUNOV ET AL. 1987; HILS ET AL. 1990; NELEMANS ET AL. 2000a). Only sources with a frequency above a certain clearing frequency (somewhere between $\sim 1-10\mathrm{mHz}$) can be resolved (e.g. EVANS ET AL. 1987).

The aim of the present paper is an accurate evaluation of the confusion limit, based on population synthesis models for compact stars and a discussion of the properties of the sample of potentially resolved binaries containing two compact objects: white dwarfs, neutron stars or black holes. We do not consider globular cluster binaries. We first discuss the gravitational wave signal from (eccentric) binaries (Sect. 9.2). Next, we summarise the properties of the Galactic disk populations of compact binaries that are relevant to the emission of gravitational waves (Sect. 9.3). In Sect. 9.4 we present a model for the background formed by the Galactic disk double white dwarfs, discuss the confusion limit and the properties of the individually resolved binaries. A discussion of the possible contribution of the halo and extra-galactic sources and a comparison with previous work follows in Sect. 9.5. Our conclusions are summarised in Sect. 9.6.

9.2 Gravitational waves from binaries

The gravitational wave luminosity of a binary in the nth harmonic is given by (PETERS AND MATTHEWS 1963)

$$L(n,e) = \frac{32}{5}\frac{G^4}{c^5}\frac{M^2\,m^2\,(M+m)}{a^5}g(n,e). \tag{9.1}$$

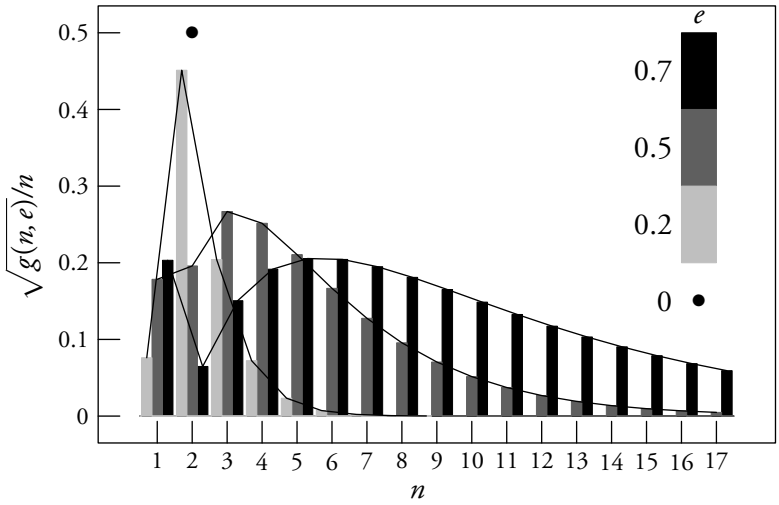

Figure 9.1: Scale factor of the GW strain amplitude $\sqrt{g(n,e)}/n$ for the different harmonics [Eq. (9.3)] for $e = 0$, 0.2, 0.5 and 0.7.

Here M and m are the masses of the components, a is their orbital separation and e is the eccentricity of the orbit. The function $g(n,e)$ is the Fourier decomposition of the GW signal.

The measurable signal for gravitational wave detectors is the amplitude of the wave – h_+ and $h_\times$ for the two polarisations. These can be computed from the GW flux at the Earth (PRESS AND THORNE 1972)

$$\frac{L_{\rm GW}}{4\pi d^2} = F = \frac{c^3}{16\pi G}\langle \dot{h}_+^2 + \dot{h}_\times^2 \rangle. \tag{9.2}$$

Assuming the waves to be sinusoidal and defining the so called strain amplitude as $h = (\frac{1}{2}[h_{+,max}^2 + h_{\times,max}^2])^{1/2}$ one obtains

$$\begin{aligned} h(n,e) &= \left[\frac{16\pi G}{c^3\,\omega_{\rm g}^2}\frac{L(n,e)}{4\pi d^2}\right]^{1/2} \\ &= 1.0\,10^{-21}\,\frac{\sqrt{g(n,e)}}{n}\left(\frac{\mathcal{M}}{\rm M_\odot}\right)^{5/3}\left(\frac{P_{orb}}{1\,\rm hr}\right)^{-2/3}\left(\frac{d}{1\rm kpc}\right)^{-1}, \end{aligned} \tag{9.3}$$

where $\mathcal{M} = (M\,m)^{3/5}/(M+m)^{1/5}$ is the so called chirp mass and $\omega_{\rm g}$ is the angular frequency of the emitted wave, which is n times the orbital angular frequency of the binary

$(2\pi n/P_{\rm orb})$[1]. In Fig. 9.1 we plot the values of $\sqrt{g(n,e)}/n$ for different eccentricities. High eccentricity binaries emit most of their energy at higher frequencies than their orbital frequency, reflecting the fact that the radiation is more effective near periastron of the orbit. Thus, eccentric compact binaries may be sources of GW signals in the low-frequency band even if their orbital frequencies are lower than the range in which low-frequency detectors like LISA are sensitive.

9.3 The Galactic disk population of binaries containing two compact objects

We calculated the Galactic disk population of binaries containing two compact objects using the population synthesis code SeBa (PORTEGIES ZWART AND VERBUNT 1996; PORTEGIES ZWART AND YUNGELSON 1998, Chapter 4). The basic assumptions used in this paper can be summarised as follows. The initial primary masses are distributed according to a power law IMF with index –2.5, the initial mass ratio distribution is taken flat, the initial semi major axis distribution flat in log a up to $a = 10^6 {\rm R}_\odot$, and the eccentricities follow $P(e) \propto 2e$. The fraction of binaries in the initial population of main-sequence stars is 50% (2/3 of all stars are in binaries). A difference with other studies of the populations of close binaries is that the mass transfer from a giant to a main sequence star of comparable mass is calculated using an angular momentum balance formalism, as described in Chapter 3. The neutron star kick distribution we use is the one proposed by HARTMAN (1997). For the star formation rate of the Galactic disk we use an exponential function:

$$\mathrm{SFR}(t) = 15\ \exp(-t/\tau) \quad {\rm M}_\odot\ {\rm yr}^{-1} \tag{9.4}$$

where $\tau = 7$ Gyr. With an age of the Galactic disk of 10 Gyr it gives a current star formation rate of $3.6\,{\rm M}_\odot\,{\rm yr}^{-1}$ compatible with observational estimates (RANA 1991; VAN DEN HOEK AND DE JONG 1997). It gives a Galactic supernova II/Ib rate of $0.02\ {\rm yr}^{-1}$ and if supernovae Ia are produced by merging double carbon-oxygen (CO) white dwarfs it gives a Galactic rate of $0.002\ {\rm yr}^{-1}$. Both are in agreement with observational estimates by CAPPELLARO ET AL. (1999).

The current birth- and merger rates and total number of systems in the Galactic disk with these assumptions are given in Table 9.1. We use a notation introduced by PORTEGIES ZWART AND VERBUNT (1996): wd, ns and bh for white dwarf, neutron star and black hole respectively; ( ) and [ ) for detached and semi-detached binaries. The fact that the numbers here are different from the numbers given in PORTEGIES ZWART AND YUNGELSON (1998), PORTEGIES ZWART AND YUNGELSON

[1] For circular orbits this equation is identical to Eq. (5) of EVANS ET AL. (1987). It is different by a factor of $\sqrt{8}$ from Eq. (20) of PRESS AND THORNE (1972), who use a factor $\sqrt{2}$ larger definition of h and possibly confuse $\omega_{\rm g}$ in Eq. 9.3 with the orbital angular frequency. It differs by a factor $2^{5/3}$ from Eq. (3.14) of DOUGLAS AND BRAGINSKY (1979) because they confuse the orbital frequency in their Eq. (3.13), with the frequency of the wave (twice the orbital frequency) in their Eq. (3.4).

TABLE 9.1: Current Galactic disk birth rates (ν) and merger rates ($\nu_{\rm merg}$) per year for binaries containing two compact objects and their total number (#) in the Galactic disk, as calculated with the SeBa population synthesis code (see text).

Type	ν	$\nu_{\rm merg}$	#
(wd, wd)	2.5×10^{-2}	1.1×10^{-2}	1.1×10^{8}
[wd, wd)	3.3×10^{-3}	-	4.2×10^{7}
(ns, wd)	2.4×10^{-4}	1.4×10^{-4}	2.2×10^{6}
(ns, ns)	5.7×10^{-5}	2.4×10^{-5}	7.5×10^{5}
(bh, wd)	8.2×10^{-5}	1.9×10^{-6}	1.4×10^{6}
(bh, ns)	2.6×10^{-5}	2.9×10^{-6}	4.7×10^{5}
(bh, bh)	1.6×10^{-4}	-	2.8×10^{6}

(1999) and NELEMANS ET AL. (2001c) is caused by the differences in the assumed IMF, initial binary frequency and star formation history.

In Fig. 9.2 we show the period distributions of the binaries of different type in the range of interest for space based gravitational wave detectors. The properties of these populations can be summarised as follows:

Detached double white dwarf binaries: (wd, wd). Our model for the Galactic disk population of double white dwarfs is described in detail in Chapter 4. It gives good agreement with the properties of the observed double white dwarfs. Most double white dwarfs have a mass ratio around unity and low-mass ($M < 0.45 M_{\odot}$) components. From Table 9.1 and Fig. 9.2 it is clear that they vastly outnumber all other binaries with compact objects in the Galactic disk.

Semi-detached double white dwarfs (AM CVn stars): [wd, wd). We include in our calculation both AM CVn stars descending from detached close double white dwarfs and from low-mass helium stars with white dwarf companions (Chapter 5). We use Model II of Chapter 5, which is most favourable for the formation of AM CVn's.

Neutron star – white dwarf binaries: (ns, wd). neutron star – white dwarf binaries fall into two families (TUTUKOV AND YUNGELSON 1993a; PORTEGIES ZWART AND YUNGELSON 1999; TAURIS AND SENNELS 2000). In the first family the neutron star is formed first. Later the secondary forms a white dwarf and in the mass transfer event the orbit circularizes (e.g. VAN DEN HEUVEL AND TAAM 1984). If both components of the initial binary are of comparable mass it can happen that the primary becomes a white dwarf, while the secondary accretes so much mass that it terminates its life as a neutron star (e.g. TUTUKOV AND YUNGELSON 1993a). In this case the orbits are eccentric. The masses of the white dwarfs are typically low in the first family and high in the second (see Fig. 9.5 below). The birth rates of both families are comparable.

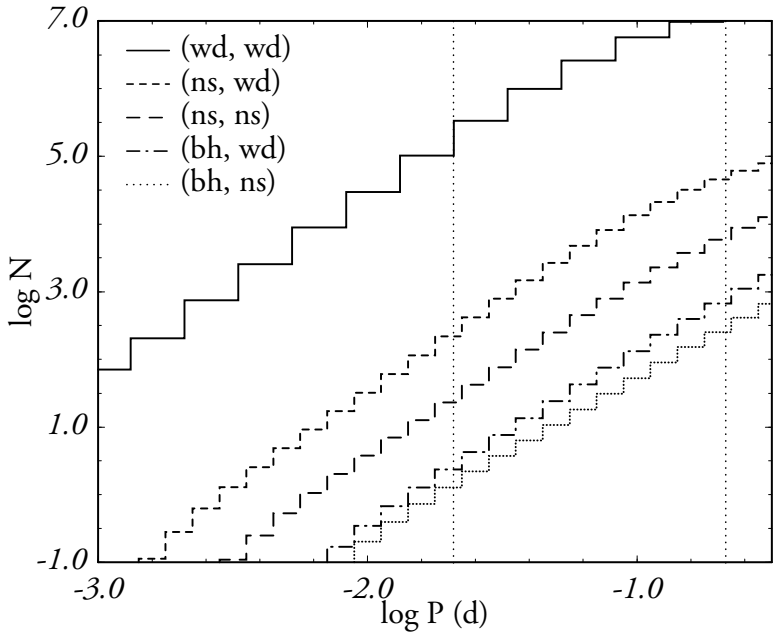

Figure 9.2: Period distribution of the binaries of different type in the period range of interest to the space based gravitational wave detectors like LISA. The vertical dotted lines give the periods at which the frequency of the fundamental (n = 2) harmonic of the gravitational wave is 1 and 0.1 mHz respectively.

Double neutron star binaries: (ns, ns). The formation and characteristics of the current population of double neutron stars is extensively studied by PORTEGIES ZWART AND YUNGELSON (1998) and we refer for all details to this study. Maybe the most important assumption, which influences the birth rate, orbital periods and eccentricities of neutron star – neutron star binaries, is the kick velocity distribution. We use the one proposed by HARTMAN (1997).

Black hole binaries: (bh, wd), (bh, ns) and (bh, bh). The knowledge of the way in which black holes are formed and the range of the masses of their progenitors are still highly uncertain (see e.g. WOOSLEY AND WEAVER 1995; PORTEGIES ZWART ET AL. 1997; ERGMA AND VAN DEN HEUVEL 1998; WELLSTEIN AND LANGER 1999; FRYER 1999). The treatment of the formation of black holes implemented in the present study is described in some detail in the Appendix 9.A. Typical black holes in our model have masses between 5 and 7 $M_\odot$. In the short orbital period range (Fig. 9.2) they are rare and their merger rates are at least an order of magnitude lower than those of the neutron star binaries (Table 9.1).

9.4 The gravitational wave signal from compact binaries in the Galactic disk

Merging of binaries containing neutron stars and black holes in distant galaxies could give measurable signals in the high frequency detectors. We do not extrapolate our merger rates to extra-galactic scales, but our inferred rates (Table 9.1) are consistent with the (very uncertain) rates derived elsewhere for the Galaxy (see for a detailed discussion KALOGERA ET AL. 2000).

The Galactic binaries with periods less than 10 hr are interesting for the low-frequency GW detectors. We calculate the expected signal for LISA, the joint ESA, NASA detector that will be launched around 2010. It consists of three satellites, 5 million kilometres apart, between which laser beams are exchanged, measuring the distance changes (MCNAMARA ET AL. 2000). A Fourier analysis provides sensitivity in the frequency domain with fixed frequency resolution equal to the inverse of the integration time. A limited angular resolution will be achieved, allowing e.g. identification of sources in globular clusters (BENACQUISTA ET AL. 2001). In our calculations we restrict ourselves to the sensitivity in frequency and do not consider the angular resolution.

Because the number of Galactic binaries drops strongly towards shorter periods (Fig. 9.2) the number of sources per frequency bin for these detectors with a fixed frequency resolution will also decrease: at low frequencies the signals in particular frequency bins will overlap, forming a so called "confusion limited noise". At higher frequencies there is not more than system per frequency bin, so the systems can be resolved individually. We discuss these regimes separately.

9.4.1 The confusion limited background due to double white dwarfs

EVANS ET AL. (1987) have shown that for space-borne detectors the confusion limit is determined by the Galactic close binary white dwarfs. In our model the total number of detached and semi-detached double white dwarfs in the Galactic disk is 1.5×10^8 (see Table 9.1). We distribute these systems randomly in the Galactic disk according to

$$\rho(R,z) = \rho_0 \, e^{-R/H} \, \mathrm{sech}(z/\beta)^2 \quad \mathrm{pc}^{-3}. \tag{9.5}$$

Here H = 2.5 kpc (SACKETT 1997) and β = 200 pc, neglecting the age and mass dependence of β. All systems are circular and for each system we calculate the strain amplitude from Eq. (9.3) taking $R_\odot$ = 8.5 kpc and $z_\odot$ = 30 pc.

To simulate the power spectrum for this population of binaries as would be detected by gravitational wave detectors in space like LISA and OMEGA we distribute the systems in frequency bins $\Delta f = 1/T$ with T the total integration time (for which we use 1 yr). In Fig. 9.3 we plot the resulting confusion limited background signal and the number of systems per bin. The contribution of the interacting double white dwarfs, which are less numerous than the detached double white dwarfs and have lower strain amplitude is concentrated in a relatively small frequency interval between $\log f = -3.5$ and -3.0 where they dominate the number of systems per bin.

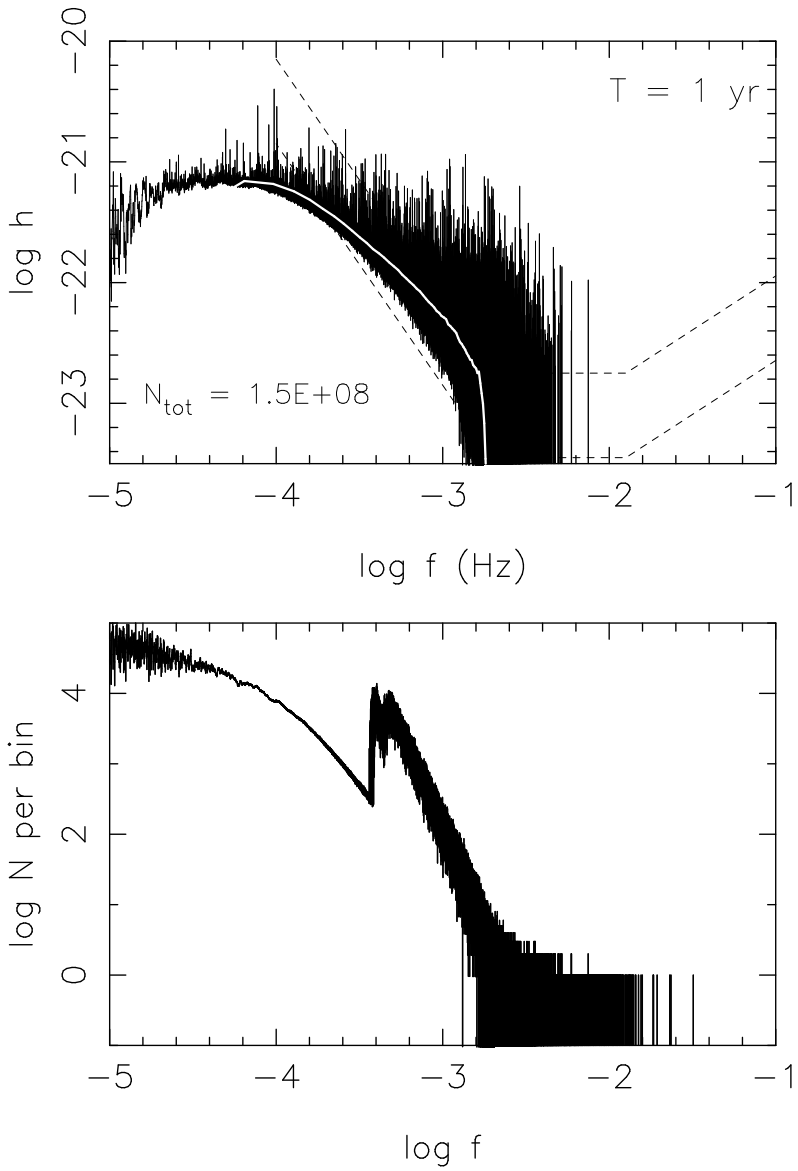

Figure 9.3: **Top:** GWR background produced by double white dwarfs (both detached and interacting). The assumed integration time is 1 yr. The 'noisy' black line gives the total power spectrum, the white line the average. The dashed lines show the expected LISA sensitivity for a S/N of 1 and 5. **Bottom:** The number of systems per bin on a logarithmic scale. The contribution of the interacting double white dwarfs between $\log f = -3.5$ and -3.0 is clearly visible.

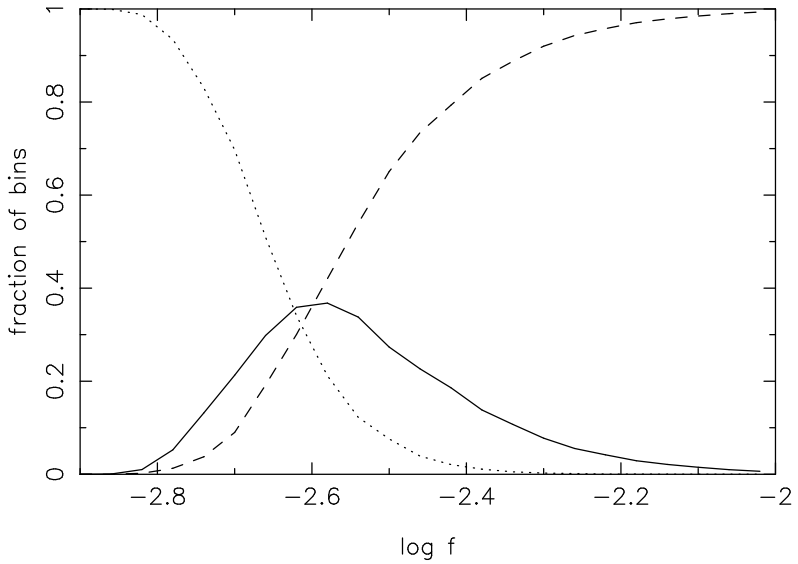

Figure 9.4: Fraction of bins that contain exactly one system (solid line), that are empty (dashed line) and contain more than one systems (dotted line) as function of the frequency of the signals. For all frequency intervals the result is normalised, because the total number of bins in a logarithmic interval changes strongly.

Most previous studies only used the average properties of the double white dwarf population to calculate the average background signal. In Fig. 9.3 we plotted the average of our model power spectrum as the white line. Note that in many bins the actual power is much larger than the average. These bins contain one system that has a much stronger signal than the rest, for example because it is close to the Earth, and may be detectable above the noise.

9.4.2 The population of resolved binaries

Given the fact that the double white dwarf background buries all underlying signals at frequencies below $\log f \approx -2.8$, we did not consider the neutron star and black hole binaries below 1 mHz. To find the binaries that will be resolved by LISA, we calculated the Galactic disk population of all binaries containing compact objects which contribute to the GW signal at frequencies above 1 mHz. Because we now also consider eccentric binaries, which emit at frequencies higher than twice the orbital frequency [Eq. (9.3)], there will be contributions from binaries with orbital periods up to $\sim$10 hr.

Considering an average background, as done e.g. by EVANS ET AL. (1987) the average number of systems per bin at a certain moment drops below one system. The frequency at which this happens is called the "confusion limit": below this limit all sources

TABLE 9.2: The number of resolved systems of different types (see Sect. 9.4.2) and the number of strong-signal systems potentially detectable above the double white dwarf background (see Sect. 9.4.3).

Type	resolved systems	detectable above noise
(wd, wd)	12124	5943
(ns, wd)	38	124
(ns, ns)	8	31
(bh, wd)	1	3
(bh, ns)	0	3
total	12171	6104

are unresolved and above it the systems are expected to be resolved. However, we model all individual systems in the Galaxy and determine, for an integration time T of 1 yr, for each frequency bin ($\Delta f = 1/T$) how many systems it contains. In Fig. 9.4 we plot the fraction of bins that contain exactly one, none and more than one system as function of frequency. The figure shows that the notion of a "confusion limit" as a unique value is too simple. At $\log f = -2.84$ the first resolved bins are found, while up to $\log f = -2.4$ bins containing more than one system are still present.

The total number of resolved bins with a signal above the sensitivity limit (S/N of 1) of LISA for an assumed integration time of 1 yr is 12171. In Table 9.2 we give the number of binaries of different types that are resolved. The eccentric binaries can contribute to more than one frequency [Eq. (9.3)], but the amplitude in the high harmonics in general is rather low. Just below the LISA sensitivity limit for $T = 1$ yr there are indeed 3 high harmonics of (ns, wd) binaries and one of a double neutron star in our model.

The change of the frequency of a binary evolving under the influence of GWR is given by (e.g. SCHUTZ 1996)

$$\dot{f} = 5.8 \times 10^{-7} (\mathcal{M}/\mathrm{M}_\odot)^{5/3} f^{11/3} \mathrm{Hz\,s}^{-1}. \tag{9.6}$$

For high-frequency systems this means that during a sufficiently long integration time the change of the frequency (the "chirp") can be detected and hence, $\mathcal{M}$ be determined. From Eq. (9.3) the distance to these sources can be found. In Fig. 9.5 we plot the frequency versus chirp mass distributions of the resolved systems for the binaries of different types to show their properties separately. In the panel with the double white dwarf systems we plot the so called chirp line, for $T = 1$ yr, as the solid line. Systems to the right of this line change their frequency during the integration by one or more bins ($\dot{f}\,T > \Delta f = 1/T$). The position at which the systems merge is plotted as the dotted line in the left two panels.

The horizontal straight dotted line in Fig. 9.5 marks the lower limit of $\mathcal{M}$ for systems with a total mass larger than the Chandrasekhar mass which may be supernova Ia (SN

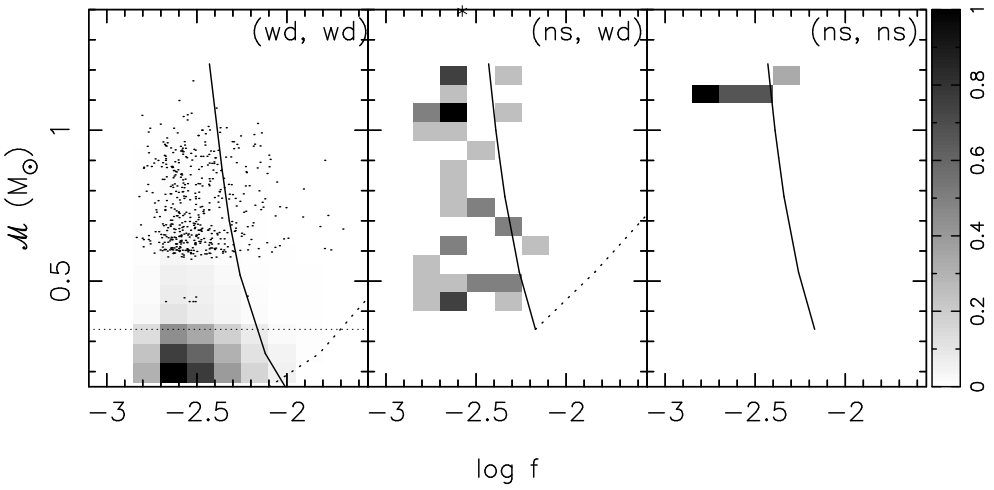

Figure 9.5: Distribution of the resolved binaries over frequency and chirp mass $\mathcal{M}$. The grey shade gives the number of systems in each bin relative to the maximum in each plot which is 1735 for (wd, wd), 5 for (ns, wd) and 3 for (ns, ns). The type of binary is denoted at the top. The dots in the (wd, wd) panel indicate the systems with a total mass above the Chandrasekhar limit. The solid line shows the chirp line for T = 1 yr (Sect. 9.4.2). The curved dotted line shows the position at which the systems merge. Double neutron stars merge at high ($f \approx$ kHz) frequencies so their merger line falls off this plot.

Ia) precursors. The resolved systems above this line are plotted as the dots, as because of their relatively small number (501 systems) the grey scales above above this line are practically invisible in the grey shade plot.

In the (ns, wd) panel we also plot the chirp and merger line, assuming for the latter that the systems emit at the fundamental (n = 2) frequency. In our model the mass of a neutron star is between 1.25 and 1.55$M_\odot$, depending on the initial mass of the progenitor. This results in a very narrow range in chirp masses for the double neutron star systems.

The quantities measured by detectors like LISA are the frequency and the strain amplitude [Eq. (9.3)]. In Fig. 9.6 we plot the distributions of the expected resolved systems over $\log f$ and $\log h$. In Fig. 9.6 we also show the sensitivity limits of LISA for monochromatic sources, for signal to noise ratios of 5 and 1 and an integration time of 1 yr (adapted from Fig. 5 and Eq. (53) of LARSON ET AL. 2000). The solid line gives the average noise background as produced by double white dwarfs (see Fig. 9.3).

9.4.3 Other detectable systems?

It may well be that the systems which produce strong signals because of their proximity to the Sun or a large chirp mass can be detected individually above the noise background

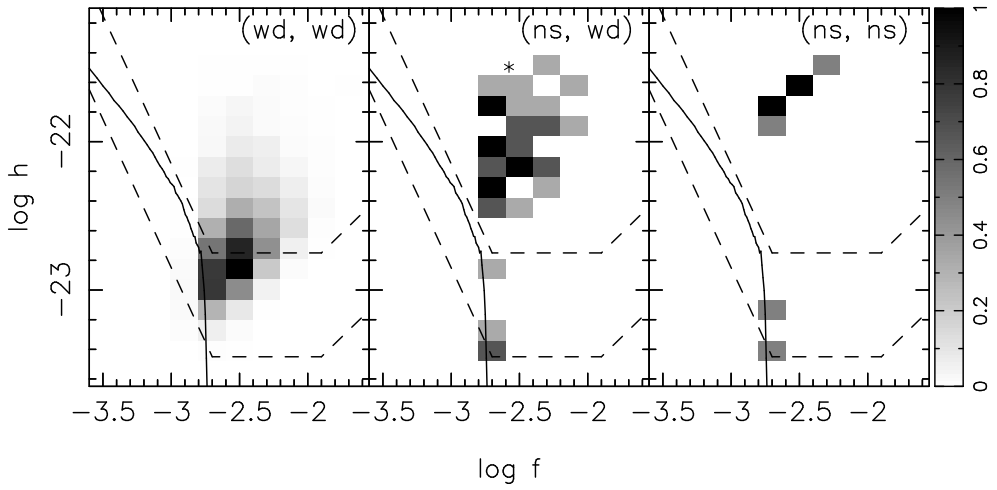

Figure 9.6: Distribution of resolved systems over the frequency and strain amplitude for the different types of binaries (indicated in the top right corner of each panel). The grey shade gives the number of systems relative to the maximum in each plot, which is 1314 for (wd, wd), 3 for (ns, wd) and 2 for (ns, ns). The star indicates the (bh, wd) system. The dashed lines give the LISA sensitivity for an integration time of 1 yr and a signal to noise ratio of 5 (top line) and 1 (bottom line). The average double white dwarfs background is plotted as the solid line.

(see Fig. 9.3). To investigate this possibility, we computed the number of systems of the different types that are not resolved, but have a strain amplitude well above the noise background (as 'well above the noise' we use the sensitivity curve for LISA for a S/N of 5, see Fig. 9.3). This adds a considerable number of potentially detectable systems to the resolved binaries (Table 9.2). It brings the total number of potentially detectable binaries containing neutron stars to almost 200, for an integration time of 1 yr.

9.5 Discussion

9.5.1 Halo and extra-galactic sources

Above, the binary confusion limit and the number of resolved sources were calculated for the Galactic disk binaries. However, for example, Galactic halo objects and extra-galactic binaries may also contribute to the GW signal in the LISA band.

The results of microlensing experiments can be considered as evidence for the existence of massive compact halo objects (MACHO's). The most likely MACHO mass is between 0.15 and 0.9 $M_\odot$, depending on the halo model, and the total mass in MACHO's out to 50 kpc is $9^{+4}_{-3} \times 10^{10}\,M_\odot$, independent of the halo model (ALCOCK ET AL. 2000). The nature of MACHO's is still unknown (e.g. GATES ET AL. 1998),

but two options are relevant to this study.

The first is that they are white dwarfs (ADAMS AND LAUGHLIN 1996), already long ago suggested to contribute a significant fraction of dark matter in the halo (TAMANAHA ET AL. 1990). A discussion is still going on whether the presence of a significant white dwarf population is compatible with constraints derived from the chemical composition of the halo and the cooling properties of the white dwarfs (e.g. CHABRIER 1999; FIELDS ET AL. 2000; HANSEN 2000). Evidently, nothing is known about the fraction of binaries in this hypothetical population. However, because the star formation in the halo happened long ago (e.g. ADAMS AND LAUGHLIN 1996), most short period double white dwarfs that could have formed will already be merged. For example, for a 1Gyr long burst of star formation, 14 Gyr ago, with an IMF similar to the IMF of the disk, currently all halo close binary white dwarfs have orbital periods longer than $\simeq 0.3$ hr, so they cannot contribute to the GW signal at frequencies higher than $\log f \simeq -2.75$. The observed deficit of halo white dwarf progenitors in distant galaxies (ADAMS AND LAUGHLIN 1996) suggests that the IMF in the halo is peaked at or above $2\,M_\odot$, limiting a hypothetical double white dwarf population to even lower frequencies. Hence, we do not expect a change in the confusion limit due to halo white dwarfs, but they could contribute to the unresolved noise below this limit.

Existing estimates of the contribution of halo binaries to the GW noise (HISCOCK ET AL. 2000) are based on a simple rescaling to the halo of the estimate of the GW signal from the disk by HILS ET AL. (1990). Because of the different evolutionary histories of disk and halo this is unrealistic. Additionally, HISCOCK ET AL. (2000) use the lowest existing observational estimates of the local white dwarf space density, probably overestimating the relative importance of a possible halo white dwarf population.

A way to circumvent the nucleosynthesis and luminosity limitations on the nature of MACHO's is to assume that they are low-mass black holes. Formation of low-mass ($\lesssim 1\,M_\odot$) black holes is possible in inflationary cosmological models (e.g. NASELSKII AND POLNAREV 1985). Further, as was shown by NAKAMURA ET AL. (1997), these black holes may form binaries. An estimate by HISCOCK (1998) shows that under certain assumptions about the separations of the components, the GW background formed by halo binary black holes can be much stronger than the signal from the Galactic binary white dwarfs. If this model is correct, the noise produced by halo objects would bury virtually all resolved signals from Galactic systems (compare our Fig.9.3, left panel and Fig. 2 of HISCOCK 1998). This would result in the non-detection of any resolved systems by LISA, and show up as an anisotropic noise.

A significant contribution from extra-galactic binaries to the background is expected only if the star formation keeps increasing at $z \gtrsim 3$ (KOSENKO AND POSTNOV 1998). A computation with a star formation rate which is almost constant at $1.5 \lesssim z \leq 5$ and roughly the same input for stellar evolution as used in this study (SCHNEIDER ET AL. 2000), showed that only just above the point where the Galactic disk double white dwarf background drops sharply (around $\log f = -2.75$) the extra-galactic background could exceed the Galactic one. However, the signals of the resolved binaries at these frequencies are at least an order of magnitude stronger than this background and will probably be detectable (see our Fig. 9.6 and Fig. 12 of SCHNEIDER ET AL. 2000).

Finally it should be noted that a few tens of double neutron stars and neutron star – white dwarf binaries in globular clusters will probably be resolved, in addition to our estimate above (BENACQUISTA ET AL. 2001).

9.5.2 Comparison with previous studies

We can compare our results to the results of earlier studies. The first quantitative calculation of the double white dwarf background was done by EVANS ET AL. (1987). Their Eq. (19) gives the expected "clearing" frequency, above which the sources are resolved, as function of birth rate and integration time. With our values ($\nu(f) \approx \nu_{\rm merg} = 0.011$ and $\Delta f_{\rm INT} = 1$ yr) one would find $\log f_{\rm c} = -2.65$, a bit higher than expected from Fig. 9.4. For the average background at $\log f = -4.0$ they find $\log h = -19.75$ and at $\log f = -3.0$ $\log h = -20.6$ for their integration time of 10^6 s. The background scales as $\sqrt{N/T}$ for different integration times and numbers of systems in the Galaxy. The fact that our average background is about $\sim$1.6 dex lower is a consequence of the lower birth rate (by a factor 7.6) and the different distribution of systems in the Galaxy that we find.

The most recent result, by WEBBINK AND HAN (1998), uses a more similar birth rate: 0.03 $\rm yr^{-1}$ but a constant star formation history and a larger age of the Galactic disk, of 15 Gyr (HAN 1998). The number distribution of these authors in Fig. 1 can be compared to our Fig. 9.3 (right panel), by dividing their number by 3.16×10^7 to account for the bin width, and by the frequency, to get $N_{\rm per\,bin}$. Their numbers then convert to $\log N_{\rm per\,bin} = 4.0$ and 1.0 for $\log f = -4.0$ and -3.0 respectively, where our calculations give $\log N_{\rm per\,bin} = 3.8$ and 1.0 for these frequencies (if we exclude the AM CVn systems, which dominate at -3.0). The slight difference in the strain amplitude (their Fig. 2), which can be compared to our Fig. 9.3 (left panel) by dividing by the square root of the integration time, may be a consequence of their higher average chirp mass (compare their average value of 0.42 for resolved binaries with Fig. 9.5) or their assumed Galactic distribution, which is slightly different from our Eq. (9.5).

The comparison with POSTNOV AND PROKHOROV (1998) is difficult since they use a very different model, with different star formation history and in particular a spheroidal Galactic distribution with a vertical scale height of 4.2 kpc instead of a disk as we use.

The number of resolved systems and their properties is briefly discussed by WEBBINK AND HAN (1998). They find a confusion limit of $\log f = -2.44$ but from a different argument. Above this limit they find 3600 resolved double white dwarfs in excellent agreement with our number of 3615 resolved double white dwarfs above $\log f = -2.44$.

The GWR signal from eccentric binaries was discussed by BARONE ET AL. (1988) and HILS (1991), but these authors do not discuss the possibility to resolve some of these. HILS (1991) calculates the average strain amplitude for double neutron stars, which clearly falls far below the double white dwarf background (his Figs. 3 and 4), again confirming our assumption that they can be excluded at low frequencies.

Finally we note that HILS AND BENDER (2000), who calculate the background due to AM CVn systems conclude (as we do) that these systems are not important for the overall background.

9.6 Conclusion

We calculated the gravitational wave signal of Galactic disk binaries containing two compact objects. We discuss three populations: (i) double white dwarfs (including interacting systems) which produce a confusion limited noise background at low frequencies ($\log f \lesssim -2.8$), (ii) resolved binaries and (iii) unresolved systems that have such a strong signal that they may be detected above the noise.

The confusion limited background is dominated by detached double white dwarfs, although in a small frequency range ($-3.4 < \log f < -3.0$) the interacting systems form the majority of the systems in each bin. The double white dwarf gravitational wave background, which in our model consists of the sum of the signal of all 150 million systems in the Galaxy, shows large spikes caused by strong-signal (i.e. close) systems, which might be detectable above the noise.

Adding the binaries containing neutron stars and black holes (which are much less numerous than white dwarf pairs), we find the distribution of bins containing one, none and more than one system and show that the "confusion limit" as a single value does not exist: at $\log f = -2.84$ the first resolved bins are found, while up to $\log f = -2.4$ bins containing more than one system are present.

We find 12171 resolved systems of which the vast majority consists of double white dwarfs. There are only 8 double neutron stars and 38 neutron star – white dwarf binaries resolved. Finally we calculate that there are 6104 systems (5943 double white dwarfs, 124 neutron star – white dwarf systems, 31 double neutron stars and 6 systems containing a black hole) which have a signal well above the double white dwarf background and the LISA sensitivity level.

Out of 12124 resolved double white dwarfs, 501 have a combined mass above the Chandrasekhar limit and periods short enough to merge in 10 Gyr and are thus potential SN Ia progenitors. Such double white dwarfs have not yet been found optically. If a system would chirp, LISA may provide a direct evidence for the total mass of the system and its distance. The number of chirping SN Ia progenitors is ~ 94 for an integration time of 1 yr. But even for these systems the actual time to coalescence is $\sim$ (4500 – 80000) yr.

Acknowledgements. LRY and SPZ acknowledge the warm hospitality of the Astronomical Institute "Anton Pannekoek". This work was supported by NWO Spinoza grant 08-0 to E. P. J. van den Heuvel, RFBR grant 99-02-16037, the Russian Ministry of Science Program "Astronomy and Space Research" and by NASA through Hubble Fellowship grant HF-01112.01-98A awarded (to SPZ) by the Space Telescope Science Institute, which is operated by the Association of Universities for Research in Astronomy, Inc., for NASA under contract NAS 5-26555.

Appendix 9.A The formation of black holes

The simplified description of evolution of massive stars used in this paper is based on results of EGGLETON ET AL. (1989) and SCHALLER ET AL. (1992) and can be summarised as follows (see also PORTEGIES ZWART AND YUNGELSON 1998)

1. The radii of the massive stars are limited to 1000 $R_\odot$ (after SCHALLER ET AL. 1992).

2. The maximum amount of mass loss for hydrogen rich massive stars is given by 0.01 M^2, unless the whole envelope is lost and the star becomes a Wolf-Rayet star. Thus stars above 85 $M_\odot$evolve off the main sequence immediately to become Wolf-Rayet stars with an initial mass of 43 $M_\odot$ (after SCHALLER ET AL. 1992).

3. Wolf-Rayet stars lose mass according to the equation proposed by LANGER (1989a).

4. In the supernova 50% of the mass of the exploding object is ejected (see also Chapter 7).

5. Exploding helium stars more massive than 10 $M_\odot$ collapse to a black hole. Thus, the lower limit for black hole masses of $M = 5M_\odot$ is consistent with observational estimates (e.g. CHARLES 1998).

6. black holes do not get a kick at birth, neutron star receive a kick according to the distribution proposed by HARTMAN (1997).

CHAPTER 10

Summary and conclusion

10.1 Summary

In this thesis some aspects of the formation and evolution of binaries containing white dwarfs, black holes and neutron stars are investigated. The formation of individual observed systems is studied and simulated populations are compared with observed samples, taking selection effects into account. These populations are used to predict the expected results of future gravitational wave detectors. Fast spectroscopy is used to study one particular source in detail, confirming its binary nature beyond any doubt. We separately summarise the results for the white dwarf and black hole binaries and end with the summary of the gravitational wave research.

10.1.1 White dwarf binaries

Chapters 2 and 3 study the formation of observed single undermassive white dwarfs and double helium white dwarfs, respectively. The formation of single undermassive white dwarfs can be explained by invoking standard common-envelope evolution with spiral-in, in 'binaries' consisting of a solar-like star and a massive planet or brown dwarf. The tidal instability causes the low-mass companion to be drawn into the solar-like star when it evolves up the giant branch. The potential energy of the low-mass companion can be sufficient to expel the envelope of the giant star, exposing the degenerate helium core and thus forming an undermassive white dwarf. The low-mass companion can either be evaporated just before the whole envelope is ejected or can still be orbiting around the white dwarf. Current limits on the radial velocity variations of the white dwarfs are not strong enough to exclude companions with masses below 0.1 $M_{\odot}$.

We show that the formation of the three observed double helium white dwarfs, all of which have mass ratios around unity, cannot be explained using the standard formation scenarios for double white dwarfs (Chapter 3): The scenario in which the binary experiences two phases of spiral-in leads to double helium white dwarfs with a mass ratio around 0.5 and the scenario in which a stable mass transfer phase is followed by a spiral-in produces binaries with mass ratios around 1.2. We reconstructed the evolution of three observed double helium white dwarfs, using the unique core mass – radius relation for giants with degenerate cores, to find the pre-mass-transfer orbital separations and came to the following conclusions: (i) The last mass-transfer phase can be described

with the spiral-in formalism with high common-envelope efficiency. (ii) The first mass-transfer phase cannot be described by a spiral-in nor by stable mass transfer but can be described very well with a formalism based on the angular momentum balance, with one free parameter which for the three observed systems has a very similar value. The fact that the angular momentum of these binaries is large enough to bring the common envelope into corotation, thus making drag forces inefficient, can explain the difference with the standard spiral-in case.

The Chapters 4 and 5 deal with population synthesis of close detached double white dwarfs and AM CVn stars, respectively. Using the results of Chapter 3, cooling curves for helium white dwarfs, and an exponentially decaying star formation rate, we improve in Chapter 4 the population synthesis for close double white dwarfs with respect to earlier studies. The main conclusions are: (i) The recently proposed cooling curves for helium white dwarfs overestimate the luminosity for the lowest mass ($M < 0.3\,\mathrm{M}_{\odot}$) helium white dwarfs (ii) The fraction of double white dwarfs among all white dwarfs can only be brought into agreement with observations if the initial binary fraction is not above 50 % (iii) The model with an exponentially decaying star formation rate gives a slightly better fit to the observed period distribution for double white dwarfs than a constant star formation rate. A well-constrained local space density of white dwarfs combined with an accurate estimate of the current planetary nebulae formation rate would improve the discrimination between models with different star formation histories. We note that the differences in the models due to different selection effects are larger than those due to different binary evolution parameters.

Chapter 5 discusses the problems of the two formation channels for AM CVn stars in detail. In a pair of close double white dwarfs, in which one of the stars starts to transfer matter to its companion, no accretion disk is formed at the onset of the mass transfer. The stability of the mass transfer then depends crucially on the (tidal) coupling between the donor and the accretor. In the case of inefficient coupling the chance for a double white dwarf to evolve into a AM CVn star is very small. The alternative channel in which a low-mass helium star transfers matter to a white dwarf companion and becomes semi-degenerate, suffers from a different problem. Before the donor becomes semi-degenerate and the system begins to look like an AM CVn star, the accreted helium on top of the white dwarf accretor may detonate and cause the underlying white dwarf to explode. We model the current population of AM CVn stars using two extreme possibilities for these channels and compare the results with the observations after applying very simple selection effects. We conclude that in order to distinguish between different models and formation channels both the theory of helium accretion disks and the homogeneity and completeness of the observations (particularly regarding the distances to the AM CVn stars) need to be improved.

In Chapter 6 we reduce and analyse high-speed spectroscopic data of AM CVn itself and find, for the first time, a clear direct signature of the binary nature of AM CVn in its spectrum. Folded on one of the proposed orbital periods (1029 s) we clearly see an emission component moving inside the He I absorption lines. With Doppler tomography this emission maps nicely onto one spot at the expected position of the hot spot (the place where the accretion stream hits the edge of the accretion disk). Folded on the other

proposed orbital period (1051 s) this signature is not seen. The orbital period of AM CVn thus is 1029 s and the system behaves as a helium equivalent to the hydrogen-rich cataclysmic variables with permanent superhumps. We confirm the 13.38 hr period in the skewness of the absorption lines and constrain the value of K_2 between 210 and 280 km s^{-1}.

10.1.2 Black hole binaries

The velocities of the black hole X-ray binaries show a remarkable property (Chapter 7). The space velocities of the two X-ray binaries with relatively massive donors are the highest. From the observed space velocity, neglecting the velocity the system already had, we could determine the amount of mass that must have been lost explosively in the supernova in which the black hole was produced. The result is that some 30 – 50% of the mass of the exploding helium star did not end up in the black hole, but was ejected from the system. The fact that the X-ray binaries with low-mass donors hardly have any space velocity is consistent with the same mass-loss fraction, since the black hole progenitors in these systems had a very low orbital velocity. This also shows that the importance of an asymmetric kick imparted on the collapsed object is negligible for black holes, in contrast to the case for neutron stars.

Chapter 8 reviews two formation scenarios for binaries in which a black hole accretes mass from a low-mass companion. The use of strong stellar winds in evolutionary calculations led to the conclusion that it is very hard to make a black hole, especially in a close binary and that the latter is only possible if the mass transfer takes place only just before the supernova occurs. We showed that such mass transfer is only possible with one of the three investigated massive star models. Furthermore, we compare the mass-loss laws used in the calculations with a recent compilation of observed mass-loss rates for Wolf-Rayet stars and find that even downward revised mass-loss laws still overestimate the mass loss. A mass-loss law more in agreement with the observed values significantly improves the possibility for the formation of black holes in binaries: we find that with these revised laws all stars in close binaries with an initial mass above 30 – 40 $M_\odot$ leave remnants at the supernova explosion of 7 $M_\odot$ or more.

10.1.3 Gravitational waves from the Galaxy

In Chapter 9 we describe the population of binaries consisting of two compact objects, either white dwarfs, neutron stars or black holes. We calculate the merger rates of binaries containing neutron stars and black holes and confirm earlier estimates of these rates which imply that the first generation high-frequency gravitational wave detectors will probably not detect these events. For the low-frequency detector in space (LISA) we calculate the unresolved noise background produced by double white dwarfs and calculate the population of resolved binaries and binaries with signals sufficiently strong that they may be detected above the noise level. For an integration time of 1 yr, we predict detection of more than ten thousand double white dwarfs, some hundred neutron star – white dwarf binaries, some tens of double neutron stars and maybe a few binaries con-

taining a black hole. Of the resolved double white dwarfs ∼500 are expected to have a total mass above the Chandrasekhar limit. They may be type Ia supernova progenitors. About 95 of them have an observable frequency change, allowing a direct measurement of their chirp mass and their distance. These will merge within the next 40000 yr.

10.2 Conclusion

The overall way in which binaries evolve and the formation of most types of binaries is understood in general terms. However many details of the evolution of single and binary stars are still unclear. This poses a serious problem in particular for population synthesis, because in order to improve its results, better understanding of these details is required. In particular the formation of some interesting populations, such as low-mass X-ray binaries, black hole binaries, and double neutron stars really depends on details like the radius evolution of massive stars and the efficiency of the common-envelope ejection. The result is that there are still large uncertainties, for example in the nature of the progenitors of type Ia supernova!e, the formation of low-mass X-ray binaries (in particular the ones with a black hole accretor) and in such fundamental questions as the applicability of the spiral-in mechanism in common-envelope evolution.

Improvements in observational techniques with larger telescopes (e.g Keck, VLT, Subaru, Gemini) and better detectors and satellites (e.g. the Parkes multi-beam receivers, ISO, RXTE, HIPPARCOS) have led to better statistics and better constrained parameters of the observed binaries. Some recent examples are the large increase in the number of known pulsars (CAMILO ET AL. 2000) and double white dwarfs (MARSH 2000), the improved parameters of black hole binaries (BAILYN ET AL. 1998; CHARLES 1998), the study of stellar winds (HAMANN AND KOESTERKE 1998; NUGIS AND LAMERS 2000) etc.

There has also been quite some progress in the modelling of specific aspects that influence the evolution of single stars. Some recent examples are the modelling of stellar wind (VINK ET AL. 2000), and of the effect of stellar rotation (MAEDER AND MEYNET 2000; HEGER ET AL. 2000). A similar step forward in binary evolution models has not yet been achieved. One basic problem for the modelling is that physical models for binaries and their evolution can not be constructed from first physical principles, because the problem is essential 3-dimensional and both the the physical theory and computer power for solving this problem are lacking. This means that the validity of the simplifications that are used in the models have to be gauged by comparison with the observations. Therefore, dedicated observations to reveal the laws governing particularly important phases of binary evolution are needed. An example of this is the applicability and properties of the spiral-in mechanism during phases of unstable mass transfer. Study of a large observed sample of pre- and post spiral-in binaries could possibly resolve this issue and bring theoretical models a step further.

From our work on the population of double white dwarfs and AM CVn stars we also concluded that, for the moment, the real problem in distinguishing between different assumptions about binary evolution is our limited knowledge of the selection effects

that govern the detection of the observed systems. To make a step forward we here again have to base ourselves on dedicated observations of a homogeneous sample of observed systems with as many parameters (magnitudes, distances etc.) as possible. In this respect it is also important to improve the absolute scaling of the population synthesis results: at present the different normalisations that are used can differ by almost an order of magnitude in particular parts of the parameter space (i.e. a factor of four in the assumed star formation rate combined with a different assumption on the IMF gives an order of magnitude difference in the expected number of massive stars in the Galaxy).

Finally, concerning the formation of black holes in binaries: Only when the evolution of massive stars and Wolf-Rayet stars is better understood will there be a prospect for solving this problem. For this again we need further observations of wind mass-loss rates of stars as well as further improved models of the evolution of (rotating) massive stars.

Nederlandse samenvatting

In deze samenvatting leg ik eerst uit wat sterren zijn en hoe ze ontstaan, vervolgens hoe ze evolueren en uiteindelijk compacte objecten worden: witte dwergen, neutronensterren of zwarte gaten worden. Dan leg ik uit wat een dubbelster is en hoe die ontstaat en evolueert. Vervolgens wat er gebeurt met een dubbelster waarvan minstens één van de sterren een compact object is. Daarna leg ik uit wat er in de verschillende hoofdstukken van mijn proefschrift beschreven is.

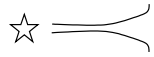

Sterren en hun evolutie

Sterren zijn gasbollen die uit het interstellaire gas zijn samengetrokken. Dat proces verloopt als volgt. Als ergens in het interstellaire gas een verdichting ontstaat komen de gasdeeltjes dichter bij elkaar waardoor ze elkaar harder gaan aantrekken en het gas nog meer gaat samentrekken. Bij die samentrekking komt energie vrij, waardoor het gas heter wordt en licht gaat uitstralen. Op het moment dat dat gebeurt is er geen houden meer aan: hoe verder de gaswolk samentrekt, hoe heter, hoe meer straling (licht), meer samentrekking, etcetera. Dit proces wordt pas gestopt als er een fundamentele verandering optreedt: het gas, dat voornamelijk uit waterstof bestaat, wordt zo heet en de druk wordt zo hoog dat waterstof gaat fuseren tot helium. Dat betekent dat de kernen van vier waterstofatomen samensmelten tot één helium atoomkern. Daarbij komt ontzettend veel energie vrij. Die energie zorgt ervoor dat het gas zo heet wordt dat er voldoende druk ontstaat om de samentrekking te stoppen. De gaswolk bereikt dan een evenwicht waarin de energieproductie in het centrum en de energieverliezen aan het oppervlak (in de vorm van licht) in evenwicht zijn. Een ster is geboren.

De verdere ontwikkeling van een ster wordt bepaald door de wisselwerking tussen de zwaartekracht en de energieproductie door kernfusie. De eerste fase van het leven van een ster is een hele rustige: in het centrum van de ster wordt waterstof in helium omgezet. Omdat deze fase langer duurt dan de rest van de evolutie van de ster, zien we de meeste sterren om ons heen in deze fase. De zon is nu bijvoorbeeld in deze fase. Dit soort sterren heten hoofdreeks-sterren, omdat ze een nauwe strook (de hoofdreeks)

vormen in een grafiek waarin je de totale hoeveelheid licht die een ster uitzendt tegen de kleur van die ster uitzet (dat heet het Hertzsprung-Russell diagram).

Deze fase kan niet eeuwig doorgaan, omdat door het omzetten van waterstof in helium de voorraad waterstof in de kern van de ster (de "brandstof" dus) langzaam opraakt. Op een gegeven moment zijn er niet genoeg waterstofatomen meer over om de kernfusie aan de gang te houden. Dan houdt dus ook de energietoevoer in het centrum van de ster op en gaat de samentrekking van de gaswolk waar de ster uit is gevormd weer verder, net als toen er nog geen kernfusie was begonnen. De temperatuur in de kern van de ster is nu echter erg hoog. Door het verder samentrekken wordt die steeds hoger. Op een gegeven moment gaat in een schil net *buiten* de kern waterstof tot helium fuseren en – wat later – *in* de kern de helium tot koolstof en zuurstof. Tijdens de 'waterstofschilverbranding' zetten de buitenste lagen van de ster (die nog steeds voornamelijk uit waterstof bestaan) uit totdat de ster honderden keren groter is dan hij op de hoofdreeks was. De buitenste lagen van de ster koelen daarbij af, waardoor de ster roder van kleur wordt. In deze fase van zijn ontwikkeling noemen we de ster een rode reus.

Afhankelijk van de massa (van de kern) van de ster zijn er drie manieren van verdere evolutie. Voor sterren die lichter zijn dan ongeveer acht keer de massa van de zon is op een gegeven moment alle helium in de kern omgezet in koolstof en zuurstof. De kernfusie stopt en de buitenste lagen van de ster worden de ruimte in geblazen. Wat overblijft is de kern, die erg heet is, omdat de kernfusie pas net is gestopt. De ster heet nu een witte dwerg, omdat hij witheet is en erg klein.

Bij zwaardere sterren wordt de temperatuur in de kern zo hoog, dat ook atoomkernen zoals die van koolstof- en zuurstof kunnen fuseren. Op een gegeven moment bestaat de kern voornamelijk uit atoomkernen van ijzer. Dan stopt de kernfusie, omdat voor kernfusie van ijzer energie toegevoegd zou moeten worden. Er is dan geen energieproductie door kernfusie meer mogelijk om de samentrekking tegen te houden. De kern van de ster stort in elkaar tot een heel klein balletje (van ongeveer 10 kilometer in doorsnede), waarin meer massa zit samengeperst dan de massa van de zon. Bij dat in elkaar storten van komt heel veel energie vrij, waardoor de buitenste lagen van de ster het heelal in worden geslingerd: dat noemen we een supernova explosie. Het balletje bestaat vrijwel helemaal uit neutronen (kerndeeltjes van atomen). Zo'n object noemen we een neutronenster.

Als de massa van de ijzerkern groter is dan zo'n twee à drie keer die van de zon, worden zelfs de neutronen in elkaar gedrukt en kan niets de samentrekking van de materie meer tegenhouden. Zo wordt een zwart gat gevormd. Een zwart gat is zo klein en zwaar dat de aantrekkingskracht zo groot wordt dat er zelfs geen licht uit kan ontsnappen. Vandaar de naam zwart gat.

Overblijfsels van sterren: compacte objecten

Overblijfsels van sterren zijn dus witte dwergen, neutronensterren of zwarte gaten, die we samenvatten onder de noemer compacte objecten.

WITTE DWERGEN zijn ongeveer net zo groot als de aarde. Omdat ze gemiddeld half zo zwaar zijn als de zon (die 300.000 keer zo zwaar is als de aarde), hebben ze een hele hoge dichtheid. Het materiaal waaruit een witte dwerg bestaat heeft een dichtheid die net zo groot is als wanneer je een olifant in een luciferdoosje zou proppen. Als witte dwergen ontstaan zijn ze erg heet. Ze hebben echter geen energiebron (er vind geen kernfusie plaats in een witte dwerg) dus ze koelen langzaam af. Dat gaat heel langzaam, omdat er in het heelal geen lucht is (op aarde zorgt de lucht ervoor, dat hete objecten snel afkoelen). Witte dwergen koelen af door straling uit te zenden. Daarom kun je een witte dwerg zien. In het begin zijn deze objecten nog vrij helder, maar al snel worden witte dwergen erg zwak en moeilijk te zien. Je kan dan ook geen enkele witte dwerg met het oog waarnemen. De meest bekende witte dwerg vormt een dubbelster met de helderste ster aan de hemel: Sirius. We noemen de witte dwerg Sirius B. Hij is ontdekt omdat de sterrenkundige Bessel opmerkte dat Sirius een slingerbeweging maakt en dus een dubbelster moest zijn. In 1862 ontdekte de Amerikaanse lenzenslijper Alvan Clark met een nieuwe telescoop inderdaad een heel zwak sterretje op de voorspelde positie van de begeleider.

NEUTRONENSTERREN zijn nog extremere objecten. Met hun doorsnede van zo'n tien kilometer en een massa van ongeveer anderhalf keer die van de zon is de dichtheid van een neutronenster net zo groot als een miljard olifanten die in een luciferdoosje zijn gepropt! Al in de jaren dertig, kort na de ontdekking van het neutron, realiseerden Baade en Zwicky zich dat er objecten kunden bestaan die uit neutronen zijn opgebouwd. Men nam aan dat je die nooit zou kunnen zien, maar aan het eind van de jaren zestig ontdekten Bell en Hewish merkwaardige signalen die werden opgevangen door hun radiotelescoop. Het bleken periodieke pulsjes te zijn van magnetische neutronensterren, die we pulsars noemen.

ZWARTE GATEN zijn helemaal moeilijk voorstelbare objecten. Het enige wat je er van kan zeggen is dat er, afhankelijk van de massa van het zwarte gat, een bolvormig volume is waaruit niets kan ontsnappen, zelfs geen licht. De rand van dit volume noemen we de horizon van een zwart gat. De vraag is natuurlijk hoe je nou een zwart gat kan ontdekken? Dat kan als een zwart gat deel uitmaakt van een dubbelster Als een zwart gat een dubbelster vormt met een begeleider die je wel kan zien, zijn er twee dingen die de aanwezigheid van het zwarte gat verraden. Ten eerste is het zwarte gat zwaar en zie je dus de gewone ster om een zwaar object – dat je niet ziet – heen bewegen. Ten tweede kan er gas van de buitenste lagen van de gewone ster naar het zwarte gat gaan stromen. Omdat het zwarte gat zwaar en klein is valt het gas heel hard naar het zwarte gat toe, waarbij het heel heet wordt. Het gaat dan Röntgenstraling uitzenden. Beide effecten komen ook voor bij neutronensterren. Omdat we vrij zeker denken te weten dat een neutronenster niet zwaarder kan zijn dan twee à drie keer de massa van de zon, moet een ongeziene begeleider die zwaarder is wel een zwart gat zijn.

Twee is leuker dan één

Het blijkt dat veel sterren niet alleen zijn, maar in paren voorkomen. Dat heeft waarschijnlijk te maken met de wijze waarop sterren ontstaan. Omdat ze ontstaan uit hele grote wolken die samentrekken, hebben ze last van een extreme vorm van het 'balletdanseres-effect': als je ronddraait met uitgestrekte armen en die dan intrekt ga je sneller draaien. Als de gaswolk waar een ster uit ontstaat een klein beetje ronddraait zal de uiteindelijke (heel veel kleinere) ster heel snel gaan ronddraaien. Als iets heel snel ronddraait krijg je een naar buiten gerichte kracht (zoals bij een centrifuge). De buitenste lagen van de ster zouden daardoor de ruimte in geslingerd worden. Om dat te vermijden worden *twee* sterren uit een gaswolk gemaakt in plaats van *één*. De draaiing kan dan in de beweging van de twee sterren om elkaar heen worden gestopt en de sterren zelf hoeven niet snel te roteren.

Dubbelsterren zijn op een heel slimme manier ontdekt. Stel dat sterren willekeurig zouden zijn verdeeld in de ruimte staan er dan soms *toevallig* twee sterren echt dicht bij elkaar. In 1767 realiseerde John Michell zich dat er aan de hemel veel meer paren voorkomen dan met dit toeval verklaard kunnen worden. Hij concludeerde daaruit dat er echte paren, dubbelsterren dus, moesten worden gevormd. In het begin van de 19^{e} eeuw ontdekte William Herschel dat twee sterren die vlak bij elkaar aan de hemel staan beiden van plek waren veranderd ten opzichte van de posities die ze tientallen jaren eerder innamen en dus een dubbelster vormen.

Dubbelsterren zijn vooral interessant als de twee componenten dicht om elkaar heen draaien. Dat zijn dus een ander soort dubbelsterren dan die waar Herschel en Michell het over hadden: de twee sterren staan zó dicht bij elkaar dat je ze ziet als één ster. Ze zijn zo interessant omdat, als een van de sterren gaat evolueren en een rode reus wordt, de buitenste lagen van deze ster de aantrekkingskracht van de begeleider net zo sterk gaan voelen als de aantrekkingskracht van zijn eigen kern. Er wordt dan dus aan twee kanten aan de materie getrokken. Als de materie nog iets dichter bij de begeleider komt gaat die nog iets harder trekken en gaat het gas naar de begeleider stromen: er treedt massa-overdracht op. Dat heeft natuurlijk zowel invloed op de verdere evolutie van de massa-verliezende ster als op de massa-opnemende ster. De eerste kan bijvoorbeeld zijn hele mantel verliezen, waardoor er in een vroeg stadium een witte dwerg (de kern van de ster) wordt gevormd. De begeleider kan door het opnemen van massa (accretie noemen we dat) zwaarder worden en bijvoorbeeld uiteindelijk een neutronenster vormen i.p.v. een witte dwerg.

Een ander effect van de massa-overdracht is dat de onderlinge beweging van de sterren verandert. Dat heeft weer te maken met het verhaal van de balletdanseres. De hoeveelheid draaiing van een object heeft te maken met iets wat we impulsmoment noemen. Hoe harder iets draait hoe meer impulsmoment het heeft, maar ook hoe groter iets is hoe meer impulsmoment het heeft. Het blijkt dat als er geen interactie plaatsvindt de hoeveelheid impulsmoment hetzelfde blijft. Vandaar dat een balletdanseres, als ze haar armen intrekt en dus kleiner wordt, harder gaat draaien om toch hetzelfde impulsmoment te houden. Bij een dubbelster geldt hetzelfde, maar nu is van belang dat het impulsmoment ook nog afhangt van de hoeveelheid massa die beweegt. Als er in de

dubbelster massa wordt overgedragen verandert de snelheid waarmee de twee sterren om elkaar heen draaien, om het impulsmoment gelijk te houden.

Wat de zaken ook nog compliceert is dat begeleider continu van plaats verandert. Het materiaal dat van de ene ster naar de begeleider wordt overgedragen stroomt daardoor niet direct naar de begeleider, maar 'mist' deze steeds, omdat hij alweer van plaats is veranderd. Het gas vormt daardoor een ring rond de begeleider en door de interne krachten in het gas spreidt deze ring zich langzaam uit tot een schijf rond de ster. Het gas beweegt langzaam door de schijf en aan de binnenkant valt het uiteindelijk op de ster. Zo'n schijf noemen we een accretieschijf.

Compacte objecten in dubbelsterren

Als de begeleider van de massa-verliezende ster een compact object is wordt het gas dat naar het compacte object stroomt hard aangetrokken en moet het heel ver 'vallen', omdat het compacte object zo klein is. Het gas valt steeds sneller en sneller en wordt heter en heter. Daarom is het gas in het binnenste van een accretieschijf rond een compact object veel heter dan rond een gewone ster. Het is het heetst rond neutronensterren en zwarte gaten, omdat die het kleinst zijn. Het wordt daar zo heet dat het gas heel veel Röntgenstraling gaat uitzenden.

Dubbelsterren waar dat het geval is heten Röntgendubbelsterren en zijn in de jaren 60 ontdekt toen men voor het eerst naar de hemel ging kijken met Röntgendetectoren. Ze zenden zóveel Röntgenstraling uit dat je met een Röntgendetector de meeste tot op hele grote afstanden kan zien, soms zelfs in andere melkwegstelsels. In het geval van een witte dwerg als compact object wordt de accretieschijf minder heet, maar ook dan wordt er Röntgenstraling uitgezonden, zij het veel minder. Dubbelsterren waar een witte dwerg massa opneemt van een gewone ster heten Cataclysmische Variabelen. Ze vertonen soms enorme uitbarstingen, waarbij ze wel een miljoen keer zo helder worden als normaal.

Het komt ook voor dat twee compacte objecten een dubbelster vormen. Omdat ze allebei klein zijn kunnen ze een hele nauwe dubbelster vormen, waarbij de sterren heel dicht om elkaar bewegen, met een hele korte omloopperiode (de tijd waarin de twee sterren precies één keer om elkaar heen draaien). Omdat er dan (meestal) geen massa-overdracht plaatsvindt kunnen we die dubbelsterren alleen ontdekken door de beweging van witte dwergen of pulsars te meten. Gelukkig kan dat bij pulsars enorm nauwkeurig, omdat door hun beweging om hun begeleider afwisselend iets verder weg van en iets dichter bij de aarde zijn. Omdat de radiostraling met een constante snelheid reist (de lichtsnelheid) komen de pulsjes dus afwisselend iets later en iets eerder aan dan het geval zou zijn als de afstand gelijk zou blijven. Bij witte dwergen kan hun beweging (minder nauwkeurig) worden bepaald uit hun spectrum. In een spectrum wordt het licht van een ster uiteengerafeld in de verschillende kleuren (golflengtes) waaruit het bestaat (zoals een regenboog). In sterspectra ontbreken vaak sommige kleuren (er zitten dan donkere lijnen in het spectrum) wat wordt veroorzaakt door absorptie van juist die golflengten door het gas in de ster. Door de beweging van de ster bewegen die donkere lijnen een heel klein beetje heen en weer. De beweging van die lijnen kan je meten.

Mijn proefschrift

Mijn proefschrift gaat over dubbelsterren die uit twee compacte objecten bestaan en over dubbelsterren die uit een compact object en een gewone ster bestaan. Het grootste deel gaat over dubbelsterren die uit twee witte dwergen bestaan. De hoofdstukken 3 en 4 gaan over dubbele witte dwergen waarbij geen massa-overdracht plaatsvindt, de hoofdstuken 5 en 6 over massa-overdragende dubbele witte dwergen. De hoofdstukken 7 en 8 gaan over dubbelsterren die bestaan uit een zwart gat en een gewone ster.

In mijn proefschrift worden verschillende technieken gebruikt om de vorming en evolutie van dubbelsterren te begrijpen. De eerste is de (re)constructie van de evolutie van individuele dubbelsterren, en wordt gebruikt in de hoofdstukken 2, 3, 7 en 8.

In HOOFDSTUK 2 bespreken we de vorming van witte dwergen die een bijzondere eigenschap hebben. Het zijn namelijk *te lichte* witte dwergen. Hun 'ondergewicht' zou als volgt verklaard kunnen worden: in een dubbelster kan een ster zijn hele mantel verliezen door massa-overdracht, waardoor de kern van de ster bloot komt te liggen en een witte dwerg wordt, voordat hij is volgroeid. Het probleem met de twee in dit hoofdstuk bestudeerde witte dwergen met ondergewicht is echter dat ze helemaal geen deel uitmaken van een dubbelster, zoals je dan zou verwachten. We hebben laten zien dat ze ook kunnen ontstaan in een 'dubbelster' die bestaat uit een ster zoals de zon en een zware planeet. De planeet vervult dan de rol van dubbelsterpartner en zorgt ervoor dat de mantel van de zon-achtige ster verloren gaat. De planeet kan in dat proces verdampen of kan het overleven. Wat het geval is geweest bij de waargenomen witte dwergen met ondergewicht weten we niet, omdat we een eventueel overgebleven planeet als begeleider niet zouden kunnen zien.

HOOFDSTUK 3 gaat wederom over witte dwergen met ondergewicht, maar dan twee samen in één dubbelster. We reconstrueren hoe de omloopperiodes van deze dubbesterren zijn veranderd tijdens de massa-overdracht fases waarin de beide witte dwergen zijn gevormd. We kunnen dat doen omdat de omloopperiode in een dubbelster behalve van de massa's van de twee sterren vooral afhangt van de *afstand* tussen de twee sterren. Die laatste kunnen we reconstrueren uit de huidige *massa* van de waargenomen witte dwergen. De diameter van de rode reuzen waar ze uit zijn ontstaan wordt namelijk bepaald door de massa van de kern (wat later de massa van de de witte dwerg is). Het blijkt dat de het idee dat we hadden over de verandering van de afstand tussen de twee sterren tijdens de massa-overdracht waarin de eerste witte dwerg is gevormd niet klopte. Uit onze reconstructie hebben we berekend hoe de afstand wel verandert. Het blijkt dat die verandering op een hele simpele manier beschreven kan worden door gebruik te maken van het feit dat het impulsmoment gedurende de massa-overdracht hetzelfde is gebleven.

De vorming van dubbelsterren waarin een zwart gat massa opneemt van een gewone ster is het onderwerp van HOOFDSTUK 7. Het gaat heel specifiek over de vraag of in de supernova explosie waarin het zwarte gat wordt gevormd alle materie van de ster in het zwarte gat verdwijnt danwel ook een deel de ruimte in wordt geslingerd. Dat laatste moet het geval zijn, want door de terugslag daarvan wordt de dubbelster de tegenovergestelde kant op geduwd. Omdat de bewegingssnelheid van een aantal van dit soort dubbelsterren gemeten is kunnen we de hoeveelheid massa berekenen die de ruimte in moet zijn

geslingerd. Het blijkt dat dat wel 30 tot 50 procent van de massa van de exploderende ster kan zijn geweest.

HOOFDSTUK 8 gaat over de massa's die deze exploderende sterren kunnen hebben. Deze soort sterren is heel zwaar op het moment dat ze ontstaan (meer dan twintig keer zo zwaar als de zon), maar verliezen veel massa in een sterrenwind. Hoe sterk die sterrenwind eigenlijk is is niet goed bekend. Tot voor kort hadden de meeste berekeningen als uitkomst dat deze sterren *zoveel* massa verliezen dat ze te licht worden om nog zwarte gaten te kunnen worden. De nieuwste waarnemingen suggereren echter dat het wel meevalt met de sterrenwind. We hebben uitgerekend wat dat voor gevolgen heeft voor de massa's van de sterren op het moment dat ze exploderen en concluderen dat ze dan toch zwaar genoeg zijn om zwarte gaten te maken. Hoe dat vervolgens gebeurt is overigens erg onzeker.

In de meeste andere hoofdstukken maken we gebruik van een andere techniek. Met computermodellen berekenen we hoeveel dubbelsterren van een bepaalde soort we verwachten in onze Melkweg en wat precies de eigenschappen zijn van deze dubbelsterpopulaties. We hebben we een computermodel verder ontwikkeld dat de evolutie van elke willekeurige dubbelster kan berekenen. We nemen aan dat dubbelsterren ontstaan met bepaalde verdelingen van de massa's van beide sterren en de omloopperiode. Vervolgens rekenen we voor een heleboel willekeurige dubbelsterren uit hoe ze evolueren. Dan selecteren we de dubbelsterren die een dubbelster worden waarin we zijn geïnteresseerd (bijvoorbeeld een dubbele neutronenster) en kijken naar de eigenschappen van deze 'model-populatie'. Die vergelijken we dan met de waargenomen dubbelsterren van dat type. Een complicerende factor hierbij is dat de waargenomen dubbelsterren soms bij toeval zijn ontdekt en dat het dus de vraag is in hoeverre ze representatief zijn voor de hele populatie van dat soort dubbelsterren in de Melkweg.

In HOOFDSTUK 4 passen we deze techniek toe op de populatie van dubbele witte dwergen. Daar zijn er op dit moment ongeveer 15 van bekend. In ons model gebruiken we de nieuwe beschrijving van de vorming van deze dubbelsterren zoals afgeleid in hoofdstuk 3. Onze model-populatie komt beter overeen met de waargenomen systemen dan de populaties die zijn berekend met andere modellen. Verder hebben we vooral beter kunnen modelleren welke van de dubbele witte dwergen in het computermodel we wel en welke we niet zouden kunnen zien, waardoor de waargenomen systemen beter zijn te vergelijken met de modelsystemen. De overeenkomst tussen model en waarnemingen is behoorlijk goed al lijken er nog wat problemen te zijn. Voordat we daar meer over kunnen zeggen moeten er eerst meer van dit soort dubbelsterren worden ontdekt.

HOOFDSTUK 5 gebruikt dezelfde techniek, maar dan om de populatie van dubbele witte dwergen te onderzoeken waarbij er massa-overdracht is van de ene witte dwerg naar de andere. Deze dubbelsterren heten AM CVn sterren, naar de naam (AM CVn) van de eerst ontdekte. Er zijn op dit moment 6 van deze dubbelsterren bekend waarvan we de omloopperiode kennen. Deze dubbelsterren kunnen op twee manieren ontstaan; o.a. uit het soort dubbelsterren waar hoofdstuk 4 over gaat. We bespreken de problemen van beide vormingspaden en de onzekerheden daarin en berekenen dan een modelpopulatie

voor dit soort dubbelsterren in de Melkweg. Welke model-dubbelsterren van de aarde het beste zichtbaar zijn en hoeveel we er verwachten te kunnen zien is bij deze dubbelsterren moeilijk te bepalen. Met een simpele schatting hiervoor vinden we dat het model redelijk goed overeenkomt met de waarnemingen.

In HOOFDSTUK 9 combineren we de modellen uit de hoofdstukken 4 en 5 met ons eerder onderzoek van de populatie van dubbelsterren die bestaan uit een neutronenster en een witte dwerg en dubbelsterren die bestaan uit twee neutronensterren. Dit doen we om de populatie van dubbelsterren die uit twee compacte objecten bestaan te berekenen die hele korte omloopperiodes hebben. De Europese en Amerikaanse ruimtevaartorganisaties zijn van plan een satelliet te lanceren die zwaartekrachtsstraling van dat soort dubbelsterren kan meten. Zwaartekrachtsstraling is een speciaal soort straling die is voorspeld door de algemene relativiteitstheorie en die wordt veroorzaakt door bewegende zware objecten. In dit hoofdstuk voorspellen we wat voor dubbelsterren die satelliet zal gaan gaan ontdekken.

De laatste techniek die in mijn proefschrift wordt toegepast is het waarnemen van dubbelsterren (HOOFDSTUK 6). We hebben uit het archief van een telescoop die op het Canarische eiland La Palma staat waarnemingen gehaald die zijn gedaan in 1996. Toen zijn er spectra van de ster AM CVn, de naamgever van de AM CVn sterren, opgemeten. We zijn er als eersten in geslaagd veranderingen van het spectrum aan te tonen die synchroon lopen met de beweging van de twee sterren om elkaar heen. Niet alle sterrenkundigen waren er helemaal van overtuigd dat AM CVn echt een dubbelster is, maar de veranderingen van het spectrum tonen dat nu duidelijk aan.

List of Publications

Refereed journals

Nelemans, G., Hartman, J. W., Verbunt, F., Bhattacharya, D., Wijers, R. A. M. J., 1997, *Modelling the variance of dispersion measures of radio pulsars*, *A&A* **322**, 489

Nelemans, G., Tauris, T. M., 1998, *Formation of undermassive single white dwarfs and the influence of planets on late stellar evolution*, *A&A* **335**, L85 (Chapter 2)

Nelemans, G., Tauris, T. M., van den Heuvel, E. P. J., 1999, *Constraints on mass ejection in black hole formation derived from black hole X-ray binaries*, *A&A* **352**, L87 (Chapter 7)

Nelemans, G., Verbunt, F., Yungelson, L. R., Portegies Zwart, S. F., 2000, *Reconstructing the evolution of double helium white dwarfs: envelope loss without spiral-in*, *A&A* **360**, 1011 (Chapter 3)

Nelemans, G., Yungelson, L. R., Portegies Zwart, S. F., Verbunt, F., 2001, *Population synthesis for double white dwarfs. I Detached systems*, *A&A* **365**, 491 (Chapter 4)

Nelemans, G., Portegies Zwart, S. F., Verbunt, F., Yungelson, L. R., 2001, *Population synthesis for double wite dwarfs. II. Semi-detached systems: AM CVn binaries*, *A&A* in press (Chapter 5)

Submitted

Nelemans, G., Steeghs, D., Groot, P. J., 2001, *Spectroscopic evidence for the binary nature of AM CVn*, *MNRAS* submitted (Chapter 6)

Everett, M. E., Huber, M. E., Howell, S. B., et al., 2001, *The Faint Sky Variability Survey II: Initial Results*, *MNRAS* submitted, astro-ph/0009479

Groot, P. J., Vreeswijk, P. M., Everett, M. E., Howell, S. B., et al., 2001, *The Faint Sky Variability Survey I: An Overview*, *MNRAS* submitted, astro-ph/0009478

Conference proceedings

Verbunt, F., Hartman, J. W., Bhattacharya, D., Wijers, R. A. M. J., Nelemans, G., 1999, in Z. Arzoumanian, F. van der Hooft, E. P. J. van den Heuvel (eds.), *Pulsar Timing, General Relativity and the Internal Structure of Neutron Stars*, p. 215, Koninklijke Nederlandse Akademie van Wetenschappen, Amsterdam

Nelemans, G., Portegies Zwart, S. F., Verbunt, F., 2000, *Gravitational waves from double white dwarfs*, in J. Trân Thanh Vân, J. Dumarchez, S. Reynaud, C. Salomon, S. Thorsett, J. Y. Vinet (eds.), *Gravitational Waves and Experimental Gravity*, XXXIVth Rencontres de Moriond, pp 119–124, World Publishers, Hanoi

Nelemans, G., Tauris, T. M., van den Heuvel, E. P. J., 2001, *Constraints on mass ejection in black hole formation derived from black hole X-ray binaries*, in L. Kaper, E. P. J. van den Heuvel, P. A. Woudt (eds.), *Black Holes in Binaries and Galactic Nuclei*, Springer-Verlag, Heidelberg, in press

Portegies Zwart, S. F., Yungelson, L. R., Nelemans, G., 2001, *Fun for Two*, in H. Zinnecker R. Mathieu (eds.), *The Formation of Binary Stars*, IAU Symposium 200, in press, astro-ph/0008033

Verbunt, F., Nelemans, G., 2001, *Binaries for LISA*, to appear in *Class. Quantum Grav.*

Yungelson, L., Nelemans, G., Portegies Zwart, S. F., Verbunt, F., 2001, *The population of close double white dwarfs in the Galaxy*, in D. Vanbeveren (ed.), *The influence of binaries on stellar population studies*, Kluwer, in press, astro-ph/0011248

Dankwoord

Als laatste rest mij nog een woord van dank aan alle mensen die hebben bijgedragen aan de totstandkoming van mijn proefschrift. Ten eerste natuurlijk mijn beide promotoren. ED en FRANK, als duopromotor vormen jullie in ieder geval een prima koppel. Weliswaar hebben jullie verschillende karakters en regelmatig verschillende meningen, jullie fundamentele houding ten opzichte van de wetenschap en jullie werkwijze lijken erg op elkaar. Ik hoop een beetje van die kijk op de zaken opgepikt te hebben.

SIMON, door de jaren hebben we veel met elkaar te maken gehad. Vaak via de e-mail, maar ook wel in levenden lijve. Dat heeft me meer opgeleverd dan reisjes naar Japan en Boston. Ik heb veel van je geleerd over programmeren, sterrenkunde en het bedrijven van wetenschap. Bovendien hebben we vooral ook erg veel plezier gehad.

LEV, our collaboration started somewhat by coincidence, but already from the chapters of my thesis it is clear that without you it would have looked quite differently. Less clear from the outside is the immense knowledge and insight in stellar evolution (no, I will not write stellar and binary evolution) you have and shared with me. I learned a lot and it was a great pleasure to work together. We will keep in touch.

THOMAS, you also played an important role in the development of two of the chapters of my thesis. During the writing of these chapters and also at other times it was always good to hear your opinion of matters (loud and clearly).

PAUL en DANNY bedankt voor het enthousiasme waarmee jullie mijn eerste stappen op het gebied van de observationele sterrenkunde hebben aangemoedigd en begeleid. Wie weet word ik nog eens een echte waarnemer.

Vervolgens wil ik mijn kamergenoot JEROEN bedanken voor de prettige en ongedwongen sfeer op onze kamer. Als ik wilde kon ik altijd mijn verhaal kwijt. Heb je je wel eens gerealiseerd dat we elkaar (op een korte onderbreking na) al 10½ jaar vrijwel dagelijks zien?

MAUREEN wil ik bedanken voor de gezellige en serieuze gesprekken als ik weer eens in Utrecht langskwam en voor het feit dat ik vorig jaar mee mocht naar La Palma, om voor het eerst waarnemingen te doen.

Zo zou ik nog wel een hele tijd door kunnen gaan, maar dat gaat misschien toch wat

ver. Ik wil iedereen op het instituut en uit Utrecht bedanken voor een gezellig gesprek hier en een praatje daar. Ik wil toch de namen van MARNIX, MARTIN, BEN, JEROENB, ALEX, RAMACH, PAULV, SACHA, ROB, JANE en ERICA niet onvermeld laten, zonder de anderen daarmee tekort te willen doen.

I also want to thank GERRY and CHANG-HWAN for inviting me to Stony Brook, where I had a very nice time and TOM and PIERRE for the hospitality in Southampton.

Er zijn ook niet-sterrenkundingen die mij (indirect) hebben bijgestaan de afgelopen jaren. MIRIAM, ALDO, ELINE, PAUL, ANNEMIEKE, CONSTANTIJN en de rest van de (ex)Kunstorkesters, ANNEMIEKE en de rest van Timber en de kleinste Johannesjes.

Ik sluit mijn proefschrift af met het bedanken van mijn OUDERS, LIJNIS, ANNEWIEKE, BERT, CATHRIEN en SOPHIE en natuurlijk

Bedankt allemaal!

☆

Bibliography

ABT H.A., 1983, ARA&A, 21, 343
ADAMS F.C., LAUGHLIN G., 1996, ApJ, 468, 586
ALCOCK C., ALLSMAN R.A., ALVES D.R., ET AL., 2000, ApJ, 542, 281
ARZOUMANIAN Z., CORDES J.M., WASSERMAN I., 1999, ApJ, 520, 696
BAILES M., 1996, In *Compact Stars in Binaries*, volume 165 of *IAU Symp.*, p. 213
BAILYN C.D., JAIN R.K., COPPI P., OROSZ J.A., 1998, ApJ, 499, 367
BAILYN C.D., OROSZ J.A., MCCLINTOCK J.E., REMILLARD R.A., 1995, Nat, 378, 157
BARKAT Z., REISS Y., RAKAVY G., 1974, ApJ, 193, L21
BARONE F., MILANO L., PINTO I., RECANO F., 1988, A&A, 199, 161
BENACQUISTA M.J., PORTEGIES ZWART S., RASIO F.A., 2001, to appear in Class. Quantum Grav., gr-qc/0010020
BERGERON P., RUIZ M.T., LEGGETT S.K., 1997, ApJS, 108, 339
BERGERON P., SAFFER R.A., LIEBERT J., 1992, ApJ, 394, 228
BETHE H.A., WILSON J.R., 1985, ApJ, 295, 14
BHATTACHARYA D., VAN DEN HEUVEL E.P.J., 1991, Physics Rep., 203, 1
BISIKALO D.V., BOYARCHUK A.A., KUZNETSOV O.A., CHECHETKIN V.M., 1998, ARep, 42, 621
BLAAUW A., 1961, BAN, 15, 165
BLÖCKER T., 1995, A&A, 299, 755
BLOOM J.S., SIGURDSSON S., POLS O.R., 1999, MNRAS, 305, 763
BOOTHROYD A.I., SACKMANN I.J., 1988, ApJ, 328, 641
BRAGAGLIA A., RENZINI A., BERGERON P., 1995, ApJ, 443, 735
BRANDT W.N., PODSIADLOWSKI P., SIGURDSSON S., 1995, MNRAS, 277, L35
BROWN G.E., 1995, ApJ, 440, 270
BROWN G.E., LEE C.H., BETHE H.A., 1999, New Astronomy, 4, 313
BROWN G.E., LEE C.H., TAURIS T.M., 2001, New Astronomy, submitted
CAMILO F., LYNE A.G., MANCHESTER R.N., ET AL., 2000, ApJ, in press, astro-ph/0012154
CAMPBELL C.G., 1984, MNRAS, 207, 433
CANNIZZO J.K., 1984, Nat, 311, 443
CAPPELLARO E., EVANS R., TURATTO M., 1999, A&A, 351, 459
CHABRIER G., 1999, ApJ, 513, L103

CHARLES P.A., 1998, In M. Abramowicz, G. Bjornsson, J. Pringle, eds., *Theory of Black Hole Accretion Disks*, pp. 1 – 21, CUP, Cambridge
CLARET A., GIMÉNEZ A., 1990, Ap&SS, 169, 215
COLGATE S.A., 1971, ApJ, 163, 221
COUNSELMAN C.I., 1973, ApJ, 180, 307
CROPPER M., HARROP-ALLIN M.K., MASON K.O., ET AL., 1998, MNRAS, 293, L57
DARWIN G.H., 1908, *Scientific papers*, volume 2, CUP, Cambridge
DE JAGER C., NIEUWENHUIJZEN H., VAN DER HUCHT K.A., 1988, A&AS, 72, 259
DE KOOL M., 1990, ApJ, 358, 189
—, 1992, A&A, 261, 188
DE KOOL M., VAN DEN HEUVEL E.P.J., PYLYSER E., 1987, A&A, 183, 47
DEWEY R.J., CORDES J.M., 1987, ApJ, 321, 780
DOUGLAS D.H., BRAGINSKY V.B., 1979, In S.W. Hawking, W. Israel, eds., *General Relativity* An Einstein centenary survey, chapter 3, pp. 90–137, CUP, Cambridge
DRIEBE T., BLÖCKER T., SCHÖNBERNER D., HERWIG F., 1999, A&A, 350, 89
DRIEBE T., SCHÖNBERNER D., BLÖCKER T., HERWIG F., 1998, A&A, 339, 123, (DSBH98)
DUQUENNOY A., MAYOR M., 1991, A&A, 248, 485
EGGLETON P.P., 1983, ApJ, 268, 368
EGGLETON P.P., FITCHETT M.J., TOUT C.A., 1989, ApJ, 347, 998
EL-KHOURY W., WICKRAMASINGHE D., 2000, A&A, 358, 154
ELVIS M., PAGE C.G., POUNDS K.A., ET AL., 1975, Nature, 257, 656
ERGMA E., FEDOROVA A., 1998, A&A, 338, 69
ERGMA E., VAN DEN HEUVEL E.P.J., 1998, A&A, 331, L29
ERGMA E.V., FEDOROVA A.V., 1990, Ap&SS, 163, 142
EVANS C.R., IBEN I. JR, SMARR L., 1987, ApJ, 323, 129
EYLES C.J., SKINNER G.K., WILLMORE A.P., ET AL., 1975, IAU Circ., 2822
FAULKNER J., FLANNERY B.P., WARNER B., 1972, ApJ, 175, L79
FESTIN L., 1998, A&A, 336, 883
FIELDS B.D., FREESE K., GRAFF D.S., 2000, ApJ, 534, 265
FLANAGAN E., 1998, In *Gravitation and Relativity: At the Turn of the Millennium*, p. 177, gr-qc/9804024
FLANNERY B.P., VAN DEN HEUVEL E.P.J., 1975, A&A, 39, 61
FRASCA A., MARILLI E., CATALANO S., 1998, A&A, 333, 205
FRYER C.L., 1999, ApJ, 522, 413
GALAMA T., ET AL., 1998, Nat, 395, 670
GATES E.I., GYUK G., HOLDER G.P., TURNER M.S., 1998, ApJ, 500, L145
GIANNONE P., GIANNUZZI M.A., 1970, A&A, 6, 309
GIANNUZZI M.A., 1981, A&A, 103, 111
GREENSTEIN J.L., MATTHEWS M.S., 1957, ApJ, 126, 14
GREINER J., HASINGER G., THOMAS H., 1994, A&A, 281, L61
GROENEWEGEN M.A.T., DE JONG T., 1993, A&A, 267, 410

GUNN J.E., OSTRIKER J.P., 1969, Nat, 221, 454
HABETS G.M.H.J., 1986, A&A, 167, 61
HAMANN W.R., KOESTERKE L., 1998, A&A, 335, 1003
HAN Z., 1998, MNRAS, 296, 1019, (HAN98)
HAN Z., PODSIADLOWSKI P., EGGLETON P.P., 1995, MNRAS, 272, 800
HAN Z., WEBBINK R.F., 1999, A&A, 349, L17
HANSEN B.M.S., 1999, ApJ, 520, 680
—, 2000, In J.W. Menzies, P.D. Sackett, eds., *Microlensing 2000: A new era of microlensing astrophysics*, ASP Conf. Ser.
HARLAFTIS E.T., COLLIER S., HORNE K., FILIPPENKO A.V., 1999, A&A, 341, 491
HARLAFTIS E.T., HORNE K., FILIPPENKO A.V., 1996, PASP, 108, 762
HÄRM R., SCHWARZSCHILD M., 1961, AJ, 66, 45
HARTMAN J.W., 1997, A&A, 322, 127
HARVEY D.A., SKILLMAN D.R., KEMP J., ET AL., 1998, ApJ, 493, L105
HEGER A., LANGER N., WOOSLEY S.E., 2000, ApJ, 528, 368
HERRERO A., KUDRITZKI R.P., GABLER R., ET AL., 1995, A&A, 297, 556
HILS D., 1991, ApJ, 381, 484
HILS D., BENDER P.L., 2000, ApJ, 537, 334
HILS D., BENDER P.L., WEBBINK R.F., 1990, ApJ, 360, 75
HIROSE M., OSAKI Y., 1990, PASJ, 42, 135
—, 1993, PASJ, 45, 595
HISCOCK W.A., 1998, ApJ, 509, L101
HISCOCK W.A., LARSON S.L., ROUTZAHN J.R., KULICK B., 2000, ApJ, 540, L5
HJELLMING M.S., TAAM R.E., 1991, ApJ, 370, 709
HORNE K., 1991, In A.W. Shafter, ed., *Proc. 12. N. AM Worksh. on CVs & XRBs*, p. 23
HUBBARD W.B., 1994, In G. Chabrier, E. Schatzman, eds., *The Equation of State in Astrophysics*, volume 147 of *IAU Coll.*, pp. 443–462, CUP, Cambridge
HULSE R.A., TAYLOR J.H., 1975, ApJ, 195, L51
HUMASON M.L., ZWICKY F., 1947, ApJ, 105, 85
HURLEY J.R., POLS O.R., TOUT C.A., 2000, MNRAS, 315, 543
IBEN I. JR, LIVIO M., 1993, PASP, 105, 1373
IBEN I. JR, TUTUKOV A.V., 1984a, ApJS, 54, 355
—, 1984b, ApJ, 284, 719
—, 1985, ApJS, 58, 661
—, 1986a, ApJ, 311, 742
—, 1986b, ApJ, 311, 753
—, 1987, ApJ, 313, 727
—, 1991, ApJ, 370, 615
IBEN I. JR, TUTUKOV A.V., FEDOROVA A.V., 1998, ApJ, 503, 344
IBEN I. JR, TUTUKOV A.V., YUNGELSON L.R., 1997, ApJ, 475, 291, (ITY97)
ISRAELIAN G., REBOLO R., BASRI G., ET AL., 1999, Nat, 401, 142
IWAMOTO K., ET AL., 1998, Nat, 395, 672
JHA S., GARNAVICH P., CHALLIS P., ET AL., 1998, IAU Circ., 6983

KALOGERA V., 1999, ApJ, 521, 723
KALOGERA V., LORIMER D.R., 2000, ApJ, 530, 890
KALOGERA V., NARAYAN R., SPERGEL D.N., TAYLOR J.H., 2000, ApJ, submitted, astro-ph/0012038
KALOGERA V., WEBBINK R.F., 1996, ApJ, 458, 301
—, 1998, ApJ, 493, 351
KAPER L., CAMERÓN A., BARZIV O., 1999, In K.A. van der Hucht, G. Koenigsberger, R.J. Eenens, eds., *Wolf-Rayet phenomena in massive stars and starburst galaxies*, IAU Symp. 193, p. 316
KIPPENHAHN R., MEYER-HOFMEISTER E., 1977, A&A, 54, 539
KIPPENHAHN R., THOMAS H.C., WEIGERT A., 1968, ZsAp, 69, 265
KIPPENHAHN R., WEIGERT A., 1967, ZsAp, 65, 251
KNOX R., HAWKINS M.R.S., HAMBLY N.C., 1999, MNRAS, 306, 736
KOEN C., OROSZ J.A., WADE R.A., 1998, MNRAS, 300, 695
KOLB U., 1993, A&A, 271, 149
KOSENKO D.I., POSTNOV K.A., 1998, A&A, 336, 786
KRAICHEVA Z.T., TUTUKOV A.V., YUNGELSON L.R., 1986, Astrophysics, 24, 167
KUDRITZKI R.P., REIMERS D., 1978, A&A, 70, 227
KUIPER G.P., 1938, ApJ, 88, 429
LANDAU L.D., LIFSHITZ E.M., 1971, *"Classical theory of fields"*, Pergamon, Oxford, 3 edition
LANDSMAN W., APARICIO J., BERGERON P., ET AL., 1997, ApJ, 481, L93
LANGER N., 1989a, A&A, 220, 135
—, 1989b, A&A, 210, 93
LARSON S.L., HISCOCK W.A., HELLINGS R.W., 2000, Phys. Rev. D, 62, 062001
LIMONGI M., TORNAMBÈ A., 1991, ApJ, 371, 317
LIPUNOV V.M., POSTNOV K.A., 1988, Ap&SS, 145, 1
LIPUNOV V.M., POSTNOV K.A., PROKHOROV M.E., 1987, A&A, 176, L1
—, 1997a, Pisma Astronomicheskii Zhurnal, 23, 563
—, 1997b, MNRAS, 288, 245
LIPUNOV V.M., POSTNOV K.A., PROKHOROV M.E., ET AL., 1995, ApJ, 454, 593
LIVIO M., 1999, In J.A. Truran, J. Niemeyer, eds., *Type Ia Supernovae: Theory and Cosmology*, CUP, Cambridge, astro-ph/9903264
LIVNE E., 1990, ApJ, 354, L53
LIVNE E., ARNETT D., 1995, ApJ, 452, 62
LIVNE E., GLASNER A., 1991, ApJ, 370, 272
LUBOW S.H., SHU F.H., 1975, ApJ, 198, 383
LYNE A.G., LORIMER D.R., 1994, Nat, 369, 127
MAEDER A., MEYNET G., 2000, ARA&A, 38, 143
MARSH T.R., 1990, ApJ, 357, 621
—, 1995, MNRAS, 275, L1
—, 1999, MNRAS, 304, 443
—, 2000, New Astronomy Review, 44, 119
—, 2001, In H. Boffin, D. Steeghs, J. Cuypers, eds., *Astro-tomography*, Lecture Notes in

Physics, Springer Verlag, astr-ph/0011020
MARSH T.R., DHILLON V.S., DUCK S.R., 1995, MNRAS, 275, 828
MARSH T.R., HORNE K., 1988, MNRAS, 235, 269
—, 1990, ApJ, 349, 593
MARSH T.R., HORNE K., ROSEN S., 1991, ApJ, 366, 535
MASSEVICH A.G., YUNGELSON L.R., 1975, MmSAI, 46, 217
MAXTED P.F.L., HILDITCH R.W., 1996, A&A, 311, 567
MAXTED P.F.L., MARSH T.R., 1998, MNRAS, 296, L34
—, 1999, MNRAS, 307, 122
MAXTED P.F.L., MARSH T.R., MORAN C.K.J., HAN Z., 2000, MNRAS, 314, 334
MAXTED P.F.L., MARSH T.R., NORTH R.C., 2000, MNRAS, 317, L41
MCCLINTOCK J.E., REMILLARD R.A., 1986, ApJ, 308, 110
MCNAMARA P.W., WARD H., HOUGH J., 2000, Advances in Space Research, 25, 1137
MENGEL J.G., DEMARQUE P., SWEIGART A.V., GROSS P.G., 1979, ApJS, 40, 733
MEURS E.J.A., VAN DEN HEUVEL E.P.J., 1989, A&A, 226, 88
MEYNET G., MAEDER A., SCHALLER G., ET AL., 1994, A&AS, 103, 97
MILLER G.E., SCALO J.M., 1979, ApJS, 41, 513
MIRONOVSKII V.N., 1965, SvA, 9, 752
MORAN C.K.J., MARSH T.R., BRAGAGLIA A., 1997, MNRAS, 288, 538
MORAN C.K.J., MAXTED P.F.L., MARSH T.R., 1999, MNRAS, 304, 535
—, 2000, MNRAS, submitted
MOTCH C., HABERL F., GUILLOUT P., ET AL., 1996, A&A, 307, 459
NAKAMURA T., SASAKI M., TANAKA T., THORNE K.S., 1997, ApJ, 487, L139
NAPIWOTZKI R., GREEN P.J., SAFFER R.A., 1999, ApJ, 517, 399
NASELSKII P.D., POLNAREV A.G., 1985, SvA, 29, 487
NATHER R.E., ROBINSON E.L., STOVER R.J., 1981, ApJ, 244, 269
NAUENBERG M., 1972, ApJ, 175, 417
NELEMANS G., PORTEGIES ZWART S.F., VERBUNT F., 2000a, In J. Trân Thanh Vân, J. Dumarchez, S. Reynaud, C. Salomon, S. Thorsett, J.Y. Vinet, eds., *Gravitational Waves and Experimental Gravity*, XXXIVth Rencontres de Moriond, pp. 119–124, World Publishers, Hanoi
NELEMANS G., PORTEGIES ZWART S.F., VERBUNT F., YUNGELSON L.R., 2001a, A&A, in press, (Chapter 5)
NELEMANS G., STEEGHS D., GROOT P.J., 2001b, MNRAS, submitted, (Chapter 6)
NELEMANS G., TAURIS T.M., VAN DEN HEUVEL E.P.J., 1999, A&A, 352, L87, (Chapter 7)
NELEMANS G., VERBUNT F., YUNGELSON L.R., PORTEGIES ZWART S.F., 2000b, A&A, 360, 1011, (Chapter 3)
NELEMANS G., YUNGELSON L.R., PORTEGIES ZWART S.F., VERBUNT F., 2001c, A&A, 365, 491 , (Chapter 4)
NOMOTO K., SUGIMOTO D., 1977, PASJ, 29, 765
NUGIS T., LAMERS H.J.G.L.M., 2000, A&A, 360, 227
OROSZ J.A., WADE R.A., 1999, MNRAS, 310, 773

OSWALT T., SMITH J., WOOD M.A., HINTZEN P., 1995, Nat, 382, 692
PACZYŃSKI B., 1967, Acta Astron., 17, 287
—, 1971, ARA&A, 9, 183
—, 1976, In P. Eggleton, S. Mitton, J. Whelan, eds., *Structure and Evolution of Close Binary Systems*, p. 75, Kluwer, Dordrecht
PACZYŃSKI B., ZIOŁKOWSKI J., 1967, Acta Astron., 17, 7
PANEI J.A., ALTHAUS L.G., BENVENUTO O.G., 2000, A&A, 353, 970
PATTERSON J., HALPERN J., SHAMBROOK A., 1993, ApJ, 419, 803
PETERS P.C., MATTHEWS J., 1963, Phys. Rev., 131, 435
PHINNEY E.S., 1991, ApJ, 380, L17
POLITANO M., WEBBINK R.F., 1989, In *White Dwarfs*, volume 114 of *IAU Colloq.*, pp. 440–442
POLS O.R., COTÉ J., WATERS F.M., HEISE J., 1991, A&A, 241, 419
POLS O.R., MARINUS M., 1994, A&A, 288, 475
PORTEGIES ZWART S.F., 1996, A&A, 296, 691
PORTEGIES ZWART S.F., MCMILLAN S.L.W., 2000, ApJ, 528, L17
PORTEGIES ZWART S.F., VERBUNT F., 1996, A&A, 309, 179
PORTEGIES ZWART S.F., VERBUNT F., ERGMA E., 1997, A&A, 321, 207
PORTEGIES ZWART S.F., YUNGELSON L.R., 1998, A&A, 332, 173
—, 1999, MNRAS, 309, 26
POSTNOV K.A., PROKHOROV M.E., 1998, ApJ, 494, 674
POTTASCH S.R., 1996, A&A, 307, 561
PRESS W., THORNE K.S., 1972, ARA&A, 10, 335
PRINGLE J.E., WEBBINK R.F., 1975, MNRAS, 172, 493
PROVENCAL J.L., WINGET D.E., NATHER R.E., ET AL., 1997, ApJ, 480, 383
RAMSAY G., CROPPER M., WU K., ET AL., 2000, MNRAS, 311, 75
RANA N.C., 1991, ARA&A, 29, 129
RAPPAPORT S.A., JOSS P.C., 1984, ApJ, 283, 232
RASIO F.A., TOUT C.A., LUBOW S.H., LIVIO M., 1996, ApJ, 470, 1187
REFSDAL S., ROTH M.L., WEIGERT A., 1974, A&A, 36, 113
REFSDAL S., WEIGERT A., 1970, A&A, 6, 426
RUIZ M.T., TAKAMIYA M., 1995, AJ, 109, 2817
SACKETT P.D., 1997, ApJ, 483, 103
SAFFER R.A., LIEBERT J., OLSZEWSKI E.W., 1988, ApJ, 334, 947
SAFFER R.A., LIVIO M., YUNGELSON L.R., 1998, ApJ, 502, 394
SALPETER E.E., 1971, ARA&A, 9, 127
SANDQUIST E.L., TAAM R.E., BURKERT A., 2000, ApJ, 533, 984
SARNA M., ERGMA E., GERSKEVITS-ANTIPOVA J., 2000, MNRAS, 316, 84
SAVONIJE G.J., DE KOOL M., VAN DEN HEUVEL E.P.J., 1986, A&A, 155, 51
SCHAERER D., MAEDER A., 1992, A&A, 263, 129
SCHALLER G., SCHAERER D., MEYNET G., MAEDER A., 1992, A&AS, 96, 269
SCHNEIDER R., FERRARI V., MATARRESE S., PORTEGIES ZWART S.F., 2000, MNRAS, submitted, astro-ph/0002055
SCHUTZ B.F., 1996, Class. Quantum Grav., 13, A219

SCHWARTZ M., 1998, IAU Circ., 6982
SHAHBAZ T., VAN DER HOOFT F., J. C., ET AL., 1999, MNRAS, 306, 89
SIMON T., FEKEL F.C., GIBSON JR D.M., 1985, ApJ, 295, 153
SKILLMAN D.R., PATTERSON J., KEMP J., ET AL., 1999, PASP, 111, 1281
SMAK J., 1967, Acta Astron., 17, 255
SMAK J., 1983, Acta Astron., 33, 333
SMARR L.L., BLANDFORD R., 1976, ApJ, 207, 574
SOKER N., 1996, ApJ, 460, L53
—, 1998, AJ, 116, 1308
SOLHEIM J.E., 1995, Baltic Astronomy, 4, 363
SOLHEIM J.E., PROVENCAL J.L., BRADLY P.A., ET AL., 1998, A&A, 332, 939
SOLHEIM J.E., ET AL., 1991, In G. Vauclair, E.M. Sion, eds., *White Dwarfs*, p. 431, Kluwer, Dordrecht
SPRUIT H.C., 1998, A&A, 333, 603
SPRUIT H.C., RUTTEN R.G.M., 1998, MNRAS, 299, 768
SWEIGART A.V., GREGGIO L., RENZINI A., 1990, ApJ, 364, 527
TAAM R.E., 1980, ApJ, 237, 142
TAGOSHI H., KANDA N., TANAKA T., ET AL., 2001, Phys. Rev. D, in press, gr-qc/0012010
TAMANAHA C.M., SILK J., WOOD M.A., WINGET D.E., 1990, ApJ, 358, 164
TAURIS T.M., 1996, A&A, 315, 453
TAURIS T.M., SENNELS T., 2000, A&A, 355, 236
TAYLOR J.H., WEISBERG J.M., 1982, ApJ, 253, 908
TOUT C.A., AARSETH S.J., POLS O.R., EGGLETON P.P., 1997, MNRAS, 291, 732
TOUT C.A., EGGLETON P.P., 1988, MNRAS, 231, 823
TSUGAWA M., OSAKI Y., 1997, PASJ, 49, 75
TUTUKOV A.V., CHEREPASHCHUK A.M., 1997, ARep, 41, 355
TUTUKOV A.V., FEDOROVA A.V., 1989, SvA, 33, 606
TUTUKOV A.V., FEDOROVA A.V., ERGMA E.V., YUNGELSON L.R., 1987, SvAL, 13, 328
TUTUKOV A.V., FEDOROVA A.V., YUNGELSON L.R., 1982, SvAL, 8, 365
TUTUKOV A.V., YUNGELSON L.R., 1973, Nauchnye Informatsii, 27, 70
—, 1979a, In C. de Loore, P.S. Conti, eds., *Mass loss and evolution of O-type stars*, p. 401, Reidel, Dordrecht
—, 1979b, Acta Astron., 29, 665
—, 1981, Nauchnye Informatsii, 49, 3
—, 1988, SvA, 14, 265
—, 1992, SvA, 36, 266
—, 1993a, ARep, 37, 411
—, 1993b, MNRAS, 260, 675
—, 1994, MNRAS, 268, 871
—, 1996, MNRAS, 280, 1035
ULLA A., 1994, Space Sci. Rev., 67, 241
—, 1995, A&A, 301, 469

VAN DEN HEUVEL E.P.J., 1983, In W.H.G. Lewin, van den Heuvel E. P. J., eds., *Accretion-driven stellar X-ray sources*, pp. 303–341, CUP, Cambridge
VAN DEN HEUVEL E.P.J., HEISE J., 1972, Nat, 239, 67
VAN DEN HEUVEL E.P.J., TAAM R.E., 1984, Nature, 309, 235
VAN DEN HOEK L.B., DE JONG T., 1997, A&A, 318, 231
VAN DER HOOFT F., HEEMSKERK H.M., ALBERTS F., VAN PARADIJS J., 1998, A&A, 329, 538
VAN KERKWIJK M.H., BELL J.F., KASPI V.M., KULKARNI S.R., 2000, ApJ, 530, 37
VAN TEESELING A., GÄNSICKE B.T., BEUERMANN K., ET AL., 1999, A&A, 351, L27
VAN TEESELING A., REINSCH K., HESSMAN F.V., BEUERMANN K., 1997, A&A, 323, L41
VERBUNT F., PHINNEY E.S., 1995, A&A, 296, 709
VERBUNT F., RAPPAPORT S., 1988, ApJ, 332, 193
VINK J.S., DE KOTER A., LAMERS H.J.G.L.M., 2000, A&A, 362, 295
WADE R.A., 1984, MNRAS, 208, 381
WARNER B., 1995, Ap&SS, 225, 249
WARNER B., ROBINSON E.L., 1972, MNRAS, 159, 101
WEBBINK R.F., 1975, MNRAS, 171, 555
—, 1977, ApJ, 211, 486
—, 1979, In *White Dwarfs and Variable Degenerate Stars*, volume 53 of *IAU Colloq.*, pp. 426–447
—, 1984, ApJ, 277, 355
WEBBINK R.F., HAN Z., 1998, In *Laser Interferometer Space Antenna*, number 456 in AIP Conf. Proc., p. 61, AIP, New York
WEBBINK R.F., RAPPAPORT R.F., SAVONIJE G.J., 1983, ApJ, 270, 678
WEBER J., 1969, Phys. Rev. Lett., 22, 1302
WELLSTEIN S., LANGER N., 1999, A&A, 350, 148
WHITE N.E., VAN PARADIJS J., 1996, ApJ, 473, L25
WHITEHURST R., 1988, MNRAS, 232, 35
WOOSLEY S.E., LANGER N., WEAVER T.A., 1995, ApJ, 448, 315
WOOSLEY S.E., WEAVER T.A., 1994, ApJ, 423, 371
—, 1995, ApJS, 101, 181
YUNGELSON L.R., LIVIO M., TUTUKOV A.V., SAFFER R., 1994, ApJ, 420, 336
YUNGELSON L.R., TUTUKOV A.V., LIVIO M., 1993, ApJ, 418, 794
ZAHN J.P., 1977, A&A, 57, 383, erratum 1978, A&A 67, 162
ZAPOLSKY H.S., SALPETER E.E., 1969, ApJ, 158, 809